Subspace-based system identification and fault detection: Algorithms for large systems and application to structural vibration analysis

Michael Döhler

N° d'ordre : 4390 ANNÉE 2011

UNIVERSITÉ DE RENNES 1

THÈSE / UNIVERSITÉ DE RENNES 1
sous le sceau de l'Université Européenne de Bretagne

pour le grade de

DOCTEUR DE L'UNIVERSITÉ DE RENNES 1

Mention : Mathématiques et Applications
Label « doctorat européen »

Ecole doctorale Matisse

présentée par

Michael Döhler

préparée à l'unité de recherche Inria

Subspace-based system identification and fault detection: Algorithms for large systems and application to structural vibration analysis

Thèse soutenue à Rennes le 10 octobre 2011

devant le jury composé de :

Albert BENVENISTE
DR Inria / président

Dionisio BERNAL
Professeur, Northeastern University, USA / rapporteur

Jean-Claude GOLINVAL
Professeur, Université de Liège, Belgique / rapporteur

Lennart LJUNG
Professeur, Linköping University, Suède / rapporteur

Palle ANDERSEN
CEO, Structural Vibration Solutions A/S, Danemark / examinateur

Laurent MEVEL
CR Inria / directeur de thèse

To Marianne and Albert.

Acknowledgments

First of all, my deepest gratitude is addressed to my *directeur de thèse* Laurent Mevel for all the support and confidence he gave me during these three years. He guided and shaped me during this thesis, was always available for discussions and was simply a wonderful mentor. His many ideas, enthusiasm and pragmatism were a great source of inspiration. Also, he opened the doors to many collaborations with partners all over the world that I could enjoy during this thesis, which was a great experience, as well as the numerous conferences that I could attend. Besides, he awoke my interest in badminton.

Professors Dionisio Bernal, Jean-Claude Golinval and Lennart Ljung acted as *rapporteurs* of this thesis. They took the time to read and review it, which is gratefully acknowledged, as well as their helpful remarks. Thanks also for taking the way to Rennes to come to the defense or being there on video conference.

The Inria Center in Rennes provided an ideal research environment and I felt more than well in the I4S team. Special thanks goes to Albert Benveniste for many fruitful discussions and helpful advice, as well as for accepting the role as president of the jury for the defense and giving helping remarks on the thesis manuscript. I would also like to thank Maurice Goursat for the interesting discussions we had on a few occasions. Further thanks goes to Dominique Siegert for an insight into civil engineering and preparing many experiments. Also thanks to the PhD students, engineers and postdocs of the I4S team for scientific exchange, pleasant atmosphere and coffee breaks. Furthermore, François Queyroi and Hongguang Zhu had not much choice but to work with me during their internships and I appreciated the collaboration. Last but not least, a great thanks goes to our assistant Laurence Dinh for preparing the *missions* and taking care of all the administrative part.

Furthermore there are many people that enriched the time inside and outside Inria and became good friends. Amongst others, I am grateful to have met Matthias, Carito, Robert, Katarzyna, Sidney, Guillaume, Noël, Ludmila, Romaric, Carole, Aurore, Florian, Phillipe to share lunch breaks, barbecues and many things more.

I am grateful for having had many international collaborations during this thesis. I wrote my first conference papers together with Marcin Luczak (LMS, Leuven), and Edwin Reynders (KU Leuven) and Filipe Magalhães (University of Porto), who I met on several occasions. I had a collaboration with Dionysius Siringoringo (University of Tokyo) including a short visit at his university. I am very grateful for an intensive collaboration with Dionisio Bernal (Northeastern University Boston) and his students. I learned a great deal while visiting him for a week in Boston and I appreciated many fruitful discussions. Within the FP7

project IRIS (whose financial support is also acknowledged) we had a good collaboration with James Brownjohn (University of Sheffield) and his postdocs Bijaya Jaishi and Ki-Young Koo. Thanks for inviting me to Sheffield. I very much enjoyed the one week visit and the occasion to see Humber Bridge and its instrumentation in reality. Another great collaboration emerging from the IRIS project is the one with Falk Hille (BAM Berlin). Each occasion to meet was a pleasure and I also enjoyed an invitation to Berlin for a week. A contribution of our collaborative work to the IRIS project was awarded with the IRIS Prize of Excellence 2011, which is also gratefully acknowledged. Thanks also go to Werner Rücker and Sebastian Thöns from BAM. Last but not least, Palle Andersen (SVS, Aalborg) has my deepest gratitude. I had the chance to participate in the collaboration with him since the beginning and see some of the algorithms developed in this thesis implemented in his software. With the support of the FP7 project ISMS (Marie Curie mobility grant), I stayed at his company for five months and got the taste of an industrial research environment, where I learned a lot about the way from research into practice. I am thankful for this unforgettable time in Denmark and all the support I got from Palle and all the SVS team with Kristine Nielsen and Henrik Vollesen.

Finally, I wish to express my gratitude to my family. They always supported me in any possible way and let me emigrate to France. Unfortunately I could not be more present for my grandparents Marianne and Albert, who both passed away during the second year of this thesis. I will never forget their curiosity, thirst of knowledge and motivation, as well as their desire for exploring and traveling the world, which undoubtedly influenced me a lot. At the end of this listing, but actually before everything, is my *PACSée* Mélissande, without whom I would not even have started this thesis. Thank you for your love and never ending support.

– Michael Döhler
Rennes, October 2011

Contents

Introduction

Context of the work

Linear system identification and the detection of changes in systems from measured signals is an area of multidisciplinary research in the fields of mathematical modeling, automatic control, statistics and signal processing. During the last ten to twenty years, system identification methods found a special interest in structural engineering for the identification of *vibration modes* and *mode shapes* of structures, as well as for detecting changes in their vibration characteristics, both under real operation conditions. This *Operational Modal Analysis (OMA)* consists of three steps: data acquisition, data analysis and evaluation of the results. Advances in data acquisition systems (low cost sensors, fiber optic sensors, wireless sensor networks, etc.) lead to larger systems that can be monitored and push for the development of data analysis methods. The evaluation step is done by the experienced structural engineer and, for example, has an impact on the design of structures, includes finite element model updating or the detection of aeroelastic flutter.

This thesis is situated in the data analysis step, where linear system identification and fault detection methods are in use. However, in the *Operational Modal Analysis* context the following unusual features must be taken into account:

(a) The number of sensors can be very large (up to hundreds, or thousands in the future with new technologies); sensors can even be moved from one measurement campaign to another;

(b) The number of modes of interest can be quite large (up to 100 or beyond), thus calling for methods that can deal with large model orders at a reasonable computation time;

(c) The excitation applied to the structure is usually unmeasured, uncontrolled and natural, thus turbulent and non-stationary.

In this thesis, methods for system identification and fault detection are developed, which take the features (a)–(c) into account. The developed techniques concern the theoretical design of these methods, but take their importance from the OMA context, where large structures equipped with many sensors under in operational noisy conditions are the norm.

System identification

The design and maintenance of mechanical, civil and aeronautical structures subject to noise and vibrations are relevant structural engineering topics. They are components of comfort, e.g. for cars and buildings, and contribute significantly to safety related aspects, e.g. for aircrafts, aerospace vehicles and payloads, civil structures, wind turbines, etc. It must be assured that dynamic loads, such as people, traffic, wind, waves or earthquakes, do not compromise the serviceability of these structures. For example, resonance or aeroelastic flutter phenomena need to be avoided. In order to study the dynamic properties of a structure, its vibration modes (natural frequencies and damping ratios) and mode shapes are analyzed.

Requirements from these application areas are numerous and demanding. In the design stage, detailed physical computer models are built, which involve the dynamics of vibrations and sometimes other physical aspects as fluid-structure interaction, aerodynamics or thermodynamics. However, not the entire structure can be accurately modeled, such as the links to the ground for civil engineering structures. Usually, laboratory and in-operation vibration tests are performed on a prototype structure in order to obtain modes and mode shapes from recorded vibration data in these tests. The results are used for updating the design model for a better fit to data from the real structure, and for certification purposes. Under operation conditions, they allow investigating the dynamic properties of the real structure and to monitor for changes in these properties, which might lead to corrective actions.

Therefore, the identification of vibration modes and mode shapes from measured data is a basic service in structural engineering in order to study and monitor the dynamic properties of a structure. These vibration characteristics are found in the eigenstructure of a linear system, which needs to be identified from the data.

Methods for system identification often originate from control theory, where they have shown to work for small system orders and controlled excitation. They are proved on the board, tested on simulated data and validated on artificially excited structures in the lab. The use of these methods on structures in the field for OMA, where the features (a)–(c) from above apply, is the last step in this development and the main motivation for this thesis. In this context, techniques are developed that remove some of the bottlenecks for system identification for OMA.

Fault detection and isolation

Fault detection and isolation are fields in control engineering concerning the detection of abnormal conditions in systems and isolating the subsystem, where the fault occurs. Applied to vibration data of dynamic structures, this corresponds to *damage detection and localization* and is done by detecting changes in the vibration characteristics or in structural parameters of a structure. *Structural Health Monitoring (SHM)* with such methods allows to monitor for example civil infrastructure and helps to identify damages at an early stage.

Major incidents due to failures in civil infrastructure, transportation, industrial plants or other areas of human activity are a great risk. Sustainable development urges to better protect the built asset, while for example transportation infrastructures are steadily aging and traffic volume is increasing. Assessment and damage detection dictate the choice of maintenance policies for these infrastructures. Since maintenance is very costly, reliable and

sensitive early damage detection capabilities would pay off world-wide. Innumerable bridges have already exceeded their estimated service life and many of them approach this limit. In the United States the Federal Highway Administration counts 100 000 highly degraded bridges, which are so deteriorated that they should be closely monitored and inspected or repaired. Even without considering the possibility of natural catastrophes like earthquakes, which in some areas of the world constitute a major concern, the structural performance of bridges decreases progressively throughout their service life due to many deterioration processes (fatigue, carbonation, etc.).

SHM has become an important emerging field, in which non-intrusive damage detection techniques are used to monitor structures. As such, SHM technologies have a large commercial and economic potential. They can help to identify damages at an early stage, where relatively minor corrective actions can be taken at the structure before the deterioration or damage grows to a state where major actions are required. Another example for SHM applications is post-earthquake damage assessment. There, they could ensure prompt reoccupation of safe civil infrastructure and transport networks, which would mitigate the huge economic losses associated with major seismic events. Also, and equally important, monitoring the infrastructure that is approaching or exceeding their initial design life would assure their reliability and support economically sensible condition-based maintenance. In general, it is desirable to detect damage in an automated way without the need of visual inspections, which would require manpower and is difficult to realize in hazardous or remote environments. SHM systems also allow engineers to learn from previous designs to improve the performance of future structures.

Methods for fault detection and isolation have primarily originated in the field of control. They have promising properties and can detect already small changes in the eigenstructure of linear systems. However, for damage detection and localization in the Structural Health Monitoring context, vibration data is recorded in operation conditions and thus the features (a)–(c) from above apply. They motivate the adaption of existing fault detection techniques in this thesis to more realistic excitation assumptions. Moreover, numerical robustness and the fast computation of the damage indicators need to be assured for large structures under operation conditions.

Proposed methods

Subspace-based system identification methods have been shown efficient for the identification of linear multi-variable time-invariant systems from measured data under realistic excitation assumptions. There are methods that deal with input/output data as well as output-only data, where the unmeasured excitation is assumed as a stochastic process. For Operational Modal Analysis of vibrating structures, the eigenstructure (eigenvalues and eigenvectors) of the underlying linear system needs to be identified, from where *natural frequencies*, *damping ratios* and *mode shapes* can be computed. The consistency of many subspace methods for eigenstructure identification under non-stationary noise conditions has been shown, making them the preferred methods for OMA.

The following methods are developed in this thesis. They are based on subspace-based

system identification and fault detection, each motivated by a practical issue of OMA.

(1) **Modular subspace-based system identification from multi-setup measurements:** One problem in OMA is the eigenstructure identification of large structures as bridges or buildings. Often, only a limited number of sensors is available. In order to obtain detailed mode shape information despite the lack of sensor availability, it is common practice to perform multiple measurements, where some of the available sensors are fixed, while others are moved between different measurement setups. In each measurement setup, ambient vibration data is recorded. By fusing in some way the corresponding data, this allows to perform system identification as if there was a very large number of sensors, even in the range of a few hundreds or thousands. A possibly different (unmeasured) excitation between the different measurements has to be taken into account. Based on [MBBG02a, MBBG02b], a global merging approach is proposed, where in a first step the data from different setups is normalized and merged, before in a second step the global system identification is done. This approach is fully automated and suitable for all subspace methods. It is modular in the sense that the data of all setups is handled sequentially, and it can handle a huge number of setups and sensors without running into memory problems. Concerning its theoretical properties, non-stationary consistency and robustness to misspecified model order are proven, which validates the use of the merging approach for system identification on real structures. It is applied successfully to several civil structures.

(2) **Fast multi-order subspace-based system identification:** A general problem in eigenstructure identification in the OMA context is the discrimination of true physical modes of the system from spurious modes that appear in the identified models, e.g. due to colored noise, non-linearities, non-stationary excitation or the over-specification of the system order. On the other hand, the system order needs to be over-specified in order to retrieve all modes due to noise contaminated data. Based on the observation that physical modes remain quite constant when estimated at different over-specified model orders, while spurious modes vary, they can be distinguished using system identification results from different model orders. In so-called *stabilization diagrams*, where the obtained natural frequencies are plotted against the model order, the final model is chosen. However, this multi-order system identification is computationally quite expensive, especially for large structures with many sensors and high model orders. A fast computation scheme is proposed in this thesis, which can be applied to all subspace identification methods. It reduces the computation cost of the system identification step from $O(n_{\max}^4)$ to $O(n_{\max}^3)$, where $n_{\max}$ is the maximal assumed model order. For example, reductions of the computation time by factor 200 could be achieved.

(3) **Robust subspace-based fault detection under changing excitation:** With a statistical subspace-based fault detection test [BAB00], data from a possibly faulty state is compared to a model from the reference state using a χ^2-test statistics on a residual function and comparing it to a threshold. Thus, it can be decided if the eigenstructure of a system corresponding to newly acquired data still corresponds to the reference state or if it has deviated from the reference state, without actually identifying

the eigenstructure in the possibly faulty state. This corresponds to damage detection when using structural vibration data. In an OMA context, the ambient excitation is unmeasured and can change, e.g. due to different traffic, wind, earthquakes etc. However, a change in the excitation also influences the χ^2-test statistics and may lead to false alarms or no alarm in case of damage. A new fault detection test based on a residual that is robust to changes in the excitation is proposed.

(4) **Robust subspace-based damage localization using mass-normalized mode shapes:** A damage localization approach is based on the detection of changes in structural parameters [BMG04, BBM$^+$08] using a χ^2-test statistics. For this approach, sensitivities with respect to these structural parameters are required, which are usually obtained from a finite element model (FEM). In this thesis, a FE model-free approach is proposed, where the required sensitivities are obtained from OMA data using measurements where a known mass perturbation is introduced on the investigated structure. Furthermore, the mutual influence of structural parameters in the χ^2-tests is investigated and a rejection scheme is proposed. This yields more contrasted damage localization results between safe and damaged elements and therefore reduces false alarms.

These methods are derived in depth and important theoretical properties are proven. They are validated on structural vibration data from real structures, when data was available. Otherwise, simulated data was used for a proof of concept.

Outline of the thesis

This thesis is organized in four parts containing nine chapters. Part I contains preliminaries. Then, in Parts II and III methods for subspace-based system identification and fault detection, respectively, are developed. Finally, Part IV is devoted to applications.

Part I comprises Chapters 1–3. In Chapter 1, some contributions from the literature related to system identification and fault detection in general are presented. In Chapter 2, the background of subspace-based system identification and fault detection is explained in detail from the literature, as well as their application to structural vibration analysis. Chapter 3 contains the introduction and development of some numerical tools, which are needed throughout this work. Furthermore, some theoretical properties and practical issues concerning the subspace-based fault detection test are derived.

Part II is devoted to developments in subspace-based system identification. It comprises Chapters 4 and 5, where the methods under (1) and (2) from above are derived. Part III contains developments in subspace-based fault detection in Chapters 6 and 7, corresponding to the methods under (3) and (4) from above. These four chapters are as far as possible self-contained and constitute the main part of this thesis.

Part IV is the application part and comprises Chapters 8 and 9. In Chapter 8, the multi-setup subspace-based system identification from Chapter 4 is successfully applied to the modal analysis of several large scale civil structures. The vibration data of these structures was obtained through numerous collaborations, where comparative studies with other multi-setup

identification algorithms are made and discussed. Chapter 9 is devoted to damage detection and localization applications. The subspace-based damage detection and localization with their improvements from Chapters 3 and 7 are applied to real monitoring data of an artificially damaged bridge and to a large-scale simulated bridge deck.

The thesis concludes with an assessment of the developed methods and perspectives for future research.

Notation

Symbols

A^T	Transposed matrix of A
A^*	Transposed conjugated complex matrix of A
A^{-1}	Inverse of A
A^{-T}	Transposed inverse of A
$A^\dagger$	Pseudoinverse of A
$\stackrel{\text{def}}{=}$	Definition
i	Imaginary unit, $\mathrm{i}^2 = -1$
$\Re(a)$, $\Im(a)$	Real and imaginary part of variable a
$\overline{A}$, $\overline{a}$	Complex conjugate
$\ker A$	Kernel, right null space of A
$\operatorname{vec} A$	Column-wise vectorization of matrix A
$A \otimes B$	Kronecker product of matrices or vectors A and B
$\widehat{X}$	Estimate of variable X
$\mathbf{E}(X)$	Expected value of variable X
$\mathbf{E}_\theta(X(\mathcal{Y}))$	Expected value of variable X, where data $\mathcal{Y}$ corresponds to parameter θ
$\mathcal{N}(M, V)$	Normal distribution with mean M and (co-)variance V
$\mathbb{N}$, $\mathbb{R}$, $\mathbb{C}$	Set of natural, real, complex numbers
I_m	Identity matrix of size $m \times m$
$0_{m,n}$	Matrix of size $m \times n$ containing zeros
$O(\cdot)$, $o(\cdot)$	Landau notation

Variables

n	System order
r	Number of sensors
$r^{(\text{ref})}$, r_0	Number of reference sensors
A	State transition matrix
C	Observation matrix
X_k	System state at index k
Y_k	System output at index k
$\mathcal{H}$	Subspace matrix
$\mathcal{J}$	Jacobian matrix
$\mathcal{O}$	Observability matrix

$\mathcal{O}^{\uparrow}$, $\mathcal{O}^{\downarrow}$	Matrices, where the last resp. first block row (usually containing r rows) of $\mathcal{O}$ are deleted
Σ	Covariance matrix
$\mathcal{Y}$	Data matrix or vector
N	Number of samples
N_s	Number of setups

Abbreviations

DOF	Degree of freedom
FEM	Finite element model
OMA	Operational modal analysis
OMAX	Operational modal analysis with exogenous inputs
SHM	Structural health monitoring
SSI	Stochastic subspace identification
SVD	Singular value decomposition
UPC	Unweighted principal component algorithm (for data-driven SSI)

Further conventions

Theorems, propositions or lemmas, which are cited (literally or equivalently) from literature, contain their source directly after their numbering in brackets.

Part I

Preliminaries

Chapter 1

State of the art

1.1 Introduction

System identification and the detection of changes in the parameters of systems ("fault detection") are research areas that emerged in the 1960s. In this thesis, methods in the field of *subspace-based* system identification and fault detection are developed and applied to structural vibration analysis.

In this chapter, some contributions from the literature related to system identification and fault detection in general are presented.

1.2 System identification

In the field of system identification, mathematical models of dynamical systems are built from measured input/output data. It emerged in the 1960s in the control community. Some of the important contributions include Ho and Kalman's work on the state-space realization problem [HK66], Åström and Bohlin's work on maximum likelihood methods [AB65], Akaike's work on stochastic realization theory [Aka74c, Aka75], Ljung's prediction-error framework [Lju78, LC79] and many more. A reference book of system identification is [Lju99]. In [Gev06] a historical overview of the development of system identification is given.

For *linear time-invariant* system identification, the main model in use is the *state-space model*

$$\begin{cases} X_{k+1} &= AX_k + BU_k + V_k \\ Y_k &= CX_k + DU_k + W_k \end{cases}$$

with the states $X_k \in \mathbb{R}^n$, the observed inputs $U_k \in \mathbb{R}^m$, the outputs $Y_k \in \mathbb{R}^r$ and the unobserved input and output noise V_k and W_k. A problem in system identification is finding the system matrices A and C from the outputs Y_k as well as the inputs U_k, in case there

are observed inputs. If there are no observed inputs, purely stochastic identification methods are used. The state-space model can be represented by an equivalent *ARMAX model (autoregressive moving average with exogenous inputs)*

$$Y_k = \sum_{i=1}^{p} A_i Y_{k-i} + \sum_{i=0}^{q} B_i E_{k-i} + \sum_{i=0}^{s} C_i U_{k-i},$$

where E_k is the common noise source of the process and the measurement noise in the innovations form of the state space recurrence. A problem here is e.g. to identify the AR parameters A_i, which can be done with the *Instrumental Variables (IV)* method [SS81]. A link between the state-space and the ARMAX models was made for example in [Aka74b].

The subspace-based system identification algorithms for stochastic inputs emerged in the 1970s. Kung presented the Balanced Realization Algorithm in [Kun78]. In 1985, Benveniste and Fuchs [BF85] proved that the Balanced Realization method for linear system eigenstructure identification is consistent under (unmeasured) non-stationary excitation. Van Overschee and De Moor introduced their own formalism and popularized subspace methods in their *data-driven* form in [VODM96]. The Balanced Realization method using a block Hankel matrix of output correlations was also popularized as *covariance-driven* stochastic subspace identification by Peeters and De Roeck in [PDR99]. Since then, the family of subspace algorithms is growing in size and popularity [Lar83, VODM94, Ver94, Vib95], mostly for its capacity to deal with problems of large scale under realistic excitation assumptions. In [MAL96, VODMDS97, Pin02, CGPV06, Akç10], subspace algorithms for frequency response data are derived. In [BM07], many subspace algorithms from literature are put in a common framework and their consistency for eigenstructure identification under non-stationary noise conditions is proven.

The application of system identification to vibrating structures yielded a new research domain in structural engineering, known as modal analysis [Ewi84, POB+91, MS97, HLS98]. There, the identified model is the modal model consisting of eigenfrequencies, damping ratios and mode shapes. Often, the state-space model is used in connection with a system identification method to identify the modal model. The emerging need for reliable identification methods for the modal analysis of vibrating structures, where noise and large system orders of structures under realistic excitation have to be considered, gave another impulse in the development of system identification methods. *Experimental Modal Analysis (EMA)*, where only deterministic inputs are considered, moved to *Operational Modal Analysis (OMA)* and *Operational Modal Analysis with eXogenous inputs (OMAX)*, where stochastic inputs and combined stochastic-deterministic inputs are considered, respectively. See e.g. [RDR08].

Another implementation of the Balanced Realization Algorithm is the Eigensystem Realization Algorithm (ERA), which was introduced by Juang and Pappa [JP85]. Originally designed for modal analysis using impulse response functions, it was adapted to output-only measurements in [JICL95] and became known as *Natural Excitation Technique (NExT-ERA)*. The latter is closely related to covariance-driven subspace identification.

A method for the direct identification of modal parameters by a decomposition of the free response data is the *Ibrahim Time Domain (ITD)* method [IM76]. In the original formulation, it was assumed that twice the number of sensors equals the system order, where all the

modes are excited. The *Random Decrement (RD) technique* was introduced in [Col68] as a method to transfer the random response of a single degree of freedom (SDOF) system to the free decays of the SDOF system, from which the modal parameters are identified. It is a simple and fast estimation technique. In [Ibr77], the RD technique was extended to multiple measurements/multiple modes in combination with the ITD algorithm. However, results may be biased. A recent analysis can be found in [MMBF07].

The simplest approach to estimate modal parameters is the *Peak Picking* method, where the eigenvalues are identified as the peaks of a spectrum plot [BG63, BP93]. However, close modes cannot be distinguished and the accuracy is limited to the frequency resolution. The *Complex Mode Indicator Function (CMIF)* method for modal analysis using frequency response functions was introduced in [STAB88]. It is based on a singular value decomposition of the frequency response functions (FRF) at each spectral line. Then, a peak in the CMIF indicates the location on the frequency axis that is nearest to the eigenvalue within the accuracy of the frequency resolution. An additional second stage procedure is needed for scaled mode shapes and an accurate eigenvalue estimation. An output-only advancement is the *Frequency Domain Decomposition (FDD)* method [BVA01, BZA01], where the power spectral density (PSD) functions are used instead of FRFs. Close modes can be identified, but user interaction is required for identifying modes from the peaks in the singular values corresponding to the spectral lines.

A non-iterative maximum likelihood approach for frequency-domain identification is the *Least-Squares Complex Frequency-domain (LSCF)* method [GVV98, VdAGVV01]. The method fits a common-denominator transfer function model to measured FRFs in a least squares sense and is the frequency-domain counterpart to the *Least Squares Complex Exponential (LSCE)* algorithm [BAZM79]. It was extended to *polyreference LSCF*, also known as *PolyMAX*, by fitting a right matrix fraction model on the FRFs in [GVV$^+$03, PVdAGL04]. This results in more accurate modal models than LSCF in the multiple inputs case. These are fast and accurate methods and produce very clear stabilization diagrams, where, however, the damping ratios of the modes might be underestimated [CGV$^+$05]. These methods can also be applied to output-only data [GVC$^+$03]. An output-only modal analysis approach using transmissibilities under different loading conditions was developed in [DDSG10], where the unknown ambient excitation can be arbitrary as long as the modes of interest are excited.

For prediction error and maximum likelihood methods, the identified parameters are often the iterative solution of an optimization problem. A broad overview of *Prediction Error Methods (PEM)* is given in [Lju99]. These methods estimate a parameter vector of the system by minimizing the prediction error, where a predictor can be described as a filter that predicts the output of a dynamic system given old measured outputs and inputs. Under convenient conditions, estimates from PEM are consistent and statistically efficient, i.e. they have the smallest possible variance given by the Cramér-Rao bound. There is also a wide range of recursive PEM methods for the identification of time-varying systems. Maximum likelihood approaches in frequency domain are e.g. addressed in [PSV97, SPVG97, PS01, CGVP03]. The solution of underlying *least squares problems* is e.g. addressed in [GP96, MWVH$^+$05].

Identification methods, where errors or measurement noises on both measured inputs and outputs are taken into account, are called *Errors In Variables (EIV)* methods. A recent survey is given by Söderström in [Söd07]. These methods play an important role when the

purpose is the determination of the physical laws that describe a process, rather than the prediction of its future behavior.

In order to track the system parameters in time-varying systems, methods as the *Instrumental Variable Projection Approximation Subspace Tracking (IV-PAST)* [Gus98] can be used. These are recursive methods for subspace tracking with application to non-stationary environments. Another recursive method based on the ARMA model of signals and wavelet-transform-based algorithms for tracking modal parameters are presented in [Uhl05]. Bayesian state and parameter estimation of uncertain dynamical systems was done in [CBP06] using particle filters. This computationally expensive method is applicable to highly nonlinear models with non-Gaussian uncertainties. For instance, it can be used in structural health monitoring to detect changes of dynamical properties of structural systems during earthquakes and, more generally, it can be used for system identification to better understand the nonlinear behavior of structures subject to seismic loading [CBP06].

1.3 Fault detection and isolation

The problem of fault detection and isolation (FDI) consists in detecting changes in the parameters of a dynamical system (detection) and distinguishing the changed parameters from the unchanged parameters (isolation). There are many FDI techniques originating from control. An overview can be found, for example, in the survey papers [Wil76, Fra90] or in the books [PFC89, BN93]. In general, these FDI problems are split in two steps: generation of residuals, which are ideally close to zero under no-fault conditions, minimally sensitive to noises and disturbances, and maximally sensitive to faults; and residual evaluation, namely design of decision rules based on these residuals [Bas98]. Many of these FDI techniques are based on the state estimation and the evaluation of the innovation of a filter, or on the identification of model parameters or related physical parameters and their comparison.

With the asymptotic local approach to change detection and model validation introduced by Benveniste et al. [BBM87], a fault detection procedure is associated with any parameter identification algorithm. Like this, a statistical test for detecting changes in the system parameters can be derived, without the need to actually estimate the parameters in the possibly faulty system. This strategy is applied to subspace-based system identification by Basseville et al. in [BAB00] and forms the basis for the fault detection tests in the subsequent chapters.

In many applications, the FDI problem is to detect and diagnose changes in the eigenstructure of a linear dynamical system. An important example is structural vibration monitoring, which is also called *Structural Health Monitoring (SHM)*, where damages of civil, mechanical or aeronautical structures lead to a change in the eigenstructure of the underlying mechanical system and thus in the modal parameters. Vibration-based damage identification methods developed extensively in the last 30 years. Rytter [Ryt93] defined a classification of these methods into four levels:

1. Damage detection,

2. Damage localization,

3. Damage quantification,

4. Prediction of the remaining service life of the investigated structure.

In [FDN01], an introduction to vibration-based damage identification is given. An overview of damage identification methods can be found in [DFP98, CF04]. In [WFMP07], Worden et al. postulate axioms as basic principles of structural health monitoring. Amongst them are the necessity of a comparison between two system states for the assessment of damage, or the necessity of feature extraction through signal processing and statistical classification to convert sensor data into damage information.

Often, damage detection is done by estimating the modal parameters of a structure in a possibly damaged state and comparing them to a reference. Especially the natural frequencies are used, as they can be reliably identified. For example, Kullaa [Kul03] uses control charts to evaluate changes in the frequencies of Z24 Bridge that are linked to damage. Magalhães et al. [MaCC08] use the modal parameters for the monitoring of a long span arch bridge. In [MaCC10], they use control charts for an evaluation of the changes. Also, in the latter contribution the influence of environmental effects on the modal parameters of a structure is considered. Such effects as temperature variation or different loading are also shown in, e.g., [RBS$^+$00, PMDR01]. Worden et al. [WMF00, WSF02] use outlier analysis for damage detection. In [YKDBG05a, YKDBG05b], Yan et al. propose a damage detection method based on a novelty measure and the principal component analysis (PCA), where the effects of environmental changes are taken into account. In beam-like structures, damage was localized, and in connection with an analytical model also quantified, using sensitivities of PCA results in [VHG10].

Other methods compare data from the possibly damaged state to a model obtained in the reference state, without actually estimating the model parameters in the damaged states. The statistical fault detection based on the asymptotic local approach [BAB00] belongs to this category, as well as in the version of Yan and Golinval [YG06]. The temperature effect on these methods was considered in [FMG03, BBB$^+$08, BBMN09]. Note that the temperature effect will not be considered in this thesis. Damage localization based on the change detection of structural parameters is considered in [BMG04, BBM$^+$08].

Some damage detection and localization methods use a direct comparison of the mode shapes. Correlation coefficients between mode shapes, such as the *Modal Assurance Criterion (MAC)* or the *Coordinate Modal Assurance Criterion (COMAC)* are used as a damage damage indicator, when many measured coordinates of a structure are available. For example, West [Wes86] used the MAC for damage localization. Ren and De Roeck [RDR02a, RDR02b] used orthogonality condition sensitivities of the mode shapes in connection with a finite element model (FEM). They concluded that there are significant difficulties regarding noise, modeling and the numerical stability of mode shape methods for practical applications. The same holds for methods using the curvature of mode shapes, which were studied by Pandey et al. [PBS91]. Promising results were obtained in [AWDR99], although techniques for improving the quality of measured mode shapes are necessary and higher order mode shapes need to be examined carefully. Methods using changes in the modal strain energy, which is computed from the mode shapes, also belong in this category, see for example Kim and Stubbs

[KS95, KS02]. With these algorithms, results for damage localization and quantification were obtained on beam-like structures.

Another class of methods exploits changes in the flexibility matrix, which is the inverse of the stiffness matrix. Pandey and Biswas [PB94] have shown that changes in the flexibility matrix can indicate the presence and location of damage, where the flexibility matrix is estimated from modal parameters of only a few lower frequency modes. Yan and Golinval [YG05] consider both changes in the flexibility and the stiffness for damage localization, where mass-normalized mode shapes are needed. Bernal [Ber02, Ber06] makes use of *Damage Locating Vectors (DLV)* from the null space of the change in flexibility. Applying these vectors as loads leads to stress fields that are zero or small over the damaged region. In [Ber10] this approach is generalized to DLVs from the null space of the change in the transfer matrix, which are estimated from output-only identification results and constraints between the realization matrices. A closely related method was proposed by Reynders et al. [RDR10] in connection with a FEM.

Many methods use FEM updating in order to localize and quantify damage. In the reference state of the structure, the parameters of a FEM are adjusted to match modal parameters with measured data. As this is an inverse problem, several numerical issues arise. Moreover, user input is necessary in the updating process (choice of parameters, ...) and engineering judgments are key to the success of the updating procedure [CF04]. A very accurate model in the reference state is necessary to avoid false alarms when comparing to data from a possibly damaged state. In [FJK98], Fritzen et al. use sensitivity based algorithms to locate damage. Jaishi and Ren [JR06] use a modal flexibility residual in connection with FEM updating for damage localization. Reynders et al. [RTDR10] use OMAX data for FEM updating and compare the computed stiffness between the reference and damaged state.

Also, wavelet transforms can be used to analyze changes in signals. For example, Liew and Wang [LW98] used changes in wavelet coefficients for damage detection on a cracked beam. Several features can be extracted from wavelet coefficients that can be used for damage detection and an overview is given in [KM04]. Zabel [Zab05] successfully used energy components of wavelet decompositions of impulse response functions and of transmissibility functions for damage localization on Z24 Bridge.

Artificial neural networks are in general used for pattern recognition. Applications to vibration based damage detection can be found in [MH99, WZ01, GZ08]. They usually require a big database in the reference state to be trained and are computationally expensive. However, they can be applied in very general settings, where it is difficult to specify an explicit algorithm. Other methods that involve some optimization procedure are based on genetic algorithms and are applied to damage detection and localization in [OKC02, GS08].

Level 4 damage identification, the prediction of the remaining service life of a structure, is hardly possible without user input from an experienced engineer. It rather belongs to the fields of fatigue-life analysis or structural design assessment. Life-cycle models of bridges were for example built by Wenzel et al. [WVE10].

1.4 Conclusion

In this chapter, different strategies for system identification and damage detection were presented from literature. In the subsequent chapters, the subspace-based system identification as well as the statistical subspace damage detection based on the local approach and their application to structural vibration analysis are investigated. In Chapter 2, the background of these algorithms from existing literature is explained in detail, before enhancing and developing new methods in this field in Chapters 3–7 with applications in Chapters 8 and 9.

Chapter 2

Background of subspace-based system identification and fault detection

2.1 Introduction

In this chapter, the theoretical background of subspace-based system identification, fault detection and its application to structural vibration analysis is introduced from literature, on which the subsequent chapters are based.

This chapter is organized as follows. In Section 2.2, the general subspace identification algorithm is presented and examples of popular identification algorithms are given. In Section 2.3, the statistical fault detection is introduced in a very general setting and its subspace-based version is explained. For an application of both algorithms to problems in structural vibration analysis, the modeling and parameters of interest are detailed in Section 2.4.

2.2 Subspace-based system identification

2.2.1 Context

Stochastic subspace-based system identification methods are efficient tools for the identification of linear time-invariant systems (LTI), fitting a linear model to input/output or output-only measurements taken from a system. The excitation of the system is assumed to be noise with certain properties. In 1985, Benveniste and Fuchs [BF85] proved that the Instrumental Variable method and what was called the Balanced Realization method for linear system eigenstructure identification are consistent under (unmeasured) non-stationary excitation. This result was obtained before [VODM96] introduced their own formalism and

popularized subspace methods in their data-driven form. Since then, the family of subspace algorithms is growing in size and popularity [Lar83, VODM94, Ver94, Vib95, MAL96], mostly for its capacity to deal with problems of large scale under realistic excitation assumptions. In [BM07], many subspace algorithms from literature are put in a common framework and their non-stationary consistency for eigenstructure identification is proven.

Concerning the theoretical properties of subspace methods, there are a number of convergence studies in a stationary context in the literature, see [DPS95, BDS99, BL02, Pin02, CP04a, CP04b, Bau05] to mention just a few of them. These papers provide deep and technically difficult results including convergence rates. They typically address the problem of identifying the system matrices or the transfer matrix, i.e. both the pole and zero parts of the system.

There is a broad range of applications of subspace algorithms in the identification of processes in automatic control, see e.g. [BNSR98, JSL01, SPG03, PL08]. During the last decade, subspace methods found a special interest in mechanical, civil and aeronautical engineering for the identification of *vibration modes* (eigenvalues) and *mode shapes* (corresponding eigenvectors) of structures. Therefore, identifying an LTI from measurements is a fundamental part of vibration monitoring, see e.g. [HVdA99, MBG03, MBB$^+$06, BMCC10].

2.2.2 The general Stochastic Subspace Identification (SSI) algorithm

Consider linear multivariable time invariant systems described by a discrete time state space model

$$\left\{ \begin{array}{rcl} X_{k+1} & = & AX_k + BU_k + V_k \\ Y_k & = & CX_k + DU_k + W_k \end{array} \right. \tag{2.1}$$

with the state $X \in \mathbb{R}^n$, the observed input $U \in \mathbb{R}^m$, the output $Y \in \mathbb{R}^r$ and the unobserved input and output disturbances V and W. The matrices $A \in \mathbb{R}^{n\times n}$ and $C \in \mathbb{R}^{r\times n}$ are the state transition and observation matrices, respectively. The parameter n denotes the system order and r the number of observed outputs, which is usually the number of sensors.

Throughout this work, we are interested in identifying only the system matrices A and C. In many cases, e.g. in Operational Modal Analysis, no observed inputs are available ($B = 0$, $D = 0$) and identification is done using the output-only data (Y_k). When some inputs (U_k) are observed, combined deterministic-stochastic subspace identification algorithms can be used. There exist many Stochastic Subspace Identification algorithms in the literature, see e.g. [VODM96, PDR99, BM07] and the related references for an overview. They all fit in the following general framework for the identification of the system matrices A and C of system (2.1) and its eigenstructure.

Denote a matrix $\mathcal{H}_{p+1,q}$ as subspace matrix, whose estimate $\widehat{\mathcal{H}}_{p+1,q}$ is built from the output or input/output data of the system (2.1) according to a chosen subspace algorithm. The subspace matrix enjoys the factorization property

$$\mathcal{H}_{p+1,q} = W\mathcal{O}_{p+1}\mathcal{Z}_q \tag{2.2}$$

into the matrix of observability

$$\mathcal{O}_{p+1} \stackrel{\text{def}}{=} \begin{bmatrix} C \\ CA \\ \vdots \\ CA^p \end{bmatrix} \in \mathbb{R}^{(p+1)r \times n},$$

and a matrix $\mathcal{Z}_q$, with an invertible weighting matrix W depending on the selected subspace algorithm. However, W is the identity matrix for many subspace algorithms.

Note that a subset of the r sensors can be used for reducing the size of the matrices in the identification process, see e.g. [PDR99, RDR08]. These sensors are called projection channels or reference sensors. Let r_0 be the number of reference sensors ($r_0 \leq r$). The parameters p and q are chosen such that $pr \geq qr_0 \geq n$. The subspace matrix has $(p+1)r$ rows and in many cases qr_0 columns.

The observation matrix C is then found in the first block-row of the observability matrix $\mathcal{O}_{p+1}$. The state transition matrix A is obtained from the shift invariance property of $\mathcal{O}_{p+1}$, namely as the least squares solution of

$$\mathcal{O}_{p+1}^{\uparrow} A = \mathcal{O}_{p+1}^{\downarrow}, \text{ where } \mathcal{O}_{p+1}^{\uparrow} \stackrel{\text{def}}{=} \begin{bmatrix} C \\ CA \\ \vdots \\ CA^{p-1} \end{bmatrix}, \ \mathcal{O}_{p+1}^{\downarrow} \stackrel{\text{def}}{=} \begin{bmatrix} CA \\ CA^2 \\ \vdots \\ CA^p \end{bmatrix} \tag{2.3}$$

and $\mathcal{O}_{p+1}^{\uparrow}, \mathcal{O}_{p+1}^{\downarrow} \in \mathbb{R}^{pr \times n}$.

Let the pairs (λ, ϕ_λ) be the eigenvalues and eigenvectors of matrix A and define the mode shape φ_λ with

$$\det(A - \lambda I) = 0, \quad A\phi_\lambda = \lambda\phi_\lambda, \quad \varphi_\lambda = C\phi_\lambda. \tag{2.4}$$

Assume that the system has no multiple eigenvalues and, thus, that the λ's and φ_λ's are pairwise complex conjugate. In particular, 0 is not an eigenvalue of state transition matrix A. The collection of pairs $(\lambda, \varphi_\lambda)$ form a canonical parameterization (invariant w.r.t. changes in the state basis) of the pole part of system (2.1), which is referred to as the system eigenstructure.

The actual implementation of this generic subspace identification algorithm uses a consistent estimate $\widehat{\mathcal{H}}_{p+1,q}$ obtained from the output or input/output data according to the selected subspace identification algorithm. The SVD

$$\widehat{\mathcal{H}}_{p+1,q} = \begin{bmatrix} \widehat{U}_1 & \widehat{U}_0 \end{bmatrix} \begin{bmatrix} \widehat{\Delta}_1 & 0 \\ 0 & \widehat{\Delta}_0 \end{bmatrix} \begin{bmatrix} \widehat{V}_1^T \\ \widehat{V}_0^T \end{bmatrix} \tag{2.5}$$

and its truncation at the model order n yields an estimate

$$\widehat{\mathcal{O}}_{p+1} = \widehat{W}^{-1} \widehat{U}_1 \widehat{\Delta}_1^{1/2} \tag{2.6}$$

for the observability matrix, from which $(\widehat{C}, \widehat{A})$ and $(\widehat{\lambda}, \widehat{\varphi}_\lambda)$ are recovered as sketched above. Also, the estimate $\widehat{\mathcal{Z}}_q = \widehat{\Delta}_1^{1/2} \widehat{V}_1^T$ can be obtained. Note that the singular values in $\widehat{\Delta}_1$ are non-zero and $\widehat{\mathcal{O}}_{p+1}$ is of full column rank.

2.2.3 Examples of SSI algorithms

2.2.3.1 Two popular SSI algorithms

Two well-known output-only subspace identification algorithms are covariance-driven subspace identification [BF85] and the data-driven Unweighted Principal Component algorithm [VODM96]. Here, they are defined using a subset of the recorded sensors at some point in the computation, so-called *reference sensors* or *projection channels* [PDR99], in order to reduce the computation effort.

Let $N+p+q$ be the number of available samples and let $Y_k^{(\text{ref})} \in \mathbb{R}^{r_0}$ ($r_0 \leq r$) be the vector containing the reference sensor data, which is a subset of Y_k for all samples. Then, define the data matrices

$$\mathcal{Y}^+ \stackrel{\text{def}}{=} \frac{1}{\sqrt{N}} \begin{bmatrix} Y_{q+1} & Y_{q+2} & \vdots & Y_{N+q} \\ Y_{q+2} & Y_{q+3} & \vdots & Y_{N+q+1} \\ \vdots & \vdots & \vdots & \vdots \\ Y_{q+p+1} & Y_{q+p+2} & \vdots & Y_{N+p+q} \end{bmatrix}, \; \mathcal{Y}^- \stackrel{\text{def}}{=} \frac{1}{\sqrt{N}} \begin{bmatrix} Y_q^{(\text{ref})} & Y_{q+1}^{(\text{ref})} & \vdots & Y_{N+q-1}^{(\text{ref})} \\ Y_{q-1}^{(\text{ref})} & Y_q^{(\text{ref})} & \vdots & Y_{N+q-2}^{(\text{ref})} \\ \vdots & \vdots & \vdots & \vdots \\ Y_1^{(\text{ref})} & Y_2^{(\text{ref})} & \vdots & Y_N^{(\text{ref})} \end{bmatrix}. \tag{2.7}$$

For *covariance-driven* subspace identification, let $R_i \stackrel{\text{def}}{=} \mathbf{E}(Y_k Y_{k-i}^{(\text{ref})T})$ and the block Hankel matrix

$$\mathcal{H}_{p+1,q}^{\text{cov}} \stackrel{\text{def}}{=} \begin{bmatrix} R_0 & R_1 & \dots & R_{q-1} \\ R_1 & R_2 & \dots & R_q \\ \vdots & \vdots & \ddots & \vdots \\ R_p & R_{p+1} & \dots & R_{p+q-1} \end{bmatrix} \stackrel{\text{def}}{=} \text{Hank}(R_i) \tag{2.8}$$

be the theoretical output-correlation and subspace matrices for some parameters p and q. Then, introducing the cross-correlation between the state and the outputs $G \stackrel{\text{def}}{=} \mathbf{E}(X_k Y_k^{(\text{ref})T})$, the correlations R_i yield $R_i = CA^iG$. In factorization property (2.2) W is the identity matrix and

$$\mathcal{Z}_q = \mathcal{C}_q(A,G) \stackrel{\text{def}}{=} \begin{bmatrix} G & AG & \dots & A^{q-1}G \end{bmatrix} \tag{2.9}$$

is the well-known controllability matrix. From the output data (Y_k), the empirical correlations can be estimated from

$$\widehat{R}_i = \frac{1}{N-i} \sum_{k=i+1}^{N} Y_k Y_{k-i}^{(\text{ref})T}, \tag{2.10}$$

which are used to fill the estimate of the subspace matrix $\widehat{\mathcal{H}}_{p+1,q}^{\text{cov}} \stackrel{\text{def}}{=} \text{Hank}(\widehat{R}_i)$ as in (2.8). Another variant of this algorithm uses the subspace matrix

$$\widehat{\mathcal{H}}_{p+1,q}^{\text{covdat}} \stackrel{\text{def}}{=} \mathcal{Y}^+ \mathcal{Y}^{-T} \tag{2.11}$$

instead of $\widehat{\mathcal{H}}_{p+1,q}^{\text{cov}}$ [BM07].

For the *Unweighted Principal Component* (UPC) algorithm, the estimate of the subspace matrix is defined as

$$\widehat{\mathcal{H}}_{p+1,q}^{\mathrm{UPC}} \stackrel{\mathrm{def}}{=} \mathcal{Y}^{+}\mathcal{Y}^{-T}(\mathcal{Y}^{-}\mathcal{Y}^{-T})^{\dagger}\mathcal{Y}^{-}, \tag{2.12}$$

where † denotes the pseudoinverse. Then, factorization property (2.2) holds asymptotically for $N \to \infty$ where W is the identity matrix and $\mathcal{Z}$ the Kalman filter state matrix. A numerically efficient and stable way to obtain an estimate of the observability matrix avoids the explicit computation of $\widehat{\mathcal{H}}_{p+1,q}^{\mathrm{UPC}}$. Instead, the partitioning of the LQ decomposition of

$$\begin{bmatrix} \mathcal{Y}^{-} \\ \mathcal{Y}^{+} \end{bmatrix} = \begin{bmatrix} R_{11} & 0 \\ R_{21} & R_{22} \end{bmatrix} \begin{bmatrix} Q_1 \\ Q_2 \end{bmatrix} \tag{2.13}$$

is used, from which the relation $\widehat{\mathcal{H}}_{p+1,q}^{\mathrm{UPC}} = R_{21}Q_1$ follows. As Q_1 is an orthogonal matrix, the estimate of the observability matrix $\widehat{\mathcal{O}}_{p+1}$ can be obtained directly from R_{21} in the implementation of the algorithm. In this sense, the subspace matrix can also be defined by

$$\widehat{\mathcal{H}}_{p+1,q}^{\mathrm{UPC},R} \stackrel{\mathrm{def}}{=} R_{21},$$

where R_{21} is obtained from (2.13).

2.2.3.2 More SSI algorithms in a general framework

In this section, several SSI algorithms are presented using the general framework from [BM07]. This notation is only used in this section in this work and reference sensors are *not* taken into account for simplicity. The subspace matrix $\widehat{\mathcal{H}}_{p+1,q}$ takes the general form

$$\widehat{\mathcal{H}}_{p+1,q} \stackrel{\mathrm{def}}{=} \begin{bmatrix} \mathcal{R}_1 \\ \mathcal{R}_2 \\ \vdots \\ \mathcal{R}_{p+1} \end{bmatrix}, \tag{2.14}$$

where $\mathcal{R}_i$ depends on the subspace algorithm. Furthermore, define for two matrices L and M of compatible dimension

$$\begin{aligned} \langle L, M \rangle &\stackrel{\mathrm{def}}{=} LM^{T}, \\ \mathrm{E}(L \mid M) &\stackrel{\mathrm{def}}{=} \langle L, M \rangle \langle M, M \rangle^{\dagger} M, \\ \mathrm{E}\Big(L \mid M^{\perp}\Big) &\stackrel{\mathrm{def}}{=} L - \mathrm{E}(L \mid M)\,. \end{aligned}$$

For the observed outputs (Y_k) and inputs (U_k) define

$$\mathcal{Y}_i \stackrel{\mathrm{def}}{=} \frac{1}{\sqrt{N}} \begin{bmatrix} Y_i & Y_{i+1} & \dots & Y_{i+N-1} \end{bmatrix}, \quad \mathcal{U}_i \stackrel{\mathrm{def}}{=} \frac{1}{\sqrt{N}} \begin{bmatrix} U_i & U_{i+1} & \dots & U_{i+N-1} \end{bmatrix}$$

and

$$\mathcal{Y}_{i,p+1}^{+} \stackrel{\text{def}}{=} \begin{bmatrix} \mathcal{Y}_{i+1} \\ \mathcal{Y}_{i+2} \\ \vdots \\ \mathcal{Y}_{i+p+1} \end{bmatrix}, \quad \mathcal{Y}_{i,q}^{-} \stackrel{\text{def}}{=} \begin{bmatrix} \mathcal{Y}_{i} \\ \mathcal{Y}_{i-1} \\ \vdots \\ \mathcal{Y}_{i-q+1} \end{bmatrix}, \quad \mathcal{U}_{i,p+1}^{+} \stackrel{\text{def}}{=} \begin{bmatrix} \mathcal{U}_{i+1} \\ \mathcal{U}_{i+2} \\ \vdots \\ \mathcal{U}_{i+p+1} \end{bmatrix}, \quad \mathcal{U}_{i,q}^{-} \stackrel{\text{def}}{=} \begin{bmatrix} \mathcal{U}_{i} \\ \mathcal{U}_{i-1} \\ \vdots \\ \mathcal{U}_{i-q+1} \end{bmatrix}.$$

All subspace algorithms summarized in [BM07] can be segmented into two families, the algorithms based on covariances

$$\mathcal{R}_i \stackrel{\text{def}}{=} \langle \mathcal{Y}_i, Z_0 \rangle$$

and the data-driven algorithms computing some conditional expectation

$$\mathcal{R}_i \stackrel{\text{def}}{=} \mathrm{E}(\mathcal{Y}_i \mid Z_0)$$

with some Z_0 and the $\mathcal{R}_i$ plugged in (2.14). Both algorithms share the same formalism. They can be expressed in function of a single process Z_0, also called instrument, the choice of this instrument being the determining factor in the design of the algorithm.

Output-only algorithms

- *Output-only covariance-driven subspace algorithm* [BF85, POB+91], see also Equation (2.8)

$$\mathcal{R}_i = \begin{bmatrix} \hat{r}_i & \hat{r}_{i+1} & \cdots & \hat{r}_{i+q-1} \end{bmatrix} \quad \text{where} \quad \hat{r}_j = \langle \mathcal{Y}_j, \mathcal{Y}_0 \rangle$$

- *Basic output-only subspace algorithm* [BM07], see also Equation (2.11)

$$\widehat{\mathcal{H}}_{p+1,q} = \langle \mathcal{Y}_{0,p+1}^{+}, \mathcal{Y}_{0,q}^{-} \rangle$$

- *Output-only data-driven subspace algorithms* [VODM96], see also Equation (2.12)

$$\widehat{\mathcal{H}}_{p+1,q} = \mathrm{E}\Big(\mathcal{Y}_{0,p+1}^{+} \mid \mathcal{Y}_{0,q}^{-}\Big)$$

  In this form, it is called *Unweighted Principal Component (UPC)* in [VODM96]. Variants of this algorithm use the subspace matrix $W_1 \widehat{\mathcal{H}}_{p+1,q} W_2$ with different weightings W_1 and W_2:

  - *Principal Component (PC):* $W_1 = I$, $W_2 = \mathcal{Y}_{0,q}^{-T} \langle \mathcal{Y}_{0,q}^{-}, \mathcal{Y}_{0,q}^{-} \rangle^{-1/2} \mathcal{Y}_{0,q}^{-}$
  - *Canonical Variate Algorithm (CVA):* $W_1 = \langle \mathcal{Y}_{0,p+1}^{+}, \mathcal{Y}_{0,p+1}^{+} \rangle^{-1/2}$, $W_2 = I$

Input-Output algorithms (combined stochastic-deterministic)

- *Covariance-driven subspace algorithms using projected past input and output as instruments* [VWO97]. They encompass the methods also known as IV, CVA, PO-MOESP and N4SID in their covariance form [VWO97]. For example, the instrumental variables (IV) method is defined by
$$\widehat{\mathcal{H}}_{p+1,q} = \langle \mathcal{Y}^+_{0,p+1}, \mathcal{L}^-_{0,q} \rangle,$$
where $\mathcal{L}^-_{0,q}$ is obtained by stacking for $i = -q+1, \ldots, 0$
$$L_i \stackrel{\text{def}}{=} \mathrm{E}\Big(W_i \,\Big|\, \big(\mathcal{U}^+_{0,p+1}\big)^\perp \Big), \quad \text{where} \quad W_i \stackrel{\text{def}}{=} \begin{bmatrix} U_i \\ Y_i \end{bmatrix}$$

- *Covariance-driven subspace algorithm with projection on the orthogonal of the input* [GM03].
$$\mathcal{R}_i = \begin{bmatrix} \hat{r}_i & \hat{r}_{i+1} & \cdots & \hat{r}_{i+q-1} \end{bmatrix} \text{ where } \hat{r}_j = \langle \mathcal{Y}_j, \mathcal{Z}_0 \rangle \text{ and } \mathcal{Z}_0 \stackrel{\text{def}}{=} \mathrm{E}\left(\mathcal{Y}_0 \,\middle|\, \begin{bmatrix} \mathcal{U}^+_{0,p+1} \\ \mathcal{U}^-_{0,q} \end{bmatrix}^\perp \right) \tag{2.15}$$

- *Data-driven subspace algorithms with projection on the orthogonal of the input* [VODM96]. This algorithm is known as the projection algorithm in [VODM96, Ch. 2.3.2] and is computed from
$$\widehat{\mathcal{H}}_{p+1,q} = \mathrm{E}\Big(\mathcal{Y}^+_{0,p+1} \mid \mathcal{Z}^-_{0,q} \Big),$$
where $\mathcal{Z}^-_{0,q}$ is defined analogous to $\mathcal{Y}^-_{0,q}$ with corresponding $\mathcal{Z}_i$ is as in (2.15).

- *Data-driven algorithms using projected inputs as instruments* [Ver93, Ver94, CP04b]. This algorithm was proposed by [Ver93, Ver94] under the name of PI-MOESP and was revisited in [CP04a, CP04b]. It results from the computation of
$$\widehat{\mathcal{H}}_{p+1,q} = \mathrm{E}\Big(\mathcal{Y}^+_{0,p+1} \mid \mathcal{L}^-_{0,q} \Big)$$
where $\mathcal{L}^-_{0,q}$ is defined by
$$L_i \stackrel{\text{def}}{=} \mathrm{E}\Big(\mathcal{U}_i \,\Big|\, \big(\mathcal{U}^+_{0,p+1}\big)^\perp \Big), \text{ for } i = -q+1, \ldots, 0.$$

Remark 2.1 (Subspace algorithms using frequency domain data) *Many subspace methods derived for time domain data have a frequency domain counterpart. Then, as pointed out in [BM07], frequency domain methods behave like their time-domain counterparts. Let $L \in \mathbb{R}^{a,N}$ and $M \in \mathbb{R}^{b,N}$ be matrices of compatible dimension and $\boldsymbol{L} \in \mathbb{R}^{a,N}$ and $\boldsymbol{M} \in \mathbb{R}^{b,N}$ their Discrete Fourier Transform (DFT) with*
$$\boldsymbol{L} = L\boldsymbol{F}, \quad \boldsymbol{M} = M\boldsymbol{F},$$

where

$$\boldsymbol{F} \stackrel{\text{def}}{=} \frac{1}{\sqrt{N}} \begin{bmatrix} e^{-2\mathrm{i}\pi\frac{0}{N}} & \dots & e^{-2\mathrm{i}\pi\frac{0N}{N}} \\ e^{-2\mathrm{i}\pi\frac{1}{N}} & \dots & e^{-2\mathrm{i}\pi\frac{1N}{N}} \\ \vdots & \vdots & \vdots \\ e^{-2\mathrm{i}\pi\frac{N-1}{N}} & \dots & e^{-2\mathrm{i}\pi\frac{(N-1)N}{N}} \end{bmatrix}$$

is the unitary Fourier matrix. Extending the definitions of $\langle \cdot, \cdot \rangle$ *and* $\mathrm{E}(\cdot \mid \cdot)$ *to complex matrices leads to*

$$\langle \boldsymbol{L}, \boldsymbol{M} \rangle = \langle L, M \rangle, \quad \mathrm{E}(\boldsymbol{L} \mid \boldsymbol{M}) = \mathrm{E}(L \mid M)\, \boldsymbol{F}.$$

Thus, the column space defined by these matrices is the same, either in frequency or in time domain, leading to the same system identification results. Frequency-domain subspace methods are detailed for example in [MAL96, VODMDS97, Pin02, CGPV06, Akç10].

2.3 Statistical subspace-based fault detection

2.3.1 Context

The considered fault detection techniques are built on an asymptotically Gaussian residual function that compares a reference model with data. They date back to Benveniste et al. 1987 [BBM87] and are based on Le Cam's local approach [LC56]. A residual function associated to subspace methods was proposed in [BAB00], on which this work is based. A summary of the local approach to change detection is found in [BBGM06].

With these methods, a χ^2-test is performed on a residual function and compared to a threshold. Like this, it can be decided if the system is still in the reference state or if the system parameters have changed. The system parameterization is only needed in the reference state, while the residual function is computed directly from the data without the need of knowing the system parameters in the tested state. An entirely non-parametric version of the χ^2-test was proposed in [BBB$^+$08].

The subspace-based fault detection test finds especially application in vibration monitoring for the detection of structural damages (see also Section 2.4). It is extended to damage localization in [BMG04, BBM$^+$08] by detecting changes of structural parameters. As structures are influenced by environmental conditions, especially temperature changes, the respective damage detection tests are also sensitive to these changes. Tests that are robust to these changes are proposed in [BBB$^+$08, BBMN09, BBM$^+$10]. There are many applications of the subspace-based fault detection tests, see e.g. [MHVdA99, MGB03, MBG03, BBM$^+$08, FK09, ZWM10].

2.3.2 The residual function and its statistical evaluation

Consider the model parameter θ of a system and its reference value θ_0, which is for instance identified from data from the reference system. In this section, the model parameter is considered as a very general parameter, but it can already be viewed as a vector containing a canonical parameterization (eigenvalues, mode shapes) of a state-space system.

Consider a new data sample $\mathcal{Y}_{k,p+1,q}^T = (Y_{k+p+1}^T, \ldots, Y_{k+1}^T, Y_k^T, \ldots, Y_{k-q+1}^T)$, $k = 1, \ldots, N$, of size N. The detection problem is to decide whether the new data – corresponding to some parameter θ – are still well described by parameter θ_0 or not. A primary residual function $\mathcal{K}(\theta', \mathcal{Y})$ is introduced and some functions are derived that originate from this primary residual. They share the common notation:

- For functions of two variables, the first variable corresponds to the model and the second to the data.
- Model parameter θ_0 corresponds to a reference state, θ to an unknown state. Often, data corresponding to θ is confronted to the model defined by θ_0.
- When computing derivatives or expected values with respect to data, the first and second variable of these functions are denoted by θ' and θ'' to be unambiguous. At the end, θ_0 or θ are plugged in.

2.3.2.1 Primary residual

The fundamental idea of the detection algorithm is to associate the model parameter θ_0 with a vector-valued differentiable primary residual function $\mathcal{K}(\theta', \mathcal{Y})$, where the data $\mathcal{Y}$ are an implicit function of parameter θ'', and $\dim \mathcal{K} \geq \dim \theta$. This primary residual is constructed to satisfy the property [Bas98]

$$\mathbf{E}_\theta \left(\mathcal{K}(\theta_0, \mathcal{Y}) \right) = 0 \quad \text{iff} \quad \theta = \theta_0, \tag{2.16}$$

where $\mathbf{E}_\theta$ is the expectation when the data $\mathcal{Y}$ correspond to the model parameter $\theta'' = \theta$. Its mean deviation with respect to the first variable is defined as

$$\mathcal{J}^{(1)}(\theta_0, \theta) \stackrel{\text{def}}{=} -\frac{\partial}{\partial \theta'} \mathbf{E}_{\theta''} \mathcal{K}\left(\theta', \mathcal{Y}\right) \Big|_{\theta' = \theta_0, \theta'' = \theta}. \tag{2.17}$$

With respect to the second variable, the mean deviation is defined as

$$\mathcal{J}^{(2)}(\theta_0, \theta) \stackrel{\text{def}}{=} \frac{\partial}{\partial \theta''} \mathbf{E}_{\theta''} \mathcal{K}\left(\theta', \mathcal{Y}\right) \Big|_{\theta' = \theta_0, \theta'' = \theta}. \tag{2.18}$$

Both matrices $\mathcal{J}^{(1)}(\theta_0, \theta)$ and $\mathcal{J}^{(2)}(\theta_0, \theta)$ can be viewed as Jacobian matrices. Because of (2.16), both expressions are equivalent for $\theta = \theta_0$ and the notation is simplified to

$$\mathcal{J}(\theta_0) \stackrel{\text{def}}{=} \mathcal{J}^{(1)}(\theta_0, \theta_0) = \mathcal{J}^{(2)}(\theta_0, \theta_0). \tag{2.19}$$

The primary residual is linked to an estimation function [DB97, BBM87], as the model parameter θ can theoretically be estimated from

$$\hat{\theta} = \arg_{\theta''} \left\{ \sum_{k=1}^{N} \mathcal{K}(\theta_0, \mathcal{Y}_{k,p+1,q}) = 0 \right\}.$$

2.3.2.2 Local approach to change detection

For a statistical evaluation of the residual its probability distribution is required, which is generally unknown for the function $\mathcal{K}$. A solution to this problem is provided by Le Cam [LC56] with the concept of local asymptotic normality to compare statistical distributions by (an infinite number of) observations under close hypotheses. With this concept, the statistical local approach to change detection was developed [BBM87, BMP90, ZBB94, Bas98], which is summarized now.

Assume the close hypotheses

$$\begin{cases} \mathbf{H}_0 : \ \theta = \theta_0 \\ \mathbf{H}_1 : \ \theta = \theta_0 + \delta\theta/\sqrt{N} \end{cases} \tag{2.20}$$

where vector $\delta\theta$ is unknown but fixed. Note that for large N, hypotheses $\mathbf{H}_1$ corresponds to small deviations in θ. From the primary residual function $\mathcal{K}$, define the residual function

$$\zeta_N(\theta_0, \theta) \stackrel{\text{def}}{=} \frac{1}{\sqrt{N}} \sum_{k=1}^{N} \mathcal{K}(\theta_0, \mathcal{Y}_{k,p+1,q}),$$

where the data $\mathcal{Y}$ corresponds to parameter θ. Define the residual covariance

$$\Sigma_N(\theta_0, \theta) \stackrel{\text{def}}{=} \mathbf{E}_\theta \left((\zeta_N(\theta_0, \theta) - \mathbf{E}_\theta \zeta_N(\theta_0, \theta)) \, (\zeta_N(\theta_0, \theta) - \mathbf{E}_\theta \zeta_N(\theta_0, \theta))^T \right), \tag{2.21}$$

and its limit

$$\Sigma(\theta_0) \stackrel{\text{def}}{=} \lim_{N\to\infty} \Sigma_N(\theta_0, \theta). \tag{2.22}$$

Note that it also holds

$$\Sigma(\theta_0) = \lim_{N\to\infty} \Sigma_N(\theta_0, \theta_0) = \lim_{N\to\infty} \mathbf{E}_{\theta_0}(\zeta_N(\theta_0, \theta_0) \, \zeta_N(\theta_0, \theta_0)^T) \tag{2.23}$$

as $\theta \to \theta_0$ for $N \to \infty$ under the assumption of close hypotheses.

Analogously to (2.17) and (2.18), define the Jacobians of the residual function as

$$\mathcal{J}_N^{(1)}(\theta_0, \theta) \stackrel{\text{def}}{=} -\frac{1}{\sqrt{N}} \frac{\partial}{\partial \theta'} \mathbf{E}_{\theta''} \zeta_N(\theta', \theta'') \Big|_{\theta'=\theta_0, \theta''=\theta}, \tag{2.24}$$

$$\mathcal{J}_N^{(2)}(\theta_0, \theta) \stackrel{\text{def}}{=} \frac{1}{\sqrt{N}} \frac{\partial}{\partial \theta''} \mathbf{E}_{\theta''} \zeta_N(\theta', \theta'') \Big|_{\theta'=\theta_0, \theta''=\theta}. \tag{2.25}$$

With (2.17)–(2.19) follows

$$\mathcal{J}^{(1)}(\theta_0, \theta) = \lim_{N\to\infty} \mathcal{J}_N^{(1)}(\theta_0, \theta), \quad \mathcal{J}^{(2)}(\theta_0, \theta) = \lim_{N\to\infty} \mathcal{J}_N^{(2)}(\theta_0, \theta) \tag{2.26}$$

as well as

$$\mathcal{J}(\theta_0) = \lim_{N\to\infty} \mathcal{J}_N^{(1)}(\theta_0, \theta) = \lim_{N\to\infty} \mathcal{J}_N^{(1)}(\theta_0, \theta_0) \tag{2.27}$$

$$= \lim_{N\to\infty} \mathcal{J}_N^{(2)}(\theta_0, \theta) = \lim_{N\to\infty} \mathcal{J}_N^{(2)}(\theta_0, \theta_0) \tag{2.28}$$

under the assumption of close hypotheses.

Under hypothesis $\mathbf{H}_1$, a small change in parameter θ, the expected value of the residual function with respect to data corresponding to (the unknown) parameter θ can be approximated by its Taylor expansion of first order, where $(\theta - \theta_0)$ is replaced by $\delta\theta/\sqrt{N}$. This Taylor expansion can be made with respect to the first or with respect to the second variable of $\zeta_N(\theta_0, \theta)$. In the first case, it holds

$$\begin{aligned}\mathbf{E}_\theta \zeta_N(\theta_0, \theta) &\approx \mathbf{E}_\theta \zeta_N(\theta, \theta) + \frac{\partial}{\partial \theta'} \mathbf{E}_\theta \zeta_N(\theta', \theta)\Big|_{\theta'=\theta} (\theta_0 - \theta) \\ &= -\frac{1}{\sqrt{N}} \frac{\partial}{\partial \theta'} \mathbf{E}_\theta \zeta_N(\theta', \theta)\Big|_{\theta'=\theta} \delta\theta \\ &= \mathcal{J}_N^{(1)}(\theta, \theta)\delta\theta, \end{aligned} \tag{2.29}$$

as $\mathbf{E}_\theta \zeta_N(\theta, \theta) = 0$ and using (2.24). In the second case, it holds

$$\begin{aligned}\mathbf{E}_\theta \zeta_N(\theta_0, \theta) &\approx \mathbf{E}_{\theta_0} \zeta_N(\theta_0, \theta_0) + \frac{\partial}{\partial \theta''} \mathbf{E}_{\theta''} \zeta_N(\theta_0, \theta'')\Big|_{\theta''=\theta_0} (\theta - \theta_0) \\ &= \frac{1}{\sqrt{N}} \frac{\partial}{\partial \theta''} \mathbf{E}_{\theta''} \zeta_N(\theta_0, \theta'')\Big|_{\theta''=\theta_0} \delta\theta \\ &= \mathcal{J}_N^{(2)}(\theta_0, \theta_0)\delta\theta, \end{aligned} \tag{2.30}$$

as $\mathbf{E}_{\theta_0} \zeta_N(\theta_0, \theta_0) = 0$ and using (2.25). Thus, in both cases the mean of the residual function asymptotically writes as $\mathcal{J}(\theta_0)\,\delta\theta$ under the assumption of close hypotheses.

The residual function $\zeta_N(\theta_0, \theta)$ is asymptotically Gaussian for a large class of primary residuals $\mathcal{K}$ and and the following Central Limit Theorem holds.

Theorem 2.2 *Provided that $\Sigma(\theta_0)$ is positive definite, the residual $\zeta_N(\theta_0, \theta)$ is asymptotically Gaussian distributed under both hypotheses $\mathbf{H}_0$ and $\mathbf{H}_1$ defined in* (2.20) *and it holds*

$$\zeta_N(\theta_0, \theta) \xrightarrow{N} \begin{cases} \mathcal{N}(0, \Sigma(\theta_0)) & \text{under } \mathbf{H}_0 \\ \mathcal{N}(\mathcal{J}(\theta_0)\,\delta\theta, \Sigma(\theta_0)) & \text{under } \mathbf{H}_1 \end{cases}$$

Hence, a change in the model parameter θ corresponds to a change of the mean of the asymptotically Gaussian distributed residual $\zeta_N(\theta_0, \theta)$.

For simplicity of notation, we will use $\zeta_N(\theta_0)$ instead of $\zeta_N(\theta_0, \theta)$ in the following, while still assuming that the data $\mathcal{Y}$ in the residual function corresponds to parameter θ.

2.3.2.3 Generalized likelihood ratio test

The generalized likelihood ratio test is a statistical test for making a decision between two hypotheses, where one hypothesis (the null hypothesis) is a special case of the other one. Consider the probability density functions p_{θ_0}, p_θ of a Gaussian random variable Z of dimension

d with mean $\mathcal{J}\delta\theta$ and covariance Σ under the hypotheses

$$\begin{cases} \mathbf{H}_0 : \delta\theta = 0 \\ \mathbf{H}_1 : \delta\theta \neq 0 \end{cases}$$

The probability density function p_θ writes as

$$p_\theta(Z) = (2\pi)^{-\frac{d}{2}} (\det(\Sigma))^{-\frac{1}{2}} \exp\left\{ -\frac{1}{2} (Z - \mathcal{J}\delta\theta)^T \Sigma^{-1} (Z - \mathcal{J}\delta\theta) \right\}$$

and the generalized log-likelihood ratio writes as

$$\begin{aligned} \Upsilon(Z) &= -2 \log \frac{p_{\theta_0}(Z)}{\sup_{\theta \in \mathbf{H}_1} p_\theta(Z)} \\ &= Z^T \Sigma^{-1} Z + \sup_{\theta \in \mathbf{H}_1} \left(-(Z - \mathcal{J}\delta\theta)^T \Sigma^{-1} (Z - \mathcal{J}\delta\theta) \right) \\ &= \sup_{\theta \in \mathbf{H}_1} \left(2\delta\theta^T \mathcal{J}^T \Sigma^{-1} Z - \delta\theta^T \mathcal{J}^T \Sigma^{-1} \mathcal{J}\delta\theta \right). \end{aligned}$$

The supremum is reached at $\delta\theta^\star = (\mathcal{J}^T \Sigma^{-1} \mathcal{J})^{-1} \mathcal{J}^T \Sigma^{-1} Z$ and it follows

$$\Upsilon(Z) = Z^T \Sigma^{-1} \mathcal{J} (\mathcal{J}^T \Sigma^{-1} \mathcal{J})^{-1} \mathcal{J}^T \Sigma^{-1} Z.$$

Consider now the asymptotically Gaussian random variable $\zeta_N(\theta_0)$ and let $\widehat{\mathcal{J}}$ and $\widehat{\Sigma}$ be consistent estimates of its sensitivity (2.24) and covariance (2.22) computed from the reference model θ_0. Then, the variable

$$\chi^2_N(\theta_0) \stackrel{\text{def}}{=} \Upsilon\left(\zeta_N(\theta_0)\right) = \zeta_N(\theta_0)^T \widehat{\Sigma}^{-1} \widehat{\mathcal{J}} (\widehat{\mathcal{J}}^T \widehat{\Sigma}^{-1} \widehat{\mathcal{J}})^{-1} \widehat{\mathcal{J}}^T \widehat{\Sigma}^{-1} \zeta_N(\theta_0)$$

is asymptotically χ^2 distributed [LC86] with $\text{rank}(\widehat{\mathcal{J}}) = \dim(\theta_0)$ degrees of freedom, if $\widehat{\mathcal{J}}$ is full column rank, and the non-centrality parameter $\delta\theta^T \widehat{\mathcal{J}}^T \widehat{\Sigma}^{-1} \widehat{\mathcal{J}}\ \delta\theta$ under $\mathbf{H}_1$.

The decision between the hypotheses $\mathbf{H}_0$ and $\mathbf{H}_1$ is hence determined by the comparison of $\chi^2_N(\theta_0)$ to a threshold γ:

$$\begin{cases} \mathbf{H}_0 : \theta = \theta_0 & \text{if } \chi^2_N(\theta_0) < \gamma \\ \mathbf{H}_1 : \theta = \theta_0 + \delta\theta/\sqrt{N} & \text{if } \chi^2_N(\theta_0) \geq \gamma \end{cases}$$

2.3.3 Covariance-driven subspace-based residual and associated fault detection test

A residual function associated to covariance-driven subspace identification and the respective fault detection test were derived by Basseville et al. [BAB00], which is summarized in this section. The theoretical foundations of this algorithm are explained in the previous section.

2.3.3.1 Definition of residual and χ^2-test

The model parameter $\theta \in \mathbb{C}^{(r+1)n}$ consists in the canonical parameterization of state-space model (2.1) by the system eigenstructure

$$\theta \stackrel{\text{def}}{=} \begin{bmatrix} \Lambda \\ \operatorname{vec} \Phi \end{bmatrix}, \quad \text{where} \quad \Lambda \stackrel{\text{def}}{=} \begin{bmatrix} \lambda_1 \\ \vdots \\ \lambda_n \end{bmatrix}, \quad \Phi \stackrel{\text{def}}{=} \begin{bmatrix} \varphi_1 & \dots & \varphi_n \end{bmatrix} \tag{2.31}$$

with the eigenvalues $\lambda_1, \dots, \lambda_n$ and respective mode shapes $\varphi_1, \dots, \varphi_n$ of system (2.1), cf. (2.4).

The characterization of the model parameter θ by the estimation function (primary residual) $\mathcal{K}(\theta, \mathcal{Y})$ is based on the factorization $\mathcal{H}_{p+1,q} = \mathcal{O}_{p+1}\mathcal{Z}_q$ of the covariance-driven subspace matrix (2.8), where $\mathcal{H}_{p+1,q} \in \mathbb{R}^{(p+1)r \times qr_0}$. Write the observability matrix in the modal basis

$$\mathcal{O}_{p+1}(\theta) = \begin{bmatrix} \Phi \\ \Phi\Delta \\ \vdots \\ \Phi\Delta^p \end{bmatrix} \in \mathbb{C}^{(p+1)r \times n}, \tag{2.32}$$

with the diagonal matrix $\Delta \stackrel{\text{def}}{=} \operatorname{diag}(\Lambda)$. Note that $A = \Psi^{-1}\Delta\Psi$, where the columns of Ψ are the eigenvectors of A, and $\Phi = C\Psi$.

The following property characterizes whether a model parameter θ_0 agrees with a subspace matrix $\mathcal{H}_{p+1,q}$:

$$\mathcal{O}_{p+1}(\theta_0) \text{ and } \mathcal{H}_{p+1,q} \text{ have the same left null space } S.$$

From a model parameter θ_0, the parametric observability matrix $\mathcal{O}_{p+1}(\theta)$ can be computed. The left null space $S \in \mathbb{R}^{(p+1)r \times s}$ can be obtained from an SVD of $\mathcal{O}_{p+1}(\theta)$ and it holds

$$S^T S = I_s \tag{2.33}$$

$$S^T \mathcal{O}_{p+1}(\theta_0) = 0, \tag{2.34}$$

where $s = (p+1)r - n$ and n is the system order. Because the left null space S implicitly depends on θ_0, it is denoted by $S(\theta_0)$, although it is not unique as $S(\theta_0)W$ with an orthonormal matrix W is also a left null space. However, the particular choice of matrix W is not important, as will be seen in Section 2.3.3.5.

Hence, the characteristic property of the subspace matrix containing data in the reference state $\theta = \theta_0$ writes as

$$S(\theta_0)^T \mathcal{H}_{p+1,q} = 0.$$

To link this result with condition (2.16) for a primary residual $\mathcal{K}$, the covariance-driven subspace matrix is written as

$$\mathcal{H}_{p+1,q} = \mathbf{E}\left(\widetilde{\mathcal{Y}}^+_{k,p+1}\widetilde{\mathcal{Y}}^{-T}_{k,q}\right), \quad (\forall k), \tag{2.35}$$

where

$$\widetilde{\mathcal{Y}}^{+}_{k,p+1} \overset{\text{def}}{=} \begin{bmatrix} Y_k \\ \vdots \\ Y_{k+p} \end{bmatrix} \in \mathbb{R}^{(p+1)r}, \quad \widetilde{\mathcal{Y}}^{-}_{k,q} \overset{\text{def}}{=} \begin{bmatrix} Y^{(\text{ref})}_k \\ \vdots \\ Y^{(\text{ref})}_{k-q+1} \end{bmatrix} \in \mathbb{R}^{qr_0}.$$

With $Z(\mathcal{Y}_k) = \widetilde{\mathcal{Y}}^{+}_{k,p+1}\widetilde{\mathcal{Y}}^{-T}_{k,q}$ the primary residual $\mathcal{K}(\theta_0, \mathcal{Y}_k) \in \mathbb{R}^{sqr_0}$ is defined as [BAB00]

$$\mathcal{K}(\theta_0, \mathcal{Y}_k) \overset{\text{def}}{=} \text{vec}\left(S(\theta_0)^T Z(\mathcal{Y}_k)\right). \tag{2.36}$$

Then, the estimate of the covariance-driven subspace matrix writes as

$$\widehat{\mathcal{H}}_{p+1,q} = \frac{1}{N}\sum_{k=1}^{N} Z(\mathcal{Y}_k) \tag{2.37}$$

and the subspace-based residual function $\zeta_N(\theta_0) \in \mathbb{R}^{sqr_0}$ is defined as

$$\zeta_N(\theta_0) \overset{\text{def}}{=} \frac{1}{\sqrt{N}}\sum_{k=1}^{N} \mathcal{K}(\theta_0, \mathcal{Y}_k) = \sqrt{N}\,\text{vec}\left(S(\theta_0)^T \widehat{\mathcal{H}}_{p+1,q}\right). \tag{2.38}$$

Note that for consistency of notation to [BAB97, BAB00, BMG04], the subspace-based residual function is denoted as $\zeta_N(\theta_0)$ instead of $\zeta_N(\theta_0, \theta)$ and the dependence on parameter θ, to which the data in $\widehat{\mathcal{H}}_{p+1,q}$ correspond, is implicit. The main properties of $\zeta_N(\theta_0)$ are summarized in the following theorem, based on Sections 2.3.2.2 and 2.3.2.3.

Theorem 2.3 ([BAB00]) *Assume the close hypotheses*

$$\begin{cases} \mathbf{H}_0: \ \theta = \theta_0 \\ \mathbf{H}_1: \ \theta = \theta_0 + \delta\theta/\sqrt{N} \end{cases}$$

where vector $\delta\theta \in \mathbb{C}^{(r+1)n}$ is unknown but fixed. Then, the residual function $\zeta_N(\theta_0)$ in (2.38) *is asymptotically Gaussian distributed under both hypotheses $\mathbf{H}_0$ and $\mathbf{H}_1$ and it holds*

$$\zeta_N(\theta_0) \xrightarrow{N} \begin{cases} \mathcal{N}\left(0, \Sigma(\theta_0)\right) & \text{under } \mathbf{H}_0 \\ \mathcal{N}\left(\mathcal{J}(\theta_0)\,\delta\theta, \Sigma(\theta_0)\right) & \text{under } \mathbf{H}_1 \end{cases}$$

where $\mathcal{J}(\theta_0) \in \mathbb{C}^{sqr_0 \times (r+1)n}$ and $\Sigma(\theta_0) \in \mathbb{R}^{sqr_0 \times sqr_0}$ are the sensitivity and covariance of the residual function. Hypothesis $\mathbf{H}_0$ can be tested against $\mathbf{H}_1$ by comparing the variable

$$\chi^2_N(\theta_0) = \zeta_N(\theta_0)^T \widehat{\Sigma}^{-1}\widehat{\mathcal{J}}(\widehat{\mathcal{J}}^T\widehat{\Sigma}^{-1}\widehat{\mathcal{J}})^{-1}\widehat{\mathcal{J}}^T\widehat{\Sigma}^{-1}\zeta_N(\theta_0) \tag{2.39}$$

with a threshold, where $\widehat{\mathcal{J}}$ and $\widehat{\Sigma}$ are consistent estimates of $\mathcal{J}(\theta_0)$ and $\Sigma(\theta_0)$. The variable $\chi^2_N(\theta_0)$ is asymptotically χ^2 distributed with $\text{rank}(\widehat{\mathcal{J}}) = \dim(\theta_0) = (r+1)n$ *degrees of freedom, if $\widehat{\mathcal{J}}$ is full column rank, and the non-centrality parameter $\delta\theta^T\widehat{\mathcal{J}}^T\widehat{\Sigma}^{-1}\widehat{\mathcal{J}}\ \delta\theta$ under $\mathbf{H}_1$.*

To evaluate the χ^2-test statistics (2.39), estimates $\widehat{\mathcal{J}}$ and $\widehat{\Sigma}$ of the residual's asymptotic sensitivity and covariance $\mathcal{J}(\theta_0)$ and $\Sigma(\theta_0)$ are needed. Note that neither the residual's sensitivity $\mathcal{J}^{(1)}_N(\theta_0, \theta)$ or $\mathcal{J}^{(2)}_N(\theta_0, \theta)$, nor its covariance $\Sigma_N(\theta_0, \theta)$ are considered here, as they converge to $\mathcal{J}(\theta_0)$ and $\Sigma(\theta_0)$, respectively (cf. Equations (2.21)–(2.30)). Thus, they can be computed in the reference state θ_0 and are detailed in the following sections.

2.3.3.2 Complex-valued Jacobian computation

The system parameter θ was defined in (2.31) and contains the eigenstructure of a system, which consists of m pairs of conjugated complex eigenvalues and mode shapes in many applications, with the system order being $n = 2m$. In this section, the general complex-valued computation of $\mathcal{J}(\theta_0)$ is introduced, while in Section 2.3.3.3 an equivalent real-valued computation for pairs of complex modes is stated.

First, the derivative of the parametric observability matrix (2.32) is introduced from [BAB00, BMG04], as the Jacobian $\mathcal{J}(\theta_0)$ will depend on it. Define

$$\Lambda_i^{(p)} \stackrel{\text{def}}{=} \begin{bmatrix} 1 & \lambda_i & \lambda_i^2 & \dots & \lambda_i^p \end{bmatrix}^T, \quad \Lambda_i'^{(p)} \stackrel{\text{def}}{=} \begin{bmatrix} 0 & 1 & 2\lambda_i & \dots & p\lambda_i^{p-1} \end{bmatrix}^T$$

for $1 \leq i \leq n$. Then the derivative of the observability matrix writes

$$\mathcal{O}'_{p+1}(\theta_0) \stackrel{\text{def}}{=} \left.\frac{\partial \operatorname{vec}\mathcal{O}_{p+1}(\theta)}{\partial\theta}\right|_{\theta=\theta_0} = \left[\begin{array}{ccc|ccc} \Lambda_1'^{(p)} \otimes \varphi_1 & & 0 & \Lambda_1^{(p)} \otimes I_r & & 0 \\ & \ddots & & & \ddots & \\ 0 & & \Lambda_n'^{(p)} \otimes \varphi_n & 0 & & \Lambda_n^{(p)} \otimes I_r \end{array}\right], \tag{2.40}$$

where $\mathcal{O}'_{p+1}(\theta_0) \in \mathbb{C}^{(p+1)rn\times(r+1)n}$.

According to Equations (2.24) and (2.25), the computation of the residual's Jacobian $\mathcal{J}(\theta_0)$ can be derived in two different ways [BAB00].

First computation In (2.24), the residual function is derived with respect to the first variable. Assume the subspace matrix $\mathcal{H}_{p+1,q} \in \mathbb{R}^{(p+1)r\times qr_0}$ in (2.35), whose data corresponds to reference state θ_0. With (2.27) follows

$$\begin{aligned} \mathcal{J}(\theta_0) &= -\left.\frac{\partial}{\partial\theta}\operatorname{vec}\left(S(\theta)^T\mathcal{H}_{p+1,q}\right)\right|_{\theta=\theta_0} \\ &= -\left(\mathcal{H}_{p+1,q}^T \otimes I_s\right)\mathcal{S}'(\theta_0), \end{aligned} \tag{2.41}$$

where $\mathcal{S}(\theta) \stackrel{\text{def}}{=} \operatorname{vec}(S(\theta)^T) \in \mathbb{R}^{s(p+1)r}$ and $\mathcal{S}'(\theta) \stackrel{\text{def}}{=} \partial/\partial\theta\,\mathcal{S}(\theta) \in \mathbb{C}^{s(p+1)r\times(r+1)n}$. The derivative of $\mathcal{S}$ is obtained from (2.34) by deriving with respect to θ. It follows

$$\frac{\partial}{\partial\theta}\operatorname{vec}\left(S(\theta)^T\mathcal{O}_{p+1}(\theta)\right) = \left(\mathcal{O}_{p+1}(\theta)^T \otimes I_s\right)\mathcal{S}'(\theta) + \left(I_n \otimes S(\theta)^T\right)\mathcal{O}'_{p+1}(\theta) = 0$$

and thus $\mathcal{S}'(\theta_0)$ in (2.41) is a solution of

$$\left(\mathcal{O}_{p+1}(\theta_0)^T \otimes I_s\right)\mathcal{S}'(\theta_0) = -\left(I_n \otimes S(\theta_0)^T\right)\mathcal{O}'_{p+1}(\theta_0). \tag{2.42}$$

As $\mathcal{O}_{p+1}(\theta_0)^T\left(\mathcal{O}_{p+1}(\theta_0)^T\right)^\dagger = I_n$, one solution is

$$\mathcal{S}'(\theta_0) = -\left(\left(\mathcal{O}_{p+1}(\theta_0)^T\right)^\dagger \otimes I_s\right)\left(I_n \otimes S(\theta_0)^T\right)\mathcal{O}'_{p+1}(\theta_0). \tag{2.43}$$

Plugging into (2.41) leads finally to

$$\mathcal{J}(\theta_0) = \left(\mathcal{O}_{p+1}(\theta_0)^\dagger\mathcal{H}_{p+1,q} \otimes S(\theta_0)\right)^T\mathcal{O}'_{p+1}(\theta_0). \tag{2.44}$$

Second computation In (2.25) the residual function is derived with respect to the second variable. With (2.28) follows

$$\mathcal{J}(\theta_0) = \frac{\partial}{\partial\theta}\mathrm{vec}\left(S(\theta_0)^T\mathcal{H}_{p+1,q}\right)\Big|_{\theta=\theta_0},$$

where $\mathcal{H}_{p+1,q}$ is an implicit function of θ. From (2.2) follows $\mathcal{H}_{p+1,q} = \mathcal{O}_{p+1}(\theta)\mathcal{Z}_q$ and thus

$$\mathcal{J}(\theta_0) = \left(\mathcal{Z}_q^T \otimes S(\theta_0)^T\right)\mathcal{O}'_{p+1}(\theta_0).$$

Then, $\mathcal{Z}_q = \mathcal{O}_{p+1}(\theta_0)^\dagger\mathcal{H}_{p+1,q}$ and

$$\mathcal{J}(\theta_0) = \left(\mathcal{O}_{p+1}(\theta_0)^\dagger\mathcal{H}_{p+1,q} \otimes S(\theta_0)\right)^T\mathcal{O}'_{p+1}(\theta_0). \tag{2.45}$$

Note that in both computations, $\mathcal{J}(\theta_0)$ does not depend on the particular scaling of the mode shapes in θ_0: Scaling the mode shapes $\varphi_1, \ldots, \varphi_n$ with some constants $\alpha_1, \ldots, \alpha_n$ leads to the parametric observability matrix $\mathcal{O}_{p+1}(\theta_0)D$, where $D = \mathrm{diag}(\alpha_1, \ldots, \alpha_n)$. Its derivative in (2.40) then writes as $(D \otimes I_{(p+1)r})\mathcal{O}'_{p+1}(\theta_0)$ and hence

$$\begin{aligned}
\mathcal{J}(\theta_0) &= \left(\left(\mathcal{O}_{p+1}(\theta_0)D\right)^\dagger\mathcal{H}_{p+1,q} \otimes S(\theta_0)\right)^T(D \otimes I_{(p+1)r})\mathcal{O}'_{p+1}(\theta_0)\\
&= \left(D^{-1}\left(\mathcal{O}_{p+1}(\theta_0)\right)^\dagger\mathcal{H}_{p+1,q} \otimes I_{(p+1)r}S(\theta_0)\right)^T(D \otimes I_{(p+1)r})\mathcal{O}'_{p+1}(\theta_0)\\
&= \left(\mathcal{O}_{p+1}(\theta_0)^\dagger\mathcal{H}_{p+1,q} \otimes S(\theta_0)\right)^T\mathcal{O}'_{p+1}(\theta_0).
\end{aligned}$$

In both computations, a consistent estimate $\widehat{\mathcal{J}}$ of $\mathcal{J}(\theta_0)$ is obtained by replacing $\mathcal{H}_{p+1,q}$ in (2.44) or (2.45) with an estimate $\widehat{\mathcal{H}}_{p+1,q}$ (cf. (2.37)) that is obtained from a data sample from the reference state corresponding to θ_0.

2.3.3.3 Real-valued Jacobian computation

If the system parameter θ consists of m pairs of conjugated complex eigenvalues and mode shapes, with the system order being $n = 2m$, the computation of the Jacobian $\mathcal{J}(\theta_0)$ can be done in real values [BAB97, BMG04]. This is for example the case for structural vibration analysis, see also Section 2.4.

Recall the definition of θ from (2.31):

$$\theta = \begin{bmatrix}\Lambda\\ \mathrm{vec}\,\Phi\end{bmatrix}, \quad \text{where} \quad \Lambda \overset{\text{def}}{=} \begin{bmatrix}\lambda_1\\ \vdots\\ \lambda_n\end{bmatrix}, \quad \Phi \overset{\text{def}}{=} \begin{bmatrix}\varphi_1 & \ldots & \varphi_n\end{bmatrix}$$

Let $\Lambda_\mathrm{c} \in \mathbb{C}^m$ and $\Phi_\mathrm{c} \in \mathbb{C}^{r\times m}$ contain one element of each pair of the conjugated complex eigenvalues and mode shapes, respectively, such that

$$\Lambda = \begin{bmatrix}\Lambda_\mathrm{c}\\ \overline{\Lambda_\mathrm{c}}\end{bmatrix}, \quad \Phi = \begin{bmatrix}\Phi_\mathrm{c} & \overline{\Phi_\mathrm{c}}\end{bmatrix}$$

and thus

$$\theta = \begin{bmatrix} \Lambda_\mathrm{c} \\ \overline{\Lambda_\mathrm{c}} \\ \operatorname{vec} \Phi_\mathrm{c} \\ \operatorname{vec} \overline{\Phi_\mathrm{c}} \end{bmatrix}.$$

Define analogously

$$\theta_\mathrm{c} \stackrel{\mathrm{def}}{=} \begin{bmatrix} \Lambda_\mathrm{c} \\ \operatorname{vec} \Phi_\mathrm{c} \end{bmatrix} \in \mathbb{C}^{(r+1)m}.$$

Then, the parametric observability matrix (2.32) writes as

$$\mathcal{O}_{p+1}(\theta) = \begin{bmatrix} \Phi_\mathrm{c} & \overline{\Phi_\mathrm{c}} \\ \Phi_\mathrm{c}\Delta_\mathrm{c} & \overline{\Phi_\mathrm{c}\Delta_\mathrm{c}} \\ \vdots & \vdots \\ \Phi_\mathrm{c}\Delta_\mathrm{c}^p & \overline{\Phi_\mathrm{c}\Delta_\mathrm{c}^p} \end{bmatrix} = \begin{bmatrix} \mathcal{O}_{p+1}(\theta_\mathrm{c}) & \mathcal{O}_{p+1}(\overline{\theta_\mathrm{c}}) \end{bmatrix},$$

where $\Delta_\mathrm{c} = \operatorname{diag}(\Lambda_\mathrm{c})$. Now define the real-valued system parameter $\tilde{\theta}$ by

$$\tilde{\theta} \stackrel{\mathrm{def}}{=} \begin{bmatrix} \Re(\theta_\mathrm{c}) \\ \Im(\theta_\mathrm{c}) \end{bmatrix} = \begin{bmatrix} \Re(\Lambda_\mathrm{c}) \\ \operatorname{vec} \Re(\Phi_\mathrm{c}) \\ \Im(\Lambda_\mathrm{c}) \\ \operatorname{vec} \Im(\Phi_\mathrm{c}) \end{bmatrix} \in \mathbb{R}^{(r+1)2m} \tag{2.46}$$

and its corresponding real-valued parametric observability matrix by

$$\mathcal{O}_{p+1}(\tilde{\theta}) \stackrel{\mathrm{def}}{=} \begin{bmatrix} \Re(\Phi_\mathrm{c}) & \Im(\Phi_\mathrm{c}) \\ \Re(\Phi_\mathrm{c}\Delta_\mathrm{c}) & \Im(\Phi_\mathrm{c}\Delta_\mathrm{c}) \\ \vdots & \vdots \\ \Re(\Phi_\mathrm{c}\Delta_\mathrm{c}^p) & \Im(\Phi_\mathrm{c}\Delta_\mathrm{c}^p) \end{bmatrix} = \begin{bmatrix} \Re\left(\mathcal{O}_{p+1}(\theta_\mathrm{c})\right) & \Im\left(\mathcal{O}_{p+1}(\theta_\mathrm{c})\right) \end{bmatrix} \in \mathbb{R}^{(p+1)r \times 2m}. \tag{2.47}$$

Then, the relation

$$\mathcal{O}_{p+1}(\tilde{\theta}) = \mathcal{O}_{p+1}(\theta)\, T$$

holds with the invertible matrix

$$T = \frac{1}{2} \begin{bmatrix} I_m & -\mathrm{i} I_m \\ I_m & \mathrm{i} I_m \end{bmatrix},$$

where $(\sqrt{2}T)(\sqrt{2}T)^* = I$. Thus, the left null space $S(\theta_0)$ of $\mathcal{O}_{p+1}(\theta_0)$ with the properties (2.33)–(2.34) is equivalent to a left null space $S(\tilde{\theta}_0)$ of $\mathcal{O}_{p+1}(\tilde{\theta}_0)$. Hence, the left null space $S(\theta_0)$ can be replaced by $S(\tilde{\theta}_0)$ in the residual computation and the system parameter $\tilde{\theta}_0$ can be used instead of θ_0.

Note that in the modal basis defined by $\mathcal{O}_{p+1}(\tilde{\theta})$, the state transition and observation matrices write as

$$\widetilde{A} = T^{-1}\Delta T = \begin{bmatrix} \Re(\Delta_\mathrm{c}) & \Im(\Delta_\mathrm{c}) \\ -\Im(\Delta_\mathrm{c}) & \Re(\Delta_\mathrm{c}) \end{bmatrix}, \quad \widetilde{C} = \Phi T = \begin{bmatrix} \Re(\Phi_\mathrm{c}) & \Im(\Phi_\mathrm{c}) \end{bmatrix}.$$

For the Jacobian computation using the real-valued system parameter $\tilde{\theta}$, the derivative

$$\mathcal{O}'_{p+1}(\tilde{\theta}_0) \stackrel{\mathrm{def}}{=} \left.\frac{\partial \operatorname{vec} \mathcal{O}_{p+1}(\tilde{\theta})}{\partial \tilde{\theta}}\right|_{\tilde{\theta}=\tilde{\theta}_0}$$

of the real-valued observability matrix is needed, where $\mathcal{O}'_{p+1}(\tilde{\theta}_0) \in \mathbb{R}^{(p+1)r2m\times(r+1)2m}$. With (2.46)–(2.47) it holds

$$\mathcal{O}'_{p+1}(\tilde{\theta}) = \begin{bmatrix} \dfrac{\partial \operatorname{vec} \Re\left(\mathcal{O}_{p+1}(\theta_\mathrm{c})\right)}{\partial \Re(\theta_\mathrm{c})} & \dfrac{\partial \operatorname{vec} \Re\left(\mathcal{O}_{p+1}(\theta_\mathrm{c})\right)}{\partial \Im(\theta_\mathrm{c})} \\ \dfrac{\partial \operatorname{vec} \Im\left(\mathcal{O}_{p+1}(\theta_\mathrm{c})\right)}{\partial \Re(\theta_\mathrm{c})} & \dfrac{\partial \operatorname{vec} \Im\left(\mathcal{O}_{p+1}(\theta_\mathrm{c})\right)}{\partial \Im(\theta_\mathrm{c})} \end{bmatrix}. \tag{2.48}$$

In (2.40), the complex-valued derivative $\mathcal{O}'_{p+1}(\theta_0) \in \mathbb{C}^{(p+1)r2m\times(r+1)2m}$ was defined. The complex-valued derivative $\mathcal{O}'_{p+1}(\theta_\mathrm{c}) \in \mathbb{C}^{(p+1)rm\times(r+1)m}$ with respect to parameter θ_c can be defined analogously. With the Wirtinger derivatives [Fis05] of a complex-valued function it follows

$$\begin{aligned} \mathcal{O}'_{p+1}(\theta_\mathrm{c}) &= \frac{\partial \operatorname{vec} \Re\left(\mathcal{O}_{p+1}(\theta_\mathrm{c})\right)}{\partial \theta_\mathrm{c}} + \mathrm{i}\frac{\partial \operatorname{vec} \Im\left(\mathcal{O}_{p+1}(\theta_\mathrm{c})\right)}{\partial \theta_\mathrm{c}} \\ &= \frac{1}{2}\left(\frac{\partial \operatorname{vec} \Re\left(\mathcal{O}_{p+1}(\theta_\mathrm{c})\right)}{\partial \Re(\theta_\mathrm{c})} - \mathrm{i}\frac{\partial \operatorname{vec} \Re\left(\mathcal{O}_{p+1}(\theta_\mathrm{c})\right)}{\partial \Im(\theta_\mathrm{c})} + \mathrm{i}\frac{\partial \operatorname{vec} \Im\left(\mathcal{O}_{p+1}(\theta_\mathrm{c})\right)}{\partial \Re(\theta_\mathrm{c})}\right. \\ &\qquad \left. + \frac{\partial \operatorname{vec} \Im\left(\mathcal{O}_{p+1}(\theta_\mathrm{c})\right)}{\partial \Im(\theta_\mathrm{c})}\right). \end{aligned}$$

Then, the elements of matrix $\mathcal{O}'_{p+1}(\tilde{\theta})$ in (2.48) are obtained from $\mathcal{O}'_{p+1}(\theta_\mathrm{c})$ by using the Cauchy-Riemann equations[1]

$$\frac{\partial \operatorname{vec} \Re\left(\mathcal{O}_{p+1}(\theta_\mathrm{c})\right)}{\partial \Re(\theta_\mathrm{c})} = \frac{\partial \operatorname{vec} \Im\left(\mathcal{O}_{p+1}(\theta_\mathrm{c})\right)}{\partial \Im(\theta_\mathrm{c})}, \quad \frac{\partial \operatorname{vec} \Re\left(\mathcal{O}_{p+1}(\theta_\mathrm{c})\right)}{\partial \Im(\theta_\mathrm{c})} = -\frac{\partial \operatorname{vec} \Im\left(\mathcal{O}_{p+1}(\theta_\mathrm{c})\right)}{\partial \Re(\theta_\mathrm{c})}$$

and it follows

$$\mathcal{O}'_{p+1}(\tilde{\theta}) = \begin{bmatrix} \Re(\mathcal{O}'_{p+1}(\theta_\mathrm{c})) & -\Im(\mathcal{O}'_{p+1}(\theta_\mathrm{c})) \\ \Im(\mathcal{O}'_{p+1}(\theta_\mathrm{c})) & \Re(\mathcal{O}'_{p+1}(\theta_\mathrm{c})) \end{bmatrix}. \tag{2.49}$$

Thus, the real-valued computation of the Jacobian $\mathcal{J}(\tilde{\theta}_0)$ analogous to (2.44) and (2.45) writes

$$\mathcal{J}(\tilde{\theta}_0) = \left(\mathcal{O}_{p+1}(\tilde{\theta}_0)^\dagger \mathcal{H}_{p+1,q} \otimes S(\tilde{\theta}_0)\right)^T \mathcal{O}'_{p+1}(\tilde{\theta}_0), \tag{2.50}$$

[1] $\mathcal{O}_{p+1}(\theta_\mathrm{c})$ is a polynomial function and thus holomorphic. Hence the Cauchy-Riemann equations are satisfied.

where the real-valued observability matrix $\mathcal{O}_{p+1}(\tilde{\theta}_0)$ is computed in (2.47), the left null space $S(\tilde{\theta}_0)$ is computed on $\mathcal{O}_{p+1}(\tilde{\theta}_0)$ and $\mathcal{O}'_{p+1}(\tilde{\theta}_0)$ is obtained from (2.49) at $\tilde{\theta} = \tilde{\theta}_0$.

A consistent estimate $\widehat{\mathcal{J}}$ of $\mathcal{J}(\tilde{\theta}_0)$ is obtained by replacing $\mathcal{H}_{p+1,q}$ in (2.50) with an estimate $\widehat{\mathcal{H}}_{p+1,q}$ that is obtained from a data sample from the reference state corresponding to $\tilde{\theta}_0$. Note that θ_0 and $\tilde{\theta}_0$ denote equivalent canonical parameterizations of the system in the reference state, where the former is complex-valued and the latter real-valued.

2.3.3.4 Covariance computation

The covariance of the residual function in the reference state is defined in (2.22) and obtained using data in the reference state in (2.23):

$$\Sigma(\theta_0) = \lim_{N\to\infty} \mathbf{E}_{\theta_0}(\zeta_N(\theta_0)\ \zeta_N(\theta_0)^T) \in \mathbb{R}^{sqr_0 \times sqr_0}$$

A consistent estimate $\widehat{\Sigma}$ of the covariance is obtained from the empirical covariance of a sample of residuals $\zeta_{N_b}^{(k)}(\theta_0)$, $k = 1, \ldots, n_b$, that are computed on different, statistically independent parts of the data, where n_b is the number of data samples that are each of length N_b. Let N be fixed, and let the n_b independent data samples be chosen such that $N = n_b N_b$. Denote the estimates (2.37) of the covariance-driven subspace matrix on each data sample of length N_b with $\widehat{\mathcal{H}}_{p+1,q}^{(k)}$ and the estimate on the data sample of length N with $\widehat{\mathcal{H}}_{p+1,q}$. Then,

$$\lim_{N\to\infty} \widehat{\mathcal{H}}_{p+1,q} = \lim_{N\to\infty} \frac{1}{n_b} \sum_{k=1}^{n_b} \widehat{\mathcal{H}}_{p+1,q}^{(k)}.$$

and thus, the covariance of ζ_N can be expressed as the covariance of the $\zeta_{N_b}^{(k)}$:

$$\widehat{\Sigma} = \mathrm{cov}(\zeta_N(\theta_0)) = \mathrm{cov}\left(\zeta_{N_b}^{(k)}(\theta_0)\right).$$

Replacing the latter with the sample covariance, where the mean $\mathbf{E}_{\theta_0}\zeta_{N_b}^{(k)}(\theta_0) = 0$ is known, yields the estimate

$$\widehat{\Sigma} = \frac{1}{n_b} \sum_{k=1}^{n_b} \zeta_{N_b}^{(k)}(\theta_0)\zeta_{N_b}^{(k)}(\theta_0)^T.$$

2.3.3.5 Invariance property of χ^2-test

The χ^2-test (2.39) possesses some important invariance properties.

Lemma 2.4 ([BAB97, Bas99, BAB00]) *The χ^2-test* (2.39) *is unchanged when the primary residual function $\mathcal{K}$ in* (2.36) *is premultiplied by an invertible matrix T.*

Proof: For the primary residual $T\mathcal{K}$, the subspace-based residual function writes $T\zeta_N(\theta_0)$ and consistent estimates of its sensitivity and covariance are $T\widehat{\mathcal{J}}$ and $T\widehat{\Sigma}T^T$, when

$\widehat{\mathcal{J}}$ and $\widehat{\Sigma}$ are consistent estimates of the sensitivity and covariance of $\zeta_N(\theta_0)$. Then,

$$\begin{aligned}\chi^2_N(\theta_0) &= (T\zeta_N(\theta_0))^T(T\widehat{\Sigma}T^T)^{-1}(T\widehat{\mathcal{J}})\left((T\widehat{\mathcal{J}})^T(T\widehat{\Sigma}T^T)^{-1}(T\widehat{\mathcal{J}})\right)^{-1}(T\widehat{\mathcal{J}})^T(T\widehat{\Sigma}T^T)^{-1}T\zeta_N(\theta_0)\\ &= \zeta_N(\theta_0)^T\widehat{\Sigma}^{-1}\widehat{\mathcal{J}}(\widehat{\mathcal{J}}^T\widehat{\Sigma}^{-1}\widehat{\mathcal{J}})^{-1}\widehat{\mathcal{J}}^T\widehat{\Sigma}^{-1}\zeta_N(\theta_0).\end{aligned}$$

□

In the definition of the left null space $S(\theta_0)$ in Section 2.3.3.1, the matrix $S(\theta_0)$ can be replaced by $S(\theta_0)W$, where W is an orthogonal matrix. This leads to a residual function

$$\zeta_{N,W}(\theta_0) = \sqrt{N}\,\mathrm{vec}\left((S(\theta_0)W)^T\widehat{\mathcal{H}}_{p+1,q}\right) = (I \otimes W^T)\zeta_N(\theta_0).$$

Thus, from Lemma 2.4 follows that the choice of W has no effect on the resulting χ^2-test statistics. Further aspects of the invariance property are considered in Section 3.4.2.

2.3.4 Non-parametric versions of the covariance-driven subspace-based fault detection test

This section addresses two implementations of the fault detection test that have proven efficient in practice and were shown in [BBB+08]. They use an entirely non-parametric version of the test, where no system parameter θ_0 needs to be known in the reference state. With this strategy, a test is proposed where an empirical null space $\widehat{S}$ is used, which is the null space of different reference states. This can be used for a test that is robust to environmental changes. Applications of the non-parametric test are found e.g. in [FM02, YG06, SBMT08, FK09, SMR+09].

2.3.4.1 Non-parametric test

In some cases, it is of interest to replace the parametric approach with a non-parametric one, based on an *empirical* null space $\widehat{S}$ computed on a reference data set and not on the parametric observability matrix (2.32) or (2.47). Such a null space may result from a SVD of the empirical subspace matrix built on the reference data set (here indexed with 0) and it holds

$$\begin{aligned}\widehat{S}^T\widehat{S} &= I_s,\\ \widehat{S}^T\widehat{\mathcal{H}}^{(0)}_{p+1,q} &= 0\end{aligned} \tag{2.51}$$

instead of (2.33)–(2.34). The subspace matrix $\widehat{\mathcal{H}}^{(0)}_{p+1,q}$ corresponds to reference parameter θ_0 in the previous sections, which is not needed to be known in this case. While θ_0 would be estimated from data in practice and thus contains only limited information about the system in the reference state, the computation of $\widehat{S}$ directly on $\widehat{\mathcal{H}}^{(0)}_{p+1,q}$ uses the entire system response.

Based on a new data set of length N from the (possibly faulty) system, the empirical subspace matrix $\widehat{\mathcal{H}}_{p+1,q}$ (corresponding to state θ) is computed and the residual then writes

$$\widehat{\zeta}_N \stackrel{\text{def}}{=} \sqrt{N}\ \text{vec}\left(\widehat{S}^T\widehat{\mathcal{H}}_{p+1,q}\right).$$

As there is no system parameterization, no sensitivity matrix needs to be taken care of. The χ^2-test statistics (2.39) boils down to

$$\widehat{\chi}^2_N \stackrel{\text{def}}{=} \widehat{\zeta}_N^T\widehat{\Sigma}^{-1}\widehat{\zeta}_N, \tag{2.52}$$

where $\widehat{\Sigma}$ is an estimate of the covariance of $\widehat{\zeta}_N$, which can be computed analogous to Section 2.3.3.4.

Note that the empirical χ^2-test statistics (2.52) corresponds to testing hypotheses $\mathbf{H}_0$ against $\mathbf{H}_1$ in Theorem 2.3, where $\mathcal{J}(\theta_0) = I$. Thus, the residual function plays the role of the underlying system parameter itself.

2.3.4.2 Merging different reference states

Assume that J reference data sets are available with corresponding subspace matrices $\widehat{\mathcal{H}}^{(0,1)}_{p+1,q}, \ldots, \widehat{\mathcal{H}}^{(0,J)}_{p+1,q}$ that relate to (slightly) different system parameters $\theta_{0,1}, \ldots, \theta_{0,J}$. This happens e.g. in structural vibration analysis, where the modal parameters of the healthy structure vary under different environmental conditions. A left null space $\widehat{S}$ is desired with the property

$$\widehat{S}^T\widehat{\mathcal{H}}^{(0,k)}_{p+1,q} = 0, \quad k = 1, \ldots, J.$$

An empirical solution to this problem was proposed in [BBB+08] by the computation of $\widehat{S}$ on the average of the subspace matrices $\widehat{\mathcal{H}}^{(k)}_{p+1,q}$, such that

$$\widehat{S}^T\sum_{k=1}^{J}\widehat{\mathcal{H}}^{(0,k)}_{p+1,q} = 0.$$

Then, the residual covariance $\widehat{\Sigma}$ is computed using the subspace matrices $\widehat{\mathcal{H}}^{(0,k)}_{p+1,q}$, $k = 1, \ldots, J$. The corresponding χ^2-test statistics (2.52) then reacts on changes in the system from the states corresponding to $\theta_{0,1}, \ldots, \theta_{0,J}$, but not from a change in the system between the reference states corresponding to some $\theta_{0,i}$ to $\theta_{0,j}$. This approach was validated e.g. in [BBM+06, RMLDR08, AMR09, SMR+09].

2.4 Structural vibration analysis

An important application of subspace-based system identification and fault detection lies in the field of vibration analysis of mechanical, civil and aeronautical structures. In this section, the underlying mechanical model is introduced and its relation to the state space model (2.1) is shown [POB+91, Jua94, PDR99]. Also, practical issues for the *modal analysis* of structures are considered.

2.4.1 Modeling and eigenstructure identification

The behavior of a mechanical structure is described by a continuous-time, time-invariant, linear dynamical system, modeled by the vector differential system

$$\begin{cases} M\ddot{\mathcal{X}}(t) + C_1\dot{\mathcal{X}}(t) + K\mathcal{X}(t) = \upsilon(t) \\ Y(t) = L\mathcal{X}(t) \end{cases} \tag{2.53}$$

where t denotes continuous time; M, C_1, and K are mass, damping, and stiffness matrices, respectively; the (high dimensional) state vector $\mathcal{X}(t)$ is the displacement vector of the degrees of freedom of the structure; the external unmeasured force υ is modeled as stationary white noise with covariance matrix $Q_\upsilon(t)$; measurements are collected in the (low dimensional) vector Y and matrix L indicates which degrees of freedom are actually measured, i.e. the sensor locations.

The matrices (M, C_1, K) cannot be recovered from measured outputs. However, the parameters to be identified are the eigenvalues (or modes) μ and mode shapes ψ_μ of system (2.53), which comprise the *modal parameters* and are solutions of

$$(\mu^2 M + \mu C_1 + K)\Psi_\mu = 0, \quad \psi_\mu = L\Psi_\mu. \tag{2.54}$$

Sampling model (2.53) at rate $1/\tau$ yields the discrete time state space model (2.1), where the state and the output are

$$X_k = \begin{bmatrix} \mathcal{X}(k\tau) \\ \dot{\mathcal{X}}(k\tau) \end{bmatrix}, \quad Y_k = Y(k\tau),$$

the state transition and observation matrices are

$$A = \mathrm{e}^{\mathcal{L}\tau}, \text{ where } \mathcal{L} = \begin{bmatrix} 0 & I \\ -M^{-1}K & -M^{-1}C_1 \end{bmatrix}, \quad C = \begin{bmatrix} L & 0 \end{bmatrix}.$$

The state noise (V_k) is stationary, zero-mean, white, with covariance

$$Q \stackrel{\text{def}}{=} \mathbf{E}\left(V_k\, V_k^T\right) = \int_{k\tau}^{(k+1)\tau} e^{\mathcal{L}s}\, \widetilde{Q}(s)\, e^{\mathcal{L}^T s} ds, \quad \text{where} \quad \widetilde{Q}(s) = \begin{bmatrix} 0 & 0 \\ 0 & M^{-1}Q_\upsilon(s)M^{-1} \end{bmatrix}.$$

The eigenstructure $(\lambda, \varphi_\lambda)$ of system (2.1) is defined by the eigenvalues and eigenvectors of A and by C:

$$(A - \lambda I)\phi_\lambda = 0, \quad \varphi_\lambda = C\phi_\lambda. \tag{2.55}$$

The desired modal parameters in (2.54) are equivalently found in the eigenstructure $(\lambda, \varphi_\lambda)$ of (2.1) and it holds

$$\mathrm{e}^{\mu\tau} = \lambda, \quad \psi_\mu = \varphi_\lambda.$$

The modal frequencies f and damping coefficients ρ are recovered directly from the eigenvalues λ by

$$f = \frac{a}{2\pi\tau}, \quad \rho = \frac{100|b|}{\sqrt{a^2 + b^2}}, \tag{2.56}$$

where $a = |\arctan \Re(\lambda)/\Im(\lambda)|$ and $b = \ln|\lambda|$.

Thus, vibration analysis is stated as the problem of identifying the eigenstructure of a linear dynamic system. Parameters of interest are modes (modal frequencies f, damping ratios ρ) and mode shapes φ_λ.

2.4.2 Further modeling issues

2.4.2.1 Sensor types

The measurement equation in (2.53) assumes that the sensors are displacement sensors such as strain gauges. If strain gauges, velocity sensors or accelerometers are available, the measurement equation in (2.53) can be written as

$$Y(t) = \begin{bmatrix} L_1 \mathcal{X}(t) \\ L_2 \dot{\mathcal{X}}(t) \\ L_3 \ddot{\mathcal{X}}(t) \end{bmatrix},$$

and the corresponding discrete time system (2.1) holds with

$$C = \begin{bmatrix} L_1 & 0 \\ 0 & L_2 \\ -L_3 M^{-1} K & -L_3 M^{-1} C_1 \end{bmatrix}.$$

Consequently, the state-space model (2.1) is valid for those three types of sensors and the nature of the sensors influences the observation matrix C only. When accelerometers are used, the sensor noise and process noise are correlated, although we ignore this effect.

2.4.2.2 Input excitation

In Section 2.4.1, the unknown excitation force $\upsilon(t)$ is assumed to be stationary Gaussian white noise for simplicity. However, it is more realistic to assume a non-stationary excitation. This is no shortcoming for the subspace algorithms, as non-stationary consistency of many subspace algorithms for eigenstructure identification was shown in [BM07].

Also, the whiteness assumption made on the input force $\upsilon(t)$ seems unrealistic. The unknown excitation forces are typically a superposition of harmonics due to rotating parts as well as colored ambient excitation noise. When processing the measured responses with subspace-based algorithms, harmonics due to rotating parts are found in the form of poles with zero damping. Since the frequency of rotation is usually known, those harmonics can be discarded from the results of the analysis. On the other hand, colored input excitation can always be represented as the output of an unknown excitation filter driven by white noise [GD91, BBGM07]. In this case, (2.53) represents the combined system including the excitation filter. Therefore, (2.54) collects the modes and mode shapes of the combined system. Since the poles corresponding to the excitation filter are generally highly damped, these poles can easily be separated from structural modes, which typically have a much lower damping coefficient.

2.4.2.3 Measurement noise

Measurement noise was neither considered in model (2.1) nor in model (2.53). This is somewhat unrealistic and the measurement equation in model (2.1) should rather be

$$Y_k = CX_k + \varepsilon_k,$$

where ε_k is a Gaussian, zero mean, moving-average sequence. However, this kind of noise can be encompassed up to an index shift when filling the subspace matrix for the subspace algorithm [VODM96, BAB00]. With this assumption on ε_k, the measurement noise does not affect the eigenstructure of the system in (2.1). This property does not hold if ε_k is an autoregressive sequence.

2.4.3 The stabilization diagram

In Operational Modal Analysis (OMA), the eigenstructure of mechanical, civil and aeronautical structures is identified from output-only data under ambient excitation. With forced excitation e.g. by shakers (exogenous inputs, OMAX), some of the inputs are available. In both cases, the selection of the model order in (2.5), and thus the parameters p and q of the subspace matrix $\widehat{\mathcal{H}}_{p+1,q}$ on one hand, and the handling of excitation and measurement noises on the other hand, are two major practical issues.

In order to retrieve a desired number of modes, an even larger model order must be assumed while performing identification. A number of spurious modes appear in the identified model due to this over-specification, as well as due to colored noise or non-linearities. Techniques from statistics to estimate the best model order, such as AIC, BIC or MDL [Aka74a, Ris78, CMK01], or model order estimation techniques specifically for subspace methods as in [Bau01] may lead to a model with the best prediction capacity. However, one is rather interested in a model containing only the physical modes of the investigated structured, while rejecting the spurious modes. Based on the observation that physical modes remain quite constant when estimated at different over-specified model orders, while spurious modes vary, they can be distinguished using so-called *stabilization diagrams* [PDR99, PDR01, VdAP04, CGV$^+$05, Bak11]. There, frequencies estimated from multi-order system identification are plotted against the model order. From the modes common to many models and using further stabilization criteria, such as a threshold on damping values, low variation between modes and mode shapes of successive orders etc., the final estimated model is obtained.

Chapter 3

Some numerical considerations for subspace-based algorithms

3.1 Introduction

This chapter has the purpose to introduce and derive some numerical tools, which are needed throughout this work. Furthermore, theoretical properties and practical issues concerning the fault detection test of Section 2.3.3 are derived.

In Section 3.2, definitions of the QR, LQ and singular value decompositions are stated, as well as properties of the vectorization operator and the Kronecker product.

In Section 3.3, an iterative least squares solution for strongly over-determined systems of equations using the QR decomposition is derived. This algorithm will be useful in Chapters 4 and 5 for an iterative solution of the least squares problem for the state transition matrix. Furthermore, an efficient computation of sensitivities of the singular vectors of a random matrix is derived in the same section, which will be useful in Chapter 6 for the covariance computation of a fault detection residual based on the left singular vectors.

In Section 3.4, additional properties of the statistical subspace-based fault detection test of Section 2.3.3 are derived and clarified. They are mainly of theoretical value and concern the computation of the asymptotic Jacobian of the residual as well as an invariance property of the associated χ^2-test. The latter concerns the selected null space and weightings for the subspace matrix. For these issues, inconsistent statements have been made in literature and this section helps to clarify them.

In Section 3.5, some practical issues of the fault detection test are addressed, which are important for the implementation of the algorithm and its application to real data. In many cases, the estimate of the residual's asymptotic covariance matrix is rank deficient due to a lack of data. For this case, a numerically robust and efficient computation of the associated χ^2-test is proposed. Furthermore, the computation of the covariance estimate

itself is explained in detail for covariance-driven SSI and extended to data-driven SSI with the UPC algorithm. These computations are applied for damage detection using ambient vibration data of a bridge in Chapter 9.

Note that Sections 3.3–3.5 can be skipped for a first reading.

3.2 Definitions

3.2.1 QR decomposition and Singular Value Decomposition

In this section, the notation for QR, LQ and singular value decompositions is defined, based on [GVL96].

Definition 3.1 *The QR decomposition of a matrix $Z \in \mathbb{R}^{a\times b}$ is denoted by*

$$Z = Q_1 R_1,$$

where $Q_1 \in \mathbb{R}^{a\times a}$ is an orthogonal matrix with $Q_1^T Q_1 = Q_1 Q_1^T = I$ and $R_1 \in \mathbb{R}^{a\times b}$ is an upper triangular matrix. For $a \geq b$ the thin QR decomposition is denoted by

$$Z = Q_2 R_2,$$

where $Q_2 \in \mathbb{R}^{a\times b}$ is a matrix with orthonormal columns ($Q_2^T Q_2 = I$) and $R_2 \in \mathbb{R}^{b\times b}$ is an upper triangular matrix.

Analogously, the LQ decomposition of a matrix $Z \in \mathbb{R}^{a\times b}$ is denoted by

$$Z = R_3 Q_3,$$

where $R_3 \in \mathbb{R}^{a\times b}$ is a lower triangular matrix and $Q_3 \in \mathbb{R}^{b\times b}$ is an orthogonal matrix with $Q_3^T Q_3 = Q_3 Q_3^T = I$. For $a \leq b$ the thin LQ decomposition is denoted by

$$Z = R_4 Q_4,$$

where $R_4 \in \mathbb{R}^{a\times a}$ is a lower triangular matrix and $Q_4 \in \mathbb{R}^{a\times b}$ is a matrix with orthonormal rows ($Q_4 Q_4^T = I$).

Note that if Z is full column rank, R_2 from the thin QR decomposition is invertible. If Z is full row rank, R_4 from the thin LQ decomposition is invertible. Still, in both cases, the thin decompositions are not unique. However, they can be defined in a unique way, e.g. by positive values on the diagonal of R_2 and R_4, respectively.

In this work, mainly the thin QR and thin LQ decompositions are used.

Definition 3.2 *The singular value decomposition (SVD) of a matrix $Z \in \mathbb{R}^{a\times b}$ is denoted by*

$$Z = U \Delta V^T$$

where $U \in \mathbb{R}^{a\times a}$ *and* $V \in \mathbb{R}^{b\times b}$ *are orthogonal matrices containing the left and right singular vectors, and*

$$\Delta = \begin{cases} \begin{bmatrix} \widetilde{\Delta} & 0 \end{bmatrix}, & \text{if } a < b, \\ \begin{bmatrix} \widetilde{\Delta} \\ 0 \end{bmatrix}, & \text{if } a > b, \\ \widetilde{\Delta}, & \text{if } a = b, \end{cases}$$

where $\widetilde{\Delta} = \operatorname{diag}(\sigma_1, \ldots, \sigma_{\min\{a,b\}})$ *is the diagonal matrix containing the singular values of* Z *with* $\sigma_1 \geq \ldots \geq \sigma_{\min\{a,b\}}$.

For $a > b$ *the thin SVD of* Z *is defined by*

$$Z = U_1 \widetilde{\Delta} V^T,$$

where $U_1 \in \mathbb{R}^{a\times b}$ *is the first block of the partitioned matrix* $U = \begin{bmatrix} U_1 & U_2 \end{bmatrix}$.

Note that again, the thin SVD of a matrix Z is not a unique decomposition, even if Z is full column rank. However, it can be defined uniquely, e.g. by positive values of the first component of each left singular vector as in the following definition.

Definition 3.3 *Let* $Z = \widetilde{U}\Delta\widetilde{V}^T$ *be an arbitrary SVD of matrix* Z*, where*

$$\widetilde{U} = \begin{bmatrix} \tilde{u}_1 & \ldots & \tilde{u}_n \end{bmatrix}, \quad \widetilde{V} = \begin{bmatrix} \tilde{v}_1 & \ldots & \tilde{v}_n \end{bmatrix}$$

and $n = \operatorname{rank}(Z)$*. For* $j = 1, \ldots, n$ *define*

$$u_j = \operatorname{sign}(\tilde{u}_{1,j})\tilde{u}_{1,j}, \quad v_j = \operatorname{sign}(\tilde{u}_{1,j})\tilde{v}_{1,j},$$

where $\tilde{u}_{1,j}$ *is the first entry of vector* $\tilde{u}_j$*, and*

$$U = \begin{bmatrix} u_1 & \ldots & u_n \end{bmatrix}, \quad V = \begin{bmatrix} v_1 & \ldots & v_n \end{bmatrix}.$$

Then, $U\Delta V^T$ *is called unique SVD of* Z*.*

In this work, the full SVD is used for the computation of left null spaces. In all other cases, the thin SVD is used.

3.2.2 Vectorization operator and Kronecker product

In this work, the vectorization operator

$$\operatorname{vec} G = \begin{bmatrix} g_1 \\ g_2 \\ \vdots \\ g_n \end{bmatrix} \quad \text{for} \quad G = \begin{bmatrix} g_1 & g_2 & \ldots & g_n \end{bmatrix} \in \mathbb{R}^{m\times n}$$

is used extensively. Here, some properties related to Kronecker products are recalled and formulas for $\operatorname{vec} G^T$ are derived. They are stated in [Fac05, Bro11] and proved in the following.

For arbitrary matrices $A \in \mathbb{R}^{p\times m}$, $B \in \mathbb{R}^{n\times q}$ the Kronecker product $A \otimes B \in \mathbb{R}^{np\times mq}$ is defined as

$$A \otimes B = \begin{bmatrix} a_{11}B & a_{12}B & \dots & a_{1m}B \\ a_{21}B & a_{22}B & \dots & a_{2m}B \\ \vdots & \vdots & \ddots & \vdots \\ a_{p1}B & a_{p2}B & \dots & a_{pm}B \end{bmatrix}, \quad \text{where} \quad A = \begin{bmatrix} a_{11} & a_{12} & \dots & a_{1m} \\ a_{21} & a_{22} & \dots & a_{2m} \\ \vdots & \vdots & \ddots & \vdots \\ a_{p1} & a_{p2} & \dots & a_{pm} \end{bmatrix}.$$

An important property of the vectorization operation is

$$\operatorname{vec}(AGB) = (B^T \otimes A)\operatorname{vec} G. \tag{3.1}$$

Definition 3.4 *For $i \in \{1, \dots, n\}$ define the unit vector*

$$e_i^{(n)} \stackrel{\text{def}}{=} \begin{bmatrix} 0 & \dots & 0 & 1 & 0 & \dots & 0 \end{bmatrix}^T \in \mathbb{R}^n,$$

where the entry 1 is at the i-th position. Then, the permutation matrix $\mathcal{P}_{m,n} \in \mathbb{R}^{mn\times mn}$ is defined as

$$\mathcal{P}_{m,n} \stackrel{\text{def}}{=} \begin{bmatrix} e_1^{(n)} \otimes e_1^{(m)T} & e_2^{(n)} \otimes e_1^{(m)T} & \dots & e_n^{(n)} \otimes e_1^{(m)T} \\ e_1^{(n)} \otimes e_2^{(m)T} & e_2^{(n)} \otimes e_2^{(m)T} & \dots & e_n^{(n)} \otimes e_2^{(m)T} \\ \vdots & \vdots & \ddots & \vdots \\ e_1^{(n)} \otimes e_m^{(m)T} & e_2^{(n)} \otimes e_m^{(m)T} & \dots & e_n^{(n)} \otimes e_m^{(m)T} \end{bmatrix} = \begin{bmatrix} I_n \otimes e_1^{(m)T} \\ I_n \otimes e_2^{(m)T} \\ \vdots \\ I_n \otimes e_m^{(m)T} \end{bmatrix}.$$

Lemma 3.5 ([Fac05, Bro11]) *Let $A \in \mathbb{R}^{p\times m}$, $B \in \mathbb{R}^{n\times q}$ and $G \in \mathbb{R}^{m\times n}$. Then, the permutation matrix $\mathcal{P}_{m,n}$ has the following properties:*

(a) $\mathcal{P}_{m,n}^T \mathcal{P}_{m,n} = \mathcal{P}_{m,n}\mathcal{P}_{m,n}^T = I_{mn}$

(b) $\mathcal{P}_{m,n}^T = \mathcal{P}_{n,m}$

(c) $\mathcal{P}_{m,n}\operatorname{vec} G = \operatorname{vec} G^T$

(d) $\mathcal{P}_{n,p}(A \otimes B)\mathcal{P}_{m,q} = B \otimes A$

Proof: Items (a) and (b) follow directly from the definition of $\mathcal{P}_{m,n}$. To prove item (c), write the vectorization operation as

$$\operatorname{vec} G = \begin{bmatrix} Ge_1^{(n)} \\ Ge_2^{(n)} \\ \vdots \\ Ge_n^{(n)} \end{bmatrix}, \quad \operatorname{vec} G^T = \begin{bmatrix} G^T e_1^{(m)} \\ G^T e_2^{(m)} \\ \vdots \\ G^T e_m^{(m)} \end{bmatrix}. \tag{3.2}$$

Then, using Definition (3.4) the k-th block of the product $\mathcal{P}_{m,n}\mathrm{vec}\, G$ writes

$$\begin{aligned}\left[\mathcal{P}_{m,n}\mathrm{vec}\, G\right]_k &\stackrel{\text{def}}{=} \begin{bmatrix} e_1^{(n)} \otimes e_k^{(m)T} & e_2^{(n)} \otimes e_k^{(m)T} & \dots & e_n^{(n)} \otimes e_k^{(m)T} \end{bmatrix} \mathrm{vec}\, G \\ &= \sum_{i=1}^{n} \left(e_i^{(n)} \otimes e_k^{(m)T} \right) G e_i^{(n)}.\end{aligned}$$

From $Ge_i^{(n)} = \mathrm{vec}(Ge_i^{(n)})$ and with property (3.1) follows

$$\begin{aligned}\left[\mathcal{P}_{m,n}\mathrm{vec}\, G\right]_k &= \sum_{i=1}^{n} \mathrm{vec}\left(e_k^{(m)T} \left(G e_i^{(n)} \right) e_i^{(n)T} \right) \\ &= \mathrm{vec}\left(e_k^{(m)T} G \sum_{i=1}^{n} e_i^{(n)} e_i^{(n)T} \right) \\ &= \mathrm{vec}\left(e_k^{(m)T} G \right).\end{aligned}$$

As $\left(e_k^{(m)T} G\right)$ is a row vector, its transposed is $\mathrm{vec}\left(e_k^{(m)T} G\right)$ and thus

$$\left[\mathcal{P}_{m,n}\mathrm{vec}\, G\right]_k = G^T e_k^{(m)}.$$

Comparing this result with the k-th block of $\mathrm{vec}\, G^T$ in (3.2) proves (c).

The proof of (d) is stated from [Fac05]: Let $C \in \mathbb{R}^{m\times q}$ be an arbitrary matrix. Then, with property (3.1) and (c) it follows

$$\begin{aligned}\mathcal{P}_{n,p}(A \otimes B)\mathcal{P}_{m,q}\mathrm{vec}\, C &= \mathcal{P}_{n,p}(A \otimes B)\mathrm{vec}\, C^T \\ &= \mathcal{P}_{n,p}\mathrm{vec}\left(BC^TA^T\right) \\ &= \mathrm{vec}\left(ACB^T\right) \\ &= (B \otimes A)\mathrm{vec}\, C.\end{aligned}$$

The fact that C is arbitrary finishes the proof. □

Remark 3.6 *The matrix $\mathcal{P}_{m,n}$ coincides with the matrix*

$$\mathcal{P} = \sum_{k_1=1}^{m} \sum_{k_2=1}^{n} E_{k_1,k_2}^{m,n} \otimes E_{k_2,k_1}^{n,m}$$

defined in [PGS07, RPDR08], where $E_{k_1,k_2}^{m,n} \in \{0,1\}^{m\times n}$ are matrices whose entries are zeros, except the entry at position (k_1, k_2) which is one.

3.3 Some numerical tools

3.3.1 Iterative QR decompositions

In some cases, thin QR decompositions of a large matrix $G \in \mathbb{R}^{m,n}$ with $m \gg n$ are necessary, where only matrix R is needed. With the following lemma, the QR decomposition of G is done iteratively on blocks of G, while in each step only the R part needs to be saved in order to obtain the corresponding R part of G.

Lemma 3.7 *Let $G_0, \ldots, G_J$, where $G_j \in \mathbb{R}^{m_j \times n}$ for $j = 0, \ldots, J$, be the $J+1$ block rows of a matrix*

$$G = \begin{bmatrix} G_0 \\ \vdots \\ G_J \end{bmatrix} \in \mathbb{R}^{m \times n},$$

where $m_0 \geq n$ and G_0 is full column rank. Let the thin QR decompositions

$$G_0 = Q_0 R_0, \tag{3.3}$$

$$\begin{bmatrix} R_{j-1} \\ G_j \end{bmatrix} = Q_j R_j, \quad j = 1, \ldots, J \tag{3.4}$$

be given iteratively, where R_j, $j = 0, \ldots, J$, are invertible matrices. Let

$$Q \stackrel{\text{def}}{=} \begin{bmatrix} Q_0 & 0 \\ 0 & I_{l_0} \end{bmatrix} \begin{bmatrix} Q_1 & 0 \\ 0 & I_{l_1} \end{bmatrix} \cdots \begin{bmatrix} Q_{J-1} & 0 \\ 0 & I_{l_{J-1}} \end{bmatrix} Q_J, \tag{3.5}$$

$$R \stackrel{\text{def}}{=} R_J, \tag{3.6}$$

where I_{l_j} are identity matrices of appropriate size. Then, a thin QR decomposition of G is given by

$$G = QR.$$

Proof: The relation $G = QR$ follows from post-multiplying (3.5) with $R = R_J$, then substituting (3.4) in backward order for $j = J, \ldots, 1$ and substituting (3.3) in the last step. R_0 is an invertible matrix, because G_0 is full column rank, and it follows iteratively from (3.4) that all the R_j, $j = 1, \ldots, J$, are invertible. As the factors in (3.5) have orthogonal columns, Q also has orthogonal columns. Furthermore, $R = R_J$ is upper triangular as it yields the QR decomposition (3.4) for $j = J$. Thus, $G = QR$ is effectively a QR decomposition of G. □

With the iterative QR decomposition of G, the least-squares solution of a large system of equations $GA = H$ can be obtained iteratively, where $G, H \in \mathbb{R}^{m \times n}$ and $A \in \mathbb{R}^{n \times n}$ with $m \gg n$.

Lemma 3.8 *Let $G_0, \dots, G_J$ and $H_0, \dots, H_J$, where $G_j, H_j \in \mathbb{R}^{m_j \times n}$ for $j = 0, \dots, J$, be the $J+1$ block rows of the matrices*

$$G = \begin{bmatrix} G_0 \\ \vdots \\ G_J \end{bmatrix}, \quad H = \begin{bmatrix} H_0 \\ \vdots \\ H_J \end{bmatrix},$$

where $G, H \in \mathbb{R}^{m \times n}$, $m_0 \geq n$ and G_0 is full column rank. Let the thin QR decompositions and products

$$G_0 = Q_0 R_0, \qquad S_0 \stackrel{\text{def}}{=} Q_0^T H_0, \tag{3.7}$$

$$\begin{bmatrix} R_{j-1} \\ G_j \end{bmatrix} = Q_j R_j, \qquad S_j \stackrel{\text{def}}{=} Q_j^T \begin{bmatrix} S_{j-1} \\ H_j \end{bmatrix}, \qquad j = 1, \dots, J \tag{3.8}$$

be given iteratively. Then, the least squares solution of

$$GA = H \tag{3.9}$$

is given by

$$A = R_J^{-1} S_J.$$

Proof: From Lemma 3.7 follows that

$$G = QR_J, \quad \text{where} \quad Q = \begin{bmatrix} Q_0 & 0 \\ 0 & I_{l_0} \end{bmatrix} \begin{bmatrix} Q_1 & 0 \\ 0 & I_{l_1} \end{bmatrix} \cdots \begin{bmatrix} Q_{J-1} & 0 \\ 0 & I_{l_{J-1}} \end{bmatrix} Q_J,$$

is a QR decomposition of G and R_J is invertible. Thus, the solution of the least squares problem (3.9) is

$$\begin{aligned} A &= R_J^{-1} Q^T H \\ &= R_J^{-1} Q_J^T \begin{bmatrix} Q_{J-1}^T & 0 \\ 0 & I_{l_{J-1}} \end{bmatrix} \cdots \begin{bmatrix} Q_1^T & 0 \\ 0 & I_{l_1} \end{bmatrix} \begin{bmatrix} Q_0^T & 0 \\ 0 & I_{l_0} \end{bmatrix} \begin{bmatrix} H_0 \\ H_1 \\ \vdots \\ H_J \end{bmatrix} \\ &= R_J^{-1} Q_J^T \begin{bmatrix} Q_{J-1}^T & 0 \\ 0 & I_{l_{J-1}} \end{bmatrix} \cdots \begin{bmatrix} Q_1^T & 0 \\ 0 & I_{l_1} \end{bmatrix} \begin{bmatrix} Q_0^T H_0 \\ H_1 \\ \vdots \\ H_J \end{bmatrix} \end{aligned}$$

Plugging in (3.7) and doing the multiplications in this product from the right to the left, where at each step (3.8) is plugged in, leads to the assertion. □

Note that Lemma 3.7 can be applied to the LQ decomposition of data matrices for data-driven subspace-based system identification in Section 2.2.3. For example, in (2.13) the LQ decomposition is done of a matrix with possibly a very large number of columns. In the case of lots of available data, this LQ decomposition may not be feasible anymore. As the factor Q is not needed, Lemma 3.7 can be applied to the transposed data matrix, without keeping the matrices Q_j on the way.

Lemma 3.8 will be useful in Chapters 4 and 5 for an iterative solution of the least squares problem for the state transition matrix.

3.3.2 Efficient computation of singular vector sensitivities

Let $u_1, \ldots, u_n$ and $v_1, \ldots, v_n$ be the first n left and right singular vectors of an estimated matrix $Z \in \mathbb{R}^{a,b}$ with $a \geq b \geq n$, and $U_1 = \begin{bmatrix} u_1 & \ldots & u_n \end{bmatrix}$ and $V_1 = \begin{bmatrix} v_1 & \ldots & v_n \end{bmatrix}$. Analogously, let $\sigma_1, \ldots, \sigma_n$ be the first n singular values of Z, such that the thin SVD of Z is given by

$$Z = \begin{bmatrix} U_1 & U_0 \end{bmatrix} \begin{bmatrix} S_1 & 0 \\ 0 & S_0 \end{bmatrix} \begin{bmatrix} V_1^T \\ V_0^T \end{bmatrix}, \tag{3.10}$$

where $S_1 = \operatorname{diag}(\sigma_1, \ldots, \sigma_n)$. The aim of this section is to compute *sensitivity matrices* $\mathcal{J}_{U_1}$ and $\mathcal{J}_{V_1}$ that link small perturbations in Z to the singular vectors in U_1 and V_1.

Assume Z as a smooth and bounded matrix function of an artificial scalar variable, where $Z(0)$ is the "true value" of Z and $Z(t)$ is a perturbed (estimated) value of Z, where t is small. Let M be a placeholder for any matrix from the SVD in (3.10), in particular $M \in \{U_1, V_1\}$, which of course depends on Z. Then, the matrix M can be analogously expressed as $M = M(t)$ when computed from an estimated Z, while $M(0)$ is their true but unknown value. Using the Taylor expansion

$$M(t) = M(0) + t\dot{M}(0) + O(t^2),$$

a first-order perturbation is denoted by $\Delta M \stackrel{\text{def}}{=} t\dot{M}(0) \approx M(t) - M(0)$ for small t [PGS07, RPDR08].

In this section, an efficient computation of the sensitivities $\mathcal{J}_{U_1}$ and $\mathcal{J}_{V_1}$ of the left and right singular vectors is derived in Proposition 3.11. These sensitivities are defined by the relations

$$\Delta(\operatorname{vec} U_1) = \mathcal{J}_{U_1} \Delta(\operatorname{vec} Z), \quad \Delta(\operatorname{vec} V_1) = \mathcal{J}_{V_1} \Delta(\operatorname{vec} Z)$$

and are finally used to express the covariances of the singular vectors using the covariance of Z: It holds for $M \in \{U_1, V_1\}$

$$\begin{aligned} \operatorname{cov}(\operatorname{vec} M) &= \operatorname{cov}(\operatorname{vec} M(t)) = \operatorname{cov}(\operatorname{vec} M(t) - \operatorname{vec} M(0)) \\ &\approx \operatorname{cov}\Delta(\operatorname{vec} M) = \operatorname{cov}\Delta(\mathcal{J}_M \operatorname{vec} Z) \\ &\approx \operatorname{cov}(\mathcal{J}_M \operatorname{vec} Z) \end{aligned}$$

and thus

$$\operatorname{cov}(\operatorname{vec} U_1) = \mathcal{J}_{U_1} \operatorname{cov}(\operatorname{vec} Z)\, \mathcal{J}_{U_1}^T, \quad \operatorname{cov}(\operatorname{vec} V_1) = \mathcal{J}_{V_1} \operatorname{cov}(\operatorname{vec} Z)\, \mathcal{J}_{V_1}^T.$$

This result will be used in Section 6.5.

The efficient sensitivity computations are based on results obtained in [PGS07, RPDR08]. Pintelon et al. [PGS07] derived the sensitivities of the singular vectors of a matrix Z as stated in the following proposition.

Proposition 3.9 ([PGS07]) *Define*

$$E_j \stackrel{\text{def}}{=} \begin{bmatrix} I_a & -\dfrac{Z}{\sigma_j} \\ -\dfrac{Z^T}{\sigma_j} & I_b \end{bmatrix}, \quad F_j \stackrel{\text{def}}{=} \frac{1}{\sigma_j} \begin{bmatrix} v_j^T \otimes (I_a - u_j u_j^T) \\ (u_j^T \otimes (I_b - v_j v_j^T))\mathcal{P}_{a,b} \end{bmatrix}, \tag{3.11}$$

where $\mathcal{P}_{a,b}$ is defined in Definition 3.4. Then, the sensitivity of the stacked j-th left and right singular vector of Z is a solution of

$$E_j \begin{bmatrix} \Delta u_j \\ \Delta v_j \end{bmatrix} = F_j \, \Delta(\operatorname{vec} Z). \tag{3.12}$$

As E_j is a rank deficient matrix with rank $a + b - 1$, one possible solution of (3.12) is $E_j^\dagger F_j$ and the following result was derived in [RPDR08].

Proposition 3.10 ([RPDR08]) *Following Proposition 3.9, the sensitivities $\mathcal{J}_{U_1}$ and $\mathcal{J}_{V_1}$ write as*

$$\mathcal{J}_{U_1} = S_1 \begin{bmatrix} E_1^\dagger F_1 \\ \vdots \\ E_n^\dagger F_n \end{bmatrix}, \quad \mathcal{J}_{V_1} = S_2 \begin{bmatrix} E_1^\dagger F_1 \\ \vdots \\ E_n^\dagger F_n \end{bmatrix},$$

where S_1 and S_2 are selection matrices with $S_1 = I_n \otimes \begin{bmatrix} I_a & 0_{a,b} \end{bmatrix}$, $S_2 = I_n \otimes \begin{bmatrix} 0_{b,a} & I_b \end{bmatrix}$.

Using an orthogonality property of the singular vectors in the computation of the sensitivities $\mathcal{J}_{U_1}$ and $\mathcal{J}_{V_1}$, the block structure of the matrices E_j can be exploited for their inversion. This leads to a more efficient computation of the sensitivities in the following proposition.

Proposition 3.11 *Define*

$$K_j \stackrel{\text{def}}{=} \left(I_b + \begin{bmatrix} 0_{b-1,b} \\ 2v_j^T \end{bmatrix} - \frac{Z^T Z}{\sigma_j^2} \right)^{-1}, \tag{3.13}$$

$$\widetilde{E}_j \stackrel{\text{def}}{=} \begin{bmatrix} I_a + \dfrac{Z}{\sigma_j} K_j \left(\dfrac{Z^T}{\sigma_j} - \begin{bmatrix} 0_{b-1,a} \\ u_j^T \end{bmatrix} \right) & \dfrac{Z}{\sigma_j} K_j \end{bmatrix}, \tag{3.14}$$

$$\widetilde{G}_j \stackrel{\text{def}}{=} \begin{bmatrix} K_j \left(\dfrac{Z^T}{\sigma_j} - \begin{bmatrix} 0_{b-1,a} \\ u_j^T \end{bmatrix} \right) & K_j \end{bmatrix}, \tag{3.15}$$

$$\widetilde{F}_j \stackrel{\text{def}}{=} \frac{1}{\sigma_j} \begin{bmatrix} v_j^T \otimes (I_a - u_j u_j^T) \\ (I_b - v_j v_j^T) \otimes u_j^T \end{bmatrix}. \tag{3.16}$$

Then, the sensitivities $\mathcal{J}_{U_1}$ and $\mathcal{J}_{V_1}$ write

$$\mathcal{J}_{U_1} = \begin{bmatrix} \widetilde{E}_1 \widetilde{F}_1 \\ \vdots \\ \widetilde{E}_n \widetilde{F}_n \end{bmatrix}, \quad \mathcal{J}_{V_1} = \begin{bmatrix} \widetilde{G}_1 \widetilde{F}_1 \\ \vdots \\ \widetilde{G}_n \widetilde{F}_n \end{bmatrix}. \tag{3.17}$$

Proof: From (3.12) follows that Δu_j and Δv_j satisfy the condition

$$E_j \begin{bmatrix} \Delta u_j \\ \Delta v_j \end{bmatrix} = F_j \, \Delta(\operatorname{vec} Z),$$

where E_j and F_j are defined in (3.11). As the singular vectors u_j and v_j, $j = 1, \ldots, n$, are orthonormal, they satisfy $u_j^T u_j = 1$ and $v_j^T v_j = 1$. It follows $u_j^T \Delta u_j = 0$ and $v_j^T \Delta v_j = 0$ and thus the condition $u_j^T \Delta u_j + v_j^T \Delta v_j = 0$ can be added to the system of equations for Δu_j and Δv_j, which was also suggested in [PGS07]. If Z is full column rank, this leads to a system of full column rank. Without loss of generality, this condition can be added to the last row of the matrices in (3.12) and a solution writes as

$$\begin{bmatrix} \Delta u_j \\ \Delta v_j \end{bmatrix} = \left(E_j + \begin{bmatrix} 0_{c,a} & 0_{c,b} \\ u_j^T & v_j^T \end{bmatrix} \right)^{-1} F_j \, \Delta(\operatorname{vec} Z), \tag{3.18}$$

where $c = a + b - 1$. The block matrix inversion formula is used for this matrix inversion. Define

$$\begin{bmatrix} O & P \\ Q & R \end{bmatrix} \stackrel{\text{def}}{=} E_j + \begin{bmatrix} 0_{c,a} & 0_{c,b} \\ u_j^T & v_j^T \end{bmatrix},$$

where

$$O \stackrel{\text{def}}{=} I_a, \quad P \stackrel{\text{def}}{=} -\frac{Z}{\sigma_j}, \quad Q \stackrel{\text{def}}{=} -\frac{Z^T}{\sigma_j} + \begin{bmatrix} 0_{b-1,a} \\ u_j^T \end{bmatrix}, \quad R \stackrel{\text{def}}{=} I_b + \begin{bmatrix} 0_{b-1,b} \\ v_j^T \end{bmatrix}.$$

With the block matrix inversion formula follows

$$\begin{bmatrix} O & P \\ Q & R \end{bmatrix}^{-1} = \begin{bmatrix} O^{-1} + O^{-1} P S_O^{-1} Q O^{-1} & -O^{-1} P S_O^{-1} \\ -S_O^{-1} Q O^{-1} & S_O^{-1} \end{bmatrix},$$

where $S_O \stackrel{\text{def}}{=} R - Q O^{-1} P$ and thus

$$S_O = I_b + \begin{bmatrix} 0_{b-1,b} \\ v_j^T \end{bmatrix} - \left(-\frac{Z^T}{\sigma_j} + \begin{bmatrix} 0_{b-1,a} \\ u_j^T \end{bmatrix} \right) \left(-\frac{Z}{\sigma_j} \right) = I_b + \begin{bmatrix} 0_{b-1,b} \\ v_j^T \end{bmatrix} + \begin{bmatrix} 0_{b-1,b} \\ u_j^T Z / \sigma_j \end{bmatrix} - \frac{Z^T Z}{\sigma_j^2}.$$

From $u_j^T Z / \sigma_j = v_j^T$ and with K_j defined in (3.13) follows $K_j = S_O^{-1}$. Then, from (3.14) and (3.15) follows

$$\left(E_j + \begin{bmatrix} 0_{c,a} & 0_{c,b} \\ u_j^T & v_j^T \end{bmatrix} \right)^{-1} = \begin{bmatrix} \widetilde{E}_j \\ \widetilde{G}_j \end{bmatrix}. \tag{3.19}$$

It remains to show $\widetilde{F}_j = F_j$ with F_j in (3.11) and $\widetilde{F}_j$ in (3.16). This follows from Lemma 3.5(d): It holds

$$\mathcal{P}_{b,1}(u_j^T \otimes (I_b - v_j v_j^T))\mathcal{P}_{a,b} = (I_b - v_j v_j^T) \otimes u_j^T.$$

From Definition 3.4 follows $\mathcal{P}_{b,1} = I_b$ and thus $\widetilde{F}_j = F_j$. Then, the assertion follows together with (3.18) and (3.19). □

Note that in Proposition 3.11 a matrix inversion only happens when computing K_j, which is of size $b \times b$. Compared to Proposition 3.10, where the pseudoinverse of matrices of size $(a+b) \times (a+b)$ is computed, the new computation in Proposition 3.11 is a significant improvement. It is of use when applied to the sensitivity computation of subspace matrices of size $a \times b = (p+1)r \times qr_0$ in Section 6.5 for a residual based on the left singular vectors in U_1, where usually $a > b$. Moreover, this computation is a significant time and memory improvement in the confidence interval computation of modal parameters from [RPDR08] and is applied in Section 9.2.5.

3.4 Remarks on theoretical properties of fault detection test

3.4.1 Jacobian computation

In Section 2.3.3.2, the asymptotic Jacobian of the subspace-based residual was derived in two ways, depending on the derived variable. In the first computation, the Jacobian $\mathcal{J}(\theta_0)$ depends on $\mathcal{S}'(\theta_0)$, which is a solution of (2.42). This equation results from the condition $S(\theta_0)^T \mathcal{O}_{p+1}(\theta_0) = 0$. However, the system of equations (2.42) is under-determined and additional conditions should be taken into account. From $S(\theta_0)^T S(\theta_0) = I_s$ results a further condition.

Lemma 3.12 *Define*

$$J_S(\theta) \stackrel{\text{def}}{=} \left(S(\theta)^T \otimes I_s\right) + \begin{bmatrix} S(\theta)^T \otimes e_1^{(s)T} \\ \vdots \\ S(\theta)^T \otimes e_s^{(s)T} \end{bmatrix},$$

where $e_j^{(s)} \in \mathbb{R}^s$ are the unit vectors. Then, a necessary condition for $S(\theta_0)^T S(\theta_0) = I_s$ is

$$J_S(\theta_0)\mathcal{S}'(\theta_0) = 0. \tag{3.20}$$

This condition is already fulfilled by the solution

$$\mathcal{S}'(\theta_0) = -\left(\left(\mathcal{O}_{p+1}(\theta_0)^T\right)^\dagger \otimes I_s\right)\left(I_n \otimes S(\theta_0)^T\right)\mathcal{O}'_{p+1}(\theta_0)$$

in (2.43).

Proof: From $S(\theta_0)^T S(\theta_0) = I_s$ follows the necessary condition

$$\frac{\partial}{\partial\theta}\mathrm{vec}\left(S(\theta)^T S(\theta)\right) = \left(S(\theta)^T \otimes I_s\right)\frac{\partial \mathrm{vec}\, S(\theta)^T}{\partial\theta} + \left(I_s \otimes S(\theta)^T\right)\frac{\partial \mathrm{vec}\, S(\theta)}{\partial\theta} = 0. \tag{3.21}$$

As $\mathcal{S}'(\theta_0)$ is defined as

$$\mathcal{S}'(\theta) = \frac{\partial \mathrm{vec}\, S(\theta)^T}{\partial\theta},$$

the derivative $\partial\,\mathrm{vec}(S(\theta))/\partial\theta$ has to be expressed in terms of $\mathcal{S}'(\theta)$. Using the conclusions of Lemma 3.5, it follows

$$\frac{\partial \mathrm{vec}\, S(\theta)}{\partial\theta} = \mathcal{P}^T_{(p+1)r,s}\frac{\partial \mathrm{vec}\, S(\theta)^T}{\partial\theta}, \quad \text{where} \quad \mathcal{P}_{a,b} = \begin{bmatrix} I_b \otimes e_1^{(a)T} \\ I_b \otimes e_2^{(a)T} \\ \vdots \\ I_b \otimes e_a^{(a)T} \end{bmatrix}$$

with the unit vectors $e_j^{(a)} \in \mathbb{R}^a$ defined in Definition 3.4. Then, condition (3.21) is equivalent to

$$\frac{\partial}{\partial\theta}\mathrm{vec}\left(S(\theta)^T S(\theta)\right) = \left(\left(S(\theta)^T \otimes I_s\right) + \left(I_s \otimes S(\theta)^T\right)\mathcal{P}^T_{(p+1)r,s}\right)\mathcal{S}'(\theta) = 0. \tag{3.22}$$

From Lemma 3.5(a) and (d) follows

$$\begin{aligned}
\left(I_s \otimes S(\theta)^T\right)\mathcal{P}^T_{(p+1)r,s} &= \mathcal{P}_{s,s}\left(S(\theta)^T \otimes I_s\right)\mathcal{P}_{(p+1)r,s}\mathcal{P}^T_{(p+1)r,s} \\
&= \mathcal{P}_{s,s}\left(S(\theta)^T \otimes I_s\right) \\
&= \begin{bmatrix} I_s \otimes e_1^{(s)T} \\ \vdots \\ I_s \otimes e_s^{(s)T} \end{bmatrix}\left(S(\theta)^T \otimes I_s\right) \\
&= \begin{bmatrix} S(\theta)^T \otimes e_1^{(s)T} \\ \vdots \\ S(\theta)^T \otimes e_s^{(s)T} \end{bmatrix}.
\end{aligned}$$

Plugging this into (3.22), a necessary condition for $S(\theta_0)^T S(\theta_0) = I_s$ writes thus

$$\left(\left(S(\theta_0)^T \otimes I_s\right) + \begin{bmatrix} S(\theta_0)^T \otimes e_1^{(s)T} \\ \vdots \\ S(\theta_0)^T \otimes e_s^{(s)T} \end{bmatrix}\right)\mathcal{S}'(\theta_0) = 0.$$

Let $\mathcal{O}_{p+1}(\theta_0) = U_1\Delta_1 V_1^T$ be a thin SVD of $\mathcal{O}_{p+1}(\theta_0)$. Then, $\mathcal{O}_{p+1}(\theta_0)^T = V_1\Delta_1 U_1^T$ and hence $\left(\mathcal{O}_{p+1}(\theta_0)^T\right)^\dagger = U_1\Delta_1^{-1}V_1^T$. Thus, $\mathcal{O}_{p+1}(\theta_0)$ and $\left(\mathcal{O}_{p+1}(\theta_0)^T\right)^\dagger$ have the same left null space.

As $S(\theta_0)^T \mathcal{O}_{p+1}(\theta_0) = 0$ it follows $S(\theta_0)^T \left(\mathcal{O}_{p+1}(\theta_0)^T\right)^\dagger = 0$ and thus

$$\left(\left(S(\theta_0)^T \otimes I_s\right) + \begin{bmatrix} S(\theta_0)^T \otimes e_1^{(s)T} \\ \vdots \\ S(\theta_0)^T \otimes e_s^{(s)T} \end{bmatrix} \right) \left(\left(\mathcal{O}_{p+1}(\theta_0)^T\right)^\dagger \otimes I_s \right) = 0,$$

which concludes the proof. □

Thus, conditions (2.42) and (3.20) lead to a square system of equations for $\mathcal{S}'(\theta_0)$

$$\left(\mathcal{O}_{p+1}(\theta_0)^T \otimes I_s\right) \mathcal{S}'(\theta_0) = -\left(I_n \otimes S(\theta_0)^T\right) \mathcal{O}'_{p+1}(\theta_0), \tag{3.23}$$

$$J_S(\theta_0)\mathcal{S}'(\theta_0) = 0, \tag{3.24}$$

where the first equation results from differentiating $S(\theta_0)^T\mathcal{O}(\theta_0) = 0$ with respect to θ_0 and the second equation results from differentiating $S(\theta_0)^T S(\theta_0) = I_s$. Note that condition $(I_s \otimes S(\theta_0)^T)\mathcal{S}'(\theta_0) = 0$ stated in [BAB00] does not result from differentiating $S(\theta_0)^T S(\theta_0) = I_s$.

The system (3.23)–(3.24) is in general not of full rank, as the matrix $J_S(\theta_0)$ is in general not full row rank. In Section 2.3.3.2 and Lemma 3.12 it was shown that one of the solutions of this system is (2.43). Fortunately, the solution $\mathcal{S}'(\theta_0)$ does not need to be unique in order to get a unique Jacobian $\mathcal{J}(\theta_0)$ in (2.41) with

$$\mathcal{J}(\theta_0) = -\left(\mathcal{H}_{p+1,q}^T \otimes I_s\right) \mathcal{S}'(\theta_0),$$

as stated in the following lemma.

Lemma 3.13 ([BAB97, BAB00]) *The Jacobian* $\mathcal{J}(\theta_0) = -\left(\mathcal{H}_{p+1,q}^T \otimes I_s\right) \mathcal{S}'(\theta_0)$ *is well-defined and does not depend on a particular solution* $\mathcal{S}'(\theta_0)$ *satisfying* (3.23).

Proof: Any element in the left null space of $\mathcal{O}_{p+1}(\theta_0)$ is also in the left null space of $\mathcal{H}_{p+1,q}$ and thus

$$\ker\left(\mathcal{O}_{p+1}(\theta_0)^T \otimes I_s\right) \subset \ker\left(\mathcal{H}_{p+1,q}^T \otimes I_s\right). \tag{3.25}$$

Assume two solutions $\mathcal{S}'_1(\theta_0)$ and $\mathcal{S}'_2(\theta_0)$ of (3.23). Then,

$$\left(\mathcal{O}_{p+1}(\theta_0)^T \otimes I_s\right) \mathcal{S}'_2(\theta_0) - \left(\mathcal{O}_{p+1}(\theta_0)^T \otimes I_s\right) \mathcal{S}'_1(\theta_0) = 0.$$

Thus $\mathcal{S}'_2(\theta_0) - \mathcal{S}'_1(\theta_0) \in \ker\left(\mathcal{O}_{p+1}(\theta_0)^T \otimes I_s\right)$ and because of (3.25) it holds $\mathcal{S}'_2(\theta_0) - \mathcal{S}'_1(\theta_0) \in \ker\left(\mathcal{H}_{p+1,q}^T \otimes I_s\right)$. It follows

$$\begin{aligned} -\left(\mathcal{H}_{p+1,q}^T \otimes I_s\right) \mathcal{S}'_1(\theta_0) &= -\left(\mathcal{H}_{p+1,q}^T \otimes I_s\right) \left(\mathcal{S}'_1(\theta_0) + (\mathcal{S}'_2(\theta_0) - \mathcal{S}'_1(\theta_0))\right) \\ &= -\left(\mathcal{H}_{p+1,q}^T \otimes I_s\right) \mathcal{S}'_2(\theta_0), \end{aligned}$$

showing that $\mathcal{J}(\theta_0)$ is well-defined. □

3.4.2 Weighting matrices and invariance property

In Section 2.3, the subspace-based fault detection test was introduced for the covariance-driven subspace matrix $\mathcal{H}_{p+1,q}$ with the factorization property $\mathcal{H}_{p+1,q} = \mathcal{O}_{p+1}\mathcal{Z}_q$. In a more general setting, the same algorithm can be written using invertible weighting matrices W_1 and W_2 for a subspace matrix $W_1\mathcal{H}_{p+1,q}W_2$ as in [BAB97, Bas99, BAB00]. Then, an invariance property holds, namely that the corresponding χ^2-test statistics is the same, either using the weighting matrices or not. In this section, special care is taken about this invariance property as there is a slight incoherence in the respective results of [BAB97, Bas99, BAB00].

Use the notation of Section 2.3 for a test corresponding to subspace matrix $\mathcal{H}_{p+1,q}$, where

$$\zeta_N(\theta_0) = \sqrt{N}\,\mathrm{vec}\left(S(\theta_0)^T\widehat{\mathcal{H}}_{p+1,q}\right),$$

and $S(\theta_0)$ is defined such that $S(\theta_0)^T\mathcal{O}_{p+1}(\theta_0) = 0$. For subspace matrix $W_1\mathcal{H}_{p+1,q}W_2$, define

$$\zeta_{N;W_1,W_2}(\theta_0) \stackrel{\text{def}}{=} \sqrt{N}\,\mathrm{vec}\left(S_{W_1}(\theta_0)^T W_1\widehat{\mathcal{H}}_{p+1,q}W_2\right),$$

where $S_{W_1}(\theta_0)$ is defined such that $S_{W_1}(\theta_0)^T W_1\mathcal{O}_{p+1}(\theta_0) = 0$. Then, there exists a unique invertible matrix T_{W_1} such that [BAB97]

$$S_{W_1}(\theta_0)^T W_1 = T_{W_1}S(\theta_0)^T,$$

as both $W_1^T S_{W_1}(\theta_0)$ and $S(\theta_0)$ are left null spaces of $\mathcal{O}_{p+1}(\theta_0)$. Then it follows

$$\zeta_{N;W_1,W_2}(\theta_0) = (W_2^T \otimes T_{W_1})\zeta_N(\theta_0). \tag{3.26}$$

Thus, with Lemma 2.4 follows that the χ^2-test statistics is the same, either using residual function $\zeta_N(\theta_0)$ or the residual function $\zeta_{N;W_1,W_2}(\theta_0)$ on the weighted subspace matrix. This also justifies why a left weighting matrix of the subspace matrix is omitted in the damage detection algorithms.

Remark 3.14 *To show the invariance property based on a relation like* (3.26)*, in [Bas99, BAB00] an invertible matrix* T_1 *is used with the property*

$$S(\theta_0)^T W_1 = T_1 S(\theta_0)^T. \tag{3.27}$$

Postmultiplying this equation with $S(\theta_0)$ *leads to*

$$T_1 = S(\theta_0)^T W_1 S(\theta_0)$$

as the only possible solution of (3.27)*. However, this is in general not a solution of* (3.27)*. A solution of* (3.27) *only exists, if* $S(\theta_0)S(\theta_0)^T W_1^T S(\theta_0) = W_1^T S(\theta_0)$*, i.e.* $W_1^T S(\theta_0)$ *is in the range of* $S(\theta_0)$*. This is the case, if* W_1 *is a multiple of the identity matrix.*

3.5 Practical issues of fault detection test

3.5.1 Numerical robustness of χ^2-test

In this section, special care is taken of numerical aspects of the computation of the χ^2-test statistics that are used for subspace-based fault detection, as matrix inversions of big and sometimes rank deficient matrices are involved. They appear for example in (2.39), (2.52), (6.13), (6.14), (6.16), (6.21), (6.24) and are always of the form

$$\chi^2 = \zeta^T \Sigma^{-1} \mathcal{J} (\mathcal{J}^T \Sigma^{-1} \mathcal{J})^{-1} \mathcal{J}^T \Sigma^{-1} \zeta \tag{3.28}$$

or, in the non-parametric version,

$$\chi^2 = \zeta^T \Sigma^{-1} \zeta. \tag{3.29}$$

Here we consider only the numerical properties of their computation and thus skip all subscripts and superscripts of χ^2, ζ, $\mathcal{J}$ and Σ. Let c be the dimension of the underlying system parameter θ in $\zeta = \zeta(\theta)$ and d the dimension of ζ, such that $\mathcal{J} \in \mathbb{R}^{d \times c}$ and $\Sigma \in \mathbb{R}^{d \times d}$.

In all computations, the covariance matrix Σ is not necessarily considered positive definite, as for an empirical estimate $\widehat{\Sigma}$ the number of samples might not be sufficient to ensure full rank of $\widehat{\Sigma}$. In this case, we assume the use of pseudoinverses, as it might be the only possibility to compute the χ^2-test statistics in practice when using real data.

Assumption 3.15 *If Σ is rank deficient, the χ^2-test statistics* (3.28) *and* (3.29) *can be approximated by*

$$\chi^2 = \zeta^T \Sigma^\dagger \mathcal{J} (\mathcal{J}^T \Sigma^\dagger \mathcal{J})^\dagger \mathcal{J}^T \Sigma^\dagger \zeta \tag{3.30}$$

and, in the non-parametric version,

$$\chi^2 = \zeta^T \Sigma^\dagger \zeta. \tag{3.31}$$

First, results from [ZB03] for a numerical stable computation of the χ^2-test are extended in Lemma 3.16 and rank conditions on the involved matrices are derived in Corollary 3.17. Second, an efficient computation of the square root inverse of the covariance matrix using sampled data is derived in Proposition 3.19, which takes a key role in the computation of the χ^2-test.

Let $\Sigma^{-1/2} \in \mathbb{R}^{e \times d}$ be a square root (pseudo-)inverse of the covariance matrix, such that

$$\Sigma^{-1} = (\Sigma^{-1/2})^T \Sigma^{-1/2},$$

if Σ is full rank, or

$$\Sigma^\dagger = (\Sigma^{-1/2})^T \Sigma^{-1/2}$$

in the rank deficient case. Note that in the full rank case, the dimensions of $\Sigma^{-1/2}$ yield $e \geq d$. In the rank deficient case, only $e \geq \operatorname{rank}(\Sigma)$ holds and thus $e < d$ is possible.

Lemma 3.16 *If*

$$\Sigma^{-1/2} \mathcal{J} \quad \textit{is full column rank,} \tag{3.32}$$

the χ^2-tests (3.28) *and* (3.30) *write as*

$$\chi^2 = \xi^T \xi \quad \textit{with} \quad \xi = Q^T \Sigma^{-1/2} \zeta \in \mathbb{R}^c, \tag{3.33}$$

where Q is obtained from the thin QR decomposition of $\Sigma^{-1/2}\mathcal{J} = QR$.

Proof: From (3.28) or (3.30) follows with the definition of $\Sigma^{-1/2}$ the relation

$$\chi^2 = \zeta^T (\Sigma^{-1/2})^T \Sigma^{-1/2} \mathcal{J} (\mathcal{J}^T (\Sigma^{-1/2})^T \Sigma^{-1/2} \mathcal{J})^\dagger \mathcal{J}^T (\Sigma^{-1/2})^T \Sigma^{-1/2} \zeta$$

Plugging $\Sigma^{-1/2}\mathcal{J} = QR$, where R is invertible and $Q^TQ = I$, into (3.30) yields

$$\begin{aligned} \chi^2 &= \zeta^T (\Sigma^{-1/2})^T QR (R^T Q^T QR)^\dagger R^T Q^T \Sigma^{-1/2} \zeta \\ &= \zeta^T (\Sigma^{-1/2})^T QQ^T \Sigma^{-1/2} \zeta \end{aligned}$$

and thus the assertion. □

From Lemma 3.16 a rank condition on the parametric χ^2-test is derived.

Corollary 3.17 *Let $\mathcal{J} \in \mathbb{R}^{d \times c}$ and $\Sigma^{-1/2} \in \mathbb{R}^{e \times d}$. If*

$$c \geq \operatorname{rank}(\Sigma^{-1/2}\mathcal{J}), \tag{3.34}$$

condition (3.32) *is violated and the χ^2-test* (3.30) *boils down to*

$$\chi^2 = \zeta^T \Sigma^\dagger \zeta = \xi^T \xi \quad \textit{with} \quad \xi = \Sigma^{-1/2} \zeta. \tag{3.35}$$

Proof: Let $f \stackrel{\text{def}}{=} \operatorname{rank}(\Sigma^{-1/2}\mathcal{J})$. Under condition (3.34), a rank-revealing QR decomposition with column pivoting [GVL96] of $\mathcal{J}^T(\Sigma^{-1/2})^T = QR\Pi^T$ is possible, where R is invertible with dimensions $f \times f$, $Q^TQ = I$ and Π is a permutation matrix with $\Pi^T\Pi = \Pi\Pi^T = I$. Plugging this QR decomposition into (3.30) yields analogously to the previous lemma

$$\chi^2 = \zeta^T (\Sigma^{-1/2})^T \Pi R^T Q^T (QR\Pi^T \Pi R^T Q^T)^\dagger QR\Pi^T \Sigma^{-1/2} \zeta.$$

As Q has orthonormal columns and R is invertible, it follows $(QRR^TQ^T)^\dagger = QR^{-T}R^{-1}Q^T$, leading to the assertion. □

An empirical estimate of Σ is often based on some samples h_k, $k = 1, \ldots, n_b$, that are obtained from instances of the subspace matrix $\widehat{\mathcal{H}}$ by cutting the sensor data into n_b statistically independent blocks (see Section 3.5.2 for some explicit formulae). Then, condition (3.34) is fulfilled, if $n_b \leq c$. This will become clear in Lemma 3.18. Thus, the number of samples must satisfy $n_b > c$ as a necessary condition for the use of a Jacobian $\mathcal{J}$. Otherwise, the residual's sensitivity will disappear in the χ^2-test statistics (3.30).

In the χ^2-test in (3.33) or (3.35), a computation of $\widehat{\Sigma}^{-1/2}$ from the estimated covariance matrix $\widehat{\Sigma}$ is needed, which can pose a numerical problem when n_b is too small for assuring full rank of $\widehat{\Sigma}$. In this work, the covariance matrix Σ of any residual function can be factorized into

$$\Sigma = \mathcal{A} \Sigma_{\mathcal{H}} \mathcal{A}^T, \tag{3.36}$$

where $\Sigma_{\mathcal{H}} = \lim_N \sqrt{N}\widehat{\mathcal{H}}$ is the asymptotic covariance of the subspace matrix and $\mathcal{A}$ is a matrix depending on the residual function ζ. For example, $\mathcal{A} = I \otimes S^T$ for residual function (2.38). Further factorizations of Σ that define $\mathcal{A}$ in (3.36) are e.g. (6.11), (6.12) or (6.23). A factorization property for an estimate of $\Sigma_{\mathcal{H}}$ will now be used for an efficient computation of $\Sigma^{-1/2}$.

Lemma 3.18 *Let $\widehat{\Sigma}_h$ be an estimate of a covariance Σ_h with*

$$\widehat{\Sigma}_h = \frac{1}{n_b - 1} \sum_{k=1}^{n_b} (h_k - \bar{h})(h_k - \bar{h})^T,$$

using samples h_k, $k = 1, \ldots, n_b$, $\bar{h} \stackrel{\text{def}}{=} \frac{1}{n_b} \sum_{k=1}^{n_b} h_k$, and

$$\mathcal{K} \stackrel{\text{def}}{=} \frac{1}{\sqrt{n_b - 1}} \begin{bmatrix} \tilde{h}_1 & \tilde{h}_2 & \ldots & \tilde{h}_{n_b} \end{bmatrix} \quad \text{with} \quad \tilde{h}_k \stackrel{\text{def}}{=} h_k - \bar{h}.$$

Then, $\widehat{\Sigma}_h = \mathcal{K}\mathcal{K}^T$.

Proposition 3.19 *Let factorization $\Sigma = \mathcal{A}\Sigma_{\mathcal{H}}\mathcal{A}^{\mathcal{T}}$ and an estimate of the covariance of the subspace matrix $\widehat{\Sigma}_{\mathcal{H}} = \mathcal{K}\mathcal{K}^T$ be given, where $\mathcal{K}$ is related to the chosen SSI algorithm. Then,*

$$\widehat{\Sigma}^{-1/2} = (\mathcal{A}\mathcal{K})^{\dagger} \tag{3.37}$$

is a square root (pseudo-)inverse of the covariance estimate $\widehat{\Sigma}$.

Proposition 3.19 provides an efficient way to compute the square root (pseudo-)inverse of the covariance matrix in case of few available samples n_b. With an empirical estimate $\widehat{\Sigma}_{\mathcal{H}} = \mathcal{K}\mathcal{K}^T$ of the covariance of the subspace matrix using Lemma 3.18, matrix $\mathcal{K}$ only has n_b columns. Then, in (3.37) the pseudoinverse of matrix $\mathcal{A}\mathcal{K} \in \mathbb{R}^{d \times n_b}$ is computed and thus $e = n_b$. If $n_b < d = \dim \zeta$, the computation of $\widehat{\Sigma}^{-1/2}$ in (3.37) is less costly than computing $\widehat{\Sigma}^{-1/2}$ directly from $\widehat{\Sigma} \in \mathbb{R}^{d \times d}$.

Moreover, the computation of the (pseudo-)inverse of matrix $\mathcal{A}\mathcal{K}$ is numerically more stable than the square root (pseudo-)inverse of the squared matrix $\widehat{\Sigma} = \mathcal{A}\mathcal{K}(\mathcal{A}\mathcal{K})^T$. Hence, using (3.37) may be favorable, even if $n_b \geq d$.

3.5.2 Covariance estimation of subspace matrix

As pointed out in the previous section, the asymptotic covariance Σ depends on the asymptotic covariance $\Sigma_{\mathcal{H}}$ of the subspace matrix. It is defined as

$$\Sigma_{\mathcal{H}} \stackrel{\text{def}}{=} \lim_{N \to \infty} \operatorname{cov}(\sqrt{N} \operatorname{vec} \widehat{\mathcal{H}}), \tag{3.38}$$

where $\widehat{\mathcal{H}}$ is computed on N data samples. The computation of $\Sigma_{\mathcal{H}}$ depends on the chosen SSI algorithm.

The difficulty in the estimation of $\widehat{\Sigma}_{\mathcal{H}}$ lies often in the availability of only comparatively small data sets. A dataset of length N, on which an estimate $\widehat{\mathcal{H}}$ of the subspace matrix

is computed, might also serve for an estimation of its covariance $\widehat{\Sigma}_{\mathcal{H}}$. Then, the available data is cut into n_b blocks of length N_b that are regarded as statistically independent, where $N = n_b \cdot N_b$. The "samples" $\widehat{\mathcal{H}}_k$ of the subspace matrix can be computed on each data block $k = 1, \ldots, n_b$. However, they cannot be used directly for the covariance computation $\widehat{\Sigma}_{\mathcal{H}}$, because they are only computed on a data sample of length N_b and thus are not samples of $\widehat{\mathcal{H}}$ (which is computed on a sample of length N). As the covariance estimate $\widehat{\Sigma}_{\mathcal{H}}$ regarding a data sample of length N is of interest, the empirical covariances of $\widehat{\mathcal{H}}$ and $\widehat{\mathcal{H}}_k$ have to be linked.

In this section, the computation of the covariance estimate $\widehat{\Sigma}_{\mathcal{H}}$ is stated for covariance-driven SSI, where the relation between $\widehat{\mathcal{H}}$ and $\widehat{\mathcal{H}}_k$ is straightforward. Then, this computation is extended to data-driven SSI with the UPC algorithm.

3.5.2.1 Notation for covariance estimation of subspace matrices of covariance- and data-driven SSI

Details of the covariance- and data-driven SSI algorithm are found in Section 2.2.3 and their notation is recalled now. From the output data, the data matrices

$$\widetilde{\mathcal{Y}}^+ \stackrel{\text{def}}{=} \begin{bmatrix} Y_{q+1} & Y_{q+2} & \vdots & Y_{N+q} \\ Y_{q+2} & Y_{q+3} & \vdots & Y_{N+q+1} \\ \vdots & \vdots & \vdots & \vdots \\ Y_{q+p+1} & Y_{q+p+2} & \vdots & Y_{N+q+p} \end{bmatrix}, \quad \widetilde{\mathcal{Y}}^- \stackrel{\text{def}}{=} \begin{bmatrix} Y_q^{(\text{ref})} & Y_{q+1}^{(\text{ref})} & \vdots & Y_{N+q-1}^{(\text{ref})} \\ Y_{q-1}^{(\text{ref})} & Y_q^{(\text{ref})} & \vdots & Y_{N+q-2}^{(\text{ref})} \\ \vdots & \vdots & \vdots & \vdots \\ Y_1^{(\text{ref})} & Y_2^{(\text{ref})} & \vdots & Y_N^{(\text{ref})} \end{bmatrix} \tag{3.39}$$

are built and normalized by the number of samples to

$$\mathcal{Y}^+ \stackrel{\text{def}}{=} \frac{1}{\sqrt{N}} \widetilde{\mathcal{Y}}^+, \quad \mathcal{Y}^- \stackrel{\text{def}}{=} \frac{1}{\sqrt{N}} \widetilde{\mathcal{Y}}^-, \tag{3.40}$$

cf. (2.7). For the *covariance-driven* SSI, the subspace matrix

$$\widehat{\mathcal{H}}^{\text{cov}} = \mathcal{Y}^+ \, \mathcal{Y}^{-\,T} \tag{3.41}$$

with $\widehat{\mathcal{H}}^{\text{cov}} \in \mathbb{R}^{(p+1)r \times qr_0}$ is built. For the *data-driven* SSI with the Unweighted Principal Component (UPC) algorithm, the matrix

$$\widehat{\mathcal{H}}^{\text{UPC}} = \mathcal{Y}^+ \, \mathcal{Y}^{-\,T} \, (\mathcal{Y}^- \, \mathcal{Y}^{-\,T})^{-1} \mathcal{Y}^- \tag{3.42}$$

with $\widehat{\mathcal{H}}^{\text{UPC}} \in \mathbb{R}^{(p+1)r \times N}$ is defined. This matrix can get very large and in practice, the thin LQ decomposition

$$\begin{bmatrix} \mathcal{Y}^- \\ \mathcal{Y}^+ \end{bmatrix} = RQ = \begin{bmatrix} R_{11} & 0 \\ R_{21} & R_{22} \end{bmatrix} \begin{bmatrix} Q_1 \\ Q_2 \end{bmatrix}, \tag{3.43}$$

is done at first, where R and Q are partitioned as stated in (3.43). Then, with (3.42) follows $\widehat{\mathcal{H}}^{\text{UPC}} = R_{21} Q_1$. As Q_1 is a matrix with orthogonal rows, the same observability matrix can also be obtained from R_{21} in the SSI algorithm. Hence, the subspace matrix estimate

$$\widehat{\mathcal{H}}^{\text{UPC,R}} = R_{21} \tag{3.44}$$

is used, with $\widehat{\mathcal{H}}^{\mathrm{UPC,R}} \in \mathbb{R}^{(p+1)r \times qr_0}$ and R_{21} from (3.43).

For the derivation of the covariance $\widehat{\Sigma}_{\mathcal{H}}$, the unnormalized data matrices $\widetilde{\mathcal{Y}}^+$ and $\widetilde{\mathcal{Y}}^-$ from (3.39) are split into n_b blocks

$$\widetilde{\mathcal{Y}}^+ = \begin{bmatrix} \widetilde{\mathcal{Y}}_1^+ & \dots & \widetilde{\mathcal{Y}}_{n_b}^+ \end{bmatrix}, \quad \widetilde{\mathcal{Y}}^- = \begin{bmatrix} \widetilde{\mathcal{Y}}_1^- & \dots & \widetilde{\mathcal{Y}}_{n_b}^- \end{bmatrix}. \tag{3.45}$$

For simplicity, each block $\widetilde{\mathcal{Y}}_j^+$ and $\widetilde{\mathcal{Y}}_j^-$ may have the same length N_b, such that $n_b \cdot N_b = N$. Each block may be long enough to assume statistical independence between the blocks. They are normalized with respect to their length to

$$\mathcal{Y}_j^+ \overset{\text{def}}{=} \frac{1}{\sqrt{N_b}} \widetilde{\mathcal{Y}}_j^+, \quad \mathcal{Y}_j^- \overset{\text{def}}{=} \frac{1}{\sqrt{N_b}} \widetilde{\mathcal{Y}}_j^-, \quad j = 1, \dots, n_b. \tag{3.46}$$

3.5.2.2 Covariance-driven case

The covariance of the subspace matrix in the covariance-driven case follows easily from the covariance of the sample mean and was used e.g. in [RPDR08]. On each normalized data block from (3.46) a subspace matrix estimate $\widehat{\mathcal{H}}_j^{\mathrm{cov}}$ is built with

$$\widehat{\mathcal{H}}_j^{\mathrm{cov}} \overset{\text{def}}{=} \mathcal{Y}_j^+ \, \mathcal{Y}_j^{-\,T}. \tag{3.47}$$

Proposition 3.20 *A covariance estimate $\widehat{\Sigma}_{\mathcal{H}^{\mathrm{cov}}}$ of the covariance-driven subspace matrix $\widehat{\mathcal{H}}^{\mathrm{cov}}$ in* (3.41) *writes as*

$$\widehat{\Sigma}_{\mathcal{H}^{\mathrm{cov}}} = \frac{N}{n_b(n_b-1)} \sum_{j=1}^{n_b} \left(\operatorname{vec} \widehat{\mathcal{H}}_j^{\mathrm{cov}} - \operatorname{vec} \widehat{\mathcal{H}}^{\mathrm{cov}} \right) \left(\operatorname{vec} \widehat{\mathcal{H}}_j^{\mathrm{cov}} - \operatorname{vec} \widehat{\mathcal{H}}^{\mathrm{cov}} \right)^T.$$

Proof: The matrices $\widehat{\mathcal{H}}_j^{\mathrm{cov}}$, $j = 1, \dots, n_b$, are independent and identically distributed (i.i.d.) random variables as the underlying data are independent. The same holds obviously for $\operatorname{vec} \widehat{\mathcal{H}}_j^{\mathrm{cov}}$, $j = 1, \dots, n_b$. From (3.40), (3.41), (3.46) and (3.47) follows

$$\widehat{\mathcal{H}}^{\mathrm{cov}} = \frac{1}{n_b} \sum_{j=1}^{n_b} \widehat{\mathcal{H}}_j^{\mathrm{cov}}. \tag{3.48}$$

As the $\operatorname{vec} \widehat{\mathcal{H}}_j^{\mathrm{cov}}$, $j = 1, \dots, n_b$, are i.i.d., they have the same covariance and it follows together with (3.48)

$$\widehat{\Sigma}_{\mathcal{H}^{\mathrm{cov}}} = \operatorname{cov}\left(\sqrt{N} \operatorname{vec} \widehat{\mathcal{H}}^{\mathrm{cov}} \right) = \frac{N}{n_b^2} \sum_{j=1}^{n_b} \operatorname{cov}\left(\operatorname{vec} \widehat{\mathcal{H}}_j^{\mathrm{cov}} \right) = \frac{N}{n_b} \operatorname{cov}\left(\operatorname{vec} \widehat{\mathcal{H}}_1^{\mathrm{cov}} \right). \tag{3.49}$$

The estimator of the sample covariance of $\operatorname{vec} \widehat{\mathcal{H}}_j^{\mathrm{cov}}$, $j = 1, \dots, n_b$, is

$$\frac{1}{n_b - 1} \sum_{j=1}^{n_b} \left(\operatorname{vec} \widehat{\mathcal{H}}_j^{\mathrm{cov}} - \operatorname{vec} \widehat{\overline{\mathcal{H}}}^{\mathrm{cov}} \right) \left(\operatorname{vec} \widehat{\mathcal{H}}_j^{\mathrm{cov}} - \operatorname{vec} \widehat{\overline{\mathcal{H}}}^{\mathrm{cov}} \right)^T$$

with the sample mean $\operatorname{vec}\widehat{\overline{\mathcal{H}}}^{\mathrm{cov}}$ with

$$\widehat{\overline{\mathcal{H}}}^{\mathrm{cov}} = \frac{1}{n_b}\sum_{j=1}^{n_b}\widehat{\mathcal{H}}_j^{\mathrm{cov}} = \widehat{\mathcal{H}}^{\mathrm{cov}},$$

and the assertion follows. □

3.5.2.3 Data-driven case

Now, the computation of the covariance of the subspace matrix $\widehat{\mathcal{H}}^{\mathrm{UPC,R}}$ (see (3.43)–(3.44)) is derived. As the LQ decomposition in (3.43) is not unique, the convergence of $\widehat{\mathcal{H}}^{\mathrm{UPC,R}}$ for $N \to \infty$ has to be assured in some sense, and thus that $\Sigma_{\mathcal{H}}$ in (3.38) is well-defined: This follows from the convergence of $\widehat{\mathcal{H}}^{\mathrm{UPC}}(\widehat{\mathcal{H}}^{\mathrm{UPC}})^T = \widehat{\mathcal{H}}^{\mathrm{UPC,R}}(\widehat{\mathcal{H}}^{\mathrm{UPC,R}})^T$ for $N \to \infty$ in the stationary case [BM07]. Thus, $\widehat{\mathcal{H}}^{\mathrm{UPC,R}}$ also converges if it is well-defined, e.g. by a unique LQ decomposition as described in Section 3.2.1.

We proceed as follows for the computation of the covariance. On each normalized data block from (3.46) a subspace matrix $\widehat{\mathcal{H}}_j^{\mathrm{UPC,R}}$ is constructed by the thin LQ decomposition of

$$\begin{bmatrix}\mathcal{Y}_j^- \\ \mathcal{Y}_j^+\end{bmatrix} = R^{(j)}Q^{(j)}, \tag{3.50}$$

where $R^{(j)}$ and $Q^{(j)}$ are partitioned into

$$R^{(j)} = \begin{bmatrix}R_{11}^{(j)} & 0 \\ R_{21}^{(j)} & R_{22}^{(j)}\end{bmatrix}, \quad Q^{(j)} = \begin{bmatrix}Q_1^{(j)} \\ Q_2^{(j)}\end{bmatrix}, \tag{3.51}$$

and $R_{11}^{(j)} \in \mathbb{R}^{qr_0\times qr_0}$, $R_{21}^{(j)} \in \mathbb{R}^{(p+1)r\times qr_0}$. Then, a subspace matrix estimate on each data block is

$$\widehat{\mathcal{H}}_j^{\mathrm{UPC,R}} \stackrel{\mathrm{def}}{=} R_{21}^{(j)}. \tag{3.52}$$

Proposition 3.21 *Let $\breve{Q}_{11}^{(j)}$, $j = 1,\ldots,n_b$, be defined from partitioning the Q matrix of the thin LQ decomposition*

$$\begin{bmatrix}R_{11}^{(1)} & \ldots & R_{11}^{(n_b)}\end{bmatrix} = \breve{R}_{11}\begin{bmatrix}\breve{Q}_{11}^{(1)} & \ldots & \breve{Q}_{11}^{(n_b)}\end{bmatrix}, \tag{3.53}$$

where the $R_{11}^{(j)}$, $j = 1,\ldots,n_b$, are defined in (3.51)*. Then, a covariance estimate $\widehat{\Sigma}_{\mathcal{H}^{\mathrm{UPC,R}}}$ of the UPC subspace matrix $\widehat{\mathcal{H}}^{\mathrm{UPC,R}}$ in* (3.42) *writes as*

$$\widehat{\Sigma}_{\mathcal{H}^{\mathrm{UPC,R}}} = \frac{N}{n_b-1}\sum_{j=1}^{n_b}\left(\operatorname{vec}\left(\widehat{\mathcal{H}}_j^{\mathrm{UPC,R}}\,\breve{Q}_{11}^{(j)\,T}\right) - \overline{M}\right)\left(\operatorname{vec}\left(\widehat{\mathcal{H}}_j^{\mathrm{UPC,R}}\,\breve{Q}_{11}^{(j)\,T}\right) - \overline{M}\right)^T,$$

where

$$\overline{M} \stackrel{\mathrm{def}}{=} \frac{1}{n_b}\sum_{j=1}^{n_b}\operatorname{vec}\left(\widehat{\mathcal{H}}_j^{\mathrm{UPC,R}}\,\breve{Q}_{11}^{(j)\,T}\right).$$

Proof: From (3.40), (3.45) and (3.46) follows

$$\begin{bmatrix} \mathcal{Y}^- \\ \mathcal{Y}^+ \end{bmatrix} = \frac{1}{\sqrt{n_b}} \begin{bmatrix} \mathcal{Y}_1^- & \dots & \mathcal{Y}_{n_b}^- \\ \mathcal{Y}_1^+ & \dots & \mathcal{Y}_{n_b}^+ \end{bmatrix}.$$

Plugging in (3.43) on the left side and (3.50) on the right side leads to

$$RQ = \frac{1}{\sqrt{n_b}} \begin{bmatrix} R^{(1)} & \dots & R^{(n_b)} \end{bmatrix} \begin{bmatrix} Q^{(1)} & & \\ & \ddots & \\ & & Q^{(n_b)} \end{bmatrix}.$$

By enlarging the thin LQ decomposition (3.53) to

$$\begin{bmatrix} R^{(1)} & \dots & R^{(n_b)} \end{bmatrix} = \breve{R}\breve{Q}, \tag{3.54}$$

it can be assumed that it holds

$$R = \frac{1}{\sqrt{n_b}}\breve{R}, \quad Q = \breve{Q} \begin{bmatrix} Q^{(1)} & & \\ & \ddots & \\ & & Q^{(n_b)} \end{bmatrix} \tag{3.55}$$

as the thin LQ decomposition is unique up to a sign change (uniqueness can be enforced by constraining the diagonal elements of the R part to positive values). Let $\breve{R}$ and $\breve{Q}$ be partitioned into

$$\breve{R} = \begin{bmatrix} \breve{R}_{11} & 0 \\ \breve{R}_{21} & \breve{R}_{22} \end{bmatrix}, \quad \breve{Q} = \begin{bmatrix} \breve{Q}_1 & \dots & \breve{Q}_{n_b} \end{bmatrix}, \tag{3.56}$$

where $\breve{R}$ is partitioned analogously to R, and the $\breve{Q}_j$ are of the same size as the $R^{(j)}$ in (3.54). As $\breve{R}$ and the $R^{(j)}$ are lower triangular in (3.54), the matrices $\breve{Q}_j$ are also lower triangular and can be partitioned accordingly into

$$\breve{Q}_j = \begin{bmatrix} \breve{Q}_{11}^{(j)} & 0 \\ \breve{Q}_{21}^{(j)} & \breve{Q}_{22}^{(j)} \end{bmatrix}, \quad j = 1, \dots, n_b. \tag{3.57}$$

Multiplying (3.54) with $\breve{Q}^T$ and replacing $\breve{Q}$ by its partition from (3.56) leads to

$$\breve{R} = \sum_{j=1}^{n_b} R^{(j)} \breve{Q}_j^T.$$

Now, replacing $\breve{R}$, $R^{(j)}$ and Q_j with their partitions from (3.56), (3.51) and (3.57), respectively, leads to

$$\begin{bmatrix} \breve{R}_{11} & 0 \\ \breve{R}_{21} & \breve{R}_{22} \end{bmatrix} = \sum_{j=1}^{n_b} \begin{bmatrix} R_{11}^{(j)} & 0 \\ R_{21}^{(j)} & R_{22}^{(j)} \end{bmatrix} \begin{bmatrix} \breve{Q}_{11}^{(j)\,T} & \breve{Q}_{21}^{(j)\,T} \\ 0 & \breve{Q}_{22}^{(j)\,T} \end{bmatrix}$$

and hence

$$\breve{R}_{21} = \sum_{j=1}^{n_b} R_{21}^{(j)} \, \breve{Q}_{11}^{(j)\,T}.$$

Then, together with (3.44), (3.52), (3.55) and (3.56) it follows

$$\widehat{\mathcal{H}}^{\mathrm{UPC,R}} = \frac{1}{\sqrt{n_b}} \sum_{j=1}^{n_b} \widehat{\mathcal{H}}_j^{\mathrm{UPC,R}} \, \breve{Q}_{11}^{(j)\,T}. \tag{3.58}$$

Now, regarding the $\mathrm{vec}(\widehat{\mathcal{H}}_j^{\mathrm{UPC,R}} \, \breve{Q}_{11}^{(j)\,T})$, $j = 1, \ldots, n_b$, as i.i.d., the relation

$$\widehat{\Sigma}_{\mathcal{H}^{\mathrm{UPC,R}}} = N \, \mathrm{cov}\left(\mathrm{vec}\left(\widehat{\mathcal{H}}_1^{\mathrm{UPC,R}} \, \breve{Q}_{11}^{(1)\,T}\right)\right)$$

follows analogously to (3.49) and the assertion follows. □

This covariance computation of the data-driven subspace matrix is applied in Section 9.2 for uncertainty quantification.

The difficulty for computing the covariance in the data-driven case lies in the non-uniqueness of the LQ decomposition and in the absence of a straightforward relation between $\widehat{\mathcal{H}}^{\mathrm{UPC,R}}$ and $\widehat{\mathcal{H}}_j^{\mathrm{UPC,R}}$. In this context, also other approaches could be considered, as linking the covariance computation of the vectorizations of $\widehat{\mathcal{H}}^{\mathrm{UPC,R}}$ and $\widehat{\mathcal{H}}^{\mathrm{UPC,R}}(\widehat{\mathcal{H}}^{\mathrm{UPC,R}})^T = \widehat{\mathcal{H}}^{\mathrm{UPC}}(\widehat{\mathcal{H}}^{\mathrm{UPC}})^T$ or employing the matrix

$$\mathcal{Y}^{+}\mathcal{Y}^{-T}(\mathcal{Y}^{-}\mathcal{Y}^{-T})^{-1/2},$$

which is related to $\widehat{\mathcal{H}}^{\mathrm{UPC,R}}$ by post-multiplying with an orthogonal matrix.

3.6 Conclusions

In this chapter, some basic numerical tools were introduced that are needed throughout this work. Additional properties of the statistical fault detection test from Section 2.3 were shown and clarified, deepening the theoretical understanding of this algorithm. Furthermore, some very practical issues of the χ^2-test computation were solved that are related to the handling of a rank deficient estimate of the covariance matrix. This situation often appears when using quite short data sets. A numerically robust implementation was suggested. The computation of the covariance matrix itself was detailed for covariance-driven SSI and extended to data-driven SSI with the UPC algorithm. These points increase the applicability of the fault detection test in practice.

3.7 Dissemination

Parts of this chapter have been published in:

[DM11d] M. Döhler and L. Mevel. Robust subspace based fault detection. In *Proc. 18th IFAC World Congress*, Milan, Italy, 2011.

Part II

System identification

Chapter 4

Modular subspace-based system identification from multi-setup measurements

4.1 Introduction

Subspace-based system identification methods have been proven efficient for the identification of the eigenstructure of linear multivariable systems [BF85, Vib95, VODM96, PDR99, BM07]. An important application of these methods is structural vibration analysis, where the vibrating characteristics (modes, mode shapes) are identified of mechanical, civil or aeronautical structures subject to uncontrolled, unmeasured and non-stationary excitation [HVdA99, MBG03].

To obtain vibration measurements at many coordinates of a structure with only few sensors, it is common practice to use multiple sensor setups for the measurements. For these *multi-setup measurements*, some of the sensors, the so-called reference sensors, stay fixed throughout all the setups, while the other sensors are moved from setup to setup. By fusing in some way the corresponding data, this allows to perform modal identification as if there was a very large number of sensors, even in the range of a few hundreds or thousands.

Processing multi-setup measurement data for structural analysis is often achieved by performing eigenstructure identification for each record separately, and then merging the results obtained for records corresponding to different sensor pools. However, pole matching may be not easy in practice, and thus the result of eigenvector gluing may not be consistent [MK00, VdALMH00, CGDV02]. Therefore the question arises to perform eigenstructure identification by merging the data of the successive records and processing them globally, instead of merging the identification results.

Global merging approaches in frequency domain were proposed for maximum likelihood

identification in [PGC03] and for NExT-ERA in [Bro03, SF09]. In time domain, an empirical global merging approach for covariance-driven subspace identification was proposed in [RMDRC09].

In [MBBG02a, MBBG02b] a merging scheme was proposed for the covariance-driven stochastic subspace identification and the non-stationary consistency of the resulting identification algorithm was proved. We generalize the merging approach from [MBBG02a, MBBG02b], which is only designed for the covariance-driven stochastic subspace identification, to arbitrary subspace-based identification algorithms.[1] Moreover, the new approach is modular, i.e. the data records from different setups are processed one after another instead of together at the same time, in order to do global system identification. Furthermore, a *scalable* modular merging algorithm is proposed in this chapter, which uses only little more than the memory needed for single-setup system identification of the setup actually being processed. Like this, there are practically no limitations on the number of setups or sensors that can be processed. Non-stationary consistency of the proposed algorithms is proved for the general class of subspace algorithms in [BM07].

In Operational Modal Analysis the true system order is unknown and recommended techniques from statistics to estimate the best model order (AIC, BIC, MDL, ...) may lead to a model with the best prediction capacity. However, one is rather interested in distinguishing between true physical modes and noise modes of the investigated system. For doing this, the identification procedure is repeated while truncating at different over-specified model orders, as the noise modes tend to vary at different orders [PDR99]. In the classical subspace algorithm, the model obtained by the selection of some lower order from an overestimated higher model order coincides with the direct truncation at this given order. We prove the same property for the proposed merging algorithms.

This chapter is organized as follows. In Section 4.2, the general subspace-based system identification algorithm is introduced and two examples of stochastic subspace identification algorithms are given. In Section 4.3, the merging problem for multi-setup measurements is addressed. The merging algorithm for the covariance-driven stochastic subspace identification from [MBBG02a, MBBG02b] is generalized in two steps to arbitrary subspace-based system identification algorithms and the scalable merging algorithm is derived. In Section 4.4, non-stationary consistency of the proposed merging algorithms is proved, with the condition of the underlying subspace algorithm being consistent to non-stationary excitation [BM07]. In Section 4.5, the robustness of these algorithms to misspecified model order is investigated. In Section 4.6, implementation details are given for the merging algorithms using data-driven subspace identification. Finally, in Section 4.7, the modal analysis of a bridge from vibration measurements is considered as an application of the merging algorithms, before some concluding remarks.

4.2 Subspace-based system identification

In this section, the basic principles of subspace-based system identification are recalled from Section 2.2.2. We consider linear multivariable systems described by a discrete time state

[1] A slight mistake in the merging procedure in [MBBG02a, MBBG02b] is also corrected in this chapter.

space model

$$\begin{cases} X_{k+1} = AX_k + V_k \\ Y_k = CX_k \end{cases} \tag{4.1}$$

where state X and observed output Y have dimensions n and r, respectively, A is the state transition and C the observation matrix. The state noise process $(V_k)_k$ is an unmeasured Gaussian white noise sequence with zero mean and, in the stationary case, constant covariance matrix Q: $\mathbf{E}(V_k V_{k'}^T) \stackrel{\text{def}}{=} Q\delta(k-k')$, where $\mathbf{E}(\cdot)$ denotes the expectation operator.

Let the pairs (λ, ϕ_λ) be the eigenvalues and eigenvectors of matrix A and define the mode shape $\varphi_\lambda \stackrel{\text{def}}{=} C\phi_\lambda$. We assume that the system has no multiple eigenvalues and, thus, that the λ's and φ_λ's are pairwise complex conjugate. In particular, 0 is not an eigenvalue of state transition matrix A. The collection of pairs $(\lambda, \varphi_\lambda)$ form a canonical parameterization (invariant w.r.t. changes in the state basis) of the pole part of system (4.1), which is referred to as the system eigenstructure.

There are many SSI algorithms in literature. Some are mentioned in Section 2.2.3 and they fit all in the following framework to identify the eigenstructure $(\lambda, \varphi_\lambda)$ of system (4.1).

From the output data (Y_k), a matrix $\widehat{\mathcal{H}}_{p+1,q}$ is built according to the selected subspace identification algorithm, which is an estimate of the *subspace matrix* $\mathcal{H}_{p+1,q}$. For all subspace identification algorithms, it satisfies the factorization property

$$\mathcal{H}_{p+1,q} = W\mathcal{O}_{p+1}\mathcal{Z}_q \tag{4.2}$$

into an invertible weighting matrix W, the matrix of observability

$$\mathcal{O}_{p+1} \stackrel{\text{def}}{=} \begin{bmatrix} C \\ CA \\ \vdots \\ CA^p \end{bmatrix} \stackrel{\text{def}}{=} \mathcal{O}_{p+1}(C, A), \tag{4.3}$$

and a matrix $\mathcal{Z}_q$, where W and $\mathcal{Z}_q$ depend on the selected subspace identification algorithm. However, W is the identity matrix for many subspace identification algorithms.

The observation matrix C is then found in the first block-row of the observability matrix $\mathcal{O}_{p+1}$, whereas exploiting the shift invariance property of $\mathcal{O}_{p+1}$ provides us with the state-transition matrix A as the least squares solution of

$$\mathcal{O}_{p+1}^{\uparrow} A = \mathcal{O}_{p+1}^{\downarrow}, \text{ where } \mathcal{O}_{p+1}^{\uparrow} \stackrel{\text{def}}{=} \begin{bmatrix} C \\ CA \\ \vdots \\ CA^{p-1} \end{bmatrix}, \ \mathcal{O}_{p+1}^{\downarrow} \stackrel{\text{def}}{=} \begin{bmatrix} CA \\ CA^2 \\ \vdots \\ CA^p \end{bmatrix}, \tag{4.4}$$

from which the eigenstructure results.

Definition 4.1 *In general, let* $^{\uparrow}$ *respectively* $^{\downarrow}$ *be operators, which remove the last respectively the first block row of an observability matrix as in* (4.4)*. The size of the removed block row is the size of the observation matrix present in the observability matrix.*

The actual implementation of this generic subspace identification algorithm uses a consistent estimate $\widehat{\mathcal{H}}_{p+1,q}$ obtained from the output data according to the selected subspace identification algorithm. The SVD

$$\widehat{\mathcal{H}}_{p+1,q} = \begin{bmatrix} \widehat{U}_1 & \widehat{U}_0 \end{bmatrix} \begin{bmatrix} \widehat{\Delta}_1 & 0 \\ 0 & \widehat{\Delta}_0 \end{bmatrix} \begin{bmatrix} \widehat{V}_1^T \\ \widehat{V}_0^T \end{bmatrix} \tag{4.5}$$

and its truncation at the model order n yields an estimate $\widehat{\mathcal{O}}_{p+1} = \widehat{W}^{-1}\widehat{U}_1\widehat{\Delta}_1^{1/2}$ for the observability matrix, from which $(\widehat{C}, \widehat{A})$ and $(\widehat{\lambda}, \widehat{\varphi}_\lambda)$ are recovered as sketched above. Also, the estimate $\widehat{\mathcal{Z}}_q = \widehat{\Delta}_1^{1/2}\widehat{V}_1^T$ can be obtained.

For simplicity, let p and q be given, and the subscripts of $\mathcal{H}_{p+1,q}$, $\mathcal{O}_{p+1}$ and $\mathcal{Z}_q$ may be skipped.

4.3 Multi-setup stochastic subspace identification

In this section, the state-space model for multi-setup measurements is introduced and the problem of merging data from different setups is stated. The merging scheme from [MBBG02a, MBBG02b] for the covariance-driven subspace identification algorithm is presented and generalized to subspace identification algorithms without a left weighting ($W = I$). In Algorithm 4.3 a modular version of this algorithm is derived, where the records of the different setups are processed one after another, instead of altogether, for a practical implementation and less numerical operations. In the next step, Algorithm 4.4 is derived that merges the observability matrices obtained from the different records to a global observability matrix and thus can be applied to arbitrary subspace identification algorithms. Finally, a scalable computation of the system matrices is derived for Algorithm 4.4 in the case of a large number of sensors and setups.

4.3.1 Modeling multi-setup measurements

Instead of a single record for the output (Y_k) of the system (4.1), N_s records

$$\underbrace{\begin{pmatrix} Y_k^{(1,\mathrm{ref})} \\ Y_k^{(1,\mathrm{mov})} \end{pmatrix}}_{\text{Record 1}} \quad \underbrace{\begin{pmatrix} Y_k^{(2,\mathrm{ref})} \\ Y_k^{(2,\mathrm{mov})} \end{pmatrix}}_{\text{Record 2}} \quad \cdots \quad \underbrace{\begin{pmatrix} Y_k^{(N_s,\mathrm{ref})} \\ Y_k^{(N_s,\mathrm{mov})} \end{pmatrix}}_{\text{Record } N_s} \tag{4.6}$$

are now available collected successively. Each record j contains data $Y_k^{(j,\mathrm{ref})}$ of dimension $r^{(\mathrm{ref})}$ from a fixed *reference* sensor pool, and data $Y_k^{(j,\mathrm{mov})}$ of dimension $r^{(j)}$ from a *moving* sensor pool. Then, the total number of sensor positions is $r^{(\mathrm{all})} \stackrel{\mathrm{def}}{=} r^{(\mathrm{ref})} + \sum_{j=1}^{N_s} r^{(j)}$. For each setup j, this corresponds to observing the state space system (4.1) at different sets of time instants k, where the observation matrices are different for every setup. The transition matrix A remains the same, since the same system is observed. As the sensor settings for the moving sensors change, the respective observation matrices mapping the states to the observations at the

moving sensors are different for each setup j, while the observation matrix with respect to the reference sensors stays the same for all setups. Denote the former observation matrices by $C^{(j,\mathrm{mov})} \in \mathbb{R}^{r^{(j)} \times n}$, $j = 1, \ldots, N_s$, and the latter by $C^{(\mathrm{ref})} \in \mathbb{R}^{r^{(\mathrm{ref})} \times n}$. Furthermore, denote the states X_k and state noise V_k from system (2.1) corresponding to record j by $X_k^{(j)}$ and $V_k^{(j)}$, respectively. Thus, to each record $j = 1, \ldots, N_s$ corresponds a state-space realization in the form [MBBG02a, MBBG02b]

$$\left\{ \begin{array}{lcll} X_{k+1}^{(j)} & = & A\, X_k^{(j)} + V_k^{(j)} & \\ Y_k^{(j,\mathrm{ref})} & = & C^{(\mathrm{ref})}\, X_k^{(j)} & (\text{reference pool}) \\ Y_k^{(j,\mathrm{mov})} & = & C^{(j,\mathrm{mov})}\, X_k^{(j)} & (\text{sensor pool n}^o j) \end{array} \right. \tag{4.7}$$

Define the global observation matrix containing information of all the sensor positions as

$$C^{(\mathrm{all})} \stackrel{\mathrm{def}}{=} \begin{bmatrix} C^{(\mathrm{ref})} \\ C^{(1,\mathrm{mov})} \\ C^{(2,\mathrm{mov})} \\ \vdots \\ C^{(N_s,\mathrm{mov})} \end{bmatrix} \in \mathbb{R}^{r^{(\mathrm{all})} \times n}, \tag{4.8}$$

corresponding to C in (4.1).

Definition 4.2 *A subspace matrix $\mathcal{H}^{(j)}$ is called local subspace matrix of record j, if its estimate is built from the output data*

$$Y_k^{(j)} \stackrel{\mathrm{def}}{=} \begin{bmatrix} Y_k^{(j,\mathrm{ref})} \\ Y_k^{(j,\mathrm{mov})} \end{bmatrix}$$

with a selected subspace identification algorithm, and whose associated observability matrix in (4.2) *is the local observability matrix*

$$\mathcal{O}^{(j)} \stackrel{\mathrm{def}}{=} \mathcal{O}\left(\begin{bmatrix} C^{(\mathrm{ref})} \\ C^{(j,\mathrm{mov})} \end{bmatrix}, A \right), \tag{4.9}$$

cf. the definition of $\mathcal{O}$ in (4.3)*. A subspace matrix $\mathcal{H}^{(\mathrm{all})}$ is called global subspace matrix, if its associated observability matrix in* (4.2) *is the global observability matrix $\mathcal{O}^{(\mathrm{all})} \stackrel{\mathrm{def}}{=} \mathcal{O}(C^{(\mathrm{all})}, A)$.*

4.3.2 The merging problem

In order to identify the eigenstructure of system (4.7) on the basis of the measurements (4.6), the output-only subspace algorithm of Section 4.2 has to be adapted. It is the aim to merge the data from the different records prior to the identification step of the algorithm, so that the identification steps (4.2)–(4.4) only have to be done once. This corresponds to merging the *local subspace matrices* $\mathcal{H}^{(j)}$, $j = 1, \ldots, N_s$, to a *global subspace matrix* $\mathcal{H}^{(\mathrm{all})}$, or merging

the *local observability matrices* $\mathcal{O}^{(j)}$ to a *global observability matrix* $\mathcal{O}^{(\text{all})}$, which is the main problem in this chapter. Then, the eigenstructure of system (4.7) can be obtained from an identified pair of system matrices $(C^{(\text{all})}, A)$ by applying the generic subspace algorithm of Section 4.2 on $\mathcal{H}^{(\text{all})}$ or on $\mathcal{O}^{(\text{all})}$.

A cornerstone in Section 4.2 is factorization (4.2), which, of course, holds for each local subspace matrix $\mathcal{H}^{(j)}$ of the N_s records with a different observability matrix $\mathcal{O}^{(j)}$ on the left and in general a different matrix $\mathcal{Z}^{(j)}$ on the right side. If the matrices $\mathcal{Z}^{(j)}$ were identical[2] for all $j = 1, \ldots, N_s$, interleaving block rows of the matrices $\mathcal{H}^{(j)}$ would lead to a global subspace matrix having a factorization property (4.2) with $\mathcal{Z} = \mathcal{Z}^{(j)}$ on the right side, which could be used for global system identification.

However, there are several reasons for possible differences between the matrices $\mathcal{Z}^{(j)}$:

- In general, the matrices $\mathcal{Z}^{(j)}$ are dependent on different sensor sets, as the moving sensor set is different for each setup j. Hence, the matrices $\mathcal{Z}^{(j)}$ are different.

- For most subspace algorithms, e.g. the data-driven algorithms in [VODM96] as UPC, the matrices $\mathcal{Z}^{(j)}$ have no expected value as their size depends on the number of samples N and the initial state $X_0^{(j)}$, or they are not uniquely defined due to LQ decompositions as in (2.13), so that in fact only some $\widehat{\mathcal{Z}}^{(j)} S_j$ with unknown matrix S_j can be estimated.

- The matrices $\mathcal{O}^{(j)}$ and $\mathcal{Z}^{(j)}$ might be in a different modal basis for each setup j, so that in fact $\widehat{\mathcal{O}}^{(j)} T_j$ and $T_j^{-1} \widehat{\mathcal{Z}}^{(j)}$ are identified with an invertible unknown change of basis matrix T_j. This is also the reason why matrix (4.8) cannot be obtained straightforward from a separate system identification of the measurement setups $j = 1, \ldots, N_s$.

- If the excitation $V_k^{(j)}$ is uncontrolled, its covariance $Q^{(j)}$ with $\mathbf{E}(V_k^{(j)} V_{k'}^{(j)}) = Q^{(j)} \delta(k-k')$ is record dependent. Hence, $\mathcal{Z}^{(j)}$ is also dependent on $Q^{(j)}$, which can be different for each record. This case appears especially in practice when ambient excitation is considered. Multi-setup measurements take place over a longer time period than a single measurement and it is likely that properties of the ambient excitation change between the measurement campaigns.

By normalizing the data in a certain way, it can be achieved that the corresponding matrices $\overline{\mathcal{Z}}^{(j)}$ are identical for all the records. Thus, the corresponding normalized subspace matrices can be merged into a global subspace matrix, on which system identification of the whole system can be done. This is the basic idea of the merging algorithms presented in the following sections.

[2] By nature, the $\mathcal{Z}^{(j)}$'s are indeed identical for $j = 1, \ldots, N_s$ in covariance-driven subspace identification under stationary excitation throughout all setups using correlations $R_i^{(j)} = \mathbf{E}(Y_k^{(j)} Y_{k-i}^{(j,\text{ref})T})$ in (2.8). However, this is a very special case.

4.3.3 Merging for covariance-driven SSI from [MBBG02a, MBBG02b]

For each setup j, the two families of cross-correlations

$$R_i^{(j,\mathrm{ref})} \stackrel{\mathrm{def}}{=} \mathbf{E}\left(Y_k^{(j,\mathrm{ref})} Y_{k-i}^{(j,\mathrm{ref})T}\right), \tag{4.10}$$

$$R_i^{(j,\mathrm{mov})} \stackrel{\mathrm{def}}{=} \mathbf{E}\left(Y_k^{(j,\mathrm{mov})} Y_{k-i}^{(j,\mathrm{ref})T}\right) \tag{4.11}$$

are defined. From their definition, they enjoy the factorization properties

$$R_i^{(j,\mathrm{ref})} = C^{(\mathrm{ref})} A^i G^{(j)}, \quad R_i^{(j,\mathrm{mov})} = C^{(j,\mathrm{mov})} A^i G^{(j)}, \tag{4.12}$$

where $G^{(j)} \stackrel{\mathrm{def}}{=} \mathbf{E}\left(X_k^{(j)} Y_{k-i}^{(j,\mathrm{ref})T}\right)$ is the cross-correlation between the state and the reference outputs of setup j.

In the *stationary case*, the state-output cross-correlations $G^{(j)}$ are equal for all the setups, $G = G^{(j)}$, $j = 1, \ldots, N_s$. Consequently, the cross-correlations of the outputs can be stacked to a block column vector

$$R_i^{(\mathrm{all})} = \begin{bmatrix} R_i^{(1,\mathrm{ref})} \\ R_i^{(1,\mathrm{mov})} \\ \vdots \\ R_i^{(N_s,\mathrm{mov})} \end{bmatrix}$$

for each lag i, which factorizes as $R_i^{(\mathrm{all})} = C^{(\mathrm{all})} A^i G$. The corresponding block Hankel matrix (see Equation (2.8)) filled with these correlations factorizes as $\mathcal{H}^{(\mathrm{all})} \stackrel{\mathrm{def}}{=} \mathrm{Hank}(R_i^{(\mathrm{all})}) = \mathcal{O}(C^{(\mathrm{all})}, A)\mathcal{C}(A, G)$. Thus, the global system identification can be performed on this merged matrix. However, this merging approach fails in the non-stationary case, as stressed in [MBBG02a, MBBG02b].

In the *non-stationary case*, some normalization of the data has to be performed prior to merging. This happens in two steps: First, the factors $\mathcal{Z}^{(j)}$ of the subspace matrix factorization are identified in the same modal basis, and second, the data of all setups is normalized and merged using the factors $\mathcal{Z}^{(j)}$.

Thanks to factorization property (4.12), the block Hankel matrices built from the cross-correlations of the output data in (4.10) and (4.11) factorize as

$$\mathcal{H}^{(j,\mathrm{ref})} \stackrel{\mathrm{def}}{=} \mathrm{Hank}(R_i^{(j,\mathrm{ref})}) = \mathcal{O}(C^{(\mathrm{ref})}, A)\, \mathcal{C}(A, G^{(j)}),$$

$$\mathcal{H}^{(j,\mathrm{mov})} \stackrel{\mathrm{def}}{=} \mathrm{Hank}(R_i^{(j,\mathrm{mov})}) = \mathcal{O}(C^{(j,\mathrm{mov})}, A)\, \mathcal{C}(A, G^{(j)}). \tag{4.13}$$

Note that a *local subspace matrix* $\mathcal{H}^{(j)}$ as in Definition 4.2 can be obtained from interleaving the block rows of $\mathcal{H}^{(j,\mathrm{ref})}$ and $\mathcal{H}^{(j,\mathrm{mov})}$, and factorization property $\mathcal{H}^{(j)} = \mathcal{O}^{(j)}\mathcal{Z}^{(j)}$ holds with $\mathcal{Z}^{(j)} = \mathcal{C}(A, G^{(j)})$. These factors $\mathcal{C}(A, G^{(j)})$ are obtained as follows. Let

$$R_i^{(\mathrm{all,ref})} \stackrel{\mathrm{def}}{=} \begin{bmatrix} R_i^{(1,\mathrm{ref})} & \ldots & R_i^{(N_s,\mathrm{ref})} \end{bmatrix} \tag{4.14}$$

be the block row vector of the reference data correlations of all setups. It factorizes as

$$R_i^{(\text{all,ref})} = C^{(\text{ref})} A^i G^{(\text{all})}, \quad G^{(\text{all})} \stackrel{\text{def}}{=} \begin{bmatrix} G^{(1)} & \dots & G^{(N_s)} \end{bmatrix}.$$

The corresponding block Hankel matrix, which factorizes as

$$\mathcal{H}^{(\text{all,ref})} \stackrel{\text{def}}{=} \text{Hank}(R_i^{(\text{all,ref})}) = \mathcal{O}(C^{(\text{ref})}, A)\, \mathcal{C}(A, G^{(\text{all})}), \tag{4.15}$$

can be obtained by interleaving block columns of $\mathcal{H}^{(j,\text{ref})}$, $j = 1, \dots, N_s$. Assume that the pair $(C^{(\text{ref})}, A)$ is observable. The factors

$$\mathcal{C}(A, G^{(j)}) = \begin{bmatrix} G^{(j)} & AG^{(j)} & \dots & A^{q-1}G^{(j)} \end{bmatrix}$$

are then obtained by juxtaposing the appropriate block columns of $\mathcal{C}(A, G^{(\text{all})})$, which is partitioned as

$$\mathcal{C}(A, G^{(\text{all})}) = \begin{bmatrix} G^{(1)} & \dots & G^{(N_s)} & AG^{(1)} & \dots & AG^{(N_s)} & \dots & A^{q-1}G^{(1)} & \dots & A^{q-1}G^{(N_s)} \end{bmatrix}. \tag{4.16}$$

For doing so, note that $\mathcal{C}(A, G^{(\text{all})})$ has to be partitioned differently than stated in [MBBG02a, MBBG02b].

Assume that for all j the pair $(A, G^{(j)})$ is controllable and that, up to a permutation on the record indices, $\mathcal{C}(A, G^{(1)})$ is the best conditioned controllability matrix among the $\mathcal{C}(A, G^{(j)})$'s. Then, the right factor $\mathcal{C}(A, G^{(j)})$ in (4.13) is removed and replaced by $\mathcal{C}(A, G^{(1)})$ in the normalized matrices

$$\overline{\mathcal{H}}^{(j,\text{mov})} \stackrel{\text{def}}{=} \mathcal{H}^{(j,\text{mov})} \mathcal{C}(A, G^{(j)})^T (\mathcal{C}(A, G^{(j)}) \mathcal{C}(A, G^{(j)})^T)^{-1} \mathcal{C}(A, G^{(1)}),$$

as defined in [MBBG02a, MBBG02b]. This notation can be simplified by using the pseudoinverse:

$$\overline{\mathcal{H}}^{(j,\text{mov})} = \mathcal{H}^{(j,\text{mov})} \mathcal{C}(A, G^{(j)})^{\dagger} \mathcal{C}(A, G^{(1)}). \tag{4.17}$$

The normalized matrix $\overline{\mathcal{H}}^{(j,\text{mov})}$ then corresponds to a block Hankel matrix filled with normalized cross-correlations $\overline{R}_i^{(j,\text{mov})} = C^{(j,\text{mov})} A^i G^{(1)}$, which can be stacked for the different setups, together with the cross-correlation of the reference sensors, to

$$\overline{R}_i^{(\text{all})} \stackrel{\text{def}}{=} \begin{bmatrix} R_i^{(1,\text{ref})} \\ \overline{R}_i^{(1,\text{mov})} \\ \vdots \\ \overline{R}_i^{(N_s,\text{mov})} \end{bmatrix} = C^{(\text{all})} A^i G^{(1)}, \tag{4.18}$$

similar to the stationary case. Hence, the corresponding block Hankel matrix $\overline{\mathcal{H}}^{(\text{all})}$ filled with these correlations fulfills the desired factorization property

$$\overline{\mathcal{H}}^{(\text{all})} \stackrel{\text{def}}{=} \text{Hank}(\overline{R}_i^{(\text{all})}) = \mathcal{O}(C^{(\text{all})}, A) \mathcal{C}(A, G^{(1)})$$

and therefore can be used for the global system identification from Section 4.2. This normalized and merged matrix $\overline{\mathcal{H}}^{(\text{all})}$ can be obtained by interleaving the block rows of $\mathcal{H}^{(1,\text{ref})}$ and $\overline{\mathcal{H}}^{(j,\text{mov})}$, $j = 1, \dots, N_s$.

The merging algorithm described in this section is summarized in Algorithm 4.1.

Algorithm 4.1 Multi-setup merging for covariance-driven SSI

Input: Subspace matrix estimates for setups $j = 1, \ldots, N_s$:

$\widehat{\mathcal{H}}^{(j,\mathrm{ref})} = \mathrm{Hank}(\widehat{R}_i^{(j,\mathrm{ref})})$ {Equation (4.10)}

$\widehat{\mathcal{H}}^{(j,\mathrm{mov})} = \mathrm{Hank}(\widehat{R}_i^{(j,\mathrm{mov})})$ {Equation (4.11)}

1: Build $\widehat{\mathcal{H}}^{(\mathrm{all,ref})}$ by interleaving the block columns of $\widehat{\mathcal{H}}^{(j,\mathrm{ref})}$, $j = 1, \ldots, N_s$, analogously to (4.14)

2: SVD of $\widehat{\mathcal{H}}^{(\mathrm{all,ref})} = \widehat{U}\widehat{\Sigma}\widehat{V}^T$ and keep $\widehat{\mathcal{C}}^{(\mathrm{all})} \stackrel{\mathrm{def}}{=} \widehat{\mathcal{C}}(A, G^{(\mathrm{all})}) = \widehat{\Sigma}^{1/2}\widehat{V}^T$ {Equation (4.15)}

3: Partition $\widehat{\mathcal{C}}^{(\mathrm{all})} = \begin{bmatrix}\mathcal{C}^{(1,1)} & \ldots & \mathcal{C}^{(1,N_s)} & \mathcal{C}^{(2,1)} & \ldots & \mathcal{C}^{(2,N_s)} & \ldots & \mathcal{C}^{(q,N_s)}\end{bmatrix}$, where each block has $r^{(\mathrm{ref})}$ columns, and set $\widehat{\mathcal{C}}_j = \begin{bmatrix}\mathcal{C}^{(1,j)} & \ldots & \mathcal{C}^{(q,j)}\end{bmatrix}$, $j = 1, \ldots, N_s$ {Equ. (4.16)}

4: Compute $\widehat{\overline{\mathcal{H}}}^{(j,\mathrm{mov})} = \widehat{\mathcal{H}}^{(j,\mathrm{mov})}\widehat{\mathcal{C}}_j^{\dagger}\widehat{\mathcal{C}}_1$ {Equation (4.17)}

5: Build $\widehat{\overline{\mathcal{H}}}^{(\mathrm{all})}$ by interleaving the block rows of $\widehat{\mathcal{H}}^{(1,\mathrm{ref})}$ and $\widehat{\overline{\mathcal{H}}}^{(j,\mathrm{mov})}$, $j = 1, \ldots, N_s$, analogously to (4.18)

Output: Global subspace matrix $\widehat{\overline{\mathcal{H}}}^{(\mathrm{all})}$ for system identification

4.3.4 Generalization of merging algorithm to SSI algorithms with $W = I$

Now, the merging approach from the previous section is generalized to subspace identification algorithms satisfying (4.2) with $W = I$, i.e. without a left weighting. From the output data of the N_s measurement setups of system (4.7), the respective local subspace matrices $\mathcal{H}^{(j)} = \mathcal{O}^{(j)}\mathcal{Z}^{(j)}$ as in Definition 4.2 are built based on the selected algorithm. Again, it is the aim to obtain a global subspace matrix $\mathcal{H}^{(\mathrm{all})}$ from them in order to do a global system identification.

First, for each setup j, the local subspace matrix $\mathcal{H}^{(j)}$ is separated into the reference sensor part $\mathcal{H}^{(j,\mathrm{ref})}$ and the moving sensor part $\mathcal{H}^{(j,\mathrm{mov})}$ by selecting the appropriate block rows, such that the factorization properties

$$\mathcal{H}^{(j,\mathrm{ref})} = \mathcal{O}(C^{(\mathrm{ref})}, A)\mathcal{Z}^{(j)}, \tag{4.19}$$

$$\mathcal{H}^{(j,\mathrm{mov})} = \mathcal{O}(C^{(j,\mathrm{mov})}, A)\mathcal{Z}^{(j)} \tag{4.20}$$

hold. Assume that $(C^{(\mathrm{ref})}, A)$ is observable. Juxtaposing the matrices $\mathcal{H}^{(j,\mathrm{ref})}$, $j = 1, \ldots, N_s$, to

$$\mathcal{H}^{(\mathrm{all,ref})} \stackrel{\mathrm{def}}{=} \begin{bmatrix}\mathcal{H}^{(1,\mathrm{ref})} & \ldots & \mathcal{H}^{(N_s,\mathrm{ref})}\end{bmatrix} \tag{4.21}$$

– instead of interleaving their block columns as in Algorithm 4.1 –, yields a matrix with factorization property

$$\mathcal{H}^{(\mathrm{all,ref})} = \mathcal{O}(C^{(\mathrm{ref})}, A)\begin{bmatrix}\mathcal{Z}^{(1)} & \ldots & \mathcal{Z}^{(N_s)}\end{bmatrix} \tag{4.22}$$

similar to (4.15), from which the matrices $\mathcal{Z}^{(1)}, \ldots, \mathcal{Z}^{(N_s)}$ can be recovered in the same modal basis.

Assume that all the $\mathcal{Z}^{(j)}$'s are full row rank, and similarly to Algorithm 4.1, that $\mathcal{Z}^{(1)}$ is the best conditioned matrix among the $\mathcal{Z}^{(j)}$'s. Then, the right factor $\mathcal{Z}^{(j)}$ in (4.20) is

removed and replaced by $\mathcal{Z}^{(1)}$ in the normalized matrices

$$\overline{\mathcal{H}}^{(j,\mathrm{mov})} \stackrel{\mathrm{def}}{=} \mathcal{H}^{(j,\mathrm{mov})}\mathcal{Z}^{(j)\dagger}\mathcal{Z}^{(1)}, \tag{4.23}$$

similar to (4.17), and factorization property $\overline{\mathcal{H}}^{(j,\mathrm{mov})} = \mathcal{O}(C^{(j,\mathrm{mov})}, A)\mathcal{Z}^{(1)}$ follows. Hence, interleaving the block rows of $\mathcal{H}^{(1,\mathrm{ref})}$ and $\overline{\mathcal{H}}^{(j,\mathrm{mov})}$, $j = 1, \ldots, N_s$, yields the desired global subspace matrix

$$\overline{\mathcal{H}}^{(\mathrm{all})} \stackrel{\mathrm{def}}{=} P \begin{bmatrix} \mathcal{H}^{(1,\mathrm{ref})} \\ \overline{\mathcal{H}}^{(1,\mathrm{mov})} \\ \vdots \\ \overline{\mathcal{H}}^{(N_s,\mathrm{mov})} \end{bmatrix} = \mathcal{O}(C^{(\mathrm{all})}, A)\mathcal{Z}^{(1)}, \tag{4.24}$$

where P is a suitable permutation matrix.

The merging algorithm described in this section is summarized in Algorithm 4.2.

Algorithm 4.2 Multi-setup merging for SSI algorithms without left weighting

Input: Local subspace matrix estimates $\widehat{\mathcal{H}}^{(j)}$ for setups $j = 1, \ldots, N_s$ {Definition 4.2}

1: Separate $\widehat{\mathcal{H}}^{(j)}$ into $\widehat{\mathcal{H}}^{(j,\mathrm{ref})}$ and $\widehat{\mathcal{H}}^{(j,\mathrm{mov})}$, $j = 1, \ldots, N_s$ {Equations (4.19), (4.20)}

2: Juxtapose $\widehat{\mathcal{H}}^{(j,\mathrm{ref})}$, $j = 1, \ldots, N_s$, to $\widehat{\mathcal{H}}^{(\mathrm{all,ref})} = \begin{bmatrix} \widehat{\mathcal{H}}^{(1,\mathrm{ref})} & \ldots & \widehat{\mathcal{H}}^{(N_s,\mathrm{ref})} \end{bmatrix}$ {Equ. (4.21)}

3: SVD of $\widehat{\mathcal{H}}^{(\mathrm{all,ref})} = \begin{bmatrix} \widehat{U}_1 & \widehat{U}_0 \end{bmatrix} \begin{bmatrix} \widehat{\Delta}_1 & 0 \\ 0 & \widehat{\Delta}_0 \end{bmatrix} \begin{bmatrix} \widehat{V}_1^T \\ \widehat{V}_0^T \end{bmatrix}$, keep $\widehat{\mathcal{Z}}^{(\mathrm{all})} \stackrel{\mathrm{def}}{=} \widehat{\Delta}_1^{1/2}\widehat{V}_1^T$ and recover $\widehat{\mathcal{Z}}^{(j)}$, $j = 1, \ldots, N_s$, from partitioning $\widehat{\mathcal{Z}}^{(\mathrm{all})} = \begin{bmatrix} \widehat{\mathcal{Z}}^{(1)} & \ldots & \widehat{\mathcal{Z}}^{(N_s)} \end{bmatrix}$ {Equation (4.22)}

4: Compute $\widehat{\overline{\mathcal{H}}}^{(j,\mathrm{mov})} = \widehat{\mathcal{H}}^{(j,\mathrm{mov})}\widehat{\mathcal{Z}}^{(j)\dagger}\widehat{\mathcal{Z}}^{(1)}$ {Equation (4.23)}

5: Build $\widehat{\overline{\mathcal{H}}}^{(\mathrm{all})}$ by interleaving the block rows of $\widehat{\mathcal{H}}^{(1,\mathrm{ref})}$ and $\widehat{\overline{\mathcal{H}}}^{(j,\mathrm{mov})}$, $j = 1, \ldots, N_s$ {Equation (4.24)}

Output: Global subspace matrix $\widehat{\overline{\mathcal{H}}}^{(\mathrm{all})}$ for system identification

4.3.5 Modular merging algorithm for SSI algorithms with $W = I$

For obtaining the right factors $\mathcal{Z}^{(j)}$ in (4.22), the subspace matrices of all the setups $j = 1, \ldots, N_s$ need to be in memory at the same time. This can be a problem in the case of a large number of setups or when it is impractical to access data from different setups at the same time. With the help of the following lemma, this step can be avoided, thus leading to a more efficient merging procedure.

Lemma 4.3 *For each setup $j \in \{1, \ldots, N_s\}$ let $\mathcal{H}^{(j,\mathrm{ref})}$ be given, which is obtained from the local subspace matrix $\mathcal{H}^{(j)}$ and fulfills factorization property* (4.19)*. Assume that the pair $(C^{(\mathrm{ref})}, A)$ is observable, i.e. $\mathcal{O}(C^{(\mathrm{ref})}, A)$ is full column rank, and $\mathcal{Z}^{(j)}$ is full row rank. Then,*

$$\mathcal{Z}^{(j)\dagger}\mathcal{Z}^{(1)} = \mathcal{H}^{(j,\mathrm{ref})\dagger}\mathcal{H}^{(1,\mathrm{ref})}.$$

Proof: From factorization property (4.19) follows

$$\mathcal{H}^{(j,\mathrm{ref})\dagger} = \mathcal{Z}^{(j)\dagger}\mathcal{O}(C^{(\mathrm{ref})}, A)^{\dagger},$$

as $\mathcal{O}(C^{(\mathrm{ref})}, A)$ is full column rank and $\mathcal{Z}^{(j)}$ is full row rank. Post-multiplying $\mathcal{H}^{(1,\mathrm{ref})} = \mathcal{O}(C^{(\mathrm{ref})}, A)\mathcal{Z}^{(1)}$ leads to the assertion, again because $\mathcal{O}(C^{(\mathrm{ref})}, A)$ is full column rank. □

Lemma 4.3 makes the explicit computation of the factors $\mathcal{Z}^{(j)}$ unnecessary for the normalization in (4.23), which is then equivalent to

$$\overline{\mathcal{H}}^{(j,\mathrm{mov})} = \mathcal{H}^{(j,\mathrm{mov})}\mathcal{H}^{(j,\mathrm{ref})\dagger}\mathcal{H}^{(1,\mathrm{ref})}. \tag{4.25}$$

The resulting modular merging algorithm is summarized in Algorithm 4.3, where the data of the different setups is processed setup after setup, instead of altogether while only keeping $\mathcal{H}^{(1,\mathrm{ref})}$ in memory all the time.

Algorithm 4.3 Modular multi-setup merging for SSI algorithms without left weighting

Input: Local subspace matrix estimates $\widehat{\mathcal{H}}^{(j)}$ for setups $j = 1, \ldots, N_s$ {Definition 4.2}

1: **for** $j = 1$ to N_s **do**
2: Separate $\widehat{\mathcal{H}}^{(j)}$ into $\widehat{\mathcal{H}}^{(j,\mathrm{ref})}$ and $\widehat{\mathcal{H}}^{(j,\mathrm{mov})}$ {Equations (4.19), (4.20)}
3: Compute $\widehat{\overline{\mathcal{H}}}^{(j,\mathrm{mov})} = \widehat{\mathcal{H}}^{(j,\mathrm{mov})}\widehat{\mathcal{H}}^{(j,\mathrm{ref})\dagger}\widehat{\mathcal{H}}^{(1,\mathrm{ref})}$ {Equation (4.25)}
4: **end for**
5: Build $\widehat{\overline{\mathcal{H}}}^{(\mathrm{all})}$ by interleaving the block rows of $\widehat{\mathcal{H}}^{(1,\mathrm{ref})}$ and $\widehat{\overline{\mathcal{H}}}^{(j,\mathrm{mov})}$, $j = 1, \ldots, N_s$ {Equation (4.24)}

Output: Global subspace matrix $\widehat{\overline{\mathcal{H}}}^{(\mathrm{all})}$ for system identification

4.3.6 Generalized merging algorithm for arbitrary SSI algorithms

Let the local subspace matrices $\mathcal{H}^{(j)}$, $j = 1, \ldots, N_s$ according to Definition 4.2 for any subspace identification algorithm be given, which fulfill the factorization property

$$\mathcal{H}^{(j)} = W^{(j)}\mathcal{O}^{(j)}\mathcal{Z}^{(j)} \tag{4.26}$$

as in (4.2), with an invertible weighting matrix $W^{(j)}$, for any setup j. The respective local observability matrices $\mathcal{O}^{(j)}$, which can be obtained from $\mathcal{H}^{(j)}$ as described in Section 4.2, are now used for merging in order to obtain a global observability matrix $\mathcal{O}^{(\mathrm{all})} \stackrel{\mathrm{def}}{=} \mathcal{O}(C^{(\mathrm{all})}, A)$, on which the system identification can be done. This is slightly different from the last sections, where it was the aim to obtain a global subspace matrix $\mathcal{H}^{(\mathrm{all})}$.

As the local observability matrices are obtained from the local subspace matrices for each setup separately, they might be in different modal bases, so in fact only $\mathcal{O}^{(j)}T_j$ can be obtained from $\mathcal{H}^{(j)}$, where T_j is an invertible change of basis matrix. The problem for merging regards now the different factors T_j instead of the different factors $\mathcal{Z}^{(j)}$ as previously.

For any j, the matrix $\mathcal{O}^{(j)}$ fulfills property (4.9) and hence can be separated into $\mathcal{O}(C^{(\mathrm{ref})}, A)$ and $\mathcal{O}(C^{(j,\mathrm{mov})}, A)$ by choosing the appropriate block rows of $\mathcal{O}^{(j)}$. Hence, separating $\mathcal{O}^{(j)}T_j$ in the same way leads to

$$\mathcal{O}^{(j,\mathrm{ref})} \stackrel{\mathrm{def}}{=} \mathcal{O}(C^{(\mathrm{ref})}, A)T_j,\ \mathcal{O}^{(j,\mathrm{mov})} \stackrel{\mathrm{def}}{=} \mathcal{O}(C^{(j,\mathrm{mov})}, A)T_j. \tag{4.27}$$

Assume that in each setup j the pair $(C^{(\mathrm{ref})}, A)$ is observable, i.e. $\mathcal{O}^{(j,\mathrm{ref})}$ is full column rank. A common modal basis for all setups can then be defined by the chosen modal basis of one of the setups. Without loss of generality, let this be setup 1, for which $T_1 = I$ is defined as the identity matrix, and hence $\mathcal{O}^{(1,\mathrm{ref})} = \mathcal{O}(C^{(\mathrm{ref})}, A)$. Another possibility to define a common modal basis is to make use of all the reference parts of the local observability matrices $\mathcal{O}^{(j,\mathrm{ref})}$, to juxtapose them and obtain $\mathcal{O}(C^{(\mathrm{ref})}, A)$ through the factorization

$$\begin{bmatrix}\mathcal{O}^{(1,\mathrm{ref})} & \dots & \mathcal{O}^{(N_s,\mathrm{ref})}\end{bmatrix} = \mathcal{O}(C^{(\mathrm{ref})}, A)\begin{bmatrix}T_1 & \dots & T_{N_s}\end{bmatrix}$$

by an SVD. In both ways, the obtained matrix $\mathcal{O}(C^{(\mathrm{ref})}, A)$ defines the modal basis, into which the other observability matrices have to be converted prior to merging.

Lemma 4.4 *For each setup $j \in \{1, \dots, N_s\}$ let $\mathcal{O}^{(j,\mathrm{ref})}$ and $\mathcal{O}^{(j,\mathrm{mov})}$ be defined as in* (4.27)*, and let $(C^{(\mathrm{ref})}, A)$ be observable. Then,*

$$\mathcal{O}(C^{(j,\mathrm{mov})}, A) = \mathcal{O}^{(j,\mathrm{mov})}\mathcal{O}^{(j,\mathrm{ref})\dagger}\mathcal{O}(C^{(\mathrm{ref})}, A). \tag{4.28}$$

Proof: From the first part of (4.27) follows $\mathcal{O}^{(j,\mathrm{ref})}T_j^{-1} = \mathcal{O}(C^{(\mathrm{ref})}, A)$ and hence

$$T_j^{-1} = \mathcal{O}^{(j,\mathrm{ref})\dagger}\mathcal{O}(C^{(\mathrm{ref})}, A),$$

as $(C^{(\mathrm{ref})}, A)$ is observable and thus $\mathcal{O}^{(j,\mathrm{ref})}$ is full column rank. Post-multiplying this to the second part of (4.27) leads to the assertion. □

Lemma 4.4 provides a way to obtain the matrices $\mathcal{O}(C^{(j,\mathrm{mov})}, A)$, $j = 1, \dots, N_s$, which are in the same modal basis as $\mathcal{O}(C^{(\mathrm{ref})}, A)$. Hence, they can be merged together to the global observability matrix $\mathcal{O}^{(\mathrm{all})}$ by interleaving their block rows

$$\mathcal{O}^{(\mathrm{all})} = P_1\begin{bmatrix}\mathcal{O}(C^{(\mathrm{ref})}, A)\\ \mathcal{O}(C^{(1,\mathrm{mov})}, A)\\ \vdots \\ \mathcal{O}(C^{(N_s,\mathrm{mov})}, A)\end{bmatrix} = \mathcal{O}(C^{(\mathrm{all})}, A), \tag{4.29}$$

where P_1 is a suitable permutation matrix as in (4.24). The resulting merging algorithm, which is suitable for arbitrary subspace identification algorithms, is summarized in Algorithm 4.4, where the modal basis is defined by $\mathcal{O}(C^{(\mathrm{ref})}, A) = \mathcal{O}^{(1,\mathrm{ref})}$ in setup 1.

Algorithm 4.4 Multi-setup merging for arbitrary SSI algorithms

Input: Local subspace matrix estimates $\widehat{\mathcal{H}}^{(j)}$ and weightings $\widehat{W}^{(j)}$ for setups $j = 1, \dots, N_s$ {Equation (4.26)}

1: **for** $j = 1$ to N_s **do**

2: SVD and truncation at model order $\widehat{\mathcal{H}}^{(j)} = \begin{bmatrix}\widehat{U}_1 & \widehat{U}_0\end{bmatrix} \begin{bmatrix}\widehat{\Delta}_1 & 0 \\ 0 & \widehat{\Delta}_0\end{bmatrix} \begin{bmatrix}\widehat{V}_1^T \\ \widehat{V}_0^T\end{bmatrix}$ {Equ. (4.5)}

3: Compute $\widetilde{\mathcal{O}}^{(j)} = \widehat{W}^{(j)-1}\widehat{U}_1\widehat{\Delta}_1^{1/2}$

4: Separate $\widetilde{\mathcal{O}}^{(j)}$ into $\widehat{\mathcal{O}}^{(j,\mathrm{ref})}$ and $\widehat{\mathcal{O}}^{(j,\mathrm{mov})}$ {Equation (4.27)}

5: Compute $\widehat{\overline{\mathcal{O}}}^{(j,\mathrm{mov})} = \widehat{\mathcal{O}}^{(j,\mathrm{mov})}\widehat{\mathcal{O}}^{(j,\mathrm{ref})\dagger}\widehat{\mathcal{O}}^{(1,\mathrm{ref})}$ {Equation (4.28)}

6: **end for**

7: Build $\widehat{\mathcal{O}}^{(\mathrm{all})}$ by interleaving the block rows of $\widehat{\mathcal{O}}^{(1,\mathrm{ref})}$ and $\widehat{\overline{\mathcal{O}}}^{(j,\mathrm{mov})}$, $j = 1, \dots, N_s$ {Equation (4.29)}

Output: Observability matrix $\mathcal{O}(\widehat{C}^{(\mathrm{all})}, \widehat{A}) = \widehat{\mathcal{O}}^{(\mathrm{all})}$ for global system identification

4.3.7 Scalable computation of $(C^{(\mathrm{all})}, A)$ for arbitrary SSI algorithms

In the previous section, the local subspace matrices $\mathcal{H}^{(j)}$, $j = 1, \dots, N_s$, are used for the computation of a global observability matrix $\mathcal{O}^{(\mathrm{all})}$, from which the system matrices $(C^{(\mathrm{all})}, A)$ are recovered for system identification as described in Section 4.2: $C^{(\mathrm{all})}$ as the first block row of $\mathcal{O}^{(\mathrm{all})}$, and A as the least squares solution of (4.4). However, if the number of sensors and setups is large, the matrix $\mathcal{O}^{(\mathrm{all})}$ may also be large, causing possibly memory problems when solving the least squares problem for A. In the following, an algorithm is described that directly computes the system matrices $(C^{(\mathrm{all})}, A)$ from the local subspace matrices, without computing $\mathcal{O}^{(\mathrm{all})}$ explicitly.

Proposition 4.5 *Let the thin QR decompositions and products*

$$\mathcal{O}(C^{(\mathrm{ref})}, A)^{\uparrow} = Q_0 R_0, \qquad S_0 \overset{\mathrm{def}}{=} Q_0^T \mathcal{O}(C^{(\mathrm{ref})}, A)^{\downarrow}, \tag{4.30}$$

$$\begin{bmatrix} R_{j-1} \\ \mathcal{O}(C^{(j,\mathrm{mov})}, A)^{\uparrow} \end{bmatrix} = Q_j R_j, \qquad S_j \overset{\mathrm{def}}{=} Q_j^T \begin{bmatrix} S_{j-1} \\ \mathcal{O}(C^{(j,\mathrm{mov})}, A)^{\downarrow} \end{bmatrix}, \quad j = 1, \dots, N_s \tag{4.31}$$

be given iteratively, where $\mathcal{O}(C^{(j,\mathrm{mov})}, A)$ is obtained from (4.28) during the iteration. Then, the least squares solution of $\mathcal{O}^{(\mathrm{all})\uparrow} A = \mathcal{O}^{(\mathrm{all})\downarrow}$ is given by

$$A = R_{N_s}^{-1} S_{N_s},$$

and the parts of $C^{(\mathrm{all})}$ are recovered as the first block row of $\mathcal{O}(C^{(\mathrm{ref})}, A)$ and each $\mathcal{O}(C^{(j,\mathrm{mov})}, A)$, $j = 1, \dots, N_s$, during the iteration.

Proof: From (4.29) follows

$$\mathcal{O}^{(\text{all})\uparrow} = P_2 \begin{bmatrix} \mathcal{O}(C^{(\text{ref})}, A)^{\uparrow} \\ \mathcal{O}(C^{(1,\text{mov})}, A)^{\uparrow} \\ \vdots \\ \mathcal{O}(C^{(N_s,\text{mov})}, A)^{\uparrow} \end{bmatrix}, \quad \mathcal{O}^{(\text{all})\downarrow} = P_2 \begin{bmatrix} \mathcal{O}(C^{(\text{ref})}, A)^{\downarrow} \\ \mathcal{O}(C^{(1,\text{mov})}, A)^{\downarrow} \\ \vdots \\ \mathcal{O}(C^{(N_s,\text{mov})}, A)^{\downarrow} \end{bmatrix},$$

with the same permutation matrix P_2 for both matrices. Thus, the least squares problem for A is equivalent to

$$\begin{bmatrix} \mathcal{O}(C^{(\text{ref})}, A)^{\uparrow} \\ \mathcal{O}(C^{(1,\text{mov})}, A)^{\uparrow} \\ \vdots \\ \mathcal{O}(C^{(N_s,\text{mov})}, A)^{\uparrow} \end{bmatrix} A = \begin{bmatrix} \mathcal{O}(C^{(\text{ref})}, A)^{\downarrow} \\ \mathcal{O}(C^{(1,\text{mov})}, A)^{\downarrow} \\ \vdots \\ \mathcal{O}(C^{(N_s,\text{mov})}, A)^{\downarrow} \end{bmatrix}$$

and the assertion follows from Lemma 3.8. □

Note that after obtaining the local observability matrices of size $(p+1)(r^{(\text{ref})} + r^{(j)}) \times n$, in this algorithm at no time matrices larger than $(p \cdot \max\{r^{(j)}\} + n) \times n$ are processed.

Then, from Proposition 4.5 the iterative computation of the system matrices is derived in Algorithm 4.5.

Remark 4.6 *In Proposition 4.5 and Algorithm 4.5 the estimate of the system matrix A is obtained iteratively at one specific model order from a least squares solution $A = R^{-1}S$. If the model order is unknown (cf. Section 4.5), the techniques from Chapter 5 can be used to obtain estimates of the system matrix at inferior model orders only by knowing the matrices R and S (cf. Section 5.3.5).*

4.3.8 Some remarks

First, a remark is in order about the condition that the pair $(C^{(\text{ref})}, A)$ needs to be observable in all setups $j = 1, \ldots, N_s$. This is a reasonable assumption, as it means that all the modes of the system need to be excited in the different data records, while the excitation may change. For the choice of the parameters in the identification algorithms it means that p has to be chosen such that $\mathcal{O}_{p+1}(C^{(\text{ref})}, A)^{\uparrow} = \mathcal{O}_p(C^{(\text{ref})}, A)$ is full column rank in all setups, while the number of columns of $\mathcal{O}_p(C^{(\text{ref})}, A)$ is the model order n. A necessary condition is hence $pr^{(\text{ref})} \geq n$. As parameter q for the subspace matrix (see e.g. (2.7) and (2.8)) is often set as $q \stackrel{\text{def}}{=} p + 1$ [BBG+01], it may be useful to construct the local subspace matrices using the fixed reference sensors as projection channels as in [PDR99] for an efficient implementation. An example is the covariance-driven merging algorithm in Section 4.3.3, where for each setup cross-correlations between all the sensor data and the reference sensor data are used. Another example will be given in Section 4.6.2, where in the data matrices $\mathcal{Y}^{(j)-}$ only data from the reference sensors is used.

Second, a remark should be made about the choice between the presented merging algorithms. Algorithm 4.1 is only suitable for the covariance-driven subspace identification.

Algorithm 4.5 Multi-setup merging for arbitrary SSI algorithms with iterative computation of system matrices

Input: Local subspace matrix estimates $\widehat{\mathcal{H}}^{(j)}$ and weightings $\widehat{W}^{(j)}$ for setups $j = 1, \ldots, N_s$ {Equation (4.26)}

1: **for** $j = 1$ to N_s **do**
2: SVD and truncation at model order $\widehat{\mathcal{H}}^{(j)} = \begin{bmatrix} \widehat{U}_1 & \widehat{U}_0 \end{bmatrix} \begin{bmatrix} \widehat{\Delta}_1 & 0 \\ 0 & \widehat{\Delta}_0 \end{bmatrix} \begin{bmatrix} \widehat{V}_1^T \\ \widehat{V}_0^T \end{bmatrix}$ {Equ. (4.5)}
3: Compute $\widetilde{\mathcal{O}}^{(j)} = \widehat{W}^{(j)-1} \widehat{U}_1 \widehat{\Delta}_1^{1/2}$
4: Separate $\widetilde{\mathcal{O}}^{(j)}$ into $\widehat{\mathcal{O}}^{(j,\mathrm{ref})}$ and $\widehat{\mathcal{O}}^{(j,\mathrm{mov})}$ {Equation (4.27)}
5: **if** $j == 1$ **then**
6: QR decomposition of $\widehat{\mathcal{O}}^{(1,\mathrm{ref})\uparrow} = QR$
7: Compute $S = Q^T \widehat{\mathcal{O}}^{(1,\mathrm{ref})\downarrow}$
8: Extract $\widehat{C}^{(\mathrm{ref})}$ from first block row of $\widehat{\mathcal{O}}^{(1,\mathrm{ref})}$ and keep it
9: **end if**
10: Compute $\widehat{\overline{\mathcal{O}}}^{(j,\mathrm{mov})} = \widehat{\mathcal{O}}^{(j,\mathrm{mov})} \widehat{\mathcal{O}}^{(j,\mathrm{ref})\dagger} \widehat{\mathcal{O}}^{(1,\mathrm{ref})}$ {Equation (4.28)}
11: QR decomposition of $\begin{bmatrix} R \\ \widehat{\overline{\mathcal{O}}}^{(j,\mathrm{mov})\uparrow} \end{bmatrix} = \tilde{Q}\tilde{R}$
12: Compute $\tilde{S} = \tilde{Q}^T \begin{bmatrix} S \\ \widehat{\overline{\mathcal{O}}}^{(j,\mathrm{mov})\downarrow} \end{bmatrix}$
13: Set $S = \tilde{S}$, $R = \tilde{R}$
14: Extract $\widehat{C}^{(j,\mathrm{mov})}$ from first block row of $\widehat{\overline{\mathcal{O}}}^{(j,\mathrm{mov})}$ and keep it
15: **end for**
16: Compute $\widehat{A} = R^{-1} S$
17: Stack $\widehat{C}^{(\mathrm{ref})}$ and $\widehat{C}^{(j,\mathrm{mov})}$, $j = 1, \ldots, N_s$, to $\widehat{C}^{(\mathrm{all})}$

Output: $\widehat{A}$, $\widehat{C}^{(\mathrm{all})}$ {system matrices after merging}

Algorithms 4.2 and 4.3, which apply to any subspace identification algorithm without a left weighting, differ in the order of data processing from the measurement setups and the number of numerical operations. As Algorithm 4.3 does not need the SVD of the juxtaposed subspace matrices related to the reference sensors and has a simpler structure, it is preferable to Algorithm 4.2. Algorithm 4.4 applies to arbitrary subspace identification algorithms. Besides the more general setting of Algorithm 4.4, it directly computes the global observability matrix that is needed for the subspace identification. The scalable computation of the system matrices A and C in Algorithm 4.5 is an extension of Algorithm 4.4 and should be chosen in the case of a very large number of sensors and setups when memory problems arise.

Third, a remark about the applicability of the presented algorithms is in order. The only condition of the merging algorithm to work with a subspace identification algorithm is factorization property (4.2) of the respective subspace matrix, and the retrieval of the system matrices from the obtained observability matrix. This is a very general condition and applies, up to our knowledge, to all output-only subspace identification algorithms in literature. It

also applies to combined deterministic-stochastic subspace identification algorithms, where some of the inputs of the system are known [VODM96], which is even a more general setting than the output-only system identification considered in this chapter.

4.4 Non-stationary consistency

Until now, we have assumed stationary excitation within each record, but with a record-dependent covariance matrix. A more realistic assumption is that the excitation is non-stationary within each record, i.e. the excitation covariance $\mathbf{E}(V_k^{(j)}V_{k'}^{(j)T}) \stackrel{\text{def}}{=} Q_k^{(j)}\delta(k-k')$ is time-varying. We show that the merging algorithms can still be applied in this case of non-stationary excitation with only little modification. Then, the identified system matrices are consistent, once the subspace identification algorithm that is used to obtain the local subspace matrices for each setup provides consistent estimates for the observation and state transition matrices. The latter is the case, when the subspace identification algorithm fulfills the following assumption.

Assumption 4.7 *For each record j there exists a triplet $(C^{(j)}, A, T_j)$ and a sequence of matrices $T_j(N)$, with $T_j(N)$ and $T_j(N)^{-1}$ uniformly bounded w.r.t. N, satisfying*

$$\begin{aligned} C^{(j)}(N)T_j(N) &\longrightarrow C^{(j)}T_j \\ T_j(N)^{-1}A_j(N)T_j(N) &\longrightarrow T_j^{-1}AT_j \end{aligned}$$

for $N \to \infty$, where

$$C^{(j)} \stackrel{\text{def}}{=} \begin{bmatrix} C^{(\text{ref})} \\ C^{(j,\text{mov})} \end{bmatrix}.$$

Matrix T_j denotes the modal basis defined by record j for $N \to \infty$ where $T_1 = I$, similar to $T_j(N)$ in (4.27). The pair $(C^{(j)}(N), A_j(N))$ corresponds to $(\widehat{C}, \widehat{A})$, which is computed with subspace system identification as in Section 4.2 from the local subspace matrix $\widehat{\mathcal{H}}^{(j)}$ using N data samples.

Assumption 4.7 is satisfied under [BM07, Assumption 1] regarding the (stochastic) inputs and [BM07, Condition 2] regarding the chosen subspace algorithm. Notice that all subspace algorithms mentioned in [BM07] satisfy these conditions, in particular the covariance-driven and data-driven algorithm that are applied in this chapter, when the factor N in (2.10) and (4.41)–(4.42) is replaced by some value s_N satisfying [BM07, Condition 2].

Theorem 4.8 *Let the pair $(C^{(\text{all})}(N), A(N))$ correspond to $(\widehat{C}^{(\text{all})}, \widehat{A})$ that can be recovered from $\widehat{\overline{\mathcal{H}}}^{(\text{all})}$ defined in Algorithm 4.3 or $\widehat{\mathcal{O}}^{(\text{all})}$ defined in Algorithm 4.4. Then, under Assumption 4.7, there exists a pair $(C^{(\text{all})}, A)$ and a sequence of matrices $T(N)$, with $T(N)$ and $T(N)^{-1}$ uniformly bounded w.r.t. N, satisfying*

$$\begin{aligned} C^{(\text{all})}(N)T(N) &\longrightarrow C^{(\text{all})}, \\ T(N)^{-1}A(N)T(N) &\longrightarrow A \end{aligned}$$

for $N \to \infty$.

Proof: From Assumption 4.7 follows

$$\begin{aligned} C^{(j,\mathrm{ref})}(N)T_j(N) &\longrightarrow C^{(\mathrm{ref})}T_j \\ C^{(j,\mathrm{mov})}(N)T_j(N) &\longrightarrow C^{(j,\mathrm{mov})}T_j \end{aligned}$$

when separating $C^{(j)}(N)$ in its reference and moving sensor part, for any setup j. For the respective local observability matrices the convergence properties

$$\begin{aligned} \mathcal{O}(C^{(\mathrm{ref})}(N), A_j(N))T_j(N) &\longrightarrow \mathcal{O}(C^{(\mathrm{ref})}, A)T_j, \\ \mathcal{O}(C^{(j,\mathrm{mov})}(N), A_j(N))T_j(N) &\longrightarrow \mathcal{O}(C^{(j,\mathrm{mov})}, A)T_j \end{aligned}$$

follow and hence for the part of the global observability matrix in Step 5 of Algorithm 4.4

$$\begin{aligned} \overline{\mathcal{O}}(C^{(j,\mathrm{mov})}(N), A_j(N)) &\overset{\mathrm{def}}{=} \mathcal{O}(C^{(j,\mathrm{mov})}(N), A_j(N))T_j(N) \left(\mathcal{O}(C^{(j,\mathrm{ref})}(N), A_j(N))T_j(N)\right)^{\dagger} \\ &\qquad \cdot \mathcal{O}(C^{(1,\mathrm{ref})}(N), A_1(N))T_1(N) \\ &\longrightarrow \mathcal{O}(C^{(j,\mathrm{mov})}, A)T_j \left(\mathcal{O}(C^{(\mathrm{ref})}, A)T_j\right)^{\dagger} \mathcal{O}(C^{(\mathrm{ref})}, A)T_1 \\ &= \mathcal{O}(C^{(j,\mathrm{mov})}, A). \end{aligned}$$

Interleaving the block rows of $\mathcal{O}(C^{(1,\mathrm{ref})}(N), A_1(N))T_1(N)$ and $\overline{\mathcal{O}}(C^{(j,\mathrm{mov})}(N), A_j(N))$, $j = 1, \ldots, N_s$, and using (4.29), the assertion follows for Algorithm 4.4.

It remains the proof for Algorithm 4.3, when the pair $(C^{(\mathrm{all})}(N), A(N))$ is recovered from $\widehat{\overline{\mathcal{H}}}^{(\mathrm{all})}$. Then, under Assumption 4.7 it follows

$$\widehat{\mathcal{H}}^{(j,\mathrm{ref})} = \mathcal{O}(C^{(\mathrm{ref})}(N), A_j(N))\mathcal{Z}^{(j)}(N) + o(1),$$

where $\mathcal{Z}^{(j)}(N)$ is the empirical counterpart of $\mathcal{Z}^{(j)}$ in (4.19) and (4.20), and $o(1)$ tends to zero when $N \to \infty$. With the same reasoning as above it follows

$$\widehat{\overline{\mathcal{H}}}^{(j,\mathrm{mov})} = \mathcal{O}(C^{(j,\mathrm{mov})}(N), A_j(N))\mathcal{Z}^{(1)}(N) + o(1)$$

in Step 3 of Algorithm 4.3. Then, together with (4.24) and [BM07, Theorem 1] the assertion follows for Algorithm 4.3. □

The previous theorem proves non-stationary consistency for system identification with Algorithms 4.3 and 4.4, once the underlying subspace method also provides non-stationary consistent estimates. The same holds for Algorithm 4.2, which provides equivalent results as Algorithm 4.3, and Algorithm 4.5 which provides equivalent results as Algorithm 4.4.

4.5 Multi-setup identification under misspecified model order

In practice, the true system order is often unknown when data are recorded under operational conditions. Recommended techniques from statistics to estimate the best model order are not useful in this context. In order to retrieve a desired number of modes, a larger model

order must be assumed. Then, the rank of the respective subspace matrices is hardly the true model order n, but full rank due to noise and a limited number of data samples. This section addresses two issues: First, the truncation at a desired model order in the merging algorithms, and second, the coherence of the merging algorithms during multi-order system identification, where the identification procedure is repeated while truncating at different model orders $n = n_{\min}, \dots, n_{\max}$. The results of the multi-order identification are displayed in *stabilization diagrams* (see Section 2.4), where system modes can be distinguished from noise modes as the latter tend to vary at different orders.

4.5.1 Considering truncation due to noise

When deriving the merging algorithms, the order of the system was assumed to be a fixed value n, with all involved subspace matrices being of rank n. However, when subspace matrices are obtained from real data, the rank of the system usually cannot be determined from them, as there is no drop in the singular values to zero due to noise and model reduction. Some assumption about the model order needs to be made for the identification, namely by the selection of an order n in (4.23), on which Algorithm 4.3 is based, or $\widetilde{\mathcal{O}}^{(j)}$ in Algorithm 4.4. However, Algorithm 4.3 is based on Lemma 4.3, which assumes that factorization property (4.19) is fulfilled exactly. This is not the case when some system order n is assumed, which is lower than the dimension of $\widehat{\mathcal{H}}^{(j,\mathrm{ref})}$. In this case, Algorithm 4.3 needs to be slightly modified.

Lemma 4.9 *For each setup $j \in \{1, \dots, N_s\}$ let $\widehat{\mathcal{H}}^{(j,\mathrm{ref})}$ be given, which can be obtained from the local subspace matrix $\widehat{\mathcal{H}}^{(j)}$. It holds*

$$\widehat{\mathcal{H}}^{(j,\mathrm{ref})} = \mathcal{O}(\widehat{C}^{(\mathrm{ref})}, \widehat{A})\widehat{\mathcal{Z}}^{(j)} + U_0^{(j)}\Delta_0^{(j)}V_0^{(j)T}$$

similar to factorization property (4.19)*, where a partitioned SVD of $\widehat{\mathcal{H}}^{(j,\mathrm{ref})}$ at model order n is given by*

$$\widehat{\mathcal{H}}^{(j,\mathrm{ref})} = \begin{bmatrix} U_1^{(j)} & U_0^{(j)} \end{bmatrix} \begin{bmatrix} \Delta_1^{(j)} & 0 \\ 0 & \Delta_0^{(j)} \end{bmatrix} \begin{bmatrix} V_1^{(j)T} \\ V_0^{(j)T} \end{bmatrix}.$$

Assume that the pair $(C^{(\mathrm{ref})}, A)$ is observable, i.e. $\mathcal{O}(\widehat{C}^{(\mathrm{ref})}, \widehat{A})$ is full column rank, and $\widehat{\mathcal{Z}}^{(j)}$ is full row rank. Then, it holds

$$\widehat{\mathcal{Z}}^{(j)\dagger}\widehat{\mathcal{Z}}^{(1)} = \widehat{\mathcal{H}}^{(j,\mathrm{ref})\dagger,n}\widehat{\mathcal{H}}^{(1,\mathrm{ref})},$$

where $\widehat{\mathcal{H}}^{(j,\mathrm{ref})\dagger,n} \overset{\mathrm{def}}{=} V_1^{(j)}\Delta_1^{(j)-1}U_1^{(j)T}$ denotes the truncated pseudoinverse of $\widehat{\mathcal{H}}^{(j,\mathrm{ref})}$ at order n.

Proof: From the definition of the truncated pseudoinverse follows that $\widehat{\mathcal{H}}^{(j,\mathrm{ref})\dagger,n}$ is equal to $\widehat{\mathcal{Z}}^{(j)\dagger}\mathcal{O}(\widehat{C}^{(\mathrm{ref})}, \widehat{A})^\dagger$ and hence

$$\widehat{\mathcal{H}}^{(j,\mathrm{ref})\dagger,n}\widehat{\mathcal{H}}^{(1,\mathrm{ref})} = \widehat{\mathcal{Z}}^{(j)\dagger}\widehat{\mathcal{Z}}^{(1)} + \widehat{\mathcal{Z}}^{(j)\dagger}\mathcal{O}(\widehat{C}^{(\mathrm{ref})}, \widehat{A})^\dagger U_0^{(1)}\Delta_0^{(1)}V_0^{(1)T}. \tag{4.32}$$

As $\mathcal{O}(\widehat{C}^{(\mathrm{ref})}, \widehat{A})\widehat{\mathcal{Z}}^{(1)} = U_1^{(1)}\Delta_1^{(1)}V_1^{(1)T}$, it follows $\mathcal{O}(\widehat{C}^{(\mathrm{ref})}, \widehat{A})^\dagger = \widehat{\mathcal{Z}}^{(1)}V_1^{(1)}\Delta_1^{(1)-1}U_1^{(1)T}$. Plugging this in (4.32), it is apparent that the second term is zero because of $U_1^{(1)T}U_0^{(1)} = 0$,

proving the assertion. □

Hence, in Algorithm 4.3 Step 3 has to be replaced by

$$\widehat{\overline{\mathcal{H}}}^{(j,\mathrm{mov})} = \widehat{\mathcal{H}}^{(j,\mathrm{mov})}\widehat{\mathcal{H}}^{(j,\mathrm{ref})\dagger,n}\widehat{\mathcal{H}}^{(1,\mathrm{ref})}$$

in the case of assuming an (unknown) model order n.

4.5.2 Multi-order system identification

It is common practice to do multi-order system identification in order to distinguish the identified true system modes from noise modes, as the latter tend to vary [PDR99]. For an efficient computation of the modal parameters at multiple model orders $n = n_{\min}, \ldots, n_{\max}$ in a single setup, usage is to truncate in (4.5) at these different orders, which is the same as computing the observability matrix estimate at the highest desired model order $n_{\max}$ and selecting the submatrices containing the first n_i columns to obtain the observability matrix estimate at a lower order n_i. However, in the merging algorithms a global observability matrix is only obtained at a specific model order, either from $\widehat{\overline{\mathcal{H}}}^{(\mathrm{all})}$ by an SVD as in (4.5), when using Algorithms 4.2 and 4.3, or directly, when using Algorithms 4.4 and 4.5. The question is whether an observability matrix estimate at a model order n_i can be obtained in a similar way by selecting columns of the global observability matrix obtained by the corresponding merging algorithm at maximal desired model order $n_{\max}$. This is indeed the case and proved first for Algorithm 4.4.

Proposition 4.10 *Let $\widehat{\mathcal{O}}_{n_i}^{(\mathrm{all})}$ and $\widehat{\mathcal{O}}_{n_{\max}}^{(\mathrm{all})}$ be the global observability matrices obtained by Algorithm 4.4 at model orders n_i and $n_{\max}$ with $n_i < n_{\max}$. Then, $\widehat{\mathcal{O}}_{n_i}^{(\mathrm{all})}$ consists of the first n_i columns of $\widehat{\mathcal{O}}_{n_{\max}}^{(\mathrm{all})}$, i.e.*

$$\widehat{\mathcal{O}}_{n_{\max}}^{(\mathrm{all})} = \begin{bmatrix} \widehat{\mathcal{O}}_{n_i}^{(\mathrm{all})} & Z \end{bmatrix}$$

with some matrix Z.

Proof: We have to prove that

$$\widehat{\overline{\mathcal{O}}}_{n_i}^{(j,\mathrm{mov})} = \widehat{\mathcal{O}}_{n_i}^{(j,\mathrm{mov})}\widehat{\mathcal{O}}_{n_i}^{(j,\mathrm{ref})\dagger}\widehat{\mathcal{O}}_{n_i}^{(1,\mathrm{ref})}, \tag{4.33}$$

obtained at model order n_i in Step 5 of Algorithm 4.4, consists of the first n_i columns of

$$\widehat{\overline{\mathcal{O}}}_{n_{\max}}^{(j,\mathrm{mov})} = \widehat{\mathcal{O}}_{n_{\max}}^{(j,\mathrm{mov})}\widehat{\mathcal{O}}_{n_{\max}}^{(j,\mathrm{ref})\dagger}\widehat{\mathcal{O}}_{n_{\max}}^{(1,\mathrm{ref})}, \tag{4.34}$$

obtained at order $n_{\max}$ for any $j \in \{1, \ldots, N_{\mathrm{s}}\}$. Note that

$$\widehat{\mathcal{O}}_{n_{\max}}^{(j,\mathrm{mov})} = \begin{bmatrix} \widehat{\mathcal{O}}_{n_i}^{(j,\mathrm{mov})} & Z_1 \end{bmatrix}, \quad \widehat{\mathcal{O}}_{n_{\max}}^{(j,\mathrm{ref})} = \begin{bmatrix} \widehat{\mathcal{O}}_{n_i}^{(j,\mathrm{ref})} & Z_2 \end{bmatrix}, \quad \widehat{\mathcal{O}}_{n_{\max}}^{(1,\mathrm{ref})} = \begin{bmatrix} \widehat{\mathcal{O}}_{n_i}^{(1,\mathrm{ref})} & Z_3 \end{bmatrix}$$

with some matrices Z_1, Z_2 and Z_3. Let

$$\widehat{\mathcal{O}}_{n_{\max}}^{(j,\mathrm{ref})} = QR = \begin{bmatrix} Q_1 & Q_2 \end{bmatrix} \begin{bmatrix} R_{11} & R_{12} \\ 0 & R_{22} \end{bmatrix} \tag{4.35}$$

be the QR decomposition of $\widehat{\mathcal{O}}_{n_{\max}}^{(j,\mathrm{ref})}$, where Q and R are partitioned such that Q_1 has n_i columns and R_{11} is of size $n_i \times n_i$. Then, from (4.34) follows

$$\begin{aligned}\widehat{\overline{\mathcal{O}}}_{n_{\max}}^{(j,\mathrm{mov})} &= \begin{bmatrix}\widehat{\mathcal{O}}_{n_i}^{(j,\mathrm{mov})} & Z_1\end{bmatrix}\begin{bmatrix}R_{11}^{-1} & -R_{11}^{-1}R_{12}R_{22}^{-1}\\ 0 & R_{22}^{-1}\end{bmatrix}\begin{bmatrix}Q_1^T\\ Q_2^T\end{bmatrix}\begin{bmatrix}\widehat{\mathcal{O}}_{n_i}^{(1,\mathrm{ref})} & Z_3\end{bmatrix}\\ &= \begin{bmatrix}\widehat{\mathcal{O}}_{n_i}^{(j,\mathrm{mov})}R_{11}^{-1} & \widetilde{Z}_1\end{bmatrix}\begin{bmatrix}Q_1^T\widehat{\mathcal{O}}_{n_i}^{(1,\mathrm{ref})} & Q_1^TZ_3\\ Q_2^T\widehat{\mathcal{O}}_{n_i}^{(1,\mathrm{ref})} & Q_2^TZ_3\end{bmatrix},\end{aligned}$$

where $\widetilde{Z}_1 = -\widehat{\mathcal{O}}_{n_i}^{(j,\mathrm{mov})}R_{11}^{-1}R_{12}R_{22}^{-1} + Z_1R_{22}^{-1}$. From (4.35) follows

$$\widehat{\mathcal{O}}_{n_i}^{(j,\mathrm{ref})} = Q_1R_{11} \tag{4.36}$$

and hence $Q_2^T\widehat{\mathcal{O}}_{n_i}^{(j,\mathrm{ref})} = 0$. Then, from (4.27) follows $Q_2^T\widehat{\mathcal{O}}_{n_i}^{(1,\mathrm{ref})} = 0$ and hence

$$\widehat{\overline{\mathcal{O}}}_{n_{\max}}^{(j,\mathrm{mov})} = \begin{bmatrix}\widehat{\mathcal{O}}_{n_i}^{(j,\mathrm{mov})}R_{11}^{-1}Q_1^T\widehat{\mathcal{O}}_{n_i}^{(1,\mathrm{ref})} & \widetilde{Z}_2\end{bmatrix},$$

where $\widetilde{Z}_2 = \widehat{\mathcal{O}}_{n_i}^{(j,\mathrm{mov})}R_{11}^{-1}Q_1^TZ_3 + \widetilde{Z}_1Q_2^TZ_3$. From (4.36) follows $\widehat{\mathcal{O}}_{n_i}^{(j,\mathrm{ref})\dagger} = R_{11}^{-1}Q_1^T$, leading with (4.33) to the assertion. □

Proposition 4.10 justifies the computation of the global observability matrix with Algorithm 4.4 at a maximal desired model order and the estimation at lower model orders directly from this matrix, as it is done in subspace identification of a single setup. In a similar way, it can be shown that Algorithm 4.3 satisfies the same property:

Corollary 4.11 *Let $\widetilde{\mathcal{O}}_{n_{\max}}^{(\mathrm{all})}$ and $\widetilde{\mathcal{O}}_{n_i}^{(\mathrm{all})}$ be recovered from $\widehat{\overline{\mathcal{H}}}_{n_{\max}}^{(\mathrm{all})}$ and $\widehat{\overline{\mathcal{H}}}_{n_i}^{(\mathrm{all})}$, which are obtained from Algorithm 4.3 assuming model order $n_{\max}$ and n_i, respectively, where in Algorithm 4.3 Lemma 4.9 is applied. Then, $\widetilde{\mathcal{O}}_{n_i}^{(\mathrm{all})}$ consists of the first n_i columns of $\widetilde{\mathcal{O}}_{n_{\max}}^{(\mathrm{all})}$ up to a change of basis, i.e.*

$$\widetilde{\mathcal{O}}_{n_{\max}}^{(\mathrm{all})} = \begin{bmatrix}\widetilde{\mathcal{O}}_{n_i}^{(\mathrm{all})}T & Z\end{bmatrix}$$

with some invertible matrix T and some matrix Z.

Proof: For each $j = 1, \ldots, N_s$, in Algorithm 4.3 it follows together with Lemma 4.9

$$\widehat{\overline{\mathcal{H}}}_{n_{\max}}^{(j,\mathrm{mov})} = \widehat{\mathcal{H}}^{(j,\mathrm{mov})}\widehat{\mathcal{H}}^{(j,\mathrm{ref})\dagger,n_{\max}}\widehat{\mathcal{H}}^{(1,\mathrm{ref})}, \quad \widehat{\overline{\mathcal{H}}}_{n_i}^{(j,\mathrm{mov})} = \widehat{\mathcal{H}}^{(j,\mathrm{mov})}\widehat{\mathcal{H}}^{(j,\mathrm{ref})\dagger,n_i}\widehat{\mathcal{H}}^{(1,\mathrm{ref})}.$$

Similarly to Lemma 4.9 it can be shown that

$$\begin{aligned}\widehat{\overline{\mathcal{H}}}_{n_{\max}}^{(j,\mathrm{mov})} &= \widehat{\mathcal{O}}_{n_{\max}}^{(j,\mathrm{mov})}\widehat{\mathcal{O}}_{n_{\max}}^{(j,\mathrm{ref})\dagger}\widehat{\mathcal{O}}_{n_{\max}}^{(1,\mathrm{ref})}\widehat{\mathcal{Z}}_{n_{\max}}^{(1)},\\ \widehat{\overline{\mathcal{H}}}_{n_i}^{(j,\mathrm{mov})} &= \widehat{\mathcal{O}}_{n_i}^{(j,\mathrm{mov})}\widehat{\mathcal{O}}_{n_i}^{(j,\mathrm{ref})\dagger}\widehat{\mathcal{O}}_{n_i}^{(1,\mathrm{ref})}\widehat{\mathcal{Z}}_{n_i}^{(1)}\end{aligned}$$

and hence

$$\widehat{\overline{\mathcal{H}}}_{n_{\max}}^{(\mathrm{all})} = \widehat{\mathcal{O}}_{n_{\max}}^{(\mathrm{all})}\mathcal{Z}_{n_{\max}}^{(1)}, \quad \widehat{\overline{\mathcal{H}}}_{n_i}^{(\mathrm{all})} = \widehat{\mathcal{O}}_{n_i}^{(\mathrm{all})}\mathcal{Z}_{n_i}^{(1)},$$

using the notations of Proposition 4.10. From Proposition 4.10 follows $\widehat{\mathcal{O}}^{(\mathrm{all})}_{n_{\max}} = \begin{bmatrix} \widehat{\mathcal{O}}^{(\mathrm{all})}_{n_i} & Z \end{bmatrix}$ and as $\widetilde{\mathcal{O}}^{(\mathrm{all})}_{n_{\max}}$ and $\widetilde{\mathcal{O}}^{(\mathrm{all})}_{n_i}$ are recovered directly from $\widehat{\overline{\mathcal{H}}}^{(\mathrm{all})}_{n_{\max}}$ and $\widehat{\overline{\mathcal{H}}}^{(\mathrm{all})}_{n_i}$ by an SVD, the assertion follows. □

Proposition 4.10 and Corollary 4.11 justify the computation of the global subspace or observability matrix using the Algorithms 4.3 or 4.4 only once at a maximal desired model order. Then, system identification is done at multiple lower model orders using this matrix. This is especially useful in vibration analysis of civil, mechanical or aeronautical structures, where multi-order identification helps to distinguish true structural modes from noise or spurious mathematical modes.

4.6 Application of merging algorithms to data-driven SSI

4.6.1 Size reduction with LQ decompositions

For so-called *data-driven* subspace identification algorithms such as the UPC algorithm in Section 2.2.3, the number of columns of the subspace matrix $\mathcal{H}$ is in the order of the available samples N, which is usually very big compared to the model order n. In this case, a thin LQ decomposition of the data like in (2.13) is done at first, leading to a factorization of subspace matrix $\mathcal{H} = \widetilde{\mathcal{H}}Q$ into the matrix $\widetilde{\mathcal{H}}$, whose number of columns is only in the order of the model order n, and a matrix Q containing orthonormal rows with $QQ^T = I$ [VODM96, PDR99]. Because of this property, the subspace identification algorithm from Section 4.2 can be called using $\widetilde{\mathcal{H}}$ instead $\mathcal{H}$, as the left side of the SVD (4.5), from which the observability matrix is retrieved, is not influenced by a different orthogonal matrix on the right side [VODM96]. Hence, matrix $\widetilde{\mathcal{H}}$ is also a subspace matrix fulfilling a factorization property (4.2). In practice, $\widetilde{\mathcal{H}}$ instead of $\mathcal{H}$ is used for system identification, as it is in general much smaller (less columns) and its computation numerically more stable than the computation of $\mathcal{H}$ itself.

Now it is shown that the same size reduction of the local subspace matrices prior to using merging algorithms 4.2–4.5 is consistent, i.e. either using $\mathcal{H}^{(j)}$, $j = 1, \ldots, N_s$, or the matrices $\widetilde{\mathcal{H}}^{(j)}$, $j = 1, \ldots, N_s$, with

$$\mathcal{H}^{(j)} = \widetilde{\mathcal{H}}^{(j)} Q_j, \quad Q_j Q_j^T = I, \tag{4.37}$$

as local subspace matrices in the merging algorithms yields the same global system identification results. Denote the respective global subspace matrices $\overline{\mathcal{H}}^{(\mathrm{all})}$ and $\overline{\widetilde{\mathcal{H}}}^{(\mathrm{all})}$, respectively.

4.6.1.1 Algorithms 4.2 and 4.3

With Lemma 4.3, the normalization step in Algorithm 4.3 is equivalent to

$$\overline{\mathcal{H}}^{(j,\mathrm{mov})} = \mathcal{H}^{(j,\mathrm{mov})} \mathcal{H}^{(j,\mathrm{ref})\dagger} \mathcal{H}^{(1,\mathrm{ref})}, \tag{4.38}$$

using $\mathcal{H}^{(j)}$, $j = 1, \ldots, N_s$, and

$$\overline{\widetilde{\mathcal{H}}}^{(j,\mathrm{mov})} = \widetilde{\mathcal{H}}^{(j,\mathrm{mov})} \widetilde{\mathcal{H}}^{(j,\mathrm{ref})\dagger} \widetilde{\mathcal{H}}^{(1,\mathrm{ref})}, \tag{4.39}$$

using $\widetilde{\mathcal{H}}^{(j)}$, $j = 1, \ldots, N_s$. Separating the subspace matrices into reference and moving sensor parts leads with (4.37) to the relation

$$\mathcal{H}^{(j,\text{ref})} = \widetilde{\mathcal{H}}^{(j,\text{ref})} Q_j, \quad \mathcal{H}^{(j,\text{mov})} = \widetilde{\mathcal{H}}^{(j,\text{mov})} Q_j.$$

Plugging this into (4.38) and using (4.39) leads to

$$\begin{aligned} \overline{\mathcal{H}}^{(j,\text{mov})} &= (\widetilde{\mathcal{H}}^{(j,\text{mov})} Q_j)(\widetilde{\mathcal{H}}^{(j,\text{ref})} Q_j)^\dagger \widetilde{\mathcal{H}}^{(1,\text{ref})} Q_1 \\ &= \widetilde{\mathcal{H}}^{(j,\text{mov})} \widetilde{\mathcal{H}}^{(j,\text{ref})\dagger} \widetilde{\mathcal{H}}^{(1,\text{ref})} Q_1 = \overline{\widetilde{\mathcal{H}}}^{(j,\text{mov})} Q_1 \end{aligned}$$

for $j = 1, \ldots, N_s$. Furthermore, $\mathcal{H}^{(1,\text{ref})} = \widetilde{\mathcal{H}}^{(1,\text{ref})} Q_1$. Hence, because of (4.24), the merged subspace matrices $\overline{\mathcal{H}}^{(\text{all})}$ and $\overline{\widetilde{\mathcal{H}}}^{(\text{all})}$ enjoy the relation

$$\overline{\mathcal{H}}^{(\text{all})} = \overline{\widetilde{\mathcal{H}}}^{(\text{all})} Q_1, \tag{4.40}$$

proving that $\overline{\mathcal{H}}^{(\text{all})}$ and $\overline{\widetilde{\mathcal{H}}}^{(\text{all})}$ yield the same global system identification results, as $Q_1 Q_1^T = I$.

4.6.1.2 Algorithms 4.4 and 4.5

Algorithms 4.4 and 4.5 compute the local observability matrix $\mathcal{O}^{(j)}$, which is used for further computations instead $\mathcal{H}^{(j)}$ or $\widetilde{\mathcal{H}}^{(j)}$. Because of (4.37), the matrices U_1 and Δ_1, on which $\mathcal{O}^{(j)}$ is computed, can be assumed to be equal without loss of generality, either coming from $\mathcal{H}^{(j)}$ or $\widetilde{\mathcal{H}}^{(j)}$.[3] Hence, global system identification results are the same for both $\mathcal{H}^{(j)}$ and $\widetilde{\mathcal{H}}^{(j)}$.

4.6.2 Example: Multi-setup reference-based SSI with UPC algorithm

The *data-driven* Unweighted Principal Component (UPC) algorithm [VODM96], [PDR99] is a popular algorithm for stochastic system identification and was described in Section 2.2.3 for a single measurement setup. In this section, implementation details are given for multi-setup system identification with the *reference-based* UPC algorithm.

Choose p such that $pr^{(\text{ref})} \geq n$ and set $q = p + 1$. For each setup j, the data matrices

$$\mathcal{Y}^{(j)+} \overset{\text{def}}{=} \frac{1}{\sqrt{N}} \begin{bmatrix} Y_{q+1}^{(j)} & Y_{q+2}^{(j)} & \cdots & Y_{N+q}^{(j)} \\ Y_{q+2}^{(j)} & Y_{q+3}^{(j)} & \cdots & Y_{N+q+1}^{(j)} \\ \vdots & \vdots & \ddots & \vdots \\ Y_{q+p+1}^{(j)} & Y_{q+p+2}^{(j)} & \cdots & Y_{N+q+p}^{(j)} \end{bmatrix}, \tag{4.41}$$

$$\mathcal{Y}^{(j)-} \overset{\text{def}}{=} \frac{1}{\sqrt{N}} \begin{bmatrix} Y_{q}^{(j,\text{ref})} & Y_{q+1}^{(j,\text{ref})} & \cdots & Y_{N+q-1}^{(j,\text{ref})} \\ Y_{q-1}^{(j,\text{ref})} & Y_{q}^{(j,\text{ref})} & \cdots & Y_{N+q-2}^{(j,\text{ref})} \\ \vdots & \vdots & \ddots & \vdots \\ Y_{1}^{(j,\text{ref})} & Y_{2}^{(j,\text{ref})} & \cdots & Y_{N}^{(j,\text{ref})} \end{bmatrix} \tag{4.42}$$

[3] By defining a unique SVD, where e.g. the first entries of the left singular vectors are positive values, the matrices U_1 and Δ_1 are identical in both SVDs of $\mathcal{H}^{(j)}$ and $\widetilde{\mathcal{H}}^{(j)}$.

are built, where

$$Y_k^{(j)} \stackrel{\text{def}}{=} \begin{bmatrix} Y_k^{(j,\text{ref})} \\ Y_k^{(j,\text{mov})} \end{bmatrix}.$$

Note that in this reference-based version, matrix $\mathcal{Y}^{(j)-}$ only contains data from the reference sensors of the setup, instead of data from all sensors. The local subspace matrix estimate is then defined as

$$\widehat{\mathcal{H}}^{(j)} = \mathcal{Y}^{(j)+}\mathcal{Y}^{(j)-T}(\mathcal{Y}^{(j)-}\mathcal{Y}^{(j)-T})^{\dagger}\mathcal{Y}^{(j)-},$$

but not explicitly computed. Instead, the thin LQ decomposition

$$\begin{bmatrix} \mathcal{Y}^{(j)-} \\ \mathcal{Y}^{(j)+} \end{bmatrix} = \begin{bmatrix} R_{11}^{(j)} & 0 \\ R_{21}^{(j)} & R_{22}^{(j)} \end{bmatrix} \begin{bmatrix} Q_1^{(j)} \\ Q_2^{(j)} \end{bmatrix} \tag{4.43}$$

is performed, from which $\widehat{\mathcal{H}}^{(j)} = R_{21}^{(j)}Q_1^{(j)}$ follows. Hence, (4.37) is satisfied with $\widetilde{\mathcal{H}}^{(j)} \stackrel{\text{def}}{=} R_{21}^{(j)}$ and $Q_j \stackrel{\text{def}}{=} Q_1^{(j)}$. Note that the number of columns of $\widetilde{\mathcal{H}}^{(j)}$ is only $qr^{(\text{ref})}$, which is in general significantly smaller than N.

Then, the merging algorithms can be called using the matrices $\widetilde{\mathcal{H}}^{(j)}$, $j = 1, \ldots, N_s$. In the case of a moderate number of sensors and setups, Algorithm 4.3 should be used to obtain the global subspace matrix, or Algorithm 4.4 should be used to obtain a global observability matrix, from which the system matrices $\widehat{A}$ and $\widehat{C}^{(\text{all})}$ are retrieved. The scalable computation of the system matrices in Algorithm 4.5 should be used in the case of a large number of sensors and setups.

It is stressed that using matrices $\widetilde{\mathcal{H}}^{(j)}$ in the merging algorithms is in general much more efficient than using the matrices $\widehat{\mathcal{H}}^{(j)}$, $j = 1, \ldots, N_s$. It should be also noted that with relation (4.40), the Kalman filter state matrix can be recovered from the merged matrix $\overline{\widetilde{\mathcal{H}}}^{(\text{all})}$ and the orthogonal matrix Q_1 from the first setup.

4.7 Structural vibration analysis example

An important instance of eigenstructure identification with subspace-based system identification algorithms is the structural vibration analysis of mechanical structures [POB+91]. In *Operational Modal Analysis*, the excitation of the structure cannot be measured and is uncontrolled, typically turbulent in nature and non-stationary. Typical examples are buildings subject to wind, or bridges, dams and offshore structures subject to wind or swell. The multi-setup system identification is of practical interest for these structures, as they can be observed at many degrees of freedom, while only using a few sensors.

In Section 2.4, the underlying mechanical model and its respective discrete time state-space model were recalled. In the following, the structural vibration analysis example of [MBBG02b] is revisited using covariance-driven and data-driven stochastic subspace identification, now showing very good eigenstructure identification results.

The proposed merging algorithms have been applied on vibrational data of the Z24 Bridge [MDR03], a benchmark of the COST F3 European network. The analyzed data is the response of the bridge to ambient excitation (traffic under the bridge) measured in 154 points, mainly

in the vertical and at some points also the transverse and lateral directions, and sampled at 100 Hz. Because at most 33 sensors were available (counting one sensor for each measured direction), $N_s = 9$ data sets have been recorded, each containing the measurements from $r^{(\mathrm{ref})} = 5$ fixed and 28 moving sensors, except dataset $j = 5$ containing only 22 moving sensors. Like this, altogether 251 sensors were mimicked. Each signal contains 65,535 samples.

The merging Algorithms 4.2–4.5 were derived for a wide range of subspace identification algorithms. Here, they are tested with subspace matrices from two popular identification algorithms, namely the covariance-driven (cf. Equation (4.13)) and the data-driven subspace identification with UPC (cf. Section 4.6.2). All available data from the nine setups was used, which includes sensor data from different directions at the same time. For the construction of the subspace matrices, the parameters $p + 1 = q = 50$ have been selected, thus leading to the maximal possible model order $pr^{(\mathrm{ref})} = 245$ of the system. The global subspace matrices obtained from Algorithm 4.3 and the global observability matrix obtained from Algorithm 4.4 are then of size 12,550 $\times$ 250 and do not pose a memory problem yet for further processing. Note that in the scalable computation of the system matrices with Algorithm 4.5, at no time matrices larger than 1,650 $\times$ 250 are processed.

In order to separate the true system modes from the noise modes, system identification was done selecting model orders from 10 to the maximal possible order 245 at every 5 orders. Then, modes showing up at successive orders and fulfilling certain stabilization criteria, such as low variability of natural frequency, damping values and mode shapes between successive orders, low damping values etc., are considered as true system modes. Their frequencies are plotted in a stabilization diagram [PDR99] to support the selection of the estimated model. Thanks to the results of Section 4.5, this multi-order system identification is done by just selecting columns of the global observability matrix obtained from the merging algorithms at the maximal desired system order, instead of redoing the merging at all desired orders. The corresponding stabilization diagram of the natural frequencies is presented in Figure 4.1.

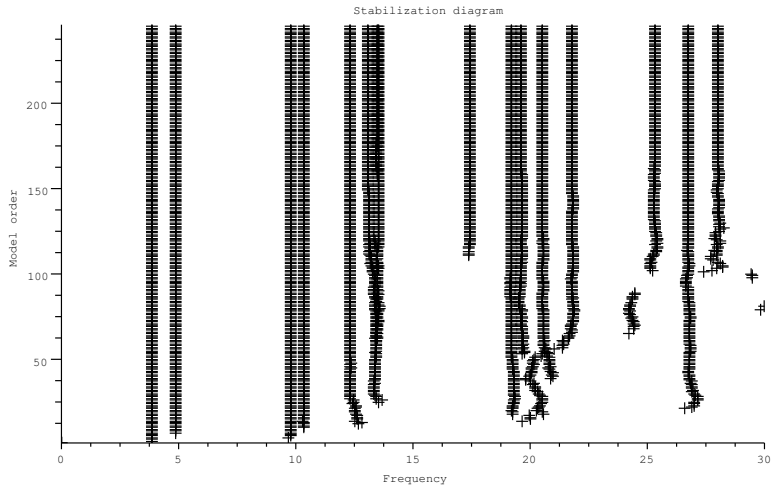

Figure 4.1 – Stabilization diagram: natural frequencies vs. model order from system identification with data-driven UPC algorithm.

Table 4.1 – Frequencies ($\widehat{f}$) and damping coefficients ($\widehat{\rho}$) of obtained modes with covariance- and data-driven approach.

	covariance-driven		data-driven	
Mode	$\widehat{f}$ (Hz)	$\widehat{\rho}$ (%)	$\widehat{f}$ (Hz)	$\widehat{\rho}$ (%)
1	3.856	0.73	3.860	0.84
2	4.884	1.36	4.893	1.28
3	9.784	1.28	9.774	1.32
4	10.31	1.65	10.33	1.89
5	12.29	3.40	12.33	3.08
6	13.02	3.93	13.08	3.32
7	17.25	5.36	17.37	7.29
8	19.23	2.75	19.21	2.99
9	19.74	4.49	19.62	3.99
10	26.69	4.94	26.75	4.21

The system identification results after applying the merging with Algorithms 4.3 and 4.4 are practically equal for each subspace method, while the results differ slightly comparing different subspace methods. The obtained frequencies and damping coefficients from the covariance- and the data-driven algorithm are summarized in Table 4.1. The differences in the obtained frequencies are less than 0.7% for all modes. For the damping coefficients, the differences are larger, but still not significant considering the large uncertainty on damping estimates [Ger74].

In Figure 4.2 the corresponding mode shapes obtained from the data-driven UPC algorithm are presented. All the obtained mode shapes are of high quality, except of the apparently lowly excited mode 7. The mode shapes obtained with the covariance-driven approach are very similar, but of slightly lesser quality.

Further applications to structural vibration problems are found in Chapter 8.

4.8 Conclusions

In this chapter, we have presented a generalization of a subspace method designed to recover modal parameters from multi-setup measurements. The new merging approach applies to a large range of subspace identification methods and is addressing the problem of size explosion for large systems. Non-stationary consistency and robustness to misspecified model order for this approach have been proven, which validates the use of the merging algorithms for system identification on real structures. They have been applied successfully to a large class of relevant examples in Chapter 8. Further work will address the computation of asymptotic efficiency for this class of modular subspace approaches and evaluate the impact of the merging approach on the uncertainty quantification of the modal parameters.

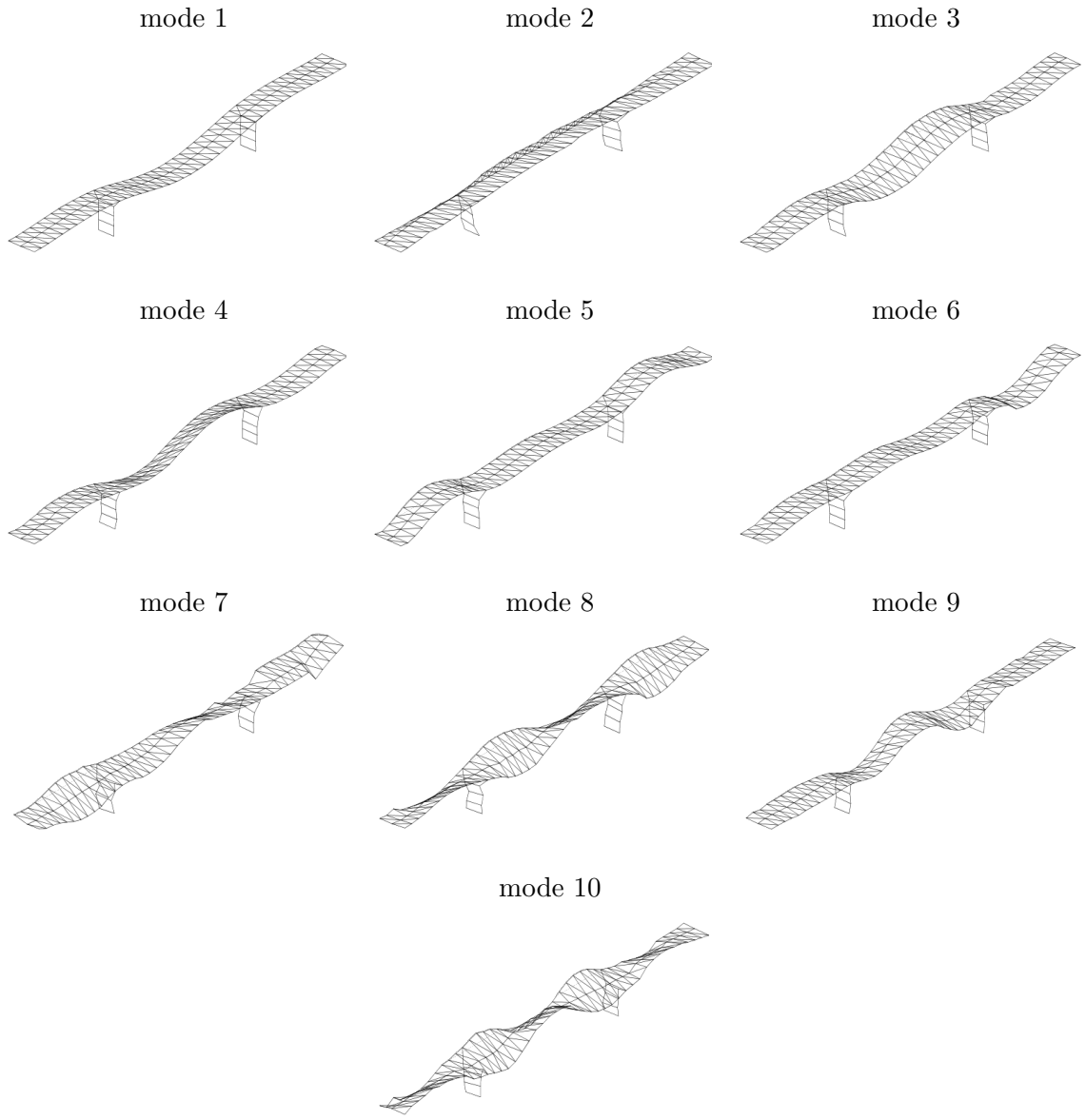

Figure 4.2 – Mode shapes identified with data-driven UPC algorithm.

4.9 Dissemination

Parts of this chapter have been published or are submitted to:

[DAM10] M. Döhler, F. Hille, X.-B. Lam, L. Mevel, and W. Rücker. Confidence intervals of modal parameters during progressive damage test. In *Proc. 29th International Modal Analysis Conference*, Jacksonville, FL, USA, 2011.

[DRM+10] M. Döhler, E. Reynders, F. Magalhães, L. Mevel, G. De Roeck, and Á. Cunha. Pre- and post-identification merging for multi-setup OMA with covariance-driven SSI. In *Proc. 28th International Modal Analysis Conference*, Jacksonville, FL, USA, 2010.

[DM10] M. Döhler and L. Mevel. Modular subspace-based system identification and damage detection on large structures. In *Proc. 34th International Symposium on Bridge and Structural Engineering*, Venice, Italy, 2010.

[DLM10b] M. Döhler, X.-B. Lam, and L. Mevel. Crystal clear data fusion in subspace system identification and damage detection. In *Proc. 5th International Conference on Bridge Maintenance, Safety and Management*, Philadelphia, PA, USA, 2010.

[DM11c] M. Döhler and L. Mevel. Modular subspace-based system identification from multi-setup measurements. 2011. *IEEE Transactions on Automatic Control*, under revision.

The merging algorithms have been transferred to the commercial software product ARTeMIS Extractor Pro [Str11].

Chapter 5

Fast multi-order subspace-based system identification

5.1 Introduction

Subspace-based system identification methods have been proven efficient for the identification of linear time-invariant systems (LTI), fitting a linear model to input/output or output-only measurements taken from a system. An overview of subspace methods can be found in [BF85, Vib95, VODM96, PDR99, BM07, Akç10]. There exists a broad range of applications in the identification of processes in automatic control, see e.g. [BNSR98, JSL01, SPG03, PL08]. During the last decade, subspace methods found a special interest in mechanical, civil and aeronautical engineering for the identification of *vibration modes* (eigenvalues) and *mode shapes* (corresponding eigenvectors) of structures. Therefore, identifying an LTI from measurements is a basic service in vibration monitoring, see e.g. [HVdA99, MBG03, MBB$^+$06, BMCC10]. Having done this allows in particular Finite Element Models (FEM) updating and structural health monitoring.

In an Operational Modal Analysis (OMA) context, however, the following unusual characteristics must be taken into account:

- The number of sensors can be very large (up to hundreds, or thousands in the future); sensors can even be moved from one measurement campaign to another;
- The number of modes of interest can be quite large (up to 100 or beyond), thus calling for non-standard approaches to model reduction;
- The excitation applied to the structure is usually uncontrolled and natural, thus turbulent and non-stationary.

Because of the features above, usual tools from linear system identification, such as the System Identification Toolbox by Matlab, cannot be used as such. In order to retrieve the

desired large number of modes, an even larger model order must be assumed while performing identification. This causes a number of spurious modes to appear in the identified models. Techniques from statistics to estimate the best model order, such as AIC, BIC or MDL [Aka74a, Ris78, CMK01], or model order estimation techniques specifically for subspace methods as in [Bau01] lead to a model with the best prediction capacity. However, one is rather interested in a model containing only the physical modes of the investigated structures, while rejecting the spurious modes. Based on the observation that physical modes remain quite constant when estimated at different over-specified model orders, while spurious modes vary, they can be distinguished using so-called *stabilization diagrams* [PDR99, PDR01]. There, the physical modes are selected from system identification results at multiple model orders in a GUI-assisted way. Methods for an automation of this selection are e.g. found in [VdAP04, SL05, RHDR11, Bak11]. As system identification is done at an over-specified model order and repeated while truncating at multiple model orders, the computational burden for this procedure is significant especially for large model orders.

A fast identification of the system parameters is of basic interest, e.g. for online structural health monitoring. Existing literature on fast subspace-based system identification covers mainly three subjects:

- Convergence rates of the system or transfer matrices for a growing sample size. They are e.g. analyzed in [DPS95, BDS99, BL02, CP04a, Bau05] and typically concern the theoretical properties of a subspace method.

- Reduction of the processed data by using only data of a subset of the recorded sensors, so-called *reference sensors* or *projection channels*, instead all the sensors at one point of the subspace algorithms. See e.g. [PDR99, RDR08].

- Fast processing of the measurement data prior to estimating the observability matrix. This is considered in [CK95, MKS$^+$01] for subspace methods using a QR decomposition of a data Hankel matrix during preprocessing, and in [Pee00, Sec. 3.2.2] for covariance-driven subspace methods.

In this chapter, the efficient computation of the system matrices from the observability matrix at multiple model orders is investigated. A fast computation scheme is derived, where the structure of the observability matrix estimates at multiple orders is exploited when solving the least squares problem to obtain the system matrices.[1] Furthermore, a fast computation of the system matrices at multiple orders is derived for the Eigensystem Realization Algorithm (ERA) [JP85, JICL95], which is closely related to covariance-driven subspace-based algorithms.

This chapter is organized as follows. In Section 5.2, the general Stochastic Subspace Identification (SSI) algorithm from Section 2.2.2 is recalled and the multi-order identification problem is addressed. In Sections 5.3 and 5.4, efficient algorithms to estimate the system matrices at multiple model orders with SSI and ERA are derived, which reduce the computational burden significantly. In Section 5.5, the computational cost of the algorithms is compared for doing the system identification on a real test case, validating their efficiency.

[1] Note that this is different from the structured total least squares problem considered in [MLVH01, MWVH$^+$05], which applies e.g. to maximum likelihood system identification.

5.2 Stochastic Subspace Identification (SSI)

5.2.1 The general SSI algorithm

Consider linear multivariable time invariant systems described by a discrete time state space model

$$\begin{cases} X_{k+1} = AX_k + BU_k + V_k \\ Y_k = CX_k + DU_k + W_k \end{cases} \tag{5.1}$$

with the state $X \in \mathbb{R}^n$, the observed input $U \in \mathbb{R}^m$, the output $Y \in \mathbb{R}^r$ and the unobserved input and output disturbances V and W. The matrices $A \in \mathbb{R}^{n\times n}$ and $C \in \mathbb{R}^{r\times n}$ are the state transition and observation matrices, respectively.

In this chapter, the identification of the system matrices A and C is of interest. In Operational Modal Analysis, typically no observed inputs are available ($B = 0$, $D = 0$) and identification is done using the output-only data (Y_k). When some inputs (U_k) are observed, combined deterministic-stochastic subspace identification algorithms can be used.

There are many SSI algorithms in literature. Some are mentioned in Section 2.2.3 and they fit in the following general framework for the identification of the system matrices A and C of system (5.1). Note that no difference is made between the theoretical matrices A, C, $\mathcal{H}_{p+1,q}$, $\mathcal{O}_{p+1}$, $\mathcal{Z}_q$ and their estimates $\widehat{A}$, $\widehat{C}$, $\widehat{\mathcal{H}}_{p+1,q}$, $\widehat{\mathcal{O}}_{p+1}$, $\widehat{\mathcal{Z}}_q$ in the following, as all derived algorithms in this chapter have a practical background and use and provide estimates computed on data.

From the output or input/output data a matrix $\mathcal{H}_{p+1,q}$ is built according to a chosen subspace algorithm. The matrix $\mathcal{H}_{p+1,q}$ will be called "subspace matrix" in the following. The subspace algorithm is chosen such that the corresponding subspace matrix enjoys (asymptotically for a large number of samples) the factorization property

$$\mathcal{H}_{p+1,q} = W\mathcal{O}_{p+1}\mathcal{Z}_q \tag{5.2}$$

into the matrix of observability

$$\mathcal{O}_{p+1} \stackrel{\text{def}}{=} \begin{bmatrix} C \\ CA \\ \vdots \\ CA^p \end{bmatrix},$$

and a matrix $\mathcal{Z}_q$, with an invertible weighting matrix W depending on the selected subspace algorithm. However, W is the identity matrix for many subspace algorithms.

Note that a subset of the r sensors can be used for reducing the size of the matrices in the identification process, see e.g. [PDR99, RDR08]. These sensors are called projection channels or reference sensors. Let r_0 be the number of reference sensors ($r_0 \leq r$). The parameters p and q are chosen such that $pr \geq qr_0 \geq n$. For simplicity, let these parameters be given and skip the subscripts of $\mathcal{H}_{p+1,q}$, $\mathcal{O}_{p+1}$ and $\mathcal{Z}_q$ in the following.

The observability matrix $\mathcal{O}$ is obtained from a thin SVD of the matrix $\mathcal{H}$ and its truncation

at the desired model order n:

$$\begin{aligned}\mathcal{H} &= U\Delta V^T \\ &= \begin{bmatrix} U_1 & U_0 \end{bmatrix} \begin{bmatrix} \Delta_1 & 0 \\ 0 & \Delta_0 \end{bmatrix} V^T, \qquad (5.3) \\ \mathcal{O} &= W^{-1} U_1 \Delta_1^{1/2}. \qquad (5.4)\end{aligned}$$

Note that the singular values in Δ_1 are non-zero and $\mathcal{O}$ is of full column rank. The observation matrix C is then found in the first block-row of the observability matrix $\mathcal{O}$. The state transition matrix A is obtained from the shift invariance property of $\mathcal{O}$, namely as the least squares solution of

$$\mathcal{O}^{\uparrow} A = \mathcal{O}^{\downarrow}, \text{ where } \mathcal{O}^{\uparrow} \stackrel{\text{def}}{=} \begin{bmatrix} C \\ CA \\ \vdots \\ CA^{p-1} \end{bmatrix}, \ \mathcal{O}^{\downarrow} \stackrel{\text{def}}{=} \begin{bmatrix} CA \\ CA^2 \\ \vdots \\ CA^{p} \end{bmatrix}. \qquad (5.5)$$

5.2.2 Multi-order SSI

In many practical applications the true system order n is unknown and it is common to do the system identification for models (5.1) at different model orders $n = n_j$, $j = 1, \ldots, t$, with

$$1 \leq n_1 < n_2 < \ldots < n_t \leq \min\{pr, qr_0\}, \qquad (5.6)$$

and where t is the number of models to be estimated [PDR99, PDR01, VdAP04]. The choice of the model orders n_j, $j = 1, \ldots, t$, is up to the user and also depends on the problem. For example, $n_j = j + c$ or $n_j = 2j + c$ with some constant c can be chosen. For example, the latter makes sense for an application as in Section 5.5: There, the eigenvalues of the state transition matrix are pairwise complex conjugate. Thus, two model orders are needed to recover one new mode.

The following notation for specifying these different model orders is used throughout this chapter. Let $\mathcal{O}_j \in \mathbb{R}^{(p+1)r \times n_j}$, $A_j \in \mathbb{R}^{n_j \times n_j}$ and $C_j \in \mathbb{R}^{r \times n_j}$ be the observability, state transition and observation matrix at model order n_j, $j \in \{1, \ldots, t\}$, respectively. Let furthermore be $\mathcal{O}_j^{\uparrow}$ and $\mathcal{O}_j^{\downarrow}$ the first respective last p block rows of $\mathcal{O}_j$, analogously to the definition in (5.5).

Note that in Section 5.2.1 model order n was used, while from now on model orders n_j will be used. The matrices A_j, C_j, $\mathcal{O}_j$, $\mathcal{O}_j^{\uparrow}$ and $\mathcal{O}_j^{\downarrow}$ fulfill the equations in Section 5.2.1, replacing A, C, $\mathcal{O}$, $\mathcal{O}^{\uparrow}$ and $\mathcal{O}^{\downarrow}$, as well as n_j replaces n.

5.2.3 Computation of system matrices

The system matrix A_j is the solution of the least squares problem (5.5) at a chosen model order n_j:

$$\mathcal{O}_j^{\uparrow} A_j = \mathcal{O}_j^{\downarrow}. \qquad (5.7)$$

A numerically stable solution is

$$A_j = \mathcal{O}_j^{\uparrow\dagger}\mathcal{O}_j^{\downarrow}, \tag{5.8}$$

where † denotes the Moore-Penrose pseudoinverse. A more efficient and also numerically stable way to solve it [GVL96], uses the thin QR decomposition

$$\mathcal{O}_j^{\uparrow} = Q_j R_j, \tag{5.9}$$

where $Q_j \in \mathbb{R}^{pr\times n_j}$ is a matrix with orthogonal columns and $R_j \in \mathbb{R}^{n_j\times n_j}$ is upper triangular. R_j is assumed to be of full rank, which is reasonable as $\mathcal{O}_j$ is of full column rank. With

$$S_j \stackrel{\text{def}}{=} Q_j^T\mathcal{O}_j^{\downarrow}, \tag{5.10}$$

$S_j \in \mathbb{R}^{n_j\times n_j}$, the solution of the least squares problem is

$$A_j = R_j^{-1}S_j. \tag{5.11}$$

The observation matrix C_j is found in the first block row of $\mathcal{O}_j$.

The conventional way to compute the system matrices A_j and C_j at the model orders n_j, $j = 1,\dots,t$, is the following [PDR01]: First, the observability matrix $\mathcal{O}_t$ is computed at the maximal desired model order n_t from (5.3)–(5.4). The observability matrix $\mathcal{O}_j$ at order n_j is obtained from the first n_j columns of $\mathcal{O}_t$. Then, the matrices A_j and C_j are the solution of least squares problem (5.7) and the first block row of $\mathcal{O}_j$, respectively. This approach is summarized in Algorithm 5.1, where the least squares solution is obtained either by using the pseudoinverse (5.8) or the QR decomposition with equations (5.9)–(5.11). Note that for a matrix X the matrix $X_{[a_1:a_2,b_1:b_2]}$ denotes the submatrix of matrix X containing the block from rows a_1 to a_2 and columns b_1 to b_2 of matrix X.

Algorithm 5.1 Multi-order SSI

Input: $\mathcal{O}_t \in \mathbb{R}^{(p+1)r\times n_t}$ {observability matrix}
$n_1,\dots,n_t$ {desired model orders satisfying (5.6)}
1: **for** $j = 1$ to t **do**
2: $\mathcal{O}_j^{\uparrow} \longleftarrow \mathcal{O}_{t[1:pr,1:n_j]}$, $\mathcal{O}_j^{\downarrow} \longleftarrow \mathcal{O}_{t[(pr+1):(p+1)r,1:n_j]}$
3: **if** method = pseudoinverse **then**
4: $A_j \longleftarrow \mathcal{O}_j^{\uparrow\dagger}\mathcal{O}_j^{\downarrow}$
5: **else if** method = QR **then**
6: QR decomposition $\mathcal{O}_j^{\uparrow} = Q_j R_j$
7: $S_j \longleftarrow Q_j^T\mathcal{O}_j^{\downarrow}$
8: $A_j \longleftarrow R_j^{-1}S_j$
9: **end if**
10: $C_j \longleftarrow \mathcal{O}_{t[1:r,1:n_j]}$
11: **end for**
Output: System matrices A_j, C_j at model orders $n_1,\dots,n_t$

5.2.4 Computational complexities

In order to compare the performance of different algorithms for the multi-order computation of the system matrices A_j and C_j, $j = 1, \ldots, t$, their number of floating point operations (flops) needs to be evaluated. Consider the observability matrix $\mathcal{O}_t$ at a maximal model order $n_{\max} \stackrel{\text{def}}{=} n_t$ be given. As C_j is always a submatrix of $\mathcal{O}_t$, only the computation of the state transition matrices A_j is considered. For comparing different algorithms, the model orders are assumed to be $n_j = j = 1, \ldots, n_{\max}$. Note that all algorithms are derived for arbitrary model orders n_j fulfilling (5.6).

The number of flops for an algorithm is determined for the computation of the system matrices at orders $n_j = 1, 2, \ldots, n_*$, where $n_* \leq n_{\max}$. Thus, the complexity of an algorithm is indicated, where the choice of the parameters is influenced by the maximal model order $n_{\max}$ and where the computation is stopped at a (possibly smaller) model order n_*. However, for a first evaluation, $n_* = n_{\max}$ can be assumed.

The subspace matrix $\mathcal{H}$ is often of size $(p+1)r \times qr_0$ and in practice it is set $p+1 = q$ and $n_{\max} = qr_0$ [BBG+01]. Define $c \stackrel{\text{def}}{=} pr/n_{\max}$ and $m \stackrel{\text{def}}{=} pr$. Then, $c \approx r/r_0$ and hence independent of p, q and $n_{\max}$. Hence, the total flop count is a function of c, n_* and $n_{\max}$. Furthermore, use the simplifications $\sum_{j=1}^{n_*} j \approx \frac{1}{2}n_*^2$, $\sum_{j=1}^{n_*} j^2 \approx \frac{1}{3}n_*^3$, $\sum_{j=1}^{n_*} j^3 \approx \frac{1}{4}n_*^4$.

For example, the SVD needed for the pseudoinverse in (5.8) takes about $14mj^2 + 8j^3$ flops and the thin Householder QR decomposition (5.9) takes about $4mj^2 - \frac{4}{3}j^3$ flops [GVL96]. Accounting the necessary multiplications, the computation of A_j takes $16mj^2 + 10j^3$ flops in (5.8) and $6mj^2 - \frac{1}{3}j^3$ flops in (5.11). Accumulating the operations for model orders $1, \ldots, n_*$ and replacing $m = cn_{\max}$ leads to a total flop count of about $\frac{16}{3}cn_{\max}n_*^3 + \frac{5}{2}n_*^4$ flops using the pseudoinverse and $2cn_{\max}n_*^3 - \frac{1}{12}n_*^4$ flops using the QR decomposition. Thus, the least squares solution for the system matrix using the QR decomposition is favorable.

5.3 Fast algorithms for multi-order SSI

The computation of the system matrices at multiple orders is a big computational burden. In the previous section it was shown that the conventional algorithm for this task (Algorithm 5.1) has a computational complexity of $O(n_{\max}^4)$ for the identification of the system matrices at model orders $1, 2, \ldots, n_{\max}$. In this section, efficient algorithms are derived for the multi-order identification of the system matrices, having a computational complexity of only $O(n_{\max}^3)$.

5.3.1 A first algorithm for fast multi-order computation of system matrices

Conventionally, the least squares problem for the state transition matrix A_j is solved at each desired model order $n_j = n_1, \ldots, n_t$. Now, an algorithm is derived that solves the least squares problem only once at the maximal desired model order n_t (Equations (5.9) to (5.11) with $j = t$), leading to matrices R_t, S_t and A_t. Then, instead of solving the least squares problems at all the orders $n_1, \ldots, n_{t-1}$, it is shown that the state transition matrices A_j at these lower orders can be computed much more efficiently from submatrices of R_t and S_t, based on the following main theorem of this chapter.

Theorem 5.1 *Let $\mathcal{O}_t$, Q_t, R_t and S_t be given at the maximal desired model order n_t with*

$$\mathcal{O}_t^{\uparrow} = Q_t R_t, \quad S_t = Q_t^T \mathcal{O}_t^{\downarrow}, \quad A_t = R_t^{-1} S_t, \tag{5.12}$$

such that A_t is the least squares solution of

$$\mathcal{O}_t^{\uparrow} A_t = \mathcal{O}_t^{\downarrow}.$$

Let $j \in \{1, \ldots, t-1\}$, and let R_t and S_t be partitioned into blocks

$$R_t = \begin{bmatrix} R_j^{(11)} & R_j^{(12)} \\ 0 & R_j^{(22)} \end{bmatrix}, \quad S_t = \begin{bmatrix} S_j^{(11)} & S_j^{(12)} \\ S_j^{(21)} & S_j^{(22)} \end{bmatrix}, \tag{5.13}$$

where $R_j^{(11)}, S_j^{(11)} \in \mathbb{R}^{n_j \times n_j}$. Then, the state transition matrix A_j at model order n_j, which is the least squares solution of

$$\mathcal{O}_j^{\uparrow} A_j = \mathcal{O}_j^{\downarrow}, \tag{5.14}$$

satisfies

$$A_j = R_j^{(11)-1} S_j^{(11)}. \tag{5.15}$$

Proof: From (5.3) and (5.4) it follows that $\mathcal{O}_j$ consists of the first n_j columns of $\mathcal{O}_t$. This holds analogously for $\mathcal{O}_j^{\uparrow}$ and $\mathcal{O}_j^{\downarrow}$. Hence, $\mathcal{O}_t^{\uparrow}$ and $\mathcal{O}_t^{\downarrow}$ can be partitioned into

$$\mathcal{O}_t^{\uparrow} = \begin{bmatrix} \mathcal{O}_j^{\uparrow} & \tilde{\mathcal{O}}_j^{\uparrow} \end{bmatrix}, \quad \mathcal{O}_t^{\downarrow} = \begin{bmatrix} \mathcal{O}_j^{\downarrow} & \tilde{\mathcal{O}}_j^{\downarrow} \end{bmatrix}, \tag{5.16}$$

where $\tilde{\mathcal{O}}_j^{\uparrow}$ and $\tilde{\mathcal{O}}_j^{\downarrow}$ consist of the remaining columns of $\mathcal{O}_t^{\uparrow}$ and $\mathcal{O}_t^{\downarrow}$. Let Q_t be partitioned into the blocks

$$Q_t = \begin{bmatrix} Q_j^{(1)} & Q_j^{(2)} \end{bmatrix}, \tag{5.17}$$

where $Q_j^{(1)} \in \mathbb{R}^{pr \times n_j}$. From (5.12) and (5.17) follows

$$\mathcal{O}_t^{\uparrow} = \begin{bmatrix} Q_j^{(1)} & Q_j^{(2)} \end{bmatrix} \begin{bmatrix} R_j^{(11)} & R_j^{(12)} \\ 0 & R_j^{(22)} \end{bmatrix} = \begin{bmatrix} Q_j^{(1)} R_j^{(11)} & B \end{bmatrix} \tag{5.18}$$

with $B = Q_j^{(1)} R_j^{(12)} + Q_j^{(2)} R_j^{(22)}$. Comparing (5.16) and (5.18), it follows

$$\mathcal{O}_j^{\uparrow} = Q_j^{(1)} R_j^{(11)}, \tag{5.19}$$

which obviously is a QR decomposition of $\mathcal{O}_j^{\uparrow}$. As A_j is the least squares solution of (5.14) and because of QR decomposition (5.19), A_j satisfies

$$A_j = R_j^{(11)-1} {Q_j^{(1)}}^T \mathcal{O}_j^{\downarrow}. \tag{5.20}$$

Furthermore, from (5.12), (5.16) and (5.17) follows

$$S_t = \begin{bmatrix} {Q_j^{(1)}}^T \\ {Q_j^{(2)}}^T \end{bmatrix} \begin{bmatrix} \mathcal{O}_j^{\downarrow} & \tilde{\mathcal{O}}_j^{\downarrow} \end{bmatrix} = \begin{bmatrix} {Q_j^{(1)}}^T \mathcal{O}_j^{\downarrow} & {Q_j^{(1)}}^T \tilde{\mathcal{O}}_j^{\downarrow} \\ {Q_j^{(2)}}^T \mathcal{O}_j^{\downarrow} & {Q_j^{(2)}}^T \tilde{\mathcal{O}}_j^{\downarrow} \end{bmatrix},$$

and comparing to (5.13) yields

$$S_j^{(11)} = {Q_j^{(1)}}^T \mathcal{O}_j^{\downarrow}.$$

Plugging this into (5.20) leads to the assertion. □

Hence, steps (5.9) and (5.10) for the least squares solution of the state transition matrix A_j are not necessary anymore for $j = 1, \ldots, t-1$, and (5.11) is replaced by (5.15).

Furthermore, matrix $R_j^{(11)-1}$ is a submatrix of R_t^{-1} due to its triangular structure. Thus, the inverse of R_t can be computed beforehand, avoiding the inversion of the matrices $R_j^{(11)}$ at each model order. The resulting algorithm for this fast multi-order computation of the system matrices is summarized in Algorithm 5.2.

Algorithm 5.2 Fast multi-order SSI – preliminary version

Input: $\mathcal{O}_t \in \mathbb{R}^{(p+1)r \times n_t}$ {observability matrix}
$n_1, \ldots, n_t$ {desired model orders satisfying (5.6)}
1: $\mathcal{O}_t^{\uparrow} \longleftarrow \mathcal{O}_{t[1:pr,1:n_t]}$, $\mathcal{O}_t^{\downarrow} \longleftarrow \mathcal{O}_{t[(pr+1):(p+1)r,1:n_t]}$
2: $C_t \longleftarrow \mathcal{O}_{t[1:r,1:n_t]}$
3: QR decomposition $\mathcal{O}_t^{\uparrow} = Q_t R_t$
4: $T \longleftarrow R_t^{-1}$, $S_t \longleftarrow Q_t^T \mathcal{O}_t^{\downarrow}$
5: **for** $j = 1$ to t **do**
6: $\quad A_j \longleftarrow T_{[1:n_j,1:n_j]} S_{t[1:n_j,1:n_j]}$
7: $\quad C_j \longleftarrow C_{t[1:r,1:n_j]}$
8: **end for**
Output: System matrices A_j, C_j at model orders $n_1, \ldots, n_t$

In Line 6 of Algorithm 5.2, A_j is computed as a matrix product with triangular matrix $T_{[1:n_j,1:n_j]}$ as one factor. This requires n_j^3 flops, when T and S_t are known. However, computing $A_j = R^{-1}_{t[1:n_j,1:n_j]} S_{t[1:n_j,1:n_j]}$ by backward substitution, without computing $R^{-1}_{t[1:n_j,1:n_j]}$ explicitly, has the same computational cost, when R_t and S_t are known. In this case, the inversion of R_t can be avoided, leading to a slightly more efficient algorithm. It is summarized in Algorithm 5.3.

5.3.2 Fast iterative multi-order computation of system matrices

The fast multi-order computation of the state transition matrix from the previous section can be further improved by expressing A_{j+1} with the help of A_j, which reduces further the number of numerical operations.

Algorithm 5.3 Fast multi-order SSI

Input: $\mathcal{O}_t \in \mathbb{R}^{(p+1)r \times n_t}$ {observability matrix}
$n_1, \ldots, n_t$ {desired model orders satisfying (5.6)}

1: $\mathcal{O}_t^{\uparrow} \longleftarrow \mathcal{O}_{t[1:pr,1:n_t]}$, $\mathcal{O}_t^{\downarrow} \longleftarrow \mathcal{O}_{t[(pr+1):(p+1)r,1:n_t]}$
2: $C_t \longleftarrow \mathcal{O}_{t[1:r,1:n_t]}$
3: QR decomposition $\mathcal{O}_t^{\uparrow} = Q_t R_t$
4: $S_t \longleftarrow Q_t^T \mathcal{O}_t^{\downarrow}$
5: **for** $j = 1$ to t **do**
6: $\quad A_j \longleftarrow R^{-1}_{t[1:n_j,1:n_j]} S_{t[1:n_j,1:n_j]}$
7: $\quad C_j \longleftarrow C_{t[1:r,1:n_j]}$
8: **end for**

Output: System matrices A_j, C_j at model orders $n_1, \ldots, n_t$

Corollary 5.2 *Let $\mathcal{O}_t$, Q_t, R_t and S_t be given at the maximal desired model order n_t. Define the submatrices*

$$\begin{aligned} \tilde{R}_j^{(11)} &= R_{t[1:n_j,1:n_j]}, & \tilde{S}_j^{(11)} &= S_{t[1:n_j,1:n_j]}, \\ \tilde{R}_j^{(12)} &= R_{t[1:n_j,(n_j+1):n_{j+1}]}, & \tilde{S}_j^{(12)} &= S_{t[1:n_j,(n_j+1):n_{j+1}]}, \\ \tilde{R}_j^{(22)} &= R_{t[(n_j+1):n_{j+1},(n_j+1):n_{j+1}]}, & \tilde{S}_j^{(21)} &= S_{t[(n_j+1):n_{j+1},1:n_j]}, \\ & & \tilde{S}_j^{(22)} &= S_{t[(n_j+1):n_{j+1},(n_j+1):n_{j+1}]}, \end{aligned} \tag{5.21}$$

and $A_1 = \tilde{R}_1^{(11)-1} \tilde{S}_1^{(11)}$. Then it holds

$$A_{j+1} = \begin{bmatrix} A_j & \tilde{R}_j^{(11)-1} \tilde{S}_j^{(12)} \\ 0 & 0 \end{bmatrix} + \begin{bmatrix} -\tilde{R}_j^{(11)-1} \tilde{R}_j^{(12)} \tilde{R}_j^{(22)-1} \\ \tilde{R}_j^{(22)-1} \end{bmatrix} \begin{bmatrix} \tilde{S}_j^{(21)} & \tilde{S}_j^{(22)} \end{bmatrix} \tag{5.22}$$

for $j = 1, \ldots, t-1$.

Proof: According to Theorem 5.1, above submatrices are defined such that $R_j = \tilde{R}_j^{(11)}$, $S_j = \tilde{S}_j^{(11)}$ and

$$R_{j+1} = \begin{bmatrix} \tilde{R}_j^{(11)} & \tilde{R}_j^{(12)} \\ 0 & \tilde{R}_j^{(22)} \end{bmatrix}, \quad S_{j+1} = \begin{bmatrix} \tilde{S}_j^{(11)} & \tilde{S}_j^{(12)} \\ \tilde{S}_j^{(21)} & \tilde{S}_j^{(22)} \end{bmatrix}.$$

Then,

$$R_{j+1}^{-1} = \begin{bmatrix} \tilde{R}_j^{(11)-1} & -\tilde{R}_j^{(11)-1} \tilde{R}_j^{(12)} \tilde{R}_j^{(22)-1} \\ 0 & \tilde{R}_j^{(22)-1} \end{bmatrix}.$$

Plugging this into $A_{j+1} = R_{j+1}^{-1} S_{j+1}$, the assertion follows using Theorem 5.1 and replacing $A_j = \tilde{R}_j^{(11)-1} \tilde{S}_j^{(11)}$. □

Hence, by using (5.22), the computation of A_{j+1} needs about $4(n_{j+1} - n_j) n_{j+1}^2$ flops, if R_t, S_t and A_j are known. Note that, again, no explicit inversion of matrix $\tilde{R}_j^{(11)}$ is necessary.

The complete algorithm for this fast iterative multi-order computation of the state transition matrix is obtained from Algorithm 5.3 by replacing Line 6 at $j+1$ with Equation (5.22). Denote the resulting algorithm by **Algorithm 5.4**.

5.3.3 Fast iterative computation of system matrices without preprocessing at the maximal model order

In the algorithms for the fast multi-order computation of the system matrices in Sections 5.3.1 and 5.3.2, the maximal desired model order must be set beforehand: The QR decomposition $\mathcal{O}_t^{\uparrow} = Q_t R_t$ and $S_t = Q_t^T \mathcal{O}_t^{\downarrow}$ are computed at the maximal desired model order n_t, from which the system matrices A_j at the model orders n_j, $j = 1, \ldots, t$, are derived.

Now, an algorithm is derived that avoids a prior QR decomposition at a maximal model order n_t. Instead, the Householder reflections to obtain the Q and R factor of the QR decomposition [GVL96] are applied only on actually required parts of the observability matrix for each j. Then, the computation of the system matrix A_j depends only on $\mathcal{O}_j$ at model order n_j in each iteration j, but not on matrices at higher model orders. This could give the advantage that the computation of A_j, $j = 1, 2, \ldots$ can be stopped at some model order depending on criteria using results that are already achieved, while avoiding additional computation needed for preprocessing at a preselected maximal model order n_t. However, note that a maximal possible model order is always given by the rank of the subspace matrix $\mathcal{H}$, thus $n_j \leq \min\{pr, qr_0\}$ for all j, cf. (5.6).

Recall the definition and properties of the well-known Householder reflections from [GVL96]:

Definition 5.3 ([GVL96]) *For a vector $x \in \mathbb{R}^m$ with the first entry $x_{[1]} \neq 0$, the Householder vector $v \in \mathbb{R}^m$ is defined as*

$$v \stackrel{\text{def}}{=} x + \operatorname{sign}(x_{[1]})||x||_2 e_1,$$

where $||\cdot||_2$ denotes the Euclidean norm and $e_1 \in \mathbb{R}^m$ is the unit vector $e_1^T = \begin{bmatrix} 1 & 0 & \cdots & 0 \end{bmatrix}$. The respective Householder reflection $H(v) \in \mathbb{R}^{m \times m}$ is defined as

$$H(x) \stackrel{\text{def}}{=} I_m - 2vv^T/(v^T v).$$

For $l \geq m$, define

$$H^{(l)}(x) \stackrel{\text{def}}{=} \begin{bmatrix} I_{l-m} & 0 \\ 0 & H(x) \end{bmatrix}.$$

Lemma 5.4 ([GVL96]) *Let $x \in \mathbb{R}^l$, $l \geq m$ and $H^{(l)}(x_{[l-m+1:l]}) \in \mathbb{R}^{l \times l}$ be the Householder reflection of Definition 5.3, which is an orthogonal matrix. Then,*

$$H^{(l)}(x_{[l-m+1:l]})x = \begin{bmatrix} x_{[1:l-m]} \\ \tilde{x}_{[l-m+1]} \\ 0_{m-1,1} \end{bmatrix},$$

where $\tilde{x}_{[l-m+1]}$ is an entry changed by the Householder reflection and $0_{a,b}$ is a matrix of size $a \times b$ containing zeros. The multiplication of $H^{(l)}(x_{[l-m+1:l]})$ with an arbitrary vector can be done with about $4m$ flops, without computing $H^{(l)}(x_{[l-m+1:l]})$ explicitly.

For $X \in \mathbb{R}^{l\times k}$, $l \geq m \geq k$, define the matrix $H^{(l)}(X_{[l-m+1:l,1:k]}) \in \mathbb{R}^{l\times l}$ as a product of Householder reflections, such that

$$H^{(l)}(X_{[l-m+1:l,1:k]})X = \begin{bmatrix} X_{[1:l-m,1:k]} \\ \tilde{X} \\ 0_{m-k,k} \end{bmatrix},$$

where $\tilde{X} \in \mathbb{R}^{k\times k}$ is an upper triangular matrix resulting from the Householder reflections. The multiplication of $H^{(l)}(X_{[l-m+1:l,1:k]})$ with an arbitrary vector can be done with about $2k(2m-k)$ flops, without computing $H^{(l)}(X_{[l-m+1:l,1:k]})$ explicitly.

With these definitions, the Householder reflections that are necessary to get the least squares solution for the system matrices can be applied stepwise on the appropriate parts of the observability matrix. Thus, the explicit computation of the factor Q of a QR decomposition is not necessary anymore.

Proposition 5.5 *Let the observability matrices $\mathcal{O}_1, \mathcal{O}_2, \ldots$ at model orders $n_1 < n_2 < \ldots$ be given. Define $H_1 = H^{(pr)}(\mathcal{O}_1^{\uparrow})$, $\tilde{R}_1 = H_1\mathcal{O}_1^{\uparrow}$ and $\tilde{S}_1 = H_1\mathcal{O}_1^{\downarrow}$. For $j = 1, 2, \ldots$ define o_{j+1} such that*

$$\mathcal{O}_{j+1} = \begin{bmatrix} \mathcal{O}_j & o_{j+1} \end{bmatrix}.$$

and

$$\tilde{o}_{j+1}^{\uparrow} = H_j \cdots H_1 o_{j+1}^{\uparrow}, \quad \tilde{o}_{j+1}^{\downarrow} = H_j \cdots H_1 o_{j+1}^{\downarrow}. \tag{5.23}$$

Let $H_{j+1} \overset{\text{def}}{=} H^{(pr)}(\tilde{o}^{\uparrow}_{j+1[(n_j+1):pr,1:(n_{j+1}-n_j)]})$ be a collection of Householder reflections and define

$$\tilde{R}_{j+1} = \begin{bmatrix} \tilde{R}_j & H_{j+1}\tilde{o}_{j+1}^{\uparrow} \end{bmatrix}, \quad \tilde{S}_{j+1} = H_{j+1}\begin{bmatrix} \tilde{S}_j & \tilde{o}_{j+1}^{\downarrow} \end{bmatrix}. \tag{5.24}$$

Then, the solution of the least squares problem $\mathcal{O}_{j+1}^{\uparrow}A_{j+1} = \mathcal{O}_{j+1}^{\downarrow}$ is given by

$$A_{j+1} = (\tilde{R}_{j+1[1:n_{j+1},1:n_{j+1}]})^{-1}\tilde{S}_{j+1[1:n_{j+1},1:n_{j+1}]}.$$

Proof: As $\tilde{R}_j$ is by construction an upper triangular matrix with $\tilde{R}_{j[(n_j+1):pr,1:n_j]} = 0$, it follows $H_{j+1}\tilde{R}_j = \tilde{R}_j$ from the definition of H_{j+1}. Then, from (5.24) follows $\tilde{R}_{j+1} = H_{j+1}\begin{bmatrix} \tilde{R}_j & \tilde{o}_{j+1}^{\uparrow} \end{bmatrix}$ and together with (5.24), it follows

$$\begin{aligned}
\tilde{R}_{j+1} &= H_{j+1}\begin{bmatrix} \tilde{R}_j & \tilde{o}_{j+1}^{\uparrow} \end{bmatrix} = H_{j+1}\begin{bmatrix} H_j\begin{bmatrix} \tilde{R}_{j-1} & \tilde{o}_j^{\uparrow} \end{bmatrix} & \tilde{o}_{j+1}^{\uparrow} \end{bmatrix} \\
&= H_{j+1}H_j\begin{bmatrix} \tilde{R}_{j-1} & H_{j-1}\cdots H_1\begin{bmatrix} o_j^{\uparrow} & o_{j+1}^{\uparrow} \end{bmatrix} \end{bmatrix} = \ldots \\
&= H_{j+1}H_j\cdots H_1\begin{bmatrix} \mathcal{O}_1^{\uparrow} & o_2^{\uparrow} & \ldots & o_{j+1}^{\uparrow} \end{bmatrix} \\
&= H_{j+1}H_j\cdots H_1\mathcal{O}_{j+1}^{\uparrow}.
\end{aligned}$$

Analogously, it holds $\tilde{S}_{j+1} = H_{j+1}H_j \cdots H_1 \mathcal{O}_{j+1}^{\downarrow}$. The Householder reflections were chosen such that $\tilde{R}_{j+1} \in \mathbb{R}^{pr \times n_{j+1}}$ is upper triangular. Hence, $\mathcal{O}_{j+1}^{\uparrow} = \tilde{Q}_{j+1}\tilde{R}_{j+1}$ with $\tilde{Q}_{j+1}^T = H_{j+1}H_j \cdots H_1 \in \mathbb{R}^{pr \times pr}$ is a full QR decomposition of $\mathcal{O}_{j+1}^{\uparrow}$ and $\tilde{S}_{j+1} = \tilde{Q}_{j+1}^T \mathcal{O}_{j+1}^{\downarrow}$. Thus, the assertion follows. □

With this proposition, the matrices $\tilde{R}_{j+1}$ and $\tilde{S}_{j+1}$ are computed iteratively. Then, Corollary 5.2 can be used to compute A_{j+1} at each iteration efficiently, using $\tilde{R}_{j+1}$ and $\tilde{S}_{j+1}$ instead of R_t and S_t, respectively. For the latter operation, about $4(n_{j+1}-n_j)n_{j+1}^2$ flops are necessary at the model order n_{j+1}, as stated in the previous section. For the computation of $\tilde{R}_{j+1}$ and $\tilde{S}_{j+1}$, $2\sum_{k=1}^{n_j} 4(pr-k)(n_{j+1}-n_j) \approx (8prn_j - 4n_j^2)(n_{j+1}-n_j)$ flops are necessary for (5.23) and $\sum_{k=n_j+1}^{n_{j+1}} 4(pr-k)(n_{j+1}-n_j+n_{j+1}) \approx (4prn_{j+1} - 4n_{j+1}^2)(n_{j+1}-n_j)$ flops are necessary for (5.24). Thus, at each model order n_{j+1} a total number of about $(12prn_{j+1} - 4n_{j+1}^2)(n_{j+1}-n_j)$ flops is necessary to compute A_{j+1}.

The complete algorithm for this fast iterative multi-order computation of the state transition matrix is obtained from Algorithm 5.3 by replacing Line 6 at $j+1$ with Equation (5.22), while replacing R_t and S_t in (5.21) by $\tilde{R}_{j+1}$ and $\tilde{S}_{j+1}$ from (5.24). Denote the resulting algorithm by **Algorithm 5.5**.

5.3.4 Comparison of multi-order algorithms

The computational complexities for the computation of the system matrices with the multi-order SSI algorithms from the last sections are summarized in Table 5.1. All results are given for the computation at model orders $1, 2, \ldots, n_*$ from an observability matrix of size $(cn_{\max} + r) \times n_{\max}$, where $n_* \leq n_{\max}$.

The conventional Algorithm 5.1, either using the pseudoinverse or the QR decomposition for the solution of the least squares problem, takes $O(n_{\max}^4)$ operations for $n_* = n_{\max}$. The simplest of the derived fast algorithms, Algorithms 5.2 and 5.3, are still dependent on n_*^4, although its constant is significantly smaller than for Algorithm 5.1, and even $(6\,c - \frac{4}{3})\,n_{\max}^3 \geq \frac{1}{4}\,n_*^4$ in many cases. Algorithm 5.3 has a slight advantage over Algorithm 5.2.

Table 5.1 – Computational complexities of multi-order system matrix identification from SSI.

Algorithm	Flops
SSI with pseudoinverse (Algorithm 5.1)	$\frac{16}{3}cn_{\max}n_*^3 + \frac{5}{2}n_*^4$
SSI with QR (Algorithm 5.1)	$2cn_{\max}n_*^3 - \frac{1}{12}n_*^4$
Fast SSI (Algorithm 5.2)	$(6c-1)n_{\max}^3 + \frac{1}{4}n_*^4$
Fast SSI (Algorithm 5.3)	$(6c-\frac{4}{3})n_{\max}^3 + \frac{1}{4}n_*^4$
Iterative Fast SSI (Algorithm 5.4)	$(6c-\frac{4}{3})n_{\max}^3 + \frac{4}{3}n_*^3$
Iterative Fast SSI (Algorithm 5.5)	$6cn_{\max}n_*^2 - \frac{4}{3}n_*^3$

Finally, the iterative fast SSI algorithms from Sections 5.3.2 and 5.3.3 (Algorithms 5.4 and 5.5) take only $O(n_{\max}^3)$ operations for $n_* = n_{\max}$. However, even if Algorithm 5.5 needs the least number of operations, it is rather of theoretical value, as a practical implementation is cumbersome. Furthermore, Algorithm 5.5 might perform less well in practice due to the manual handling of matrix operations.

5.3.5 Iterative computation of R_t and S_t

In the Algorithms 5.2–5.4 the matrices R_t and S_t are computed from $\mathcal{O}_t$ at the maximal desired model order n_t. From these matrices, the state transition matrix A_j is derived at inferior model orders n_j, $j = 1, \ldots, t$.

However, $\mathcal{O}_t$ can be a very large matrix with $(p+1)r \gg n_t$, for example in the case of a large number of sensors r or using multiple sensor setups as in Chapter 4. Then, the computation of R_t and S_t could pose a memory problem. In this case, the matrices R_t and S_t can be computed iteratively by cutting $\mathcal{O}_t$ in block rows and using an iterative QR decomposition. This solves the possible memory problem as R_t and S_t are only of size $n_t \times n_t$. The iterative computation of R_t and S_t was already detailed in Propositions 3.8 and 4.5. It can be applied to any separation of $\mathcal{O}_t$ into block rows $\mathcal{O}_t^{(0)}, \ldots, \mathcal{O}_t^{(J)}$, where each block $\mathcal{O}_t^{(j)}$ relates to a sensor set defined by partial observation matrices $C_t^{(j)}$, $j = 0, \ldots, J$, such that the observation matrix C_t writes

$$C_t = \begin{bmatrix} C_t^{(0)} \\ C_t^{(1)} \\ \vdots \\ C_t^{(J)} \end{bmatrix}, \quad \text{and} \quad \mathcal{O}_t = \begin{bmatrix} \mathcal{O}_t^{(0)} \\ \mathcal{O}_t^{(1)} \\ \vdots \\ \mathcal{O}_t^{(J)} \end{bmatrix} \quad \text{with} \quad \mathcal{O}_t^{(j)} = \begin{bmatrix} C_t^{(j)} \\ C_t^{(j)} A_t \\ \vdots \\ C_t^{(j)} A_t^p \end{bmatrix}$$

for $j = 0, \ldots, J$. Thus, R_t and S_t can be obtained iteratively from the blocks $\mathcal{O}_t^{(0)}, \ldots, \mathcal{O}_t^{(J)}$. Then, the estimates of the state transition matrices A_j at model orders n_j, $j = 1, \ldots, t$ can be obtained from R_t and S_t by one of the Algorithms 5.2–5.4. Estimates of C_j are obtained from C_t.

5.4 Eigensystem Realization Algorithm (ERA)

5.4.1 System identification with ERA

System identification with NExT-ERA is closely related to covariance-driven stochastic subspace identification. The Natural Excitation Technique (NExT) [JICL95, FJI97] states that the cross-correlation function between two responses made on unknown ambient excitation has the same form as the system's impulse response function under convenient assumptions. Then, the Eigensystem Realization Algorithm (ERA) [JP85], which was developed to analyze impulse response functions, can be applied for system identification.

For ERA, the subspace matrix $\mathcal{H}$ is built as a block Hankel matrix

$$\mathcal{H}_k \overset{\text{def}}{=} \begin{bmatrix} M_k & M_{k+1} & \dots & M_{k+q-1} \\ M_{k+1} & M_{k+2} & \dots & M_{k+q} \\ \vdots & \vdots & \ddots & \vdots \\ M_{k+p} & M_{k+p+1} & \dots & M_{k+p+q-1} \end{bmatrix},$$

where parameters p and q are used as in Section 5.2.1, parameter $k \in \mathbb{N}_0$ indicates a time lag and the so-called Markov parameters M_i at time lag i can be chosen as one of the following functions [SF08]:

- Impulse response functions;
- Inverse Fast Fourier Transform (FFT) of frequency response functions;
- Cross-correlation functions of outputs under ambient excitation;
- Inverse FFT of cross-spectral densities under ambient excitation.

Then, $\mathcal{H}_k$ possesses the factorization property

$$\mathcal{H}_k = \mathcal{O} A^k \mathcal{Z}$$

analogous to (5.2). Using the SVD decomposition

$$\mathcal{H}_k = \begin{bmatrix} U_1 & U_0 \end{bmatrix} \begin{bmatrix} \Delta_1 & 0 \\ 0 & \Delta_0 \end{bmatrix} \begin{bmatrix} V_1^T \\ V_0^T \end{bmatrix}, \tag{5.25}$$

and truncation at some model order n analogous to (5.3), the state transition matrix A is computed as

$$A = \Delta_1^{-1/2} U_1^T \mathcal{H}_{k+1} V_1 \Delta_1^{-1/2}, \tag{5.26}$$

similar to (5.4) and (5.5). The observation matrix C is obtained as the first block row of $U_1 \Delta_1^{1/2}$ as in Section 5.2.1.

5.4.2 Fast multi-order computation of the system matrices

When the model order n in the truncation of the SVD in (5.25) is unknown, it is useful to do multi-order system identification at model orders $1 \leq n_1 < n_2 < \ldots < n_t$ as in Section 5.2. This corresponds to the partition of the SVD in (5.25) at model orders n_j, $j = 1, \ldots, t$, such that

$$\mathcal{H}_k = U \Delta V^T = \begin{bmatrix} U_j & \breve{U}_j \end{bmatrix} \begin{bmatrix} \Delta_j & 0 \\ 0 & \breve{\Delta}_j \end{bmatrix} \begin{bmatrix} V_j^T \\ \breve{V}_j^T \end{bmatrix}, \tag{5.27}$$

where U_j and V_j have n_j columns and $\Delta_j \in \mathbb{R}^{n_j \times n_j}$. Then, the state transition matrix at model order n_j writes as

$$A_j = \Delta_j^{-1/2} U_j^T \mathcal{H}_{k+1} V_j \Delta_j^{-1/2}. \tag{5.28}$$

Proposition 5.6 *Let A_t from* (5.27) *and* (5.28) *at a maximal desired model order n_t be given. Then, A_j satisfying* (5.28) *at model order n_j is a submatrix of A_t and fulfills*

$$A_j = A_{t[1:n_j,1:n_j]}.$$

Proof: From (5.27) and (5.28), A_t is defined as

$$A_t = \Delta_t^{-1/2} U_t^T \mathcal{H}_{k+1} V_t \Delta_t^{-1/2}.$$

For any $j = 1, \ldots, t$, it holds by definition

$$U_t = \begin{bmatrix} U_j & \tilde{U}_j \end{bmatrix}, \quad \Delta_t^{-1/2} = \begin{bmatrix} \Delta_j^{-1/2} & 0 \\ 0 & \tilde{\Delta}_j^{-1/2} \end{bmatrix}, \quad V_t = \begin{bmatrix} V_j & \tilde{V}_j \end{bmatrix}$$

with some matrices $\tilde{U}_j$, $\tilde{\Delta}_j$ and $\tilde{V}_j$. Thus, plugging this in the definition of A_t it follows

$$A_t = \begin{bmatrix} \Delta_j^{-1/2} U_j^T \mathcal{H}_{k+1} V_j \Delta_j^{-1/2} & \Delta_j^{-1/2} U_j^T \mathcal{H}_{k+1} \tilde{V}_j \tilde{\Delta}_j^{-1/2} \\ \tilde{\Delta}_j^{-1/2} \tilde{U}_j^T \mathcal{H}_{k+1} V_j \Delta_j^{-1/2} & \tilde{\Delta}_j^{-1/2} \tilde{U}_j^T \mathcal{H}_{k+1} \tilde{V}_j \tilde{\Delta}_j^{-1/2} \end{bmatrix}$$

and comparing with the definition of A_j in (5.28), the assertion follows. □

Hence, for multi-order system identification with ERA, only A_t at the maximal desired model order n_t needs to be computed. Then, the matrices A_j, $j = 1, \ldots, t-1$, are simply submatrices of A_t and do not require further computations.

With the following corollary, the prior computation of A_t at the maximal desired model order n_t can be avoided and the matrices A_j are defined iteratively, analogous to Section 5.3.3.

Corollary 5.7 *Let $\mathcal{H}_k$, $\mathcal{H}_{k+1}$ and the SVD* (5.27) *be given. Define $T_1 = \Delta_1^{-1/2} U_1^T \mathcal{H}_{k+1}$ and $A_1 = T_1 V_1 \Delta_1^{-1/2}$. For $j = 1, 2, \ldots$ define u_{j+1}, σ_{j+1} and v_{j+1} such that*

$$U_{j+1} = \begin{bmatrix} U_j & u_{j+1} \end{bmatrix}, \quad \Delta_{j+1} = \begin{bmatrix} \Delta_j & 0 \\ 0 & \sigma_{j+1} \end{bmatrix}, \quad V_{j+1} = \begin{bmatrix} V_j & v_{j+1} \end{bmatrix},$$

and

$$t_{j+1} = \sigma_{j+1}^{-1/2} u_{j+1}^T \mathcal{H}_{k+1}, \quad T_{j+1} = \begin{bmatrix} T_j \\ t_{j+1} \end{bmatrix}. \tag{5.29}$$

Then,

$$A_{j+1} = \begin{bmatrix} A_j & T_j v_{j+1} \sigma_{j+1}^{-1/2} \\ t_{j+1} V_j \Delta_j^{-1/2} & t_{j+1} v_{j+1} \sigma_{j+1}^{-1/2} \end{bmatrix}. \tag{5.30}$$

Proof: Replace A_t, U_t, Δ_t and V_t in the proof of Proposition 5.6 by A_{j+1}, U_{j+1}, Δ_{j+1} and V_{j+1}. □

For a comparison of the computational complexity of this algorithm with the results of Section 5.3.4, it is assumed that the SVD (5.27) is the starting point of the computation, which is analogous to assume that the observability matrix used for SSI algorithms is already known. The notation of Sections 5.2.4 and 5.3.4 is used and $\mathcal{H}_k$ is assumed to be of size $cn_{\max} \times n_{\max}$.

About $(2c+2)n_{\max}^3$ flops are necessary to compute A_t at model order $n_t = n_{\max}$, from which the state transition matrices at inferior orders are selected in Proposition 5.6. In Corollary 5.7, the computation of A_j at some order j takes about $2cn_{\max}^2 + 4n_{\max}j$ flops, amounting to $2cn_{\max}^2 n_* + 2n_{\max}n_*^2$ flops when computing at all orders $1, 2, \ldots, n_*$. Note that the conventional computation of A_j for all $j = 1, \ldots, t$ from (5.28) needs about $(\frac{1}{2}c + \frac{1}{2})n_*^4$ flops.

The computational complexities of the derived multi-order ERA algorithms are summarized in Table 5.2.

Table 5.2 – Computational complexities of multi-order system matrix identification from ERA.

Algorithm	Flops
Conventional Computation	$(\frac{1}{2}c + \frac{1}{2})n_*^4$
Fast Computation (Proposition 5.6)	$(2c+2)n_{\max}^3$
Iterative Fast Computation (Corollary 5.7)	$2cn_{\max}^2 n_* + 2n_{\max}n_*^2$

5.5 Structural vibration analysis example

In this section, the fast multi-order computation of the system matrices is applied to a practical test case from vibration analysis. In Section 2.4, the underlying mechanical model and its respective discrete time state-space model were recalled. For eigenstructure identification, so-called stabilization diagrams (cf. Section 2.4.3) are used that contain the system identification results at multiple model orders. At each of these model orders, the system matrices have to be computed first in order to get the eigenstructure of the respective systems. For system identification with SSI algorithms or with ERA, this can be done efficiently and fast with the new algorithms derived in this chapter.

5.5.1 Numerical results of multi-order system identification

All system identification algorithms of this chapter are applied to the system identification of the Z24 Bridge [MDR03, Par03] as in Section 4.7. It was a prestressed concrete bridge with three spans, supported by two intermediate piers and a set of three columns at each end. Both types of supports are rotated with respect to the longitudinal axis which results in a skew bridge. The overall length is 58 m.

The ambient vibration data was measured in nine setups of up to 33 sensors each, with five reference sensors common to all setups. Altogether, the structure was measured at

$r = 251$ sensor positions, of which are $r_0 = 5$ reference sensors. In each setup, 65,536 samples were collected for each sensor with a sampling frequency of 100 Hz. The common subspace matrix of all setups was obtained with the merging approach described in Chapter 4 using data-driven SSI with the Unweighted Principal Component Algorithm.

The different algorithms presented in this chapter are tested on an Intel Xeon CPU 3.40 GHz with 16 GByte in Matlab 7.10.0.499 using one processor kernel. With these algorithms, the system matrices A_j and C_j are computed at model orders $n_j = 1, 2, \ldots, n_{\max}$. From these results, the modal parameters of the system can be identified using the stabilization diagram. To compare the performance of the algorithms, the system matrices are computed for stabilization diagrams with different maximal model orders $n_{\max}$.

- For SSI algorithms, a subspace matrix $\mathcal{H}$ of size $(p+1)r \times qr_0$ is built from the data, where $p + 1 = q$ is chosen, as recommended in [BBG+01]. $\mathcal{O}_t$ is obtained from $\mathcal{H}$, where the maximal model order is $n_{\max} = n_t = qr_0$. Then, the time is recorded for the computation of A_j and C_j from $\mathcal{O}_t$ at model orders $n_j = j = 1, 2, \ldots, n_{\max}$.

- For ERA, the matrix $\mathcal{H}$ from the subspace algorithm is used for simplicity. Set $n_{\max} = qr_0$, $\mathcal{H}_k = \mathcal{H}_{[1:pr,1:qr_0]}$ and $\mathcal{H}_{k+1} = \mathcal{H}_{[(r+1):(p+1)r,1:qr_0]}$. Then, the SVD of $\mathcal{H}_k$ is performed and the time is recorded for the computation of A_j and C_j from U, Δ, V and $\mathcal{H}_{k+1}$ at model orders $n_j = j = 1, 2, \ldots, n_{\max}$.

To evaluate the computational time for obtaining the set of A_j's and C_j's from order 1 until a maximal model order $n_{\max} = qr_0$, these steps are repeated for $q = 2, \ldots, 100$. As the computation time is also dependent on the constant $c \approx r/r_0$ (see Section 5.2.4), first a computation is done with all $r = 251$ sensors ($c \approx 50$), and second a computation with only a subset of $r = 5$ sensors ($c \approx 1$).

5.5.1.1 Computation times of multi-order SSI algorithms at different maximal model orders

The computation times for the computation of the system matrices at model orders $1, 2, \ldots, n_{\max}$ from an observability matrix $\mathcal{O}_{n_{\max}}$ with the SSI algorithms are presented in Figure 5.1 for different maximal model orders $n_{\max}$. It can be seen that the solution of the least squares problem with the QR decomposition is more efficient than using the pseudoinverse in the conventional Algorithm 5.1, as expected. The Algorithms 5.2–5.4 derived in this chapter yield a significant reduction in the computation times. Although Algorithm 5.5 theoretically needs the least number of operations, it does not perform well in practice, which is already explained in Section 5.3.4. Besides the latter algorithm, all other algorithms seem to be consistent with their theoretical performance.

At each maximal model order, the computation time in Figure 5.1 corresponds to the total time that is needed to compute all the system matrices for a stabilization diagram having this maximal model order. It is clearly shown that the new fast iterative multi-order SSI with Algorithm 5.4 outperforms the other algorithms. For $n_{\max} = 500$ it takes a total of 13.7 s, while the conventional multi-order Algorithm 5.1 using the pseudoinverse takes 2873 s, thus being more than 200 times faster.

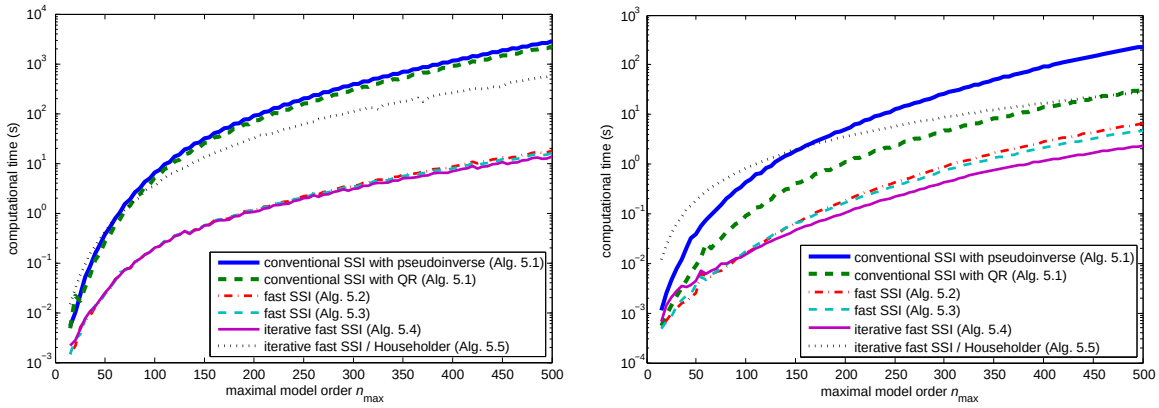

(a) $r = 251$, $r_0 = 5$, $c \approx 50$ (b) $r = r_0 = 5$, $c \approx 1$

Figure 5.1 – Computation times for multi-order SSI system identification of system matrices A_j and C_j, $n_j = j = 1, \ldots, n_{\max}$ from $\mathcal{O}_{n_{\max}}$ at different maximal model orders $n_{\max}$.

5.5.1.2 Computation times of multi-order SSI algorithms for maximal model order 500

The accumulated computation times of the system matrices at model orders $1, 2, \ldots, n_*$ for the maximal model order $n_{\max} = 500$ are presented in Figure 5.2 for $n_* = 1, \ldots, 500$. This corresponds to the time that is needed to compute the system matrices up to each order n_* for a stabilization diagram of maximal model order $n_{\max} = 500$.

Due to a preprocessing step at the maximal model order in Algorithms 5.2–5.4, the

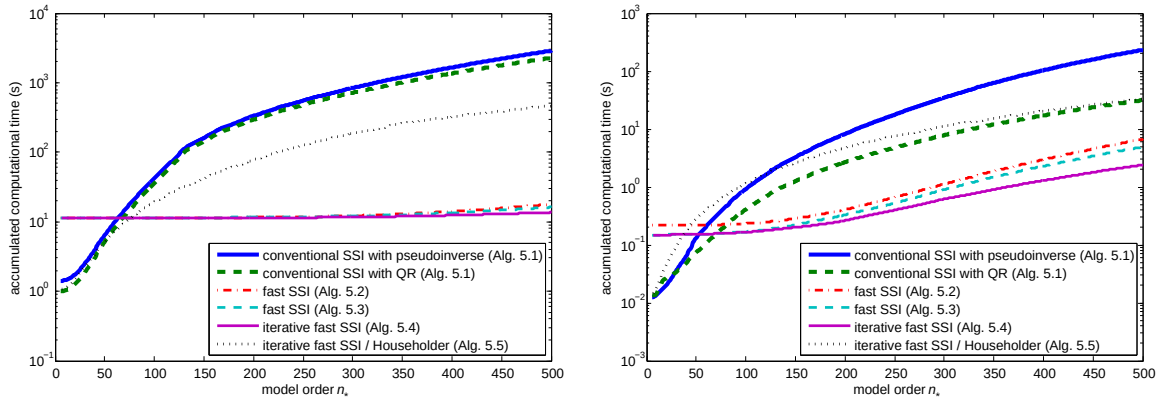

(a) $r = 251$, $r_0 = 5$, $c \approx 50$ (b) $r = r_0 = 5$, $c \approx 1$

Figure 5.2 – Accumulated computation times for multi-order SSI system identification up to different model orders n_* with maximal model order $n_{\max} = 500$.

accumulated computation time for the first model orders n_* is higher in these fast algorithms than for the conventional algorithms. However, this changes quickly at higher model orders and the new algorithms outperform the conventional ones, with Algorithm 5.4 being the fastest. It is also noted that the preprocessing step takes the main part of the computation, while after that, the computation of the system matrices at all orders $1, 2, \ldots, 500$ take only about 2.4 seconds for Algorithm 5.4 in Figures 5.2(a) and 5.2(b).

5.5.1.3 Computation times of multi-order ERA algorithms

The computation times for the computation of the system matrices at model orders $1, 2, \ldots, n_{\max}$ from an observability matrix $\mathcal{O}_{n_{\max}}$ with the ERA algorithms are presented in Figure 5.3 for different maximal model orders $n_{\max}$. The accumulated computation times of the system matrices at model orders $1, 2, \ldots, n_*$ for the maximal model order $n_{\max} = 500$ are presented in Figure 5.4 for $n_* = 1, \ldots, 500$.

From both figures it can be seen that the new multi-order algorithms for ERA developed in this chapter are significantly faster than the conventional ERA algorithm. Due to its implementation, the fast ERA algorithm from Proposition 5.6 outperforms its iterative variant from Corollary 5.7, except when stopping the computation at a low model order. For the computation of the system matrices at orders $1, 2, \ldots, 500$ with $n_{\max} = 500$, the fast multi-order ERA algorithm takes a total of 5 s, while the conventional multi-order ERA algorithm takes 980 s, thus being about 200 times faster.

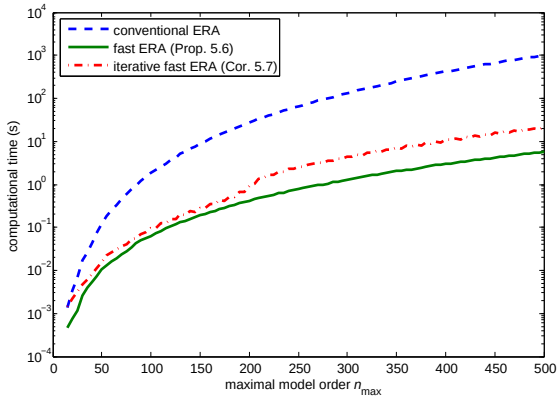

Figure 5.3 – Computation times for multi-order ERA system identification of system matrices A_j and C_j, $n_j = j = 1, \ldots, n_{\max}$ from $\mathcal{O}_{n_{\max}}$ at different maximal model orders $n_{\max}$ with $r = 251$, $r_0 = 5$, $c \approx 50$.

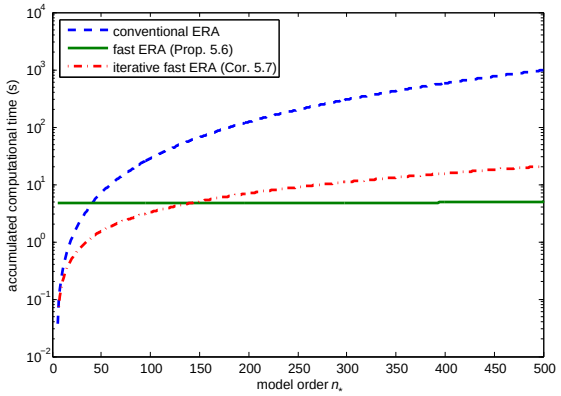

Figure 5.4 – Accumulated computation times for multi-order ERA system identification up to different model orders n_* with maximal model order $n_{\max} = 500$ and $r = 251$, $r_0 = 5$, $c \approx 50$.

5.5.1.4 Discussion of the results

In Figure 5.1, computation times are obtained for multi-order system identification with SSI for different maximal model orders, where for each maximal order $n_{\max}$ the system matrices are computed at orders $1, 2, \ldots, n_{\max}$. In Figure 5.2, the accumulated computation times at

each of these orders $1, 2, \ldots, n_{\max}$ are obtained for $n_{\max} = 500$. With these results, the performance of the algorithms proposed in this chapter can be evaluated for the computation of the system matrices up to a maximal model order $n_{\max}$ as well as up to a lower order $n_* \leq n_{\max}$. From both figures it can be seen that the conventional algorithm (Algorithm 5.1 using the pseudoinverse), which is widely used, is the slowest except when stopping the computation at a very small model order. Using the QR decomposition in Algorithm 5.1 yields already faster results, while the new Algorithms 5.2–5.4 yield significant improvements in the computation time. Algorithm 5.2 yields slightly slower results than Algorithm 5.3. Algorithm 5.4 is in general the fastest of these algorithms, except at very low model orders, where computation times are lower than 0.01 s. Algorithm 5.5 theoretically needs even less operations (cf. Table 5.1), but is in practice slower due to its implementation. As the theoretical performances of Algorithms 5.4 and 5.5 are very close, Algorithm 5.4 is favorable.

In Figures 5.3 and 5.4 corresponding results for the ERA algorithms from Section 5.4 are obtained. Although the fast multi-order computation (Proposition 5.6) and its iterative variant (Corollary 5.7) theoretically need the same number of operations for $n_* = n_{\max}$ in Figure 5.3, the former algorithm is faster due to implementation reasons. When stopping the computation at lower model orders in Figure 5.4, the iterative algorithm is faster only at very low model orders. In both cases, the conventional multi-order algorithm is the slowest.

5.5.2 Modal parameter estimation and stabilization diagram

In order to obtain the modal parameters of the vibration analysis example (cf. Section 2.4), the multi-order system identification performed in the previous section is one part of the task. From these results, the eigenstructure of the investigated structure is obtained from the system matrices at the multiple orders using (2.55) and (2.56) in the next step. Note that

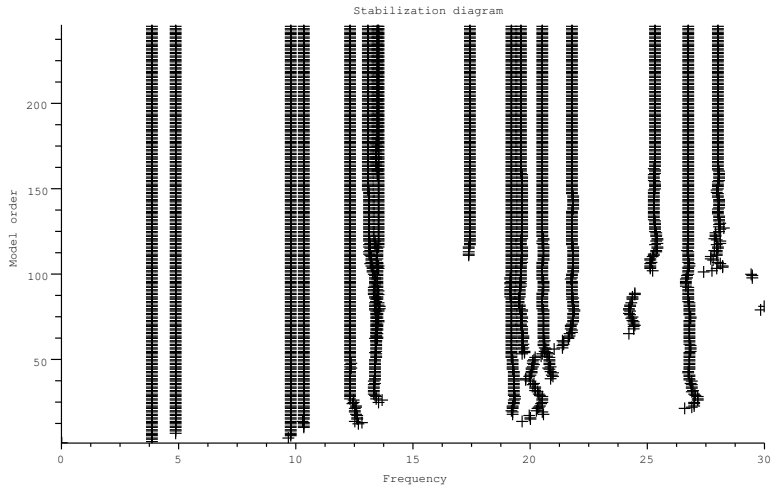

Figure 5.5 – Stabilization diagram of Z24 Bridge containing the identified natural frequencies at model orders $1, \ldots, 250$ *using the fast iterative SSI (Algorithm 5.4).*

the eigenstructure computation has a complexity of $O(n_j^3)$ at each model order n_j and thus $O(n_{\max}^4)$ for the entire computation. However, for $n_{\max} = 500$ this step took a total time of 168 s, thus being a small part compared to the conventional multi-order system identification algorithms. It is beyond the scope of this chapter to optimize this process.

A stabilization diagram containing the natural frequencies of the Z24 Bridge at model orders $1, \ldots, 250$ is presented in Figure 5.5. Note that some of the modes – the ones that might not be very well excited – stabilize late in the diagram, making it necessary to use high model orders for system identification. Using even higher model orders than 250 can still improve the identification results, although there are only 10 modes present in this case [Par03].

5.6 Conclusions

In this chapter, new algorithms were derived to efficiently compute the system matrices at multiple model orders in stochastic subspace-based system identification (SSI) and the closely related Eigensystem Realization Algorithm (ERA). The computational complexity for this task was reduced from $O(n_{\max}^4)$ to $O(n_{\max}^3)$, where $n_{\max}$ is the maximal desired model order. These algorithms are especially applied in the modal analysis of mechanical, civil or aeronautical structures, where eigenstructure identification results at multiple model orders are used to distinguish physical from spurious modes using stabilization diagrams.

The efficiency of the new algorithms was shown on a real test case and computation time was reduced up to a factor of 200 and more. These fast algorithms can e.g. be exploited in online monitoring, where incoming data has to be processed quickly.

5.7 Dissemination

Parts of this chapter have been published or are submitted to:

[DM11a] M. Döhler and L. Mevel. Fast multi-order stochastic subspace-based system identification. 2011. *Control Engineering Practice*, under revision.

[DM11b] M. Döhler and L. Mevel. Fast multi-order stochastic subspace identification. In *Proc. 18th IFAC World Congress*, Milan, Italy, 2011.

The fast multi-order identification algorithms have been transferred to the commercial software product ARTeMIS Extractor Pro [Str11].

Part III

Fault detection

Chapter 6

Robust subspace-based fault detection under changing excitation

6.1 Introduction

Subspace methods enjoy some popularity, especially in vibration analysis of civil, aeronautical or mechanical structures, where large model orders have to be considered. The excitation is ambient and mostly unmeasured. In most cases it is impractical to use artificial excitation sources, such as shakers, where a part of the excitation is measured. Details of the modeling of the underlying mechanical system are found in Section 2.4.

In the last twenty years, monitoring the integrity of the civil infrastructure has been an active research topic, including in connected areas such as automatic control, for mastering the aging of bridges, or the resistance to seismic events and the protection of the cultural heritage. It is assumed that changes in the structural properties lead to changes in the eigenstructure of a system.

In order to detect changes in the modal parameters linked to the structural parameters, often eigenstructure identification results are used and evaluated for changes, e.g. [Kul03, MaCC08, MaCC10, RML$^+$10]. The modal parameters are not afflicted by different ambient excitations, but their automatic estimation and matching from measurements of different states of the structure might require an extensive preprocessing step.

A subspace-based residual function that is robust to excitation change is considered in [YG06]. Recently, a modified whiteness test for damage detection, which is is robust to changes in the excitation, was proposed in [BB11, Ber11b] using Kalman filter innovations.

In this chapter, the subspace-based fault detection approach from [BAB97, BAB00, BMG04] is considered. It uses a subspace-based residual built on the left null space of a nominal observability matrix of the system in a reference state, which is the same as the corresponding subspace matrix built from the output data. In a possibly damaged state it is

then checked, whether the corresponding subspace matrix is still well described by the null space of the reference state, using a χ^2-test on the residual. The statistical theory behind the χ^2-test and the subspace-based fault detection are explained in detail in Section 2.3.

However, the subspace matrix is influenced by the properties of the unmeasured ambient excitation. Most works on the subspace-based fault detection test assume that these properties stay constant between measurements of the investigated structure in the reference and possibly damaged condition, which is hardly the case for real applications. Robustness to non-stationary excitation *within* one measurement has already been addressed in [MB86]. We assume stationary excitation during one measurement, while the excitation covariance may change *between* measurements. In this chapter, the problem of robustness to changes in the excitation of this fault detection method is addressed. Two modifications of the fault detection test are proposed to make it robust to excitation changes.

After recalling the basic principles of subspace-based system identification and statistical fault detection in Section 6.2, the impact of a changing ambient excitation between measurements on the fault detection test is discussed in Section 6.3. Using strategies for the normalization of the subspace matrices with respect to different excitations of Chapter 4, a first modification of the test is proposed in Section 6.4. A more general approach for robustness to changing excitation is proposed in Section 6.5, where a robust residual function and its corresponding χ^2-test are derived. In Section 6.6, numerical results of the proposed algorithms are presented.

6.2 Statistical subspace-based fault detection

In Sections 6.2.1 and 6.2.2 the basic concepts of stochastic subspace-based system identification and fault detection are recalled from Chapter 2 and generalized to SSI algorithms without a left weighting matrix.

6.2.1 General SSI algorithm

Consider the discrete time model in state space form:

$$\begin{cases} X_{k+1} &= AX_k + V_k \\ Y_k &= CX_k \end{cases} \tag{6.1}$$

with the state $X \in \mathbb{R}^n$, the output $Y \in \mathbb{R}^r$, the state transition matrix $A \in \mathbb{R}^{n\times n}$ and the observation matrix $C \in \mathbb{R}^{r\times n}$. The excitation $(V_k)_k$ is an unmeasured Gaussian white noise sequence with zero mean and constant covariance matrix Q: $\mathbf{E}(V_k V_{k'}^T) \stackrel{\text{def}}{=} Q\delta(k-k')$, where $\mathbf{E}(\cdot)$ denotes the expectation operator.

A subset of the r sensors may be used for reducing the size of the matrices in the identification process. These sensors are called projection channels or reference sensors. Let r_0 be the number of reference sensors ($r_0 \leq r$) and p and q chosen parameters with $pr \geq qr_0 \geq n$.

Denote a matrix $\mathcal{H}_{p+1,q} \in \mathbb{R}^{(p+1)r\times qr_0}$ as subspace matrix, whose estimate $\widehat{\mathcal{H}}_{p+1,q}$ is built from the output data $(Y_k)_{k=1,\ldots,N+p+q}$ according to a chosen SSI algorithm. In this chapter,

only SSI algorithms without a left weighting matrix are considered. The subspace matrix enjoys the factorization property

$$\mathcal{H}_{p+1,q} = \mathcal{O}_{p+1}\mathcal{Z}_q \tag{6.2}$$

into the matrix of observability

$$\mathcal{O}_{p+1} = \begin{bmatrix} C \\ CA \\ \vdots \\ CA^p \end{bmatrix}$$

and a matrix $\mathcal{Z}_q$ depending on the selected SSI algorithm. The observation matrix C is then found in the first block-row of the observability matrix $\mathcal{O}_{p+1}$. The state transition matrix A is obtained from the shift invariance property of $\mathcal{O}_{p+1}$ and the eigenstructure $(\lambda, \varphi_\lambda)$ of system (6.1) results from

$$\det(A - \lambda I) = 0, \quad A\phi_\lambda = \lambda\phi_\lambda, \quad \varphi_\lambda = C\phi_\lambda,$$

where λ ranges over the set of eigenvalues of A. The collection of modes and mode shapes $(\lambda, \varphi_\lambda)$ is a canonical parameterization of system (6.1) and considered as the system parameter θ with

$$\theta \stackrel{\text{def}}{=} \begin{bmatrix} \Lambda \\ \operatorname{vec}\Phi \end{bmatrix}, \tag{6.3}$$

where Λ is the vector whose elements are the eigenvalues λ and Φ is the matrix whose columns are the mode shapes φ.

The actual implementation of this generic subspace identification algorithm uses a consistent estimate $\widehat{\mathcal{H}}_{p+1,q}$ obtained from the output data according to the selected subspace identification algorithm. The SVD

$$\widehat{\mathcal{H}}_{p+1,q} = \begin{bmatrix} \widehat{U}_1 & \widehat{U}_0 \end{bmatrix} \begin{bmatrix} \widehat{\Delta}_1 & 0 \\ 0 & \widehat{\Delta}_0 \end{bmatrix} \begin{bmatrix} \widehat{V}_1^T \\ \widehat{V}_0^T \end{bmatrix} \tag{6.4}$$

and its truncation at the model order n yields an estimate

$$\widehat{\mathcal{O}}_{p+1} = \widehat{U}_1 \widehat{\Delta}_1^{1/2}$$

for the observability matrix, from which $(\widehat{C}, \widehat{A})$ and $(\widehat{\lambda}, \widehat{\varphi}_\lambda)$ are recovered as sketched above. Note that the singular values in $\widehat{\Delta}_1$ are non-zero and $\widehat{\mathcal{O}}_{p+1}$ is of full column rank. The matrices

$$\widehat{U}_1 = \begin{bmatrix} u_1 & \dots & u_n \end{bmatrix}, \widehat{V}_1 = \begin{bmatrix} v_1 & \dots & v_n \end{bmatrix}, \widehat{\Delta}_1 = \operatorname{diag}\{\sigma_1, \dots, \sigma_n\} \tag{6.5}$$

contain the first n left and right singular vectors, and singular values of $\widehat{\mathcal{H}}_{p+1,q}$.

6.2.2 Subspace-based fault detection algorithm

In [BAB00] the statistical subspace-based fault detection method was described, which is designed for subspace algorithms satisfying factorization property (6.2). Let θ be the vector containing a canonical parameterization of the actual state of the system and θ_0 the parameterization of the reference state, as defined in (6.3). A residual function compares the system parameter θ_0 of a reference state with a subspace matrix $\widehat{\mathcal{H}}_{p+1,q}$ computed on a new data sample $(Y_k)_{k=1,\ldots,N+p+q}$, corresponding to an unknown, possibly damaged state with system parameter θ. Assume that $\widehat{\mathcal{H}}_{p+1,q}$ is a consistent estimate of $\mathcal{H}_{p+1,q}$.

To compare the states, the left null space matrix $S = S(\theta_0)$ of the observability matrix of the reference state is computed, which is also the left null space of the subspace matrix at the reference state because of factorization property (6.2). The characteristic property of a system in the reference state then writes $S^T\widehat{\mathcal{H}}_{p+1,q} = 0$ and the residual vector $\zeta_N = \zeta_N(\theta_0)$ with

$$\zeta_N = \sqrt{N}\mathrm{vec}(S^T\widehat{\mathcal{H}}_{p+1,q}) \tag{6.6}$$

describes the difference between the unknown state θ of matrix $\widehat{\mathcal{H}}_{p+1,q}$ and the reference state θ_0.

The damage detection problem is to decide whether the subspace matrix $\widehat{\mathcal{H}}_{p+1,q}$ from the (possibly damaged) system (corresponding to θ) is still well described by the characteristics of the reference state (corresponding to θ_0) or not. This is done by testing between the hypotheses

$$\begin{array}{ll} \mathbf{H}_0 : \ \theta = \theta_0 & \text{(reference system)}, \\ \mathbf{H}_1 : \ \theta = \theta_0 + \delta\theta/\sqrt{N} & \text{(faulty system)}, \end{array} \tag{6.7}$$

where δ is unknown but fixed. This is called the local approach, and the following proposition is used to test between both hypotheses.

Proposition 6.1 ([BAB00]) *The residual ζ_N is asymptotically Gaussian for $N \to \infty$ with*

$$\zeta_N \xrightarrow{N} \begin{cases} \mathcal{N}(0, \Sigma_\zeta) & \text{under } \mathbf{H}_0 \\ \mathcal{N}(\mathcal{J}_\zeta\delta\theta, \Sigma_\zeta) & \text{under } \mathbf{H}_1, \end{cases}$$

where $\mathcal{J}_\zeta$ and Σ_ζ are the asymptotic sensitivity and covariance of the residual ζ_N. The test between the hypotheses $\mathbf{H}_0$ and $\mathbf{H}_1$ is achieved through the asymptotic χ^2-test statistics

$$\chi^2_N = \zeta_N^T\widehat{\Sigma}_\zeta^{-1}\widehat{\mathcal{J}}_\zeta(\widehat{\mathcal{J}}_\zeta^T\widehat{\Sigma}_\zeta^{-1}\widehat{\mathcal{J}}_\zeta)^{-1}\widehat{\mathcal{J}}_\zeta^T\widehat{\Sigma}_\zeta^{-1}\zeta_N \tag{6.8}$$

and comparing it to a threshold, where $\widehat{\mathcal{J}}_\zeta$ and $\widehat{\Sigma}_\zeta$ are consistent estimates of $\mathcal{J}_\zeta$ and Σ_ζ. Both can be estimated in the reference state under the assumption that the covariance Q of the excitation of the system does not change between the reference state and the possibly damaged state. The test χ^2_N is asymptotically χ^2 distributed with $\mathrm{rank}(\mathcal{J}_\zeta)$ *degrees of freedom and non-centrality parameter $\delta\theta^T F\delta\theta$, where $F = \mathcal{J}_\zeta^T\Sigma_\zeta^{-1}\mathcal{J}_\zeta$ is the asymptotic Fisher information on θ_0 contained in $\zeta_N = \zeta_N(\theta_0)$.*

Remark 6.2 *The notation of the residual function, its sensitivity and covariance is slightly changed here compared to Chapter 2. For simplicity, the argument θ_0 of $\zeta_N = \zeta_N(\theta_0)$, $\chi^2_N = \chi^2_N(\theta_0)$, $\mathcal{J}_\zeta = \mathcal{J}_\zeta(\theta_0)$ and $\Sigma_\zeta = \Sigma_\zeta(\theta_0)$ is omitted. The index ζ of $\mathcal{J}_\zeta$ and Σ_ζ emphasizes that these matrices are the asymptotic sensitivity and covariance of residual ζ_N, while $\widehat{\mathcal{J}}_\zeta$ and $\widehat{\Sigma}_\zeta$ are consistent estimates of residual ζ_N.*

The computation of the Jacobian $\mathcal{J}_\zeta$ needs a parameterization of the system, where the eigenvalues and mode shapes of the reference system must be known. It is explained in detail in Chapter 2. In [BBB+08] a non-parametric version of the test is proposed, where $\mathcal{J}_\zeta$ is set as the identity matrix. In this case, the χ^2-test boils down to

$$\widehat{\chi}^2_N = \widehat{\zeta}_N^T \widehat{\Sigma}_\zeta^{-1} \widehat{\zeta}_N, \tag{6.9}$$

see also Section 2.3.4.

The computation of the residual covariance matrix Σ_ζ depends on the *covariance of the subspace matrix*

$$\Sigma_{\mathcal{H}} \stackrel{\text{def}}{=} \lim_{N\to\infty} \operatorname{cov}(\sqrt{N}\operatorname{vec} \widehat{\mathcal{H}}_{p+1,q}), \tag{6.10}$$

which is dependent on the chosen subspace algorithm. Then, the covariance matrix Σ_ζ can be obtained from

$$\Sigma_\zeta = (I \otimes S^T)\Sigma_{\mathcal{H}}(I \otimes S) \tag{6.11}$$

due to (6.6), where $\otimes$ denotes the Kronecker product and an estimate $\widehat{\Sigma}_{\mathcal{H}}$ of $\Sigma_{\mathcal{H}}$ is computed on data of the reference state of the system. With this notation, the covariance computation of the covariance-driven subspace-based residual as in Section 2.3.3.4 can be extended to other SSI algorithms. In Section 3.5.2, its computation was explained in detail for covariance-driven SSI and extended to SSI with the Unweighted Principal Component algorithm.

6.3 Impact of changing excitation on fault detection test

In the introductory Section 2.3.3 of Chapter 2 and when recalling the fault detection test in Section 6.2.2, it was assumed that the unmeasured excitation $(V_k)_k$ is stationary and does not change between the reference state θ_0 and a possibly damaged state θ of the system. In practice, however, its covariance $Q = \mathbf{E}(V_k V_k^T)$ may change between different measurements of the system due to different environmental factors (wind, traffic, ...), while the excitation is still assumed to be stationary during one measurement. A change in the state noise covariance Q leads to a change in the subspace matrix $\mathcal{H}_{p+1,q}$ and its estimate $\widehat{\mathcal{H}}_{p+1,q}$ and thus changes the residual function ζ_N in (6.6). Thus, the estimates $\widehat{\mathcal{J}}_\zeta$ and $\widehat{\Sigma}_\zeta$ of the residual's sensitivity and covariance are influenced by a change in the state noise. To be unambiguous, write $\zeta_N(\theta_0, \theta)$ for the residual function, where the null space is computed on the reference state θ_0 and the tested data correspond to the unknown state θ as in Section 2.3.

The derivation of the residual's sensitivity and covariance in Section 2.3 then depends on

the actual Q, under which the residual $\zeta_N(\theta_0,\theta) = \zeta_N(\theta_0,\theta,Q)$ is obtained and it holds

$$\zeta_N(\theta_0,\theta,Q) \xrightarrow{N} \begin{cases} \mathcal{N}\left(0,\Sigma_\zeta^Q\right) & \text{under } \mathbf{H}_0 \\ \mathcal{N}\left(\mathcal{J}_\zeta^Q\,\delta\theta,\Sigma_\zeta^Q\right) & \text{under } \mathbf{H}_1 \end{cases},$$

where

$$\mathcal{J}_\zeta^Q = \lim_{N\to\infty} \mathcal{J}_N^{(1)}(\theta_0,\theta,Q) = \lim_{N\to\infty} \mathcal{J}_N^{(2)}(\theta_0,\theta,Q), \quad \Sigma_\zeta^Q = \lim_{N\to\infty} \Sigma_N(\theta_0,\theta,Q),$$

cf. Equations (2.21), (2.26). The argument Q indicates a dependence on the actual excitation, under which the residual function is computed. Note that the system parameters θ_0 or θ are independent of Q.

However, the excitation and thus Q is in general unknown. Thus, consistent estimates of $\mathcal{J}_\zeta^Q$ and Σ_ζ^Q of the asymptotic sensitivity and covariance of the residual $\zeta_N(\theta_0,\theta_0,Q)$ might not correspond to consistent estimates of $\mathcal{J}_\zeta^{\widetilde{Q}}$ and $\Sigma_\zeta^{\widetilde{Q}}$ related to $\zeta_N(\theta_0,\theta,\widetilde{Q})$ in some unknown state. In this case, consistent estimates $\widehat{\mathcal{J}}_\zeta^Q$ and $\widehat{\Sigma}_\zeta^Q$ of $\mathcal{J}_\zeta^Q$ and Σ_ζ^Q can only be obtained using the data corresponding to the excitation covariance Q, i.e. data of the actually tested state. As this state is also unknown, it corresponds to parameter θ.

With the generalized likelihood ratio test of Section 2.3.2.3, the close hypotheses $\mathbf{H}_0$ and $\mathbf{H}_1$ are tested against each other, amounting to the χ^2-test statistics. Note that in the case of a changed excitation covariance $\widetilde{Q}$, both hypotheses are related to the actual excitation $\widetilde{Q}$ and the residual function $\zeta_N(\theta_0,\theta,\widetilde{Q})$, where $\theta = \theta_0 + \delta\theta/\sqrt{N}$ is tested. There is no relation to the residual function $\zeta_N(\theta_0,\theta_0,Q)$ using data from the reference state. If the null hypothesis $\mathbf{H}_0$ relates to distribution $\mathcal{N}(0,\Sigma_\zeta^Q)$, while hypothesis $\mathbf{H}_1$ relates to a distribution $\mathcal{N}(\mathcal{J}_\zeta^{\widetilde{Q}}\delta\theta,\Sigma_\zeta^{\widetilde{Q}})$ with a different covariance, the generalized likelihood ratio test does not boil down to a χ^2-distributed variable anymore.

Assuming close hypotheses, where $\theta \to \theta_0$ for $N \to \infty$, and using the results of Sections 2.3.3.2–2.3.3.4 and Equation (2.21), consistent estimates of $\mathcal{J}_\zeta^Q$ and Σ_ζ^Q write

$$\begin{aligned} \widehat{\mathcal{J}}_\zeta^Q &= \left(\mathcal{O}_{p+1}(\theta_0)^\dagger \widehat{\mathcal{H}}_{p+1,q} \otimes S\right)^T \mathcal{O}'_{p+1}(\theta_0) \\ \widehat{\Sigma}_\zeta^Q &= \frac{1}{n_b-1}\sum_{k=1}^{n_b}\left(\zeta_{N_b}^{(k)} - \overline{\zeta}_{N_b}\right)\left(\zeta_{N_b}^{(k)} - \overline{\zeta}_{N_b}\right)^T, \quad \overline{\zeta}_{N_b} = \frac{1}{n_b}\sum_{k=1}^{n_b}\zeta_{N_b}^{(k)}, \end{aligned}$$

where $\zeta_{N_b}^{(k)} = \sqrt{N_b}\,\mathrm{vec}\left(S^T\widehat{\mathcal{H}}_{p+1,q}^{(k)}\right)$. All used subspace matrices are computed on new data corresponding to Q and the unknown state θ. Then, with (6.11) follows

$$\widehat{\Sigma}_\zeta^Q = (I\otimes S^T)\widehat{\Sigma}_{\mathcal{H}}(I\otimes S), \tag{6.12}$$

where $\widehat{\Sigma}_{\mathcal{H}}$ is obtained using new data corresponding to the unknown state θ. The corresponding χ^2-test statistics as in (6.8) thus writes as

$$\chi_N^2 = \zeta_N^T(\widehat{\Sigma}_\zeta^Q)^{-1}\widehat{\mathcal{J}}_\zeta^Q\left((\widehat{\mathcal{J}}_\zeta^Q)^T(\widehat{\Sigma}_\zeta^Q)^{-1}\widehat{\mathcal{J}}_\zeta^Q\right)^{-1}(\widehat{\mathcal{J}}_\zeta^Q)^T(\widehat{\Sigma}_\zeta^Q)^{-1}\zeta_N, \tag{6.13}$$

where $\zeta_N = \zeta_N(\theta_0, \theta, Q)$. Its non-parametric counterpart as in (6.9) writes

$$\widehat{\chi}_N^2 = \widehat{\zeta}_N^T (\widehat{\Sigma}_\zeta^Q)^{-1} \widehat{\zeta}_N. \tag{6.14}$$

This computation of the residual's sensitivity and covariance using new data from the unknown state was already applied successfully, e.g. in [RMLDR08]. However, the computation of $\widehat{\Sigma}_\mathcal{H}$ requires many samples and hence it would be favorable to compute it in the reference state.

In the following sections, two solutions are proposed that take into account a change in the excitation.

6.4 Residual with excitation normalization

A first attempt to take a different excitation between measurements into account makes use of the strategies of Chapter 4, where subspace matrices under possibly different excitation are normalized and merged. Only the non-parametric test variant without the use of the Jacobian of the residual are derived in this section.

6.4.1 Single setup

The set of r available sensors is divided in two parts, into r_0 reference sensors and $r^{(\mathrm{mov})} \stackrel{\mathrm{def}}{=} r - r_0$ remaining sensors, which are also called *moving sensors*, in view of using multiple sensor setups with moving sensors. Analogously, the sensor data and the observation matrix are separated into reference and moving sensor parts, such that

$$Y_k = \begin{bmatrix} Y_k^{(\mathrm{ref})} \\ Y_k^{(\mathrm{mov})} \end{bmatrix}, \quad C = \begin{bmatrix} C^{(\mathrm{ref})} \\ C^{(\mathrm{mov})} \end{bmatrix}.$$

Then, with an appropriate permutation matrix P, the subspace and observability matrix are separated into reference and moving sensor part, such that

$$\mathcal{H}_{p+1,q} = P \begin{bmatrix} \mathcal{H}_{p+1,q}^{(\mathrm{ref})} \\ \mathcal{H}_{p+1,q}^{(\mathrm{mov})} \end{bmatrix}, \quad \mathcal{O}_{p+1} = P \begin{bmatrix} \mathcal{O}_{p+1}^{(\mathrm{ref})} \\ \mathcal{O}_{p+1}^{(\mathrm{mov})} \end{bmatrix}, \tag{6.15}$$

where the observation matrices in $\mathcal{O}_{p+1}^{(\mathrm{ref})}$ and $\mathcal{O}_{p+1}^{(\mathrm{mov})}$ are $C^{(\mathrm{ref})}$ and $C^{(\mathrm{mov})}$, respectively. Then,

$$\begin{bmatrix} \mathcal{H}_{p+1,q}^{(\mathrm{ref})} \\ \mathcal{H}_{p+1,q}^{(\mathrm{mov})} \end{bmatrix} = \begin{bmatrix} \mathcal{O}_{p+1}^{(\mathrm{ref})} \\ \mathcal{O}_{p+1}^{(\mathrm{mov})} \end{bmatrix} \mathcal{Z}_q,$$

and the product

$$\mathcal{H}_{p+1,q}^{(\mathrm{mov})} \mathcal{H}_{p+1,q}^{(\mathrm{ref})-1} = \mathcal{O}_{p+1}^{(\mathrm{mov})} \mathcal{O}_{p+1}^{(\mathrm{ref})-1}$$

is independent of the excitation. Then, the null space $\widehat{S}$ is defined such that

$$\widehat{S}^T \widehat{\mathcal{H}}_{p+1,q}^{0,(\mathrm{mov})} = \widehat{S}^T \widehat{\mathcal{O}}_{p+1}^{0,(\mathrm{mov})} = 0,$$

where the additional index 0 indicates matrices from the reference state. Define the residual function

$$\widehat{\zeta}_N^{\mathrm{r}} \stackrel{\mathrm{def}}{=} \sqrt{N}\,\mathrm{vec}\left(\widehat{S}^T\widehat{\mathcal{H}}_{p+1,q}^{(\mathrm{mov})}\widehat{\mathcal{H}}_{p+1,q}^{(\mathrm{ref})-1}\right),$$

where $\widehat{\mathcal{H}}_{p+1,q}^{(\mathrm{ref})}$ and $\widehat{\mathcal{H}}_{p+1,q}^{(\mathrm{mov})}$ are obtained from $\widehat{\mathcal{H}}_{p+1,q}$ in (6.15), which is computed on N data samples. The covariance $\widehat{\Sigma}_\zeta^{\mathrm{r}}$ of residual $\widehat{\zeta}_N^{\mathrm{r}}$ is obtained in the reference state as follows. Assume a first order perturbation

$$\begin{aligned}
\Delta\widehat{\zeta}_N^{\mathrm{r}} &= \sqrt{N}(I\otimes\widehat{S}^T)\,\mathrm{vec}\left(\Delta\left(\widehat{\mathcal{H}}_{p+1,q}^{0,(\mathrm{mov})}\widehat{\mathcal{H}}_{p+1,q}^{0,(\mathrm{ref})-1}\right)\right)\\
&= \sqrt{N}(I\otimes\widehat{S}^T)\,\mathrm{vec}\left(\Delta\left(\widehat{\mathcal{H}}_{p+1,q}^{0,(\mathrm{mov})}\right)\widehat{\mathcal{H}}_{p+1,q}^{0,(\mathrm{ref})-1} - \widehat{\mathcal{H}}_{p+1,q}^{0,(\mathrm{mov})}\widehat{\mathcal{H}}_{p+1,q}^{0,(\mathrm{ref})-1}\Delta\left(\widehat{\mathcal{H}}_{p+1,q}^{0,(\mathrm{ref})}\right)\widehat{\mathcal{H}}_{p+1,q}^{0,(\mathrm{ref})-1}\right)\\
&= \sqrt{N}(I\otimes\widehat{S}^T)\left(\widehat{\mathcal{H}}_{p+1,q}^{0,(\mathrm{ref})-1}\otimes I\right)\mathrm{vec}\left(\begin{bmatrix}-\widehat{\mathcal{H}}_{p+1,q}^{0,(\mathrm{mov})}\widehat{\mathcal{H}}_{p+1,q}^{0,(\mathrm{ref})-1} & I\end{bmatrix}\Delta\begin{bmatrix}\widehat{\mathcal{H}}_{p+1,q}^{0,(\mathrm{ref})}\\ \widehat{\mathcal{H}}_{p+1,q}^{0,(\mathrm{mov})}\end{bmatrix}\right)\\
&= \sqrt{N}(I\otimes\widehat{S}^T)\left(\widehat{\mathcal{H}}_{p+1,q}^{0,(\mathrm{ref})-T}\otimes\begin{bmatrix}-\widehat{\mathcal{H}}_{p+1,q}^{0,(\mathrm{mov})}\widehat{\mathcal{H}}_{p+1,q}^{0,(\mathrm{ref})-1} & I\end{bmatrix}P^T\right)\Delta(\mathrm{vec}\,\widehat{\mathcal{H}}_{p+1,q}^{(0)}),
\end{aligned}$$

leading to the residual covariance

$$\widehat{\Sigma}_\zeta^{\mathrm{r}} = (I\otimes\widehat{S}^T)\widehat{\mathcal{J}}_{\mathrm{r}}\widehat{\Sigma}_{\mathcal{H}}\widehat{\mathcal{J}}_{\mathrm{r}}^T(I\otimes\widehat{S}),\quad\text{where}\quad\widehat{\mathcal{J}}_{\mathrm{r}}\stackrel{\mathrm{def}}{=}\widehat{\mathcal{H}}_{p+1,q}^{0,(\mathrm{ref})-T}\otimes\begin{bmatrix}-\widehat{\mathcal{H}}_{p+1,q}^{0,(\mathrm{mov})}\widehat{\mathcal{H}}_{p+1,q}^{0,(\mathrm{ref})-1} & I\end{bmatrix}P^T$$

and $\widehat{\Sigma}_{\mathcal{H}}$ is an estimate of the covariance of the subspace matrix, which are computed in the reference state. The respective χ^2-test statistics writes thus

$$\chi_N^{\mathrm{r}\,2} = \widehat{\zeta}_N^{\mathrm{r}\,T}(\widehat{\Sigma}_\zeta^{\mathrm{r}})^{-1}\widehat{\zeta}_N^{\mathrm{r}}. \tag{6.16}$$

Some comments are in order about the χ^2-test statistics (6.16). This test corresponds to testing the product

$$\widehat{S}^T\,\widehat{\mathcal{H}}_{p+1,q}^{(\mathrm{mov})}\,\widehat{T}$$

for a change, where $\widehat{T}\stackrel{\mathrm{def}}{=}\widehat{\mathcal{H}}_{p+1,q}^{(\mathrm{ref})-1}\widehat{\mathcal{H}}_{p+1,q}^{0,(\mathrm{ref})}$ is the matrix that artificially introduces the same excitation to $\widehat{\mathcal{H}}_{p+1,q}^{(\mathrm{mov})}$ as it is present in the reference state. However, if $\widehat{\mathcal{H}}_{p+1,q}^{(\mathrm{ref})}$ is not in the reference state anymore, matrix $\widehat{T}$ is not just simply a matrix that accounts for excitation change, but also contains information about the poles and thus the eigenstructure of the currently tested and the reference state. However, the effects of this influence are not clear.

Note also, that with this kind of test, the information for fault detection is only obtained from the moving sensors, while the reference only serve to normalize the data with respect to a different excitation.

6.4.2 Multiple setups

For fault detection of multiple setups, where a structure is measured using fixed reference sensors and moving sensors as in Chapter 4, the different excitation in the data between the

setups needs to be taken into account. Instead of a single record for the output (Y_k) of the system (4.1), N_s records

$$\underbrace{\begin{pmatrix} Y_k^{(1,\mathrm{ref})} \\ Y_k^{(1,\mathrm{mov})} \end{pmatrix}}_{\text{Record 1}} \quad \underbrace{\begin{pmatrix} Y_k^{(2,\mathrm{ref})} \\ Y_k^{(2,\mathrm{mov})} \end{pmatrix}}_{\text{Record 2}} \quad \cdots \quad \underbrace{\begin{pmatrix} Y_k^{(N_s,\mathrm{ref})} \\ Y_k^{(N_s,\mathrm{mov})} \end{pmatrix}}_{\text{Record } N_s}$$

are now available collected successively. Each record j contains data $Y_k^{(j,\mathrm{ref})}$ of dimension $r^{(\mathrm{ref})} = r_0$ from a fixed *reference* sensor pool, and data $Y_k^{(j,\mathrm{mov})}$ of dimension $r^{(j)}$ from a *moving* sensor pool. Details of the modeling are found in Section 4.3.1. With a chosen subspace algorithm, a local subspace matrix $\widehat{\mathcal{H}}^{(j)}$ can be built for each of the setups, which can be separated into reference sensor part $\widehat{\mathcal{H}}^{(j,\mathrm{ref})}$ and moving sensor part $\widehat{\mathcal{H}}^{(j,\mathrm{mov})}$ analogously to (6.15).

A first way to derive a χ^2-test for these multiple measurements uses the argument that the data from different setups is uncorrelated, without taking a different excitation into account. The *local residual functions* $\zeta_N^{(j)}$ are defined analogously to Section 6.2.2 as

$$\zeta_N^{(j)} \overset{\mathrm{def}}{=} \sqrt{N}\,\mathrm{vec}\left(\widehat{S}^{(j)T}\widehat{\mathcal{H}}_{p+1,q}^{(j,\mathrm{mov})}\right),$$

where $\widehat{S}^{(j)}$ is computed on reference data such that $\widehat{S}^{(j)T}\widehat{\mathcal{H}}_{p+1,q}^{0,(j,\mathrm{mov})} = 0$. Denote the local residual's covariance by $\widehat{\Sigma}_\zeta^{\mathrm{r}(j)}$. This leads to the χ^2-test statistics

$$\chi_N^2 = \sum_{j=1}^{N_s} \widehat{\zeta}_N^{(j)T}(\widehat{\Sigma}_\zeta^{(j)})^{-1}\widehat{\zeta}_N^{(j)}. \tag{6.17}$$

Another way to build a residual for multiple setups uses the global subspace matrix built with a merging algorithm from Chapter 4. However, in the case of many setups and many sensors this can lead to a high dimensional residual function with a very large covariance matrix. Instead, the property is used that data from different setups is statistically uncorrelated. Then, define the *normalized local residual function* as

$$\widehat{\zeta}_N^{\mathrm{r}\,(j)} \overset{\mathrm{def}}{=} \sqrt{N}\,\mathrm{vec}\left(\widehat{S}^{(j)T}\widehat{\mathcal{H}}_{p+1,q}^{(j,\mathrm{mov})}\widehat{\mathcal{H}}_{p+1,q}^{(j,\mathrm{ref})-1}\right),$$

where the null space $\widehat{S}^{(j)}$ is obtained in the reference state from the condition

$$\widehat{S}^{(j)T}\left(\widehat{\mathcal{H}}_{p+1,q}^{0,(j,\mathrm{mov})}\widehat{\mathcal{H}}_{p+1,q}^{0,(j,\mathrm{ref})-1}\widehat{\mathcal{H}}_{p+1,q}^{0,(1,\mathrm{ref})}\right) = 0.$$

Note that $\widehat{S}^{(j)}$ is computed on the normalized local subspace matrix here, where the excitation from setup 1 is introduced artificially. Denote the covariance of $\widehat{\zeta}_N^{\mathrm{r}\,(j)}$ by $\widehat{\Sigma}_\zeta^{\mathrm{r}(j)}$, which can be computed as in the previous section.

As the data sets from different setups are uncorrelated, a χ^2-test of all the setups thus writes

$$\chi_N^{\mathrm{r}\,2} = \sum_{j=1}^{N_s} \widehat{\zeta}_N^{\mathrm{r}\,(j)T}(\widehat{\Sigma}_\zeta^{\mathrm{r}(j)})^{-1}\widehat{\zeta}_N^{\mathrm{r}\,(j)}, \tag{6.18}$$

taking a different excitation between the setups into account.

6.5 Residual robust to excitation change

6.5.1 Definition of residual and χ^2-test

A new possibility to compensate a change in the excitation covariance $Q = \mathbf{E}(V_k V_k^T)$ is the use of a residual function that is robust to these changes. In this section, a χ^2-test on such a residual is derived.

The subspace-based fault detection test was derived based on the property that some system parameter θ_0 agrees with a subspace matrix $\mathcal{H}_{p+1,q}$ iff

$$\mathcal{O}_{p+1}(\theta_0) \text{ and } \mathcal{H}_{p+1,q} \text{ have the same left null space } S.$$

In Section 6.3 it was argued that subspace matrix $\mathcal{H}_{p+1,q}$ depends on the excitation covariance Q. Let U_1 be the matrix of the left singular vectors of $\mathcal{H}_{p+1,q}$. Then the analogous property

$$\mathcal{O}_{p+1}(\theta_0) \text{ and } U_1 \text{ have the same left null space } S$$

holds. However, as U_1 is a matrix with orthonormal columns, it is regarded as independent of the excitation Q. Matrix U_1 is defined by a unique SVD to ensure no changing modal basis, cf. Definition 3.3.

Let $\widehat{\mathcal{H}}_{p+1,q}$ be an estimate of the subspace matrix from a data sample of length N corresponding to the unknown, possibly faulty state θ and unknown state excitation covariance Q. From a unique SVD

$$\widehat{\mathcal{H}}_{p+1,q} = \begin{bmatrix} \widehat{U}_1 & \widehat{U}_0 \end{bmatrix} \begin{bmatrix} \widehat{\Delta}_1 & 0 \\ 0 & \widehat{\Delta}_0 \end{bmatrix} \begin{bmatrix} \widehat{V}_1^T \\ \widehat{V}_0^T \end{bmatrix} \tag{6.19}$$

the matrix $\widehat{U}_1$ is obtained, whose number of columns is the system order n. Note that the singular values in $\widehat{\Delta}_0$ are very small and tend to zero for $N \to \infty$. Then, a residual that is robust to a change in the excitation covariance can be defined as

$$\xi_N \overset{\text{def}}{=} \sqrt{N}\text{vec}(S^T \widehat{U}_1). \tag{6.20}$$

Proposition 6.3 *The residual ξ_N is asymptotically Gaussian for $N \to \infty$ with*

$$\xi_N \xrightarrow{N} \begin{cases} \mathcal{N}(0, \Sigma_\xi) & \text{under } \mathbf{H}_0 \\ \mathcal{N}(\mathcal{J}_\xi \delta\theta, \Sigma_\xi) & \text{under } \mathbf{H}_1, \end{cases}$$

where $\mathcal{J}_\xi$ and Σ_ξ are the asymptotic sensitivity and covariance of the residual ξ_N and the close hypotheses $\mathbf{H}_0$ and $\mathbf{H}_1$ are defined in (6.7).

The test between the hypotheses $\mathbf{H}_0$ and $\mathbf{H}_1$ is achieved through the asymptotic χ^2-test statistics

$$\gamma_N^2 = \xi_N^T \widehat{\Sigma}_\xi^{-1} \widehat{\mathcal{J}}_\xi (\widehat{\mathcal{J}}_\xi^T \widehat{\Sigma}_\xi^{-1} \widehat{\mathcal{J}}_\xi)^{-1} \widehat{\mathcal{J}}_\xi^T \widehat{\Sigma}_\xi^{-1} \xi_N \tag{6.21}$$

and comparing it to a threshold, where $\widehat{\mathcal{J}}_\xi$ and $\widehat{\Sigma}_\xi$ are consistent estimates of $\mathcal{J}_\xi$ and Σ_ξ.

Proof: Let the unique SVDs of $\widehat{\mathcal{H}}_{p+1,q}$ in (6.19) and $\mathcal{H}_{p+1,q} = U_1 \Delta_1 V_1^T$ be given, where $\widehat{\mathcal{H}}_{p+1,q}$ is an estimate of the subspace matrix $\mathcal{H}_{p+1,q}$. From [MB86] and [BP08, Corollary 1] follows that $\widehat{U}_1$ is asymptotically Gaussian with

$$\sqrt{N} \operatorname{vec}\left(\widehat{U}_1 - U_1\right) \xrightarrow{N} \mathcal{N}\left(0, \Sigma_{U_1}\right),$$

where

$$\Sigma_{U_1} = \lim_{N\to\infty} \operatorname{cov}(\sqrt{N}\operatorname{vec}\widehat{U}_1) = \left(\Delta_1^{-1} V_1^T \otimes I\right) \Sigma_{\mathcal{H}} \left(V_1 \Delta_1^{-1} \otimes I\right).$$

It follows that the residual ξ_N is asymptotically Gaussian, with a covariance satisfying $\Sigma_\xi = (I \otimes S^T)\, \Sigma_{U_1}\, (I \otimes S)$. The proof finishes as in Proposition 6.1. □

Note that the asymptotic sensitivity $\mathcal{J}_\xi$ and covariance Σ_ξ of residual ξ_N can be computed on data corresponding to the reference state, as they do not depend on the excitation covariance Q.

The computation of the sensitivity $\mathcal{J}_\xi$ is analogous to the computation of the sensitivity $\mathcal{J}_\zeta$ of ζ_N, where $\mathcal{H}_{p+1,q}$ has to be replaced by U_1. From (2.44) and (2.45) follows

$$\mathcal{J}_\xi = \left(\mathcal{O}_{p+1}(\theta_0)^\dagger\, U_1 \otimes S\right)^T \mathcal{O}'_{p+1}(\theta_0).$$

A consistent estimate $\widehat{\mathcal{J}}_\xi$ is obtained by replacing U_1 by $\widehat{U}_1$.

Following the proof of Proposition 6.3, the asymptotic covariance Σ_ξ of ξ_N can be obtained from

$$\Sigma_\xi = \left(\Delta_1^{-1} V_1^T \otimes S^T\right) \Sigma_{\mathcal{H}} \left(V_1 \Delta_1^{-1} \otimes S\right),$$

where $\mathcal{H}_{p+1,q} = U_1 \Delta_1 V_1^T$. A consistent estimate thus writes as

$$\widehat{\Sigma}_\xi = \left(\widehat{\Delta}_1^{-1} \widehat{V}_1^T \otimes S^T\right) \widehat{\Sigma}_{\mathcal{H}} \left(\widehat{V}_1 \widehat{\Delta}_1^{-1} \otimes S\right).$$

Another possibility to compute the estimate $\widehat{\Sigma}_\xi$ is to propagate the covariance of the subspace matrix to the covariance of the singular vectors by a sensitivity analysis [PGS07, RPDR08]. Then it holds

$$\operatorname{cov}(\sqrt{N} \operatorname{vec}\widehat{U}_1) = \mathcal{J}_{\widehat{U}_1} \operatorname{cov}(\sqrt{N} \operatorname{vec}\widehat{\mathcal{H}}_{p+1,q}) \mathcal{J}_{\widehat{U}_1}^T, \tag{6.22}$$

where $\mathcal{J}_{\widehat{U}_1}$ is the sensitivity of the left singular vectors $\operatorname{vec}\widehat{U}_1$ with respect to $\operatorname{vec}\widehat{\mathcal{H}}_{p+1,q}$. It follows

$$\widehat{\Sigma}_\xi = (I \otimes S^T)\, \mathcal{J}_{\widehat{U}_1}\, \widehat{\Sigma}_{\mathcal{H}}\, \mathcal{J}_{\widehat{U}_1}^T\, (I \otimes S). \tag{6.23}$$

The computation of $\mathcal{J}_{\widehat{U}_1}$ is numerically costly and was proposed in [PGS07, RPDR08] (see Proposition 3.10 in Section 3.3.2). A more efficient computation of singular vector sensitivities was proposed in Proposition 3.11. Its results for the computation of $\mathcal{J}_{\widehat{U}_1}$ are summarized now.

Proposition 6.4 *Let the SVD of $\widehat{\mathcal{H}}_{p+1,q}$ in (6.4) with singular vectors and values (6.5) be given. For $j = 1, \ldots, n$ define*

$$\begin{aligned}
\widetilde{K}_j &\overset{\text{def}}{=} \frac{\widehat{\mathcal{H}}_{p+1,q}}{\sigma_j} \left(I_{qr_0} + \begin{bmatrix} 0_{qr_0-1,qr_0} \\ 2v_j^T \end{bmatrix} - \frac{\widehat{\mathcal{H}}_{p+1,q}^T \widehat{\mathcal{H}}_{p+1,q}}{\sigma_j^2} \right)^{-1}, \\
\widetilde{E}_j &\overset{\text{def}}{=} \left[I_{(p+1)r} + \widetilde{K}_j \left(\frac{\widehat{\mathcal{H}}_{p+1,q}^T}{\sigma_j} - \begin{bmatrix} 0_{qr_0-1,(p+1)r} \\ u_j^T \end{bmatrix} \right) \quad \widetilde{K}_j \right], \\
\widetilde{F}_j &\overset{\text{def}}{=} \frac{1}{\sigma_j} \begin{bmatrix} v_j^T \otimes (I_{(p+1)r_0} - u_j u_j^T) \\ (I_{qr_0} - v_j v_j^T) \otimes u_j^T \end{bmatrix}.
\end{aligned}$$

Then the sensitivity of the left singular vectors of $\widehat{\mathcal{H}}_{p+1,q}$ writes

$$\mathcal{J}_{\widehat{U}_1} = \begin{bmatrix} \widetilde{E}_1 \widetilde{F}_1 \\ \vdots \\ \widetilde{E}_n \widetilde{F}_n \end{bmatrix}.$$

Remark 6.5 *The computation of $\mathcal{J}_{\widehat{U}_1}$ in Proposition 6.4 involves n matrix inversions of size qr_0 and is less costly than computing n pseudoinverses of square matrices of size $(p+1)r+qr_0$ that are necessary for the computation in [RPDR08] as stated in Proposition 3.10 in Section 3.3.2.*

Remark 6.6 *In this section, the matrix $\widehat{U}_1$ obtained from a unique SVD of the subspace matrix is assumed to be independent of the excitation. A similar problem, where the excitation between different setups needs to be normalized, is the merging of the subspace or observability matrices obtained from data of different measurement setups in Chapter 4. However, computing the matrices $\widehat{U}_1^{(j)}$ from a unique SVD for each measurement setup j and merging them straightforward is not possible, as each of these matrices still can be in a different modal basis with respect to the reference sensor part, although being independent of the excitation itself. Thus, the techniques of Section 4.3.6 would still need to be applied on the matrices $\widehat{U}_1^{(j)}$ for merging.*

6.5.2 Non-parametric version of robust fault detection test

6.5.2.1 Non-parametric test

Analogous to Section 2.3.4, a non-parametric version of the fault detection test can be defined by using an empirical left null space $\widehat{S}$ with

$$\begin{aligned}
\widehat{S}^T \widehat{S} &= I_s, \\
\widehat{S}^T \widehat{\mathcal{H}}_{p+1,q}^{(0)} &= 0,
\end{aligned}$$

where $\widehat{\mathcal{H}}_{p+1,q}^{(0)}$ is an estimate of the subspace matrix corresponding to reference parameter θ_0 that is unknown. The null space $\widehat{S}$ can be obtained in SVD (6.19) from $\widehat{S} = \widehat{U}_0$.

Based on a new data set of length N from the (possibly faulty) system, the empirical subspace matrix $\widehat{\mathcal{H}}_{p+1,q}$ (corresponding to the unknown state θ) is computed and the residual then writes

$$\widehat{\xi}_N \stackrel{\text{def}}{=} \sqrt{N}\ \text{vec}\left(\widehat{S}^T\widehat{U}_1\right),$$

where $\widehat{U}_1$ is obtained from unique SVD (6.19) of $\widehat{\mathcal{H}}_{p+1,q}$. As there is no system parameterization, no sensitivity matrix is to be taken care of. The χ^2-test statistics (6.21) boils down to

$$\widehat{\gamma}_N^2 \stackrel{\text{def}}{=} \widehat{\xi}_N^T\widehat{\Sigma}_\xi^{-1}\widehat{\xi}_N \tag{6.24}$$

where $\widehat{\Sigma}_\xi$ is an estimate of the covariance of $\widehat{\xi}_N$, which can be computed in the reference state as in the previous section.

6.5.2.2 Merging different reference states under possibly different excitation

As in 2.3.4, assume that J reference data sets are available with corresponding subspace matrices $\widehat{\mathcal{H}}_{p+1,q}^{(0,1)},\dots,\widehat{\mathcal{H}}_{p+1,q}^{(0,J)}$ that relate to (slightly) different system parameters $\theta_{0,1},\dots,\theta_{0,J}$. Now it is also assumed that they are estimated under possibly different excitation with excitation covariances $Q_1,\dots,Q_J$.

A left null space $\widehat{S}$ is desired with the property

$$\widehat{S}^T\widehat{\mathcal{H}}_{p+1,q}^{(0,k)} = 0, \quad k = 1,\dots,J.$$

As the subspace matrices correspond to different excitations, computing $\widehat{S}$ on their sum is not meaningful as this sum can be seen as weighted with respect to different excitations. Instead it is proposed to compute $\widehat{S}$ on the juxtaposed subspace matrices from the reference states such that

$$\widehat{S}^T\widehat{\mathcal{H}}^{(\text{jux})} = 0, \quad \text{where} \quad \widehat{\mathcal{H}}^{(\text{jux})} \stackrel{\text{def}}{=} \begin{bmatrix}\widehat{\mathcal{H}}_{p+1,q}^{(0,1)} & \widehat{\mathcal{H}}_{p+1,q}^{(0,2)} & \dots & \widehat{\mathcal{H}}_{p+1,q}^{(0,J)}\end{bmatrix}.$$

This can be done by computing the SVD $\widehat{\mathcal{H}}^{(\text{jux})} = \widehat{U}\widehat{\Delta}\widehat{V}^T$ of $\widehat{\mathcal{H}}^{(\text{jux})} \in \mathbb{R}^{(p+1)r\times Jqr_0}$, where $\widehat{U} \in \mathbb{R}^{(p+1)r\times(p+1)r}$. Then, $\widehat{S}$ is obtained from the last s columns of $\widehat{U}$. Alternatively, especially in the case of a large number J of reference states, an iterative QR decomposition of $\widehat{\mathcal{H}}^{(\text{jux})T}$ as in Lemma 3.7 can be made to obtain the factor R, such that $\widehat{\mathcal{H}}^{(\text{jux})} = RQ$ with an orthogonal matrix Q that is not computed. Then, $\widehat{S}$ can be obtained from an SVD of R.

Let $\widehat{\Sigma}_\xi^{(0,k)}$ be a covariance estimate of ξ_N using the data of $\widehat{\mathcal{H}}_{p+1,q}^{(0,k)}$. Then, a better estimate of the residual covariance on a sample of length N can be obtained from

$$\widehat{\Sigma}_\xi = \frac{1}{J}\sum_{k=1}^{J}\widehat{\Sigma}_\xi^{(0,k)},$$

using the data from all the reference states. In this covariance computation, the possibly different excitation of each data set is taken into account, as the residual function is independent of the excitation.

6.6 Numerical results

In this section, the new fault detection tests of Sections 6.4 and 6.5 are applied to structural vibration examples (cf. Section 2.4).

6.6.1 Fault detection with excitation normalization

The multi-setup damage detection algorithm from Section 6.4 is applied on three nominally identical glass reinforced composite panels (specimen I, II and III). They are similar to the load carrying laminate in a wind turbine blade and described in detail in [LS10]. They were provided by the Risø laboratory at DTU, Denmark, and vibration tests were made at LMS, Belgium.

Due to a non-repeatable manufacturing process, the three specimen differ slightly. Vibration data was recorded in the healthy state and after loading specimen I with the force of 210 kN, specimen II with 220 kN and specimen III with 230 kN. Each time, vibration measurements were done in $N_s = 4$ sensor setups, where 3 of them contained 14 moving sensors and 1 contained 7 moving sensors, with $r_0 = 1$ reference sensor that stayed fixed all the time.

As there are 3 reference specimen, the null space matrices were computed on the averaged subspace matrices (using the covariance-driven approach) of the three specimen in the reference state. The χ^2-test statistics were computed in the healthy and damaged state on 12 different parts of the recorded data containing each 50 000 samples and averaged to avoid outliers. All χ^2-test values are divided by the values of the reference states to be comparable.

The χ^2-test values from test (6.17) are presented in Figure 6.1. The corresponding values from test (6.18), which normalizes different excitation between the setups, are presented in Figure 6.2. It can be seen that the latter test is more reactive and its χ^2-test values grow with the extent of the damage, which is to be expected.

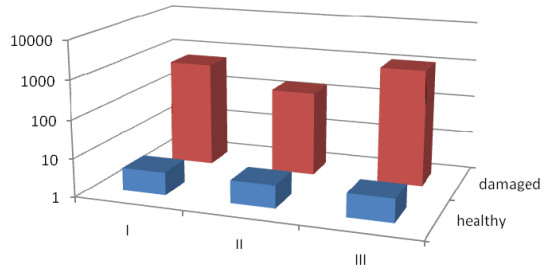

Figure 6.1 – Multi-setup χ^2-test (6.17).

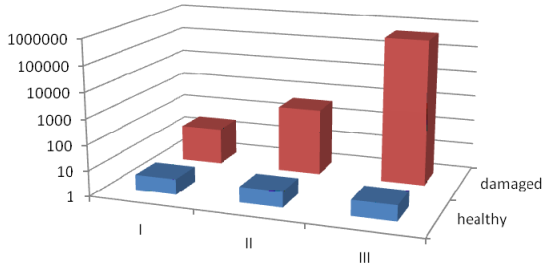

Figure 6.2 – Multi-setup χ^2-test (6.18) *with excitation normalization.*

6.6.2 Fault detection robust to excitation change

To validate the described robust fault detection algorithm from Section 6.5, a simulation study was made using a mass-spring model of six degrees of freedom (DOF), see Figure 6.3,

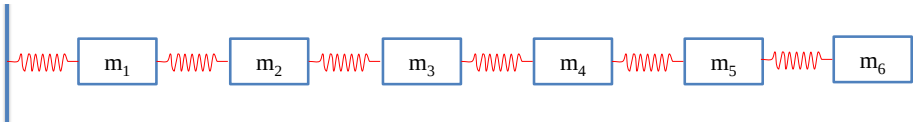

Figure 6.3 – Simulated mass-spring chain.

which is observed at all six DOFs. Four cases of Gaussian stationary white noise excitation having a different covariance $Q = \mathbf{E}(V_k V_k^T)$ of the system were simulated:

1. $Q = I_6$, represented by ○ in the figures,
2. $Q = 4^2 I_6$ (□),
3. $Q = 0.25^2 I_6$ (×),
4. $Q = \mathrm{diag}(1, 2, 3, 4, 5, 6)^2$ (+).

Using this model, output-only data with 100 000 samples was generated to obtain measurements in the reference state with each of the different excitations. Then, the stiffness of spring 2 was reduced by 5% and 10% compared to the reference state, and the simulations were repeated with newly generated excitations.

On this simulated data, the performance of the fault detection algorithms was tested. The χ^2-test statistics is used in its empirical form. Three variants were tested:

- test $\widehat{\chi}^2_N = \widehat{\zeta}_N^T \widehat{\Sigma}_\zeta^{-1} \widehat{\zeta}_N$ in (6.9), where the residual's covariance $\widehat{\Sigma}_\zeta$ is computed only once in the reference state (Section 6.2.2), in Figure 6.4,
- test $\widehat{\chi}^2_N = \widehat{\zeta}_N^T (\widehat{\Sigma}_\zeta^Q)^{-1} \widehat{\zeta}_N$ in (6.14), where the residual's covariance $\widehat{\Sigma}_\zeta^Q$ is computed each time in the tested state, where the excitation covariance is Q (Section 6.3), in Figure 6.5,

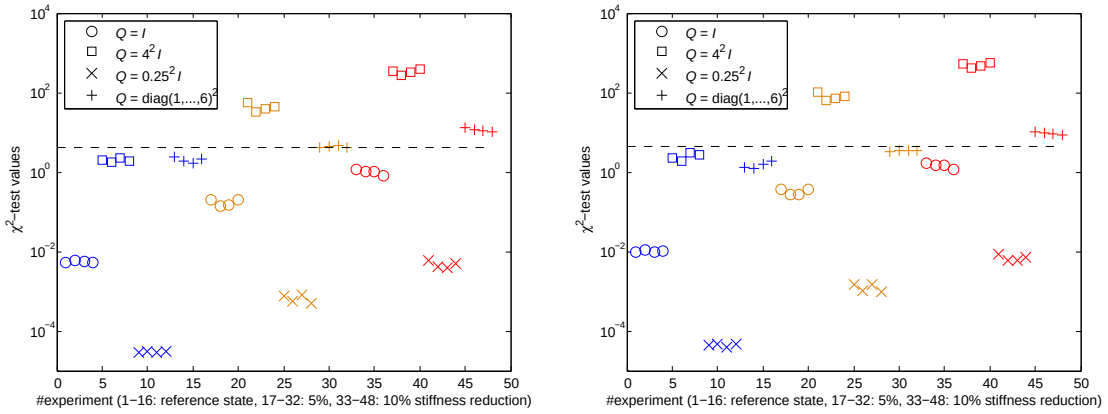

(a) kernel and covariance on states 1–4

(b) kernel and covariance on states 1,2,5,6,9,10

Figure 6.4 – χ^2-test (6.9) with the residual's covariance computed once in the reference state (Section 6.2.2).

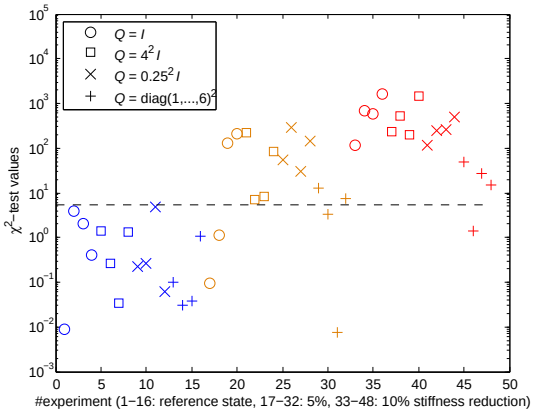

(a) kernel on states 1–4

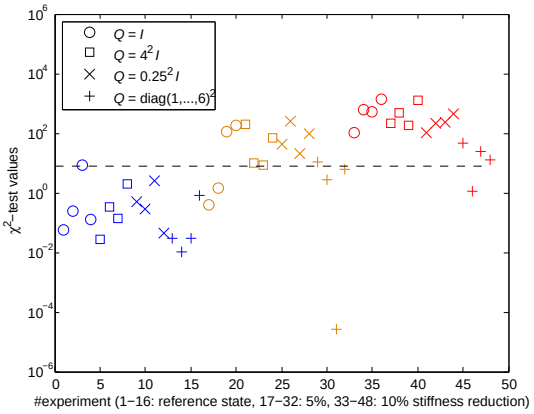

(b) kernel on states 1,2,5,6,9,10

Figure 6.5 – χ^2-test (6.14) *with the residual's covariance computed in the tested state (Section 6.3).*

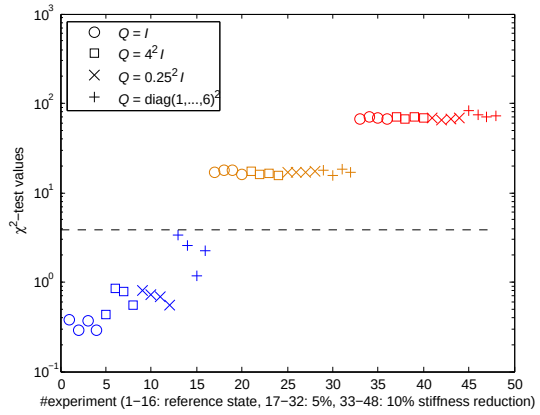

(a) kernel and covariance on states 1–4

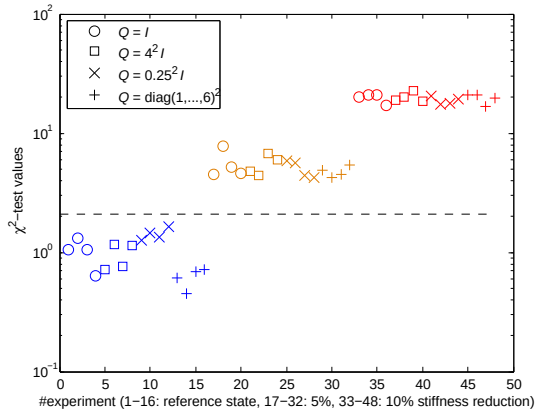

(b) kernel and covariance on states 1,2,5,6,9,10

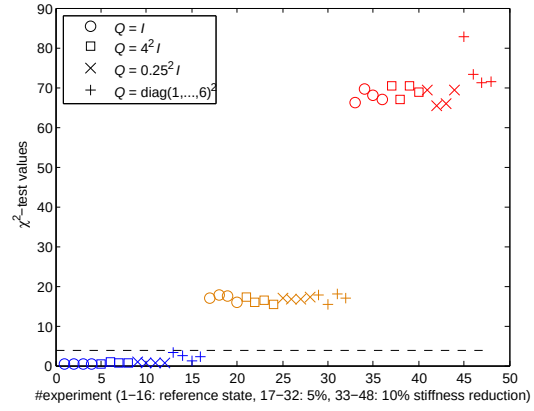

(c) kernel and covariance on states 1–4

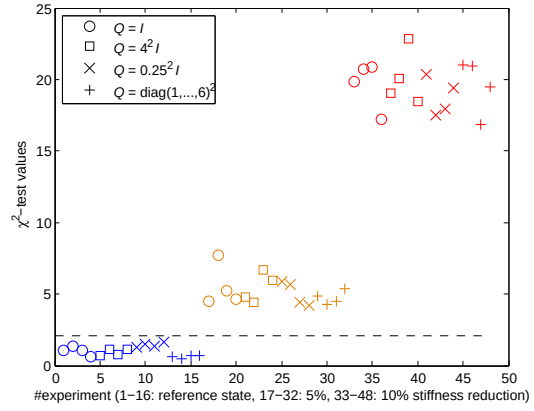

(d) kernel and covariance on states 1,2,5,6,9,10

Figure 6.6 – Newly derived χ^2-test (6.24) *with the residual's covariance computed once in the reference state (Section 6.5) in logarithmic scale (top) and linear scale (bottom).*

- newly derived robust test $\widehat{\gamma}_N^2 = \widehat{\xi}_N^T \widehat{\Sigma}_\xi^{-1} \widehat{\xi}_N$ in (6.24), where the residual's covariance $\widehat{\Sigma}_\xi$ is computed only once in the reference state (Section 6.5), in Figure 6.6.

For each state and excitation covariance, the 100 000 available samples were cut into 4 parts with sample length $N = 25\,000$. The resulting χ^2-test values of the three different tests on this data are plotted in Figures 6.4, 6.5 and 6.6 in the following order: the first 16 test values are computed in the reference state, the next 16 values with 5% stiffness reduction and the last 16 values with 10% stiffness reduction. In each of these states, 4 values correspond to one of the 4 different excitation covariances mentioned above. An empirical threshold (horizontal dashed line) to distinguish between reference states and damaged states is computed on the mean and variance of the χ^2-test values of the 16 reference states.

As can be seen in Figure 6.4, the classical χ^2-test is strongly influenced by a different excitation covariance and no separation of the χ^2-test values between reference and damaged states is possible. Recomputing the residual covariance on data of the currently tested state in Figure 6.5 already leads to a better separation between reference and damaged states, where less than 1/5 of the values in the damaged states are below the threshold established by the reference states. With the new robust χ^2-test in Figure 6.6, a clear separation between reference and damaged states is possible. Note also that the magnitude of damage is apparently linked to the obtained χ^2-test values: Increasing the damage by factor 2 leads to χ^2-test values that are approximately increased to factor 4, which is to be expected.

6.7 Conclusions

In this chapter, the influence of changing excitation between the reference state and the possibly damaged state using the subspace-based fault detection test was clearly pointed out. Two modifications of the test are presented that take into account a changing ambient excitation of the investigated system. The resulting fault detection tests thus contribute to the applicability of the tests under operation conditions, where the unmeasured ambient excitation naturally varies. Especially the statistical fault detection test based on a noise-robust residual in Section 6.5 seems to be theoretically and practically promising. A study on real data under varying excitation has to be made to validate the algorithms under operation conditions.

6.8 Dissemination

Parts of this chapter have been published in:

[LPS+09] M. Luczak, B. Peeters, W. Szkudlarek, L. Mevel, M. Döhler, W. Ostachowicz, K. Martyniuk, and K. Branner. Comparison of the three different approaches for damage detection in the part of the composite wind turbine blade. In *Proc. 7th International Workshop on Structural Health Monitoring*, Stanford, CA, USA, 2009.

[DLM10b] M. Döhler, X.-B. Lam, and L. Mevel. Crystal clear data fusion in subspace system identification and damage detection. In *Proc. 5th International Conference on Bridge Maintenance, Safety and Management*, Philadelphia, PA, USA, 2010.

[DM10] M. Döhler and L. Mevel. Modular subspace-based system identification and damage detection on large structures. In *Proc. 34th International Symposium on Bridge and Structural Engineering*, Venice, Italy, 2010.

[DM11d] M. Döhler and L. Mevel. Robust subspace based fault detection. In *Proc. 18th IFAC World Congress*, Milan, Italy, 2011.

Chapter 7

Robust subspace-based damage localization using mass-normalized mode shapes

7.1 Introduction

Statistical subspace-based methods using output-only data have been shown to offer a robust solution to the damage detection task where changes in the modal parameters of a structure are detected [MHVdA99, BAB00]. These techniques have also been combined with sensitivities extracted from finite element models to localize damages: the detection of changes in local structural parameters (e.g. stiffness) indicates the location of a damage [BMG04, BBM$^+$08]. Like this, the damage localization problem is formulated as detection problem.

In the formulation of this detection problem, all available structural parameters are tested separately for a change using a χ^2-test statistics. Comparing their values the damage can be localized, when structural parameters are linked to a location, as high χ^2 values indicate a high change. In the derivation of these tests in [BMG04, BBM$^+$08], no special care was taken of the mutual influence of close structural parameters. The main drawback for localization is then the possible reaction when testing an undamaged element due to the lack of orthogonality in the parametric space defined by the corresponding χ^2-metric. A robust version of this test is derived in this chapter. It yields more contrasted damage localization results between safe and damaged elements and thus reduces false alarms.

For damage localization, sensitivities of the modal parameters with respect to the monitored structural parameters are needed, that were computed from an a FEM of the investigated structure in [BMG04, BBM$^+$08]. In some applications, though, the formulation of the FEM makes implementation impractical and this motivates the search for model-free damage localization alternatives. Without a FEM, sensitivities with respect to structural parameters

can still be computed at the measured coordinates of a structure using mass-normalized mode shapes, which can be obtained by adding a known perturbation to the mass distribution of the structure and repeating the output-only identification [PVGVO02, BA03, Ber04, Ber11d]. In this chapter, the corresponding model-free statistical damage localization test is derived and illustrated on simulated data.

This chapter is organized as follows. In Section 7.2, the basic principles of subspace-based system identification and statistical fault detection on vibrating structures are recalled from Chapter 2, as well as the damage localization test from [BMG04, BBM$^+$08]. In Section 7.3, the problem of the mutual influence of structural parameters in the χ^2-tests is addressed and a robust min-max test is considered. In Section 7.4, the FE model-free damage localization test is derived, using mass perturbations to obtain required sensitivities with respect to the structural parameters in the reference state. The performance of the robust damage localization, where all required parameters are obtained without a model, are demonstrated in a simulation study in Section 7.5.

7.2 Statistical subspace-based damage localization

7.2.1 Models and parameters

The behaviour of a mechanical system is assumed to be described by a stationary linear dynamical system

$$\left\{ \begin{array}{rcl} M\ddot{\mathcal{X}}(t) + C_1\dot{\mathcal{X}}(t) + K\mathcal{X}(t) &=& \upsilon(t) \\ Y(t) &=& L\mathcal{X}(t) \end{array} \right. \tag{7.1}$$

where t denotes continuous time, $M, C_1, K \in \mathbb{R}^{m\times m}$ are the mass, damping and stiffness matrices, high-dimensional vector $\mathcal{X}$ collects the displacements of the m degrees of freedom of the structure, the non-measured external force ν modeled as non-stationary Gaussian white noise, the measurements are collected in the vector Y and matrix L indicates the sensor locations. The eigenstructure of (7.1) with the modes μ and mode shapes φ_μ is a solution of

$$\det(\mu^2 M + \mu C_1 + K) = 0, \quad (\mu^2 M + \mu C_1 + K)\phi_\mu = 0, \quad \varphi_\mu = L\phi_\mu. \tag{7.2}$$

Sampling model (7.1) at some rate $1/\tau$ yields the discrete model in state-space form

$$\left\{ \begin{array}{rcl} X_{k+1} &=& AX_k + V_k \\ Y_k &=& CX_k \end{array} \right. \tag{7.3}$$

of model order $n = 2m$, whose eigenstructure is given by

$$\det(A - \lambda I) = 0, \quad (A - \lambda I)\phi_\lambda = 0, \quad \varphi_\lambda = C\phi_\lambda. \tag{7.4}$$

Then, the eigenstructure of the continuous system (7.1) is related to the eigenstructure of the discrete system (7.3) by

$$\mathrm{e}^{\tau\mu} = \lambda, \quad \varphi_\mu = \varphi_\lambda. \tag{7.5}$$

The modal frequencies f and damping coefficients ρ are recovered directly from the eigenvalues λ by

$$f = \frac{a}{2\pi\tau}, \quad \rho = \frac{100|b|}{\sqrt{a^2+b^2}}, \tag{7.6}$$

where $a = |\arctan \Re(\lambda)/\Im(\lambda)|$ and $b = \ln|\lambda|$.

The collection of modes and mode shapes $(\lambda, \varphi_\lambda)$ is a canonical parameterization of system (7.3) and considered as the system parameter θ with

$$\theta = \begin{bmatrix} \Lambda \\ \operatorname{vec} \Phi \end{bmatrix}, \tag{7.7}$$

where Λ is the vector whose elements are the eigenvalues λ and Φ is the matrix whose columns are the mode shapes φ_λ.

7.2.2 Stochastic Subspace Identification

To obtain the system parameter θ from output-only measurements $(Y_k)_{k=1,\dots,N}$, a SSI method from Section 2.2.3 is used. From the data, a subspace matrix $\widehat{\mathcal{H}}$ is computed, which is an estimate of a theoretical subspace matrix $\mathcal{H}$ according to the selected method. It possesses the factorization property

$$\mathcal{H} = \mathcal{O}\,\mathcal{Z} \tag{7.8}$$

into observability matrix

$$\mathcal{O} = \begin{bmatrix} C \\ CA \\ \vdots \\ CA^p \end{bmatrix}$$

and another matrix $\mathcal{Z}$ according to the selected method. An estimate $\widehat{\mathcal{O}}$ is obtained from $\widehat{\mathcal{H}}$ by an SVD and truncation at the desired model order of

$$\widehat{\mathcal{H}} = \begin{bmatrix} \widehat{U}_1 & \widehat{U}_0 \end{bmatrix} \begin{bmatrix} \widehat{\Delta}_1 & 0 \\ 0 & \widehat{\Delta}_0 \end{bmatrix} V^T, \quad \widehat{\mathcal{O}} = \widehat{U}_1 \widehat{\Delta}_1^{1/2}.$$

From the observability matrix $\widehat{\mathcal{O}}$ an estimate of matrix C is obtained from its first block row. An estimate of A is obtained from a least squares solution using the shift invariance property of $\widehat{\mathcal{O}}$. Estimates of the eigenstructure $(\lambda, \varphi_\lambda)$ of the system (7.3) and hence the system parameter θ are then obtained in (7.4).

7.2.3 Damage detection

In this section, the statistical subspace-based damage detection from Section 2.3 is recalled, where a residual function for damage detection is associated with the covariance-driven

output-only subspace identification described in the previous section. This function compares the system parameter θ_0 of a reference state with a subspace matrix $\widehat{\mathcal{H}}$ computed on new data corresponding to an unknown, possibly damaged state.

Assume that the eigenvectors of A are chosen as the basis for the state space of system (7.3). Then, the observability matrix writes as

$$\mathcal{O}(\theta) = \begin{bmatrix} \Phi \\ \Phi\Delta \\ \vdots \\ \Phi\Delta^p \end{bmatrix}$$

with Φ and Λ as in (7.7) and $\Delta = \operatorname{diag}(\Lambda)$. Let $S(\theta_0)$ be the left null space of $\mathcal{O}(\theta_0)$, which can be obtained by an SVD of $\mathcal{O}(\theta_0)$. Then, because of (7.8), the characteristic property of the system in the reference state writes

$$S(\theta_0)^T \widehat{\mathcal{H}} = 0.$$

For checking whether new data agree with the reference state corresponding to θ_0, the residual function

$$\zeta_N(\theta_0) = \sqrt{N}\,\operatorname{vec}(S(\theta_0)^T \widehat{\mathcal{H}}) \tag{7.9}$$

is introduced in Section 2.3. Let $\mathcal{J}(\theta_0)$ and $\Sigma(\theta_0)$ be the residual sensitivity and covariance matrices. The residual function is asymptotically Gaussian with

$$\zeta_N(\theta_0) \xrightarrow{N} \begin{cases} \mathcal{N}(0, \Sigma(\theta_0)) & \text{no change} \\ \mathcal{N}(\mathcal{J}(\theta_0)\,\delta\theta, \Sigma(\theta_0)) & \text{change } \delta\theta \end{cases} \tag{7.10}$$

Hence, a change in the system parameter θ corresponds to a change in the mean value of the residual function. It manifests itself in the χ^2-test statistics

$$\chi^2_N = \zeta_N(\theta_0)^T \widehat{\Sigma}^{-1} \widehat{\mathcal{J}} (\widehat{\mathcal{J}}^T \widehat{\Sigma}^{-1} \widehat{\mathcal{J}})^{-1} \widehat{\mathcal{J}}^T \widehat{\Sigma}^{-1} \zeta_N(\theta_0),$$

where $\widehat{\mathcal{J}}$ and $\widehat{\Sigma}$ are consistent estimates of $\mathcal{J}(\theta_0)$ and $\Sigma(\theta_0)$ (cf. Section 2.3.3). To assess the occurrence of damage, the value χ^2_N should be compared with a threshold.

7.2.4 Damage localization

In [BMG04, BBM+08], the damage localization problem is stated as a detection problem as follows: Let a set of structural parameters $p_1, \ldots, p_P$ be given, which are physically linked to locations at the investigated structure. Assume that a change δp_k occurs in one of the parameters p_k. Then, the mean of the residual function $\zeta_N(\theta_0)$ in (7.10) can be expressed as

$$\mathcal{J}(p_k)\delta p_k, \quad k = 1, \ldots, P,$$

where $\mathcal{J}(p_k)$ is the sensitivity of the residual function with respect to p_k and is usually obtained as

$$\mathcal{J}(p_k) = \mathcal{J}(\theta_0)\frac{\partial \theta_0}{\partial p_k}. \tag{7.11}$$

Then, testing the parameters p_k separately for a change consists in computing the residual $\zeta_N(\theta_0)$ once in (7.9) and computing the χ^2-test statistics

$$\chi^2_N(p_k) = \zeta_N(\theta_0)^T \widehat{\Sigma}^{-1} \widehat{\mathcal{J}}_k (\widehat{\mathcal{J}}_k^T \widehat{\Sigma}^{-1} \widehat{\mathcal{J}}_k)^{-1} \widehat{\mathcal{J}}_k^T \widehat{\Sigma}^{-1} \zeta_N(\theta_0) \tag{7.12}$$

for each $k = 1, \ldots, P$, where $\widehat{\mathcal{J}}_k$ is a consistent estimate of $\mathcal{J}(p_k)$. Then, the values $\chi^2_N(p_k)$, $k = 1, \ldots, P$, indicate the changes in the structural parameters p_k. As the parameters are related to locations at the structure, high values of $\chi^2_N(p_k)$ indicate the location of the damage. The χ^2-test statistics (7.12) is also called sensitivity test.

However, the sensitivity test assumes that a change happens in the tested structural parameter and that every other parameter remains unchanged. This condition is violated in two occasions, firstly when damage happen simultaneously at two or more locations, and more important, when testing for a change in an unchanged structural element. In that case, the test will still react by statistical influence of the damage element. This effect will be considered in the next section.

7.3 Mutual influence of structural parameters in change detection test

7.3.1 Focused change detection in structural parameters

In the previous section, the sensitivity test (7.12) is computed to test a change in each parameter $p_k, k = 1, \ldots, P$. Formally, $\delta p_k = 0$ is tested against $\delta p_k \neq 0$, by assuming no change in the other parameters. This also means that $\chi^2_N(p_k)$ might be sensitive to a change in some other parameters p_i with $i \neq k$ [Bas97, BBMN09]. In the following, the min-max approach [Bas97] is described that consists in viewing the parameters p_i, $i \neq k$, as nuisance. They are rejected by replacing them in the likelihood with their least favorable value. Then, for each parameter p_k, the min-max approach detects a change in its corresponding direction of the parameter space, orthogonal to every direction corresponding to the set of the remaining parameters. Thus, changes in the remaining parameters do not affect the min-max test of the actually tested parameter. It also means that testing an undamaged element will not yield a false alarm provoked by some other close damaged element. Note that for simplicity of the notation, the symbol $\widehat{\ }$ indicating a consistent estimate of the underlying variable, is omitted on the Jacobians $\mathcal{J}$ and the covariance matrix Σ.

Fix some k and define the Jacobians

$$\begin{aligned} \mathcal{J}_a &\stackrel{\text{def}}{=} \mathcal{J}(p_k), \\ \mathcal{J}_b &\stackrel{\text{def}}{=} \begin{bmatrix} \mathcal{J}(p_1) & \cdots & \mathcal{J}(p_{k-1}) & \mathcal{J}(p_{k+1}) & \cdots & \mathcal{J}(p_P) \end{bmatrix}. \end{aligned} \tag{7.13}$$

The asymptotic Fisher information on the set of parameters $\{p_1, \ldots, p_P\}$ contained in $\zeta_N(\theta_0)$ is defined as

$$F \stackrel{\text{def}}{=} \begin{bmatrix} \mathcal{J}_a & \mathcal{J}_b \end{bmatrix}^T \Sigma^{-1} \begin{bmatrix} \mathcal{J}_a & \mathcal{J}_b \end{bmatrix} = \begin{bmatrix} F_{aa} & F_{ab} \\ F_{ba} & F_{bb} \end{bmatrix}, \tag{7.14}$$

where

$$F_{aa} = \mathcal{J}_a^T \Sigma^{-1} \mathcal{J}_a, \qquad F_{ab} = \mathcal{J}_a^T \Sigma^{-1} \mathcal{J}_b,$$
$$F_{ba} = \mathcal{J}_b^T \Sigma^{-1} \mathcal{J}_a, \qquad F_{bb} = \mathcal{J}_b^T \Sigma^{-1} \mathcal{J}_b.$$

Furthermore, define the matrices

$$F_a^* \stackrel{\text{def}}{=} F_{aa} - F_{ab} F_{bb}^{-1} F_{ba},$$

the partial residuals

$$\tilde{\zeta}_a \stackrel{\text{def}}{=} \mathcal{J}_a^T \Sigma^{-1} \zeta_N(\theta_0), \quad \tilde{\zeta}_b \stackrel{\text{def}}{=} \mathcal{J}_b^T \Sigma^{-1} \zeta_N(\theta_0) \tag{7.15}$$

and the robust residual

$$\zeta_a^* \stackrel{\text{def}}{=} \tilde{\zeta}_a - F_{ab} F_{bb}^{-1} \tilde{\zeta}_b. \tag{7.16}$$

Then, the corresponding χ^2-test statistics detecting a change in parameter p_k writes as

$$\chi_N^{*2} = \zeta_a^{*T} F_a^{*-1} \zeta_a^* \tag{7.17}$$

and is not affected by a change in the parameters p_i, $i \neq k$. Test (7.17) is called the min-max test. Hence, repeating the steps (7.13)–(7.17) for all $k = 1, \ldots, P$ leads to values of the χ^2-test statistics (7.17) for each monitored structural parameter. A change in a parameter is linked with a high value of its corresponding χ^2-test statistics and thus can be located.

Some comments are in order. First, it is obvious that the min-max test does not depend on the *magnitude* of the Jacobians, but only on the change directions defined by them. This is proven in the following lemma.

Lemma 7.1 *The min-max test* (7.17) *is invariant to post-multiplication of the Jacobians $\mathcal{J}_a$ and $\mathcal{J}_b$ with some invertible matrices.*

Proof: Use the notation from Equations (7.14)–(7.17) for the min-max test with the Jacobians $\mathcal{J}_a$ and $\mathcal{J}_b$. Now consider $\mathcal{J}_a A$ and $\mathcal{J}_b B$ instead of $\mathcal{J}_a$ and $\mathcal{J}_b$ for the min-max test, where A and B are some invertible matrices, and use the notation with a tilde $\widetilde{\ }$ for the respective variables in the min-max test. Then,

$$\widetilde{F} = \begin{bmatrix} \widetilde{F}_{aa} & \widetilde{F}_{ab} \\ \widetilde{F}_{ba} & \widetilde{F}_{bb} \end{bmatrix} = \begin{bmatrix} A^T \mathcal{J}_a^T \Sigma^{-1} \mathcal{J}_a A & A^T \mathcal{J}_a^T \Sigma^{-1} \mathcal{J}_b B \\ B^T \mathcal{J}_b^T \Sigma^{-1} \mathcal{J}_a A & B^T \mathcal{J}_b^T \Sigma^{-1} \mathcal{J}_b B \end{bmatrix} = \begin{bmatrix} A^T F_{aa} A & A^T F_{ab} B \\ B^T F_{ba} A & B^T F_{bb} B \end{bmatrix}$$

and, furthermore,

$$\widetilde{F}_a^* = \widetilde{F}_{aa} - \widetilde{F}_{ab} \widetilde{F}_{bb}^{-1} \widetilde{F}_{ba} = A^T F_a^* A.$$

Then, from (7.15) and (7.16) follows

$$\widetilde{\zeta}_a^* = A^T \zeta_a^*$$

and thus

$$\widetilde{\chi}_N^{*2} = \widetilde{\zeta}_a^{*T} \widetilde{F}_a^{*-1} \widetilde{\zeta}_a^* = \left(A^T \zeta_a^*\right)^T \left(A^T F_a^* A\right)^{-1} \left(A^T \zeta_a^*\right) = \zeta_a^{*T} F_a^{*-1} \zeta_a^* = \chi_N^{*2},$$

proving the assertion. □

There are many numerically sensitive operations involved in computing the min-max test in Equations (7.14)–(7.17). In [ZB03] the following practical and numerically stable computation was derived.

Lemma 7.2 ([ZB03]) *Let $\Sigma^{-1/2}$ be a square root inverse of Σ, such that*

$$\Sigma^{-1} = (\Sigma^{-1/2})^T \Sigma^{-1/2}.$$

If $\Sigma^{-1/2}\mathcal{J}_a$ and $\Sigma^{-1/2}\mathcal{J}_b$ are full column rank, then the min-max test (7.17) *writes as*

$$\chi^{*2}_N = \xi^T \xi \quad \textit{where} \quad \xi = Q_c^T \Sigma^{-1/2} \zeta_N(\theta_0),$$

where Q_c is obtained from the thin QR decompositions

$$\begin{aligned} \Sigma^{-1/2}\mathcal{J}_a &= Q_a R_a, \\ \Sigma^{-1/2}\mathcal{J}_b &= Q_b R_b, \\ Q_a - Q_b Q_b^T Q_a &= Q_c R_c. \end{aligned}$$

Note that for the computation of $\Sigma^{-1/2}$ in the previous lemma from an estimate of Σ, the same techniques as in Section 3.5.1 can be used.

7.3.2 Change directions and separability of structural parameters

With the described χ^2-tests, structural parameters are tested for a change. This corresponds to testing directions in the structural parameter space for a change that are defined by the sensitivities of the structural parameters. These parameters might show some dependence, i.e. a change in one parameter might raise the χ^2-test value of another parameter and vice versa. For checking the *separability* of these parameters, the angles between their respective change directions can be analyzed.

To be coherent with the χ^2-metric, define the k-th change direction as [BMG04]

$$d_k \stackrel{\text{def}}{=} \Sigma(\theta_0)^{-1/2} \mathcal{J}(p_k), \quad k = 1, \ldots, P, \tag{7.18}$$

where $\Sigma(\theta_0)^{-1/2}$ is a matrix square root of the inverse of $\Sigma(\theta_0)$. The sensitivity test (7.12), testing separately for changes in the parameters p_k, $k = 1, \ldots, P$, is hence a directional test, where the residual function $\zeta_N(\theta_0)$ is tested for a change in the directions d_k in the structural parameter space. Let the cosine of the angle between two change directions be given as

$$\alpha_{ij} \stackrel{\text{def}}{=} \frac{d_i^T d_j}{\|d_i\| \, \|d_j\|}, \quad \text{where} \quad \|d\| = \sqrt{d^T d}. \tag{7.19}$$

Thus, if $\alpha_{ij} \approx 0$ the change directions d_i and d_j are nearly orthogonal and clearly separable. However, if $|\alpha_{ij}| \approx 1$, the change directions d_i and d_j are nearly parallel and not separable anymore. In the latter case, changes in the parameters p_i and p_j are not distinguishable. Then, a change in parameter p_i leads to similar values of the corresponding sensitivity test for parameters p_i and p_j for $|\alpha_{ij}| \approx 1$.

7.3.3 Clustering and rejection

Often, the number of structural parameters P is very high and especially higher than the number of modal parameters $\dim \theta_0 = 2m(r+1)$. Then, many of the respective change directions d_k, $k = 1, \ldots, P$, cf. (7.18), are nearly parallel with respect to the χ^2-metric. Testing them separately in the sensitivity test then yields nearly the same results. For this problem, a clustering step was suggested in [BMG04, BBM$^+$08] prior to testing all the parameters, where each cluster contains nearly parallel change directions. Then, in the test only a barycenter of each cluster is tested and the resulting χ^2-value is assigned to all elements of the cluster. As the elements in one cluster are not (or very poorly) separable, all the elements of a cluster are either recognized as healthy or as damaged. Changing the sensor positions could lead to a separation of the cluster elements.

This clustering is even more important for the min-max test than the sensitivity test regarding the rejected parameters. It is not meaningful to test a parameter for a change in the min-max test while rejecting another parameter whose change direction is nearly parallel to the tested parameter. This might lead to a low (false negative) result of the test, even if a change in the parameter happened.

A clustering algorithm usually works in two steps. In the first step, small change directions d_k are removed, as vectors with a low magnitude are likely to blur the results of the aggregation. Then, the remaining vectors d_k are normed to 1, as only their direction is of interest, and clustered. In [BMG04, BBM$^+$08], a vector quantization method [LBG80, Gra84] is suggested for clustering, which performs a hierarchical classification while controlling the variability in each cluster. However, any appropriate clustering algorithm can be used.

Let N_c the number of clusters and c_k, $k = 1, ..., N_c$, be their barycenters. The barycenters are arbitrarily scaled, but because of Lemma 7.1 they can be directly used for the min-max test. With the definition of the change directions in (7.18) and with Lemma 7.2, the min-max test for each cluster k is performed as follows:

1. Define $C_a = c_k$, $C_b = \begin{bmatrix} c_1 & \ldots & c_{k-1} & c_{k+1} & \ldots & c_{N_c} \end{bmatrix}$;

2. Do thin QR decompositions

$$\begin{aligned} C_a &= Q_a R_a, \\ C_b &= Q_b R_b, \\ Q_a - Q_b Q_b^T Q_a &= Q_c R_c; \end{aligned}$$

3. Compute $\xi = Q_c^T \Sigma^{-1/2} \zeta_N(\theta_0)$ and finally $\chi^{*2}_N(c_k) = \xi^T \xi$. Assign value $\chi^{*2}_N(c_k)$ to all elements in cluster k.

In Section 9.3, the damage localization using the min-max approach with clustering is performed on a simulated bridge deck with almost 10 000 elements.

7.4 Damage localization using mass-normalized mode shapes from mass perturbations

For the statistical damage localization approach in [BMG04, BBM+08], the monitored structural parameters p_k are stiffness parameters of a FEM. The sensitivities $\partial\theta_0/\partial p_k$ in (7.11) of the modal parameters with respect to the structural parameters are obtained from the settings of a FEM. They are needed for the sensitivity test (7.12) or the min-max test (7.17).

In this section, this approach is modified to work without a FEM. The considered structural parameters p_k are masses and stiffnesses with respect to the measured coordinates of the structure. The required sensitivities for these structural parameters can be computed using mass-normalized mode shapes, which can be obtained from Operational Modal Analysis by two measurements of a structure, where a known mass perturbation is introduced on the structure between the measurements.

7.4.1 Mass-normalization of mode shapes using mass perturbations

Output-only system identification cannot provide mode shapes that are mass-normalized, such that the collection of eigenvectors ϕ from (7.2) yields

$$\Omega^T M \Omega = I, \tag{7.20}$$

where the columns of Ω are the eigenvectors ϕ. In order to solve this problem, Parloo et al. [PVGVO02] proposed a method using system identification results from two measurements of the structure where a known mass perturbation ΔM is introduced at (some or all of) the measured coordinates between the two measurements. Since, further mass-normalization methods using mass perturbations have been developed, see e.g. [BA03, Ber04, Ber11d], and a review in [Ber11a]. It turns out that the mode shapes φ, which are obtained only at the measured degrees of freedom, can be normalized without knowing the unobserved part. In the following, we use the receptance based approach from [Ber11d] using the normal mode model, where the modal parameters are obtained from

$$\det(K - \omega^2 M) = 0, \quad K\phi = \omega^2 M\phi, \quad \varphi = L\phi,$$

cf. (7.2). For the natural frequencies f holds $\omega = 2\pi f$.

Denote a mode and corresponding mode shape of the structure in the original state by ω_i and φ_i and after the mass perturbation ΔM on the structure by ω_i^* and φ_i^*, for $i = 1, \cdots, m$. The modal scaling factors β_i are defined such that

$$\psi_i = \beta_i \varphi_i \tag{7.21}$$

are the mass-normalized mode shapes fulfilling (7.20). With the receptance based approach from [Ber11d], the squares of the modal scaling factors $\gamma_i \overset{\text{def}}{=} \beta_i^2$ are obtained from the linear set of equations described by

$$\sum_{l=1}^{m} \frac{\varphi_l (\varphi_l^T \Delta M \varphi_j^*) \omega_j^{2*}}{\omega_l^2 - \omega_j^{2*}} \gamma_l = \varphi_j^*, \quad j = 1, \ldots, m, \tag{7.22}$$

by a least squares solution. Then, with the mass-normalized mode shapes (7.21), sensitivities with respect to some structural parameters can be computed.

Remark 7.3 *In this section, the normal mode model was used without considering damping, while in* (7.2) *the complex mode model was used. While the latter model is probably more appropriate for vibrating structures under operation conditions, the imaginary parts of the mode shapes and the estimated damping values are possibly not very reliable for the sensitivity computation in the following. These figures were already skipped in the sensitivity computations using FEM data in [BBM+08]. This is also the reason why the complex mode mass normalization as e.g. in [Ber11c] is not used here.*

7.4.2 Sensitivities of modal parameters with respect to structural parameters

Using the mass-normalized mode shapes $\psi_i, i = 1, \dots, m$, the sensitivities of the modal parameters with respect to a mass m_s at the measured coordinate s or with respect to a stiffness k_{st}, which is assumed between the measured coordinates s and t, can be computed as described in [HLS98]. Let ψ_{ji} be the j-th entry of mode shape ψ_i. Then, the desired sensitivities are

$$\begin{aligned} \frac{\partial \omega_i}{m_s} &= -\frac{1}{2}\omega_i \psi_{si}^2 \\ \frac{\partial \psi_{ji}}{m_s} &= -\frac{1}{2}\psi_{si}^2 \psi_{ji} + \psi_{si} \sum_{l=1, l\neq i}^{m} \frac{\omega_i^2}{\omega_l^2 - \omega_i^2} \psi_{sl} \psi_{jl} \end{aligned} \tag{7.23}$$

for the sensitivities with respect to mass and

$$\begin{aligned} \frac{\partial \omega_i}{k_{st}} &= -\frac{1}{2\omega_i}(\psi_{si} - \psi_{ti})^2 \\ \frac{\partial \psi_{ji}}{k_{st}} &= (\psi_{si} - \psi_{ti}) \sum_{l=1, l\neq i}^{m} \frac{1}{\omega_l^2 - \omega_i^2} (\psi_{sl} - \psi_{tl}) \psi_{jl} \end{aligned} \tag{7.24}$$

for the sensitivities with respect to stiffness.

7.4.3 Sensitivities for χ^2-tests

For localization of changes in the mass at the measured coordinates of the structure and localization of changes in the stiffness of assumed structural elements between pairs of measured coordinates of the structure, the considered structural parameters are $p_k = m_s$ or $p_k = k_{st}$. In (7.23) and (7.24) sensitivities of modal parameters with respect to these structural parameters are given. It remains the computation of $\mathcal{J}(p_k) = \mathcal{J}(\theta_0)\partial\theta_0/\partial p_k$ in (7.11) for the sensitivity test (7.12) or min-max test (7.17).

In Section 2.3.3 the residual sensitivity $\mathcal{J}(\theta_0)$ with respect to the modal parameter is derived. The modal parameter θ_0 contains the modes λ of the discrete system (7.4). However, in the previous section sensitivities of the pulsations ω of the continuous system (7.1) are given w.r.t. structural parameters. To compute the sensitivity $\mathcal{J}(p_k)$ of the residual $\zeta_N(\theta_0)$ with

respect to the structural parameters, the sensitivity $\mathcal{J}_{\lambda\omega}$ of the eigenvalues λ with respect to the pulsations $\omega = 2\pi f$ is needed, which results directly from relation (7.6) and is detailed in [BMG04]. Then, the desired sensitivities of the residual w.r.t. structural parameters write as

$$\mathcal{J}(p_k) = \mathcal{J}(\theta_0)\mathcal{J}_{\lambda\omega}\mathcal{J}_{p_k}, \tag{7.25}$$

where $\mathcal{J}_{p_k}$ is the collection of sensitivities of (7.23) or (7.24) in a column vector, depending on the kind of structural parameter. Note that in this derivation the system parameter θ_0 (on which $\mathcal{J}(\theta_0)$ is computed) must contain the mass-normalized mode shapes to be coherent.

7.4.4 Summary of model-free damage localization algorithm

Damage localization usually corresponds to finding the element(s) of a structure with the highest change of stiffness compared to a reference state. With the derivations in the previous sections we can detect changes in mass ($p_k = m_s$) or in stiffness ($p_k = k_{st}$) with a statistical test. The resulting algorithm for model free damage localization consists of the following steps:

1. Output-only measurement of the structure in the reference state, retrieval of modal parameter $\theta_{0,1}$ from Stochastic Subspace Identification (SSI) (Section 7.2.2),
2. Add a mass perturbation ΔM near one or more sensor positions, do output-only measurements and retrieve modal parameter $\theta_{0,2}$ from SSI,
3. Compute mass-normalized mode shapes using $\theta_{0,1}$ and $\theta_{0,2}$ (Equations (7.21), (7.22)) and replace arbitrarily scaled mode shapes from $\theta_{0,1}$ by mass-normalized mode shapes to obtain system parameter θ_0,
4. Computation of $\widehat{\mathcal{J}}(p_k)$, $k = 1, \ldots, P$, (Equations (7.23)–(7.25)) and $\widehat{\Sigma}(\theta_0)$ in the reference state,
5. Computation of $\chi^{*2}_N(p_k), k = 1, \ldots, P$, in possibly damaged states (Equations (7.13)–(7.17)) and comparison of their values. A high value $\chi^{*2}_N(p_k)$ is linked to a high change in p_k.

7.5 Numerical results

To validate the proposed min-max test for a focused change detection in the structural parameters and the statistical-based model-free damage localization algorithm, a simulation study was made using a mass-spring model of six degrees of freedom (Figure 7.1). Using this model, output-only data was generated at all 6 DOFs to obtain the necessary measurements in the reference states for the mass-normalization of the mode shapes and in the damaged states with different introduced damage scenarios.

In the reference state, the modal parameter $\theta_{0,1}$ was obtained from SSI. After an increase of the mass at DOF 2 of 5%, the modal parameter $\theta_{0,2}$ was obtained from SSI. Both were used to compute the mass-normalized mode shapes, which are also inserted in the reference

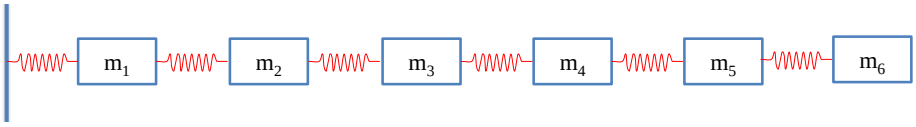

Figure 7.1 – Simulated mass-spring chain.

modal parameter θ_0. Using the mass-normalized mode shapes, the sensitivities of the modal parameters with respect to the masses at each of the 6 DOFs and with respect to the stiffnesses between every pair of DOFs were computed.

7.5.1 Detection of changes in stiffness or mass

After obtaining all the test parameters from the reference state, the following scenarios were simulated:

- Decrease of stiffness of element between DOF 1 and 2 of 5% (Figure 7.2);
- Decrease of stiffness of element between DOF 1 and 2 of 10% (Figure 7.3);
- Increase of mass at DOF 2 of 5% (Figure 7.4);
- Increase of mass at DOF 3 of 10% (Figure 7.5).

For each of these scenarios the χ^2-tests (7.12) and (7.17) were performed for the stiffnesses as structural parameters for the first two scenarios and for the masses as structural parameters for the last two scenarios. In Figures 7.2–7.5 the corresponding χ^2-values are shown.

Note that when testing the stiffness change of the *structural elements* in Figures 7.2–7.3, these elements are only defined from the information contained in the mode shape ("model-free"). Between all pairs of measured DOFs, a structural element is assumed whose stiffness

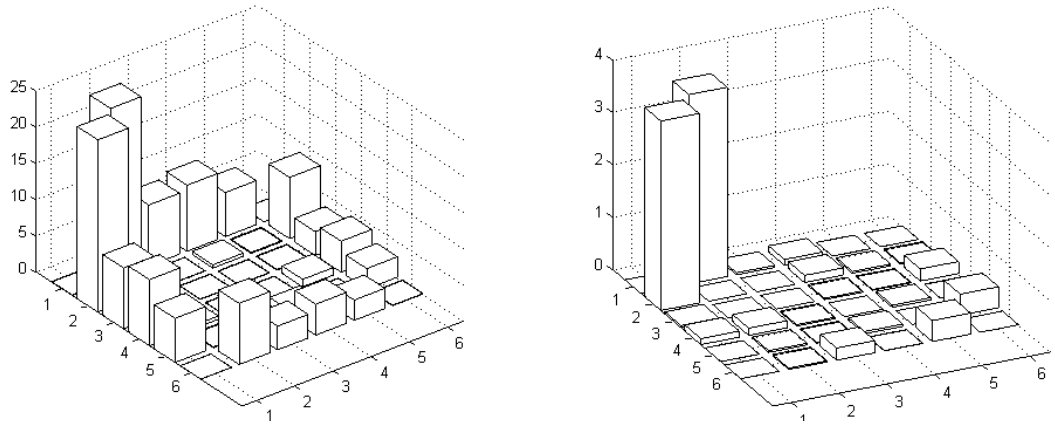

(a) Sensitivity test (7.12) (b) Min-max test (7.17)

Figure 7.2 – Stiffness decrease of 5% between DOFs 1 and 2.

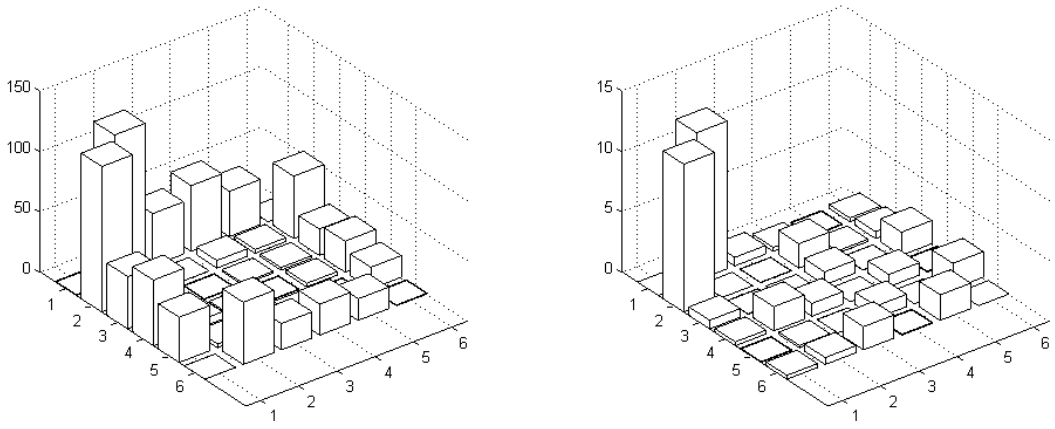

(a) Sensitivity test (7.12) (b) Min-max test (7.17)

Figure 7.3 – Stiffness decrease of 10% between DOFs 1 and 2.

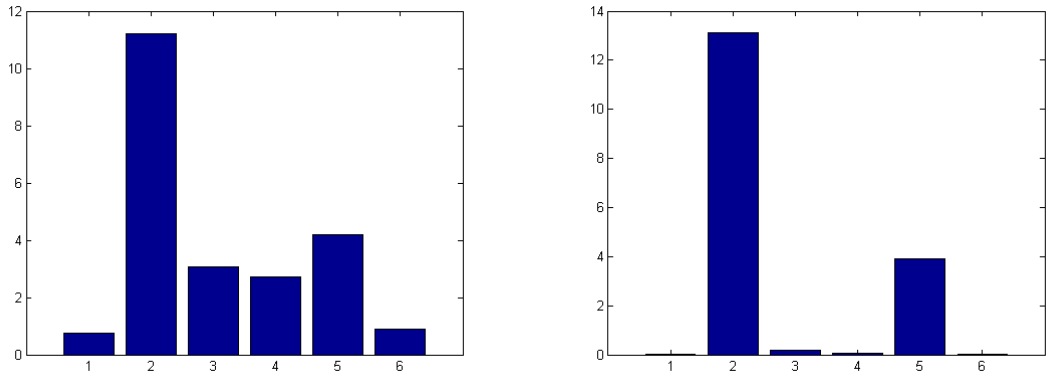

(a) Sensitivity test (7.12) (b) Min-max test (7.17)

Figure 7.4 – Mass of 5% added at DOF 2.

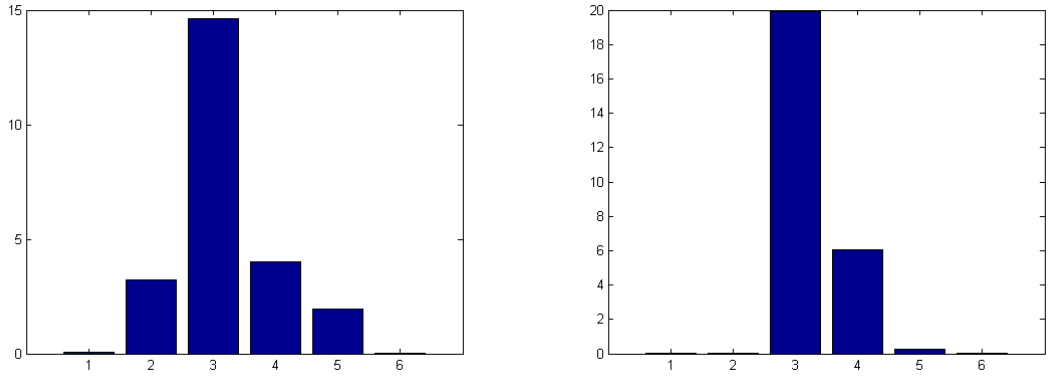

(a) Sensitivity test (7.12) (b) Min-max test (7.17)

Figure 7.5 – Mass of 5% added at DOF 3.

change is tested. Hence, also elements are tested that do not exist in the underlying simulated model (e.g. elements (1,3), (1,4), ...), as no information of this model is used. For testing the mass change in Figures 7.4–7.5, the mass at each measured DOF is tested.

In each case, the location of the change of the structural parameter could be clearly identified. The min-max test (7.17) using the rejection approach gives higher contrasted test results and thus outperforms the sensitivity test (7.12).

7.5.2 Detection of changes in stiffness while rejecting changes in mass

In another simulated scenario, both the mass and stiffness of the model were changed with a 5% increase of mass at DOF 2 and 5% stiffness reduction between DOFs 1 and 2. For

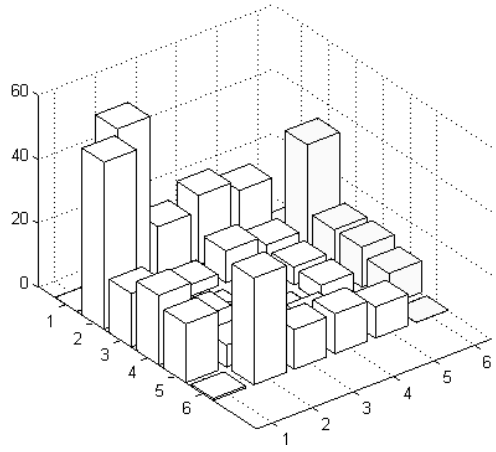

(a) Sensitivity test (7.12)

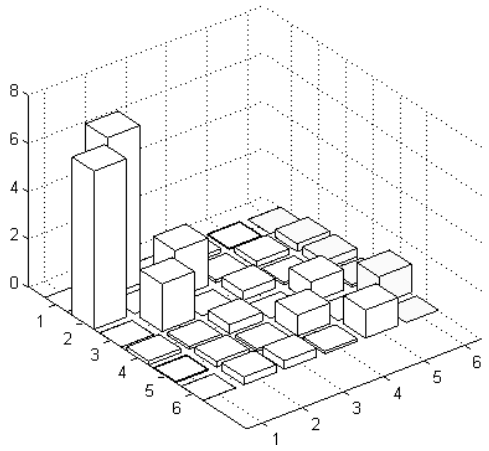

(b) Min-max test (7.17) rejecting other stiffness parameters

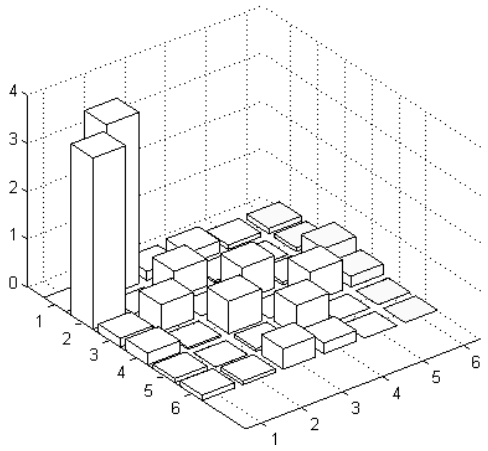

(c) Min-max test (7.17) rejecting other stiffness and mass parameters

Figure 7.6 – Mass of 5% added at DOF 2 and stiffness decrease of 5% between DOFs 1 and 2.

example, such a situation can happen in practice when monitoring a bridge for damage, where the traffic is regarded as a nuisance. Not the added weight to the bridge should be detected, but the damage in the bridge, i.e. the stiffness change of the bridge's structural elements. Similarly, the changes due to the mass of water in an aqueduct or at a dam should be rejected, while monitoring the structural integrity. Of course, the presented example on the 6 DOF mass-spring chain only reflects this idea, but not an entire structure.

In Figure 7.6(a), the sensitivity test is shown, where many elements besides the damaged element (1,2) clearly react. In a first step, the non-tested stiffness parameters were rejected with the min-max test in Figure 7.6(b), similar to the previous section. In the last step, also the mass parameters were rejected in Figure 7.6(c), leading to the highest contrasted result of the test and underlining the importance of the rejection approach. Note also, that only in Figure 7.6(c), the χ^2-value of the damaged element of around $\chi^2 \approx 3$ corresponds to Figure 7.2(b), where the stiffness of element (1,2) was also decreased by 5%. Thus, the rejection approach seems to be indispensable for a quantification of the damages.

7.5.3 Orthogonality of change directions

Although only one parameter was changed in each of the experiments in Figures 7.2–7.5, the χ^2-test statistics also reacted for some of the structural quantities that were not changed. For the sensitivity tests (7.12) in the figures, the reason for this reaction is obvious: Computing this test on unaffected structural parameters (mass or stiffness) is performed while still being sensitive to changes in other parameters (amongst them one modified parameter) and thus might lead to a false alarm.

Now consider the min-max test (7.17) in Figures 7.2(b)–7.5(b). The χ^2 value corresponding to an unmodified structural parameter reacts less. Still, for some elements the min-max test reacts, e.g. for testing a change in the stiffness of the elements (1,3), (2,4), (3,6), (4,5) or (5,6), even if only the stiffness of element (1,2) was reduced (see Figures 7.2(b) and 7.3(b)). Similarly, when testing for a mass change at DOF 5, the test reacts, when the mass at DOF 2 was increased in Figure 7.4(b). Also, the test at DOF 4 reacts, when the mass at DOF 3 was increased in Figure 7.5(b). This can be explained by looking at the angles between the underlying change directions that are tested: In all these cases, the cosine of the angle between

Table 7.1 – Cosine of angles between change direction corresponding to change of stiffness of element (1,2) and the elements (a,b)

a \ b	1	2	3	4	5	6
1	–	1.00	**0.83**	0.16	0.87	0.30
2	1.00	–	0.22	**0.82**	0.27	0.28
3	**0.83**	0.22	–	0.18	0.11	**0.86**
4	0.16	**0.82**	0.18	–	**0.87**	0.80
5	0.87	0.27	0.11	**0.87**	–	**0.86**
6	0.30	0.28	**0.86**	0.80	**0.86**	–

Table 7.2 – Cosine of angles between change direction corresponding to change of mass of DOF a and DOF b

a \ b	1	2	3	4	5	6
1	1.00	0.34	0.22	0.30	0.36	0.87
2	0.34	1.00	0.77	0.79	**0.91**	0.30
3	0.22	0.77	1.00	**0.90**	0.74	0.14
4	0.30	0.79	**0.90**	1.00	0.79	0.22
5	0.36	**0.91**	0.74	0.79	1.00	0.32
6	0.87	0.30	0.14	0.22	0.32	1.00

the corresponding change directions computed from (7.19) was quite high (see Tables 7.1 and 7.2), thus indicating a poor separability of the underlying structural parameters. Nevertheless, the test of the changed parameter still reacts stronger than the test of (unchanged) parameter having a nearly parallel change direction.

7.6 Conclusions

In this chapter, a model-free subspace-based statistical damage localization test was derived for output-only data using known mass perturbations of the structure in the reference state. Its performance to detect changes in the stiffness or mass between the measured coordinates of a structure was demonstrated using simulated data. When testing the structural parameters for a change, special care was taken of the rejection of the influence of the other structural parameters that are not actually tested. The effectiveness of this rejection was demonstrated as well and it seems to be important for future damage quantification. An application of the damage localization to a simulated bridge deck using the clustering and rejection approach is demonstrated in Section 9.3. Future work contains the validation of the proposed algorithms on a real structure.

7.7 Dissemination

Parts of this chapter have been published in:

[DBMS11] M. Döhler, D. Bernal, L. Mevel, and D. Siegert. Statistical-based model-free damage localization. In *Proc. 4th International Operational Modal Analysis Conference*, Istanbul, Turkey, 2011.

[DMB11] M. Döhler, L. Mevel, and D. Bernal. Statistical subspace-based model-free damage localization. In *Proc. Engineering Mechanics Institute Conference*, Boston, USA, 2011.

Part IV

Applications

Chapter 8

Modal analysis with multi-setup system identification

8.1 Introduction

In this chapter, the merging algorithms for multi-setup system identification from Chapter 4 are applied to the eigenstructure identification of a composite plate and four civil structures using output-only vibration data. The data of all structures was recorded under operational conditions, except for the composite plate, which was recorded in the lab. The analyses of the structures were made in the framework of numerous collaborations, which are gratefully acknowledged.

The underlying mechanical model for vibration analysis and the transformation to a state-space model was presented in Section 2.4. Using the merging methods from Chapter 4 for multi-setup subspace system identification, the system matrices are identified at multiple model orders, where the fast multi-order algorithms from Chapter 5 are used. From their eigenstructure, the *natural frequencies* $\widehat{f}$, *damping ratios* $\widehat{\rho}$ and *mode shapes* $\widehat{\varphi}$ of the investigated structure are determined. With the help of a stabilization diagram (see Section 2.4.3), where the natural frequencies are plotted against model order, the true system modes are distinguished from spurious modes and the final model is obtained. This final model is chosen manually from the stabilization diagram. One example of multi-setup and multi-order system identification is Z24 Bridge, which were detailed in Sections 4.7 and 5.5.

For the application of the merging algorithms, one of the Algorithms 4.1–4.5 is used either with covariance-driven SSI or the data-driven UPC algorithm. As the merging algorithms mainly differ in their implementation and no SSI algorithm with left weighting is used, any one of them can be used, yielding practically identical identification results. In the implementation of the merging algorithm the results of Section 4.5 are used, as the true model order is unknown.

Often, a comparison for multi-setup system identification with further, empirical merging methods is made by the collaborating partners. Their notation and schematic is introduced in Section 8.2, before the modal analysis of the mentioned structures is made in Section 8.3. In Section 8.4, the results of the multi-setup identification are discussed and the relevance of the new merging algorithms from Chapter 4 is pointed out.

8.2 Notation and comparison to other methods

For eigenstructure identification from multiple sensor setups, mainly three strategies are in use [Par03, Sec. 3.3], [RMDRC09] that consist of the general steps

- normalization (scaling) due to different ambient excitation or identification results,
- merging of the data or identification results,
- eigenstructure identification.

According to the order of these steps, they are called *Pre Global Estimation Re-Scaling (PreGER)*, *Post Separate Estimation Re-Scaling (PoSER)* and *Post Global Estimation Re-Scaling (PoGER)* in [Par03, RMDRC09]. For the application with SSI algorithms we will use these notations.

The *Pre Global Estimation Re-Scaling (PreGER)* consists in the steps normalization – merging – identification. It comprises the algorithms from Chapter 4 and its schematics are illustrated in Figure 8.1.

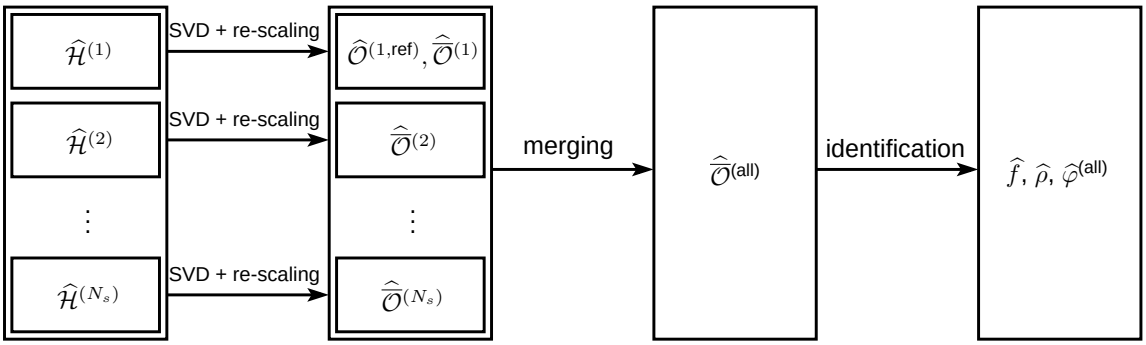

Figure 8.1 – Scheme of PreGER approach (Algorithm 4.4).

The *Post Separate Estimation Re-Scaling (PoSER)* [MK00, VdALMH00, CGDV02, Par03, RMDRC09, Au11] consists in the steps identification – normalization – merging. It is the common practice approach for multi-setup system identification in Operational Modal Analysis. The data of each setup is processed separately, yielding a set of model parameters $(\widehat{f}_j, \widehat{\rho}_j, \widehat{\varphi}^{(j)})$ for each setup j. Then, the identified modes are matched between all setups and final estimates of frequencies and damping ratios are obtained by averaging. Before merging

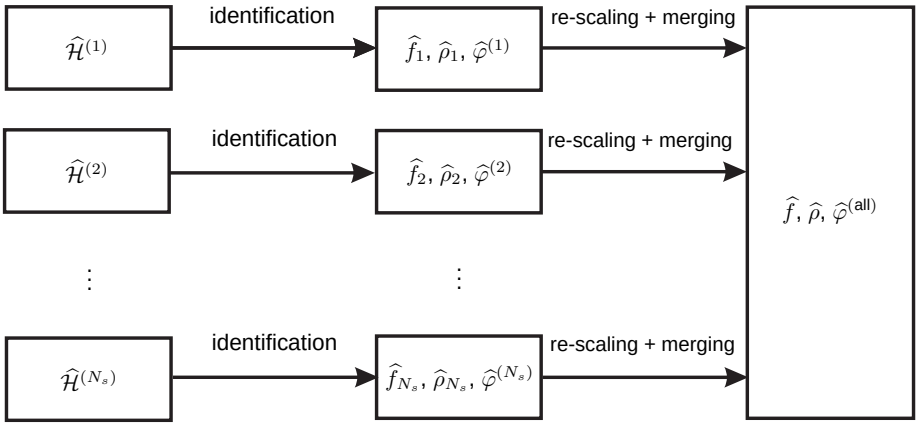

Figure 8.2 – Scheme of PoSER approach.

the partial mode shapes from each setup, they are re-scaled in a least-squares sense, for instance to the reference sensor part of the first setup. The whole procedure is summarized in Figure 8.2. For a large number of setups, this approach is time consuming as many stabilization diagrams have to be analyzed. Moreover, not all modes may be well excited in all setups, and often mode pairing between different setups is difficult due to closely spaced modes.

The *Post Global Estimation Re-Scaling (PoGER)* [Par03, PGC03, RMDRC09] consists in the steps merging – identification – normalization. For SSI algorithms, this empirical merging approach consists in the computation of the subspace matrix for each setup separately and merging them directly to a global subspace matrix. Then, system identification is performed, yielding one set of global modal parameters. Due to a possibly different excitation in each setup, the mode shape estimates are finally rescaled in a least squares sense with respect to their reference sensor part. The procedure is summarized in Figure 8.3.

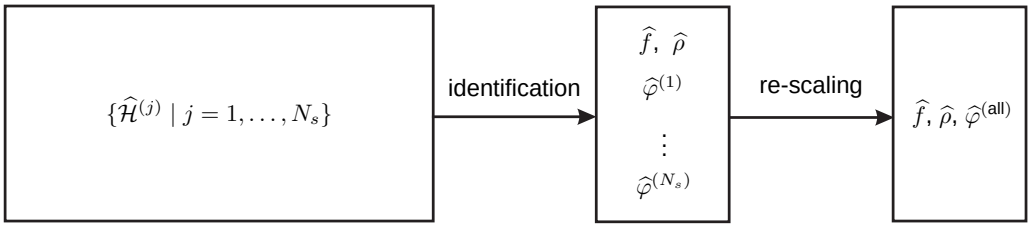

Figure 8.3 – Scheme of PoGER approach.

For a comparison of mode shapes obtained from different methods and for evaluating the orthogonality between a set of mode shapes, the *Modal Assurance Criterion (MAC)* is used, which is the angle between two mode shapes and defined as

$$\mathrm{MAC}(\varphi_1, \varphi_2) \overset{\mathrm{def}}{=} \frac{|\varphi_1^* \varphi_2|}{\sqrt{\varphi_1^* \varphi_1}\sqrt{\varphi_2^* \varphi_2}}.$$

A MAC value near to 1 indicates thus a strong similarity between two mode shapes, and a value near to 0 rather orthogonal mode shapes.

8.3 Case studies

8.3.1 A composite plate

Within a collaboration with LMS (Belgium), the Risø laboratory (Denmark) and the Polish Academy of Sciences, glass reinforced composite panels of dimension $20 \times 320 \times 320\,\text{mm}$ were investigated. They are similar to the load carrying laminate in a wind turbine blade [LS10] and are illustrated in Figure 8.4. They were also used for excitation robust damage detection in Section 6.6.1.

Vibration measurements of the composite panels were made in the lab at a sampling rate

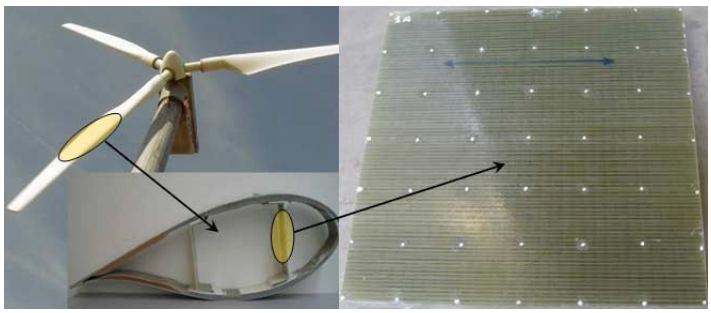

Figure 8.4 – Glass reinforced composite panel [LS10].

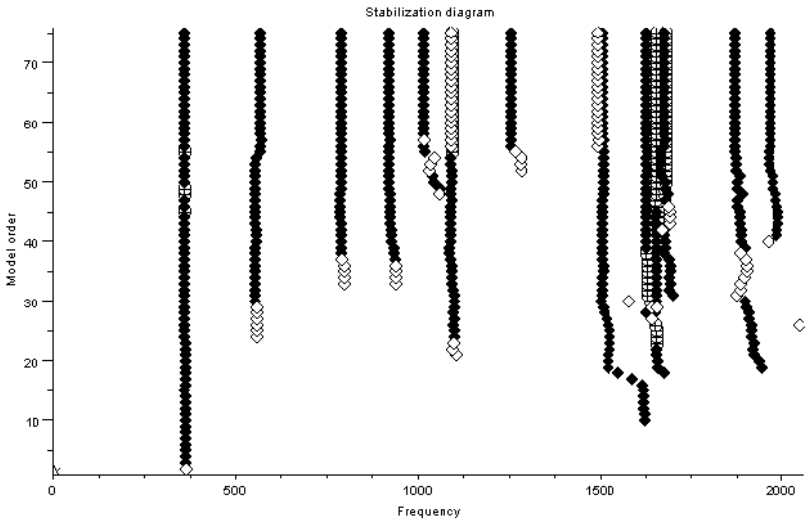

Figure 8.5 – Stabilization diagram containing the natural frequencies composite plate from covariance-driven SSI with Algorithm 4.4.

of $1/\tau = 4096\,\text{Hz}$ in $N_s = 4$ setups, where 3 of them contained 14 moving sensors and 1 contained 7 moving sensors, with $r^{(\text{ref})} = 1$ reference sensor that stayed fixed all the time. Thus, the structure was recorded at altogether 49 measurement points.

With merging Algorithm 4.4 using covariance-driven SSI, a stabilization diagram was obtained in Figure 8.5, from which the system modes were selected. Nine modes in the range $[0 - 2048\,\text{Hz}]$ were obtained. Their mode shapes with their natural frequencies and damping ratios are displayed in Figure 8.6.

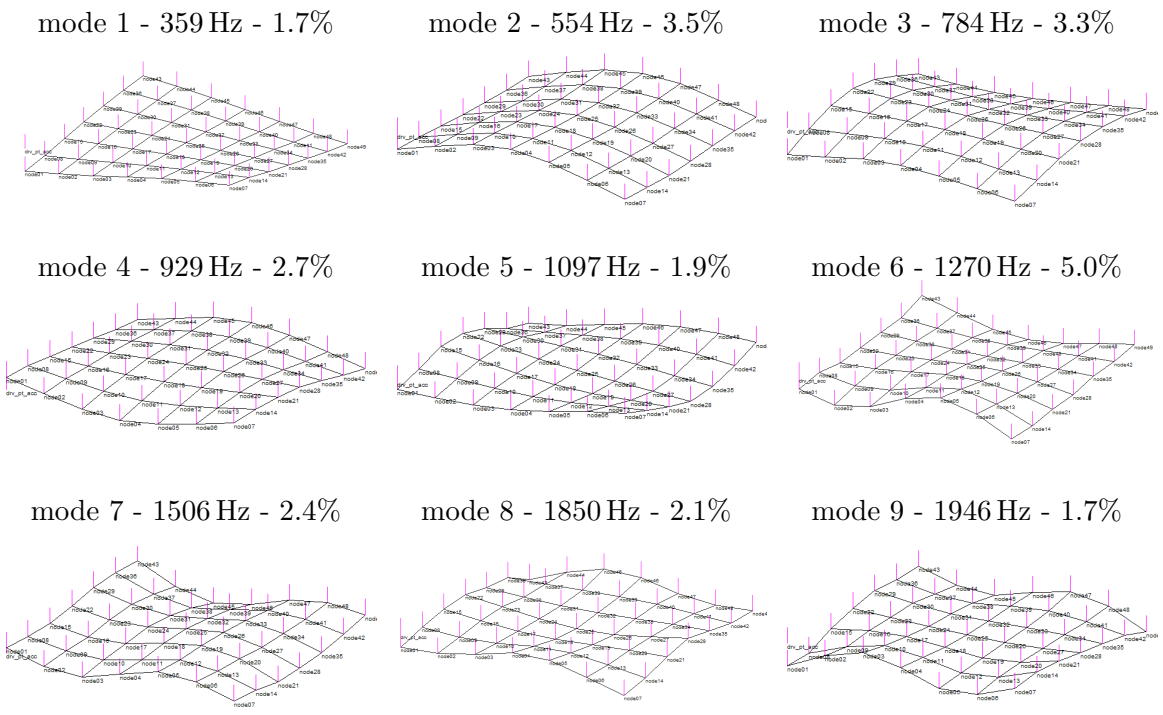

Figure 8.6 – Obtained natural frequencies, damping ratios and mode shapes of composite plate.

8.3.2 Luiz I Bridge

The multi-setup system identification of Luiz I Bridge was investigated within a collaboration with KU Leuven (Belgium) and the Faculty of Engineering of University of Porto (Portugal). A prior study comparing different merging approaches on Luiz I Bridge was made in [RMDRC09], which is extended to the merging approach from Chapter 4.

8.3.2.1 Bridge description and ambient vibration test

The Luiz I Bridge (Figure 8.7) is a 172 m tied metallic arch bridge over the Douro River at the city of Porto, in the north of Portugal, built in 1885 by Eiffel's former engineer Theophile

Seyrig. The bridge is composed by a hinged metallic arch supporting two different decks: one at the top of the arch and another one at the level of the respective supports. The arch spans 172 m between abutments and rises 45.1 m. It has a variable thickness, between 16.7 m near the supports and 7.1 m at midspan, and presents a parabolic geometry both in vertical and plan views. The upper deck is 391.25 m long and 5 m height, and it is supported by the arch, at midspan and at two intermediate sections, by 5 piers and the abutments. The lower deck has a height of 3.25 m, is suspended from the arch by four ties and provides a roadway connection between the cities of Porto and Vila Nova de Gaia.

The Laboratory of Vibrations and Monitoring (VIBEST) of the Civil Engineering Department of the Faculty of Engineering of the University of Porto (FEUP) was contracted to perform the ambient vibration tests on the Luiz I Bridge. This dynamic test was conducted without disturbing the normal use of the bridge, so the measured accelerations were mainly induced by the wind, by the roadway traffic on the lower deck and by the metro passing over the upper deck. The dynamic response of the bridge was recorded with four seismographs equipped with triaxial force-balance accelerometers and duly synchronized by GPS. Because of the limited number of available sensors and the need to measure a high number of points, the measurements were carried out in 26 different setups during two days. For the vibration recordings, two recorders served as references, permanently located at section 15 (Figure 8.7), at both the upstream and downstream sides, while the other two recorders scanned the bridge deck in 18 consecutive setups, measuring the acceleration along the 3 orthogonal directions, at both the upstream and downstream sides. During the ambient vibration test of the lower deck, the reference sensors of the upper deck kept their positions and an additional reference was introduced at the downstream side at section 22 (Figure 8.7). For each setup, time series of 16 minutes were collected with a sampling frequency of 100 Hz. Further details of the

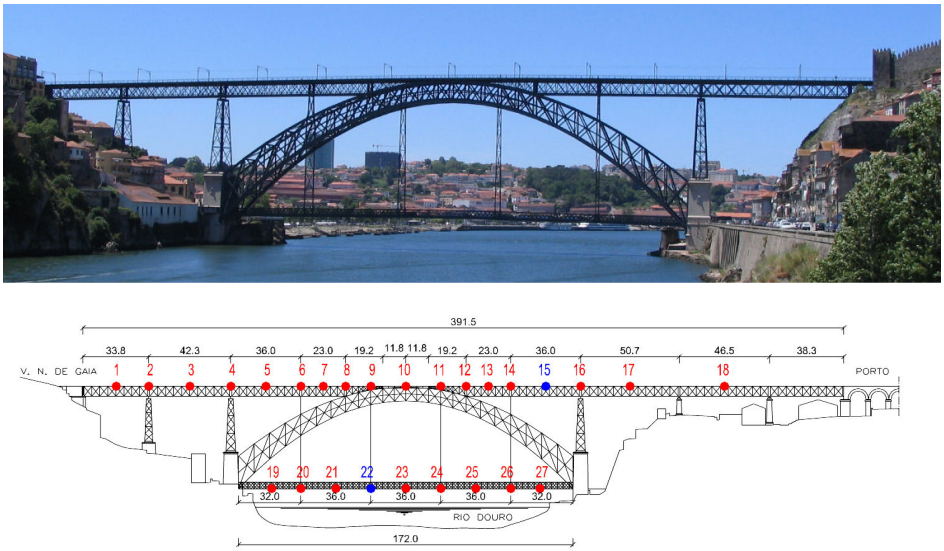

Figure 8.7 – Luiz I Bridge.

dynamic test can be found in [CMC06].

The data to be processed consists of the lateral and vertical accelerations of the bridge, is low-pass filtered at 4 Hz and re-sampled with the sampling frequency 20 Hz.

8.3.2.2 Multi-setup system identification

In [RMDRC09], system identification results were obtained using the PoSER and PoGER approaches with covariance-driven SSI. Altogether, 14 modes were identified. These results are not repeated here, but used for a comparison in the following section.

For the analysis with the PreGER approach (Algorithm 4.2) we separated the data into their lateral and vertical components and processed them separately. This led to better results than processing the data from both directions together as the mode shape of a lateral bending mode would contain noise in the vertical direction, and vice versa. Apart from this separation, all setups were processed together. For the analysis the parameters $p + 1 = q = 150$ were chosen and the model order ranged from 1 to 150. The modes were manually chosen in a stable model order band in the resulting stabilization diagrams.

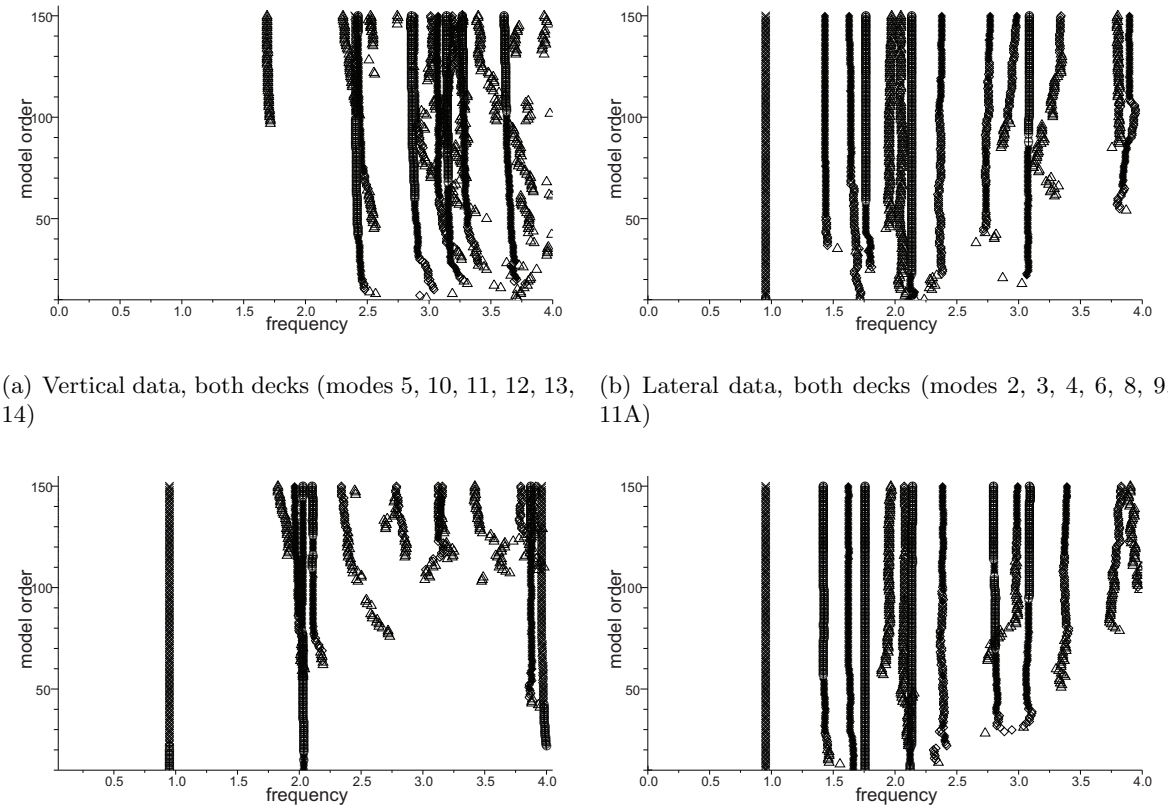

(a) Vertical data, both decks (modes 5, 10, 11, 12, 13, 14)

(b) Lateral data, both decks (modes 2, 3, 4, 6, 8, 9, 11A)

(c) Lateral data, lower deck (modes 1, 7, 15)

(d) Lateral data, upper deck (mode 13A)

Figure 8.8 – Stabilization diagrams used to identify the modes in the PreGER approach.

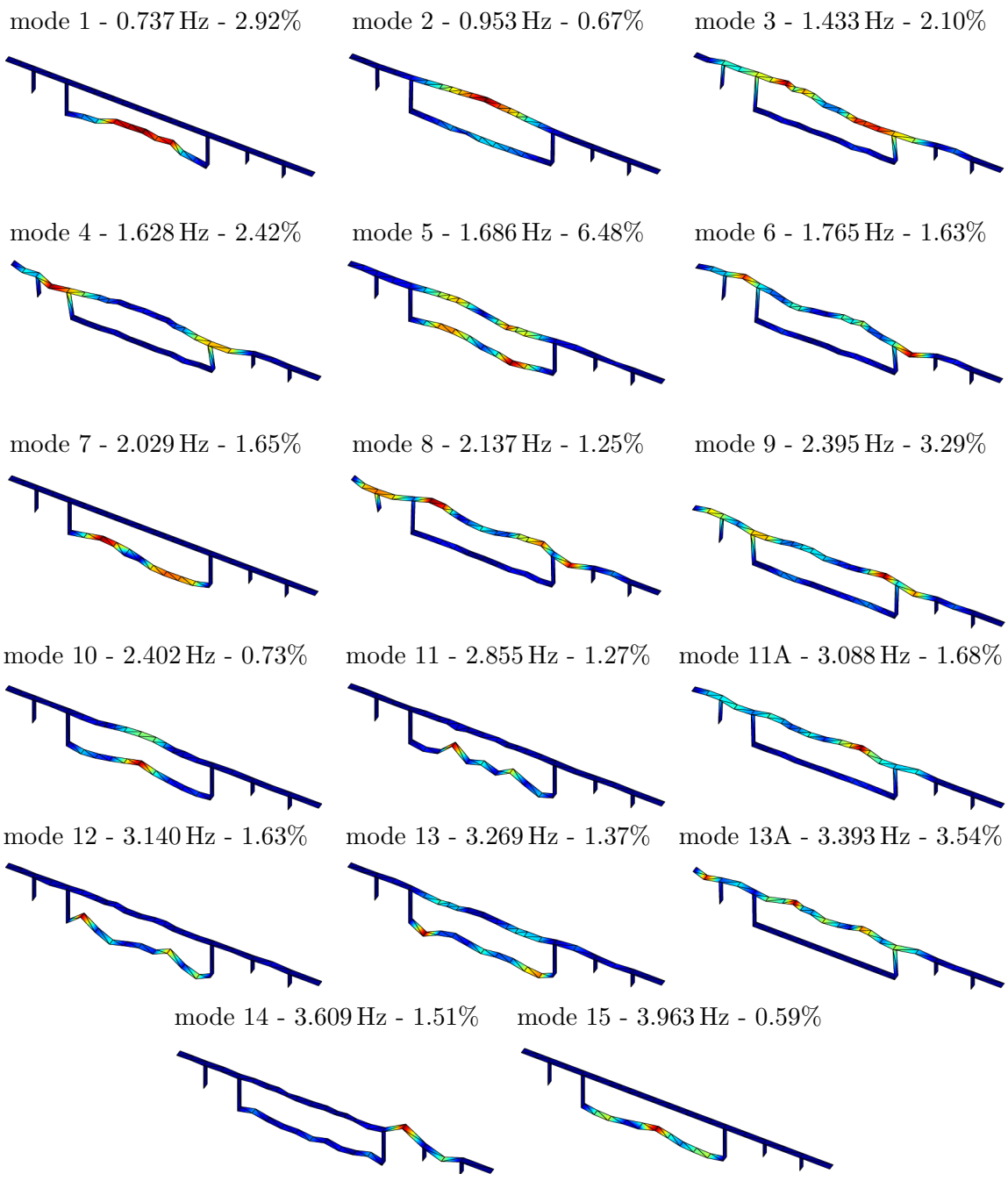

Figure 8.9 – Modes identified of Luiz I Bridge with covariance-driven SSI using merging Algorithm 4.2.

For the lateral components, one reference sensor common to all setups was available on the upper deck, and for the vertical components, two reference sensors were available on the upper deck. With these settings all modes from the PoSER approach could be identified (Figures 8.8(a) and 8.8(b)), except mode 1 and 7 like in the PoGER approach in [RMDRC09]. These are local lateral bending modes of the lower deck, and the lateral reference sensor only from the upper deck was used. Besides, an additional lateral bending mode compared to the identification in [RMDRC09] was identified at 3.088 Hz (mode 11A).

In order to identify the local lateral bending modes of the lower deck, we continued the analysis only with the setups containing data from the lower deck, including the reference sensor from the lower deck. This led to the identification of modes 1 and 7, and an additional local lateral bending mode at 3.963 Hz (mode 15) in Figure 8.8(c). Another separate analysis of the upper deck (with the reference sensor from there) led to the identification of a local lateral bending mode of the upper deck at 3.393 Hz (mode 13A) in Figure 8.8(d). None of the modes 1, 7, 13A and 15 were present on both decks.

All in all, the following modes were identified with the new merging algorithms:

- Modes 1, 7 and 15 are lateral bending modes of the lower deck.
- Modes $2, 3, 4, 6, 8, 9, 11\text{A}$ and 13A are lateral bending modes of the upper deck. Only for mode 2, there is a clear but minor deformation of the lower deck.
- Modes 5 and 10 are vertical bending modes were both decks move in phase.
- Modes 11, 12 and 13 are vertical bending modes of the lower deck.
- Mode 14 is a local bending mode at the side spans of the Porto side of the bridge.

The identified frequencies, damping ratios and mode shapes are displayed in Figure 8.9.

8.3.2.3 Summary of results

Table 8.1 provides a comparative overview of the natural frequencies and damping ratios estimated with the different merging approaches (PoSER, PoGER and PreGER) using

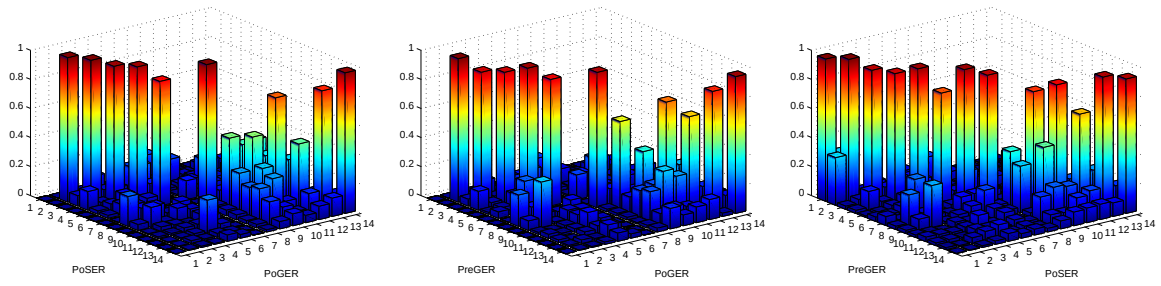

Figure 8.10 – MAC values between the mode shapes from the PoSER and PoGER approach (left), from the PreGER and PoGER approach (middle) and from the PreGER and PoSER approach (right).

Table 8.1 – Frequencies ($\widehat{f}$) and damping coefficients ($\widehat{\rho}$) of Luiz I Bridge with different merging approaches.

	PoSER		PoGER		PreGER	
Mode	$\widehat{f}$ (Hz)	$\widehat{\rho}$ (%)	$\widehat{f}$ (Hz)	$\widehat{\rho}$ (%)	$\widehat{f}$ (Hz)	$\widehat{\rho}$ (%)
1	0.741	1.20	–	–	0.737	2.92
2	0.954	0.80	0.953	0.85	0.953	0.67
3	1.418	1.25	1.421	0.95	1.433	2.10
4	1.618	0.96	1.619	0.76	1.628	2.42
5	1.640	1.75	1.639	1.48	1.686	6.48
6	1.758	0.86	1.758	0.78	1.765	1.63
7	2.044	1.19	–	–	2.029	1.65
8	2.137	1.04	2.134	1.02	2.137	1.25
9	2.395	1.05	2.397	0.56	2.378	3.29
10	2.396	0.67	2.398	1.71	2.402	0.73
11	2.848	0.77	2.849	0.70	2.855	1.27
11A	–	–	–	–	3.088	1.68
12	3.126	1.14	3.132	0.91	3.140	1.63
13	3.252	0.78	3.251	0.60	3.269	1.37
13A	–	–	–	–	3.393	3.54
14	3.589	0.60	3.590	0.61	3.609	1.51
15	–	–	–	–	3.963	0.59

covariance-driven SSI. For a comparison of the mode shapes we use the Modal Assurance Criterion (MAC) in Figure 8.10.

The following observations can be made:

- Modes 1, 7 and 15 were not observed in the PoGER and initial PreGER estimates, due to the lack of a lateral reference sensor at the lower deck that is common to all setups; however they were observed in the PreGER estimates after analyzing the lower deck separately.

- Modes 11A, 13A and 15 were not observed in the PoSER and PoGER estimates, but in the PreGER estimates.

- The differences in natural frequencies for the PoSER approaches and the PoGER approach are negligibly small. Their differences to the PreGER approach are slightly larger, but still less than 1 %.

- For the damping ratios, the differences between PoSER and PoGER estimates are larger but still not significant considering the large standard deviations on the estimates

[Ger74]. For some modes however, the damping ratios of the PreGER estimates are considerably higher than the PoSER and PoGER estimates.

- The MAC values between the mode shapes of the different merging approaches are very high (> 0.9) for most of the modes, meaning that the identified mode shapes are very similar. Only the mode shapes of modes 6 and 11 show larger differences, and, as expected, the double modes 9 and 10.

- The double mode 9 and 10 turns out to be the superposition of a lateral and vertical bending mode and could be clearly separated with the PreGER approach. With the PoSER and PoGER approaches, no clear separation was possible.

8.3.3 Humber Bridge

The multi-setup system identification of the Humber Bridge was carried out in a collaboration with the Department of Civil & Structural Engineering of the University of Sheffield within the IRIS project. A prior study on its system identification was made in [BMCC10]. Now, system identification is done with the data-driven SSI with the UPC algorithm, either using the merging with Algorithm 4.4 (PreGER) or with the PoSER approach.

8.3.3.1 Bridge description and ambient vibration test

The Humber Bridge (Figure 8.11), which was opened in July 1981, has a main span of 1410 m with side spans of 280 m and 530 m. The spans comprise 124 units of 18.1 m long 4.5 m deep prefabricated sections 28.5 m wide including two 3 m walkways. At the ends of each span there is a pair of A-frame rocker bearings that provide restraint in three degrees of freedom. The slip-formed reinforced concrete towers rise 155.5 m above the caisson foundations and carry the two main cables which have a sag of 115.5 m.

Figure 8.11 – Views of Humber Bridge from north and south.

The bridge was previously tested in July 1985 [BDST87]. The testing was motivated by a requirement to validate FE procedures for suspensions bridges. After 23 years, the original signals and resulting digital mode shapes were no longer available, just the values in published papers and reports. Because of the quality uncertainties and lack of digital data, a retest of the bridge was necessary. The current test was conducted during the week 14th-18th in July 2008 as part of EPSRC funded research project. To avoid lengthy post-processing of data a different strategy was required for the system identification, making use of autonomous recorders with precise timing of GPS-synchronized clocks. A team from FEUP in Portugal brought their recorders and assisted in the testing and post-processing. Between FEUP and University of Sheffield ten GEOSIG recorders were available. These recorders used either internal force balance accelerometers, external Guralp CMG5 accelerometers of a triaxial arrangement of QA750 accelerometers.

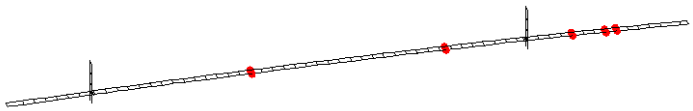

Figure 8.12 – Sensor locations for setup 24: sidespan measurement.

With up to five days of measurement available with a maximum of 10 hours per day due to recorder batteries, an optimal plan was formulated that involved separate setups to cover 76 positions. Sensor locations for one of the setups is shown in Figure 8.12. In each setup, two pairs of triaxial recorders are maintained at two permanent reference locations, leaving the remaining three pairs to rove either deck or in East/West tower pylons. Each measurement generated one hour of 30-channel (10 in each direction) acceleration records, in four 15-minutes segments. The entire day of measurements was pre-programmed into each recorder, leaving 10-minute periods between measurements to move the six rovers. The details of the measurement procedure can be found in [BMCC10].

Here, only vertical direction data from 26 different setups are processed. The analysis of the experimental data involved initial preprocessing operations of trend removal, low-pass filtering and resampling, considering that the range of frequencies of interest is rather low, of the order of 1 Hz, compared to the original sampling rate of 100 Hz.

8.3.3.2 PreGER approach

For the PreGER merging approach, all 26 setups were processed together with Algorithm 4.4. For the analysis $p+1 = q = 50$ was selected to build the data-driven subspace matrices. With 4 available reference sensors the maximal model order was 200. The stabilization diagram obtained from the global merged subspace matrix is presented in Figure 8.13, from where the 18 modes where chosen. All the identified modes can be seen in Figure 8.14. Modes 7, 10, 13 and 16 are torsional modes, and the other modes are vertical bending modes.

Note that the closely spaced modes 6 and 7 are well separated. All mode shape estimates show high quality.

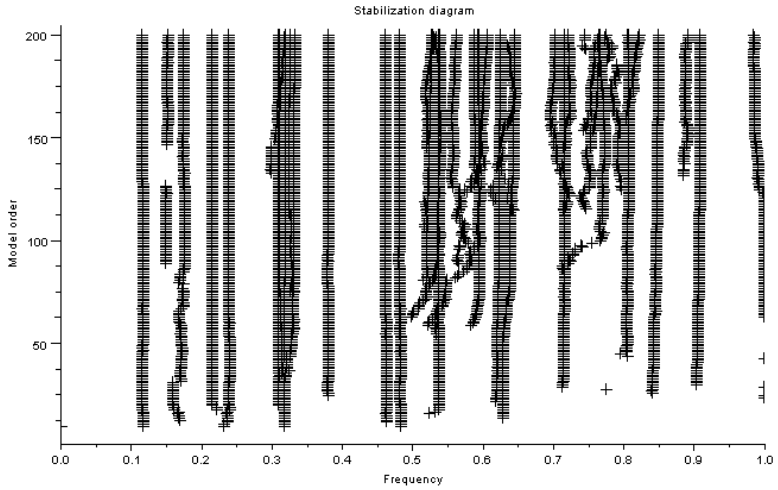

Figure 8.13 – Stabilization diagram containing the natural frequencies of Humber Bridge from the PreGER approach.

8.3.3.3 PoSER approach

For system identification with the PoSER approach, 26 stabilization diagrams were analyzed separately. The extracted modal parameters are in good agreement with other methods that are reported in [BMCC10] as well as the results of the PreGER approach. However, the mode shapes of modes 6 and 7 are poorly separated due to difficulty in analyzing the very closely spaced mode in the stabilization diagrams. Moreover, mode shapes 3 and 7 are of lower quality than in the PreGER approach.

8.3.3.4 Summary of results and comparison

For a comparison of the mode shapes the Modal Assurance Criterion (MAC) of the real parts of the mode shapes between PoSER and PreGER approach is shown in Figure 8.16. The following observations can be made:

- The differences in natural frequencies for the PoSER and the PreGER approach are less than 1 %.
- For the damping ratios, the differences between PoSER and PreGER estimates are larger but still not significant considering the large standard deviations on the estimates.
- The MAC values between most of the mode shapes of the different merging approaches are mostly close to one, meaning that the identified mode shapes are very similar. However, mode shape 6 that could not be identified clearly in the PoSER approach shows a bigger difference. Also mode shape 11 shows some difference, due to some noise in the mode shape estimate of the PoSER approach in the side span of the bridge, that is not present in the PreGER approach.

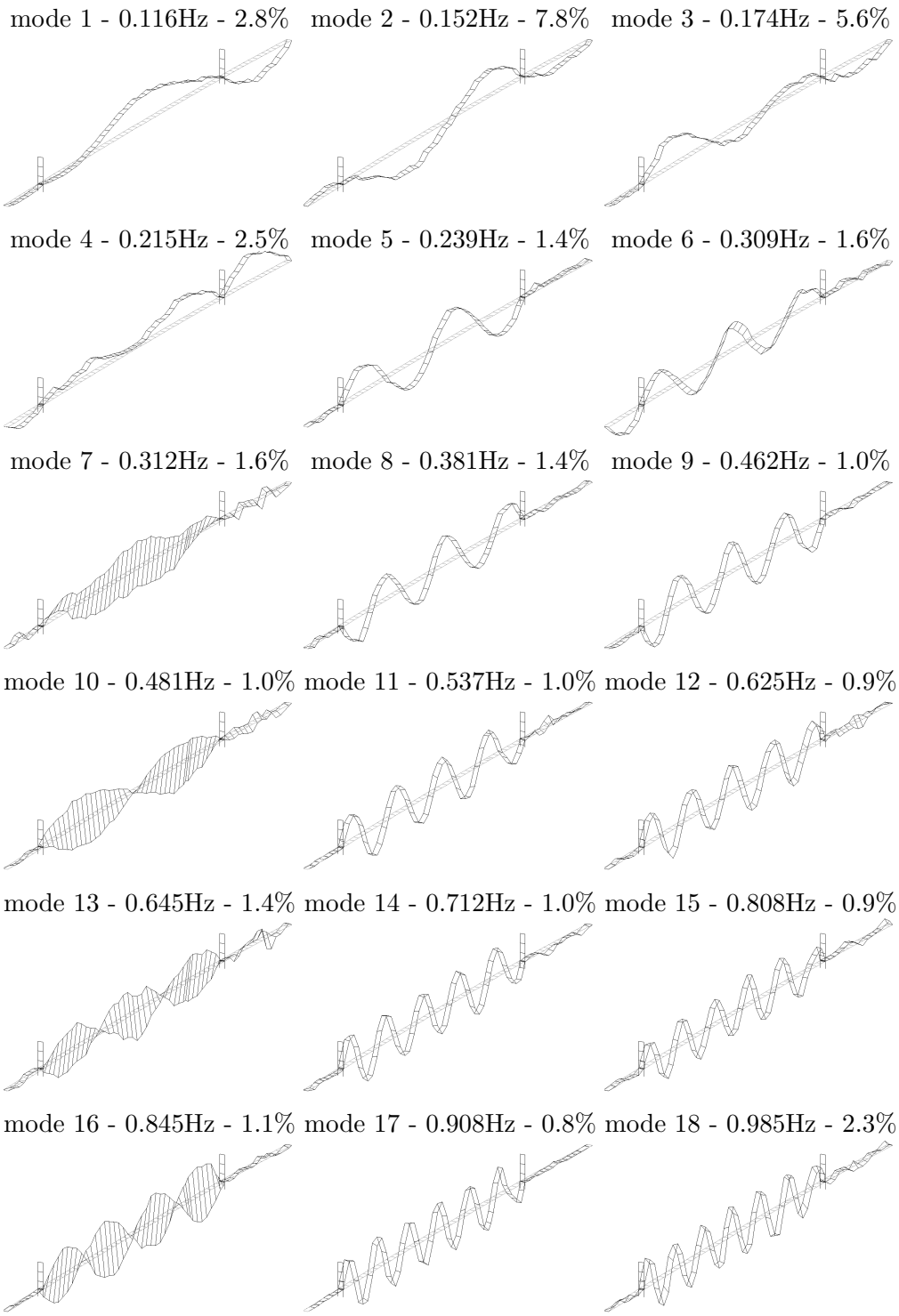

Figure 8.14 – Modes identified with data-driven SSI from the modular PreGER approach (Algorithm 4.4).

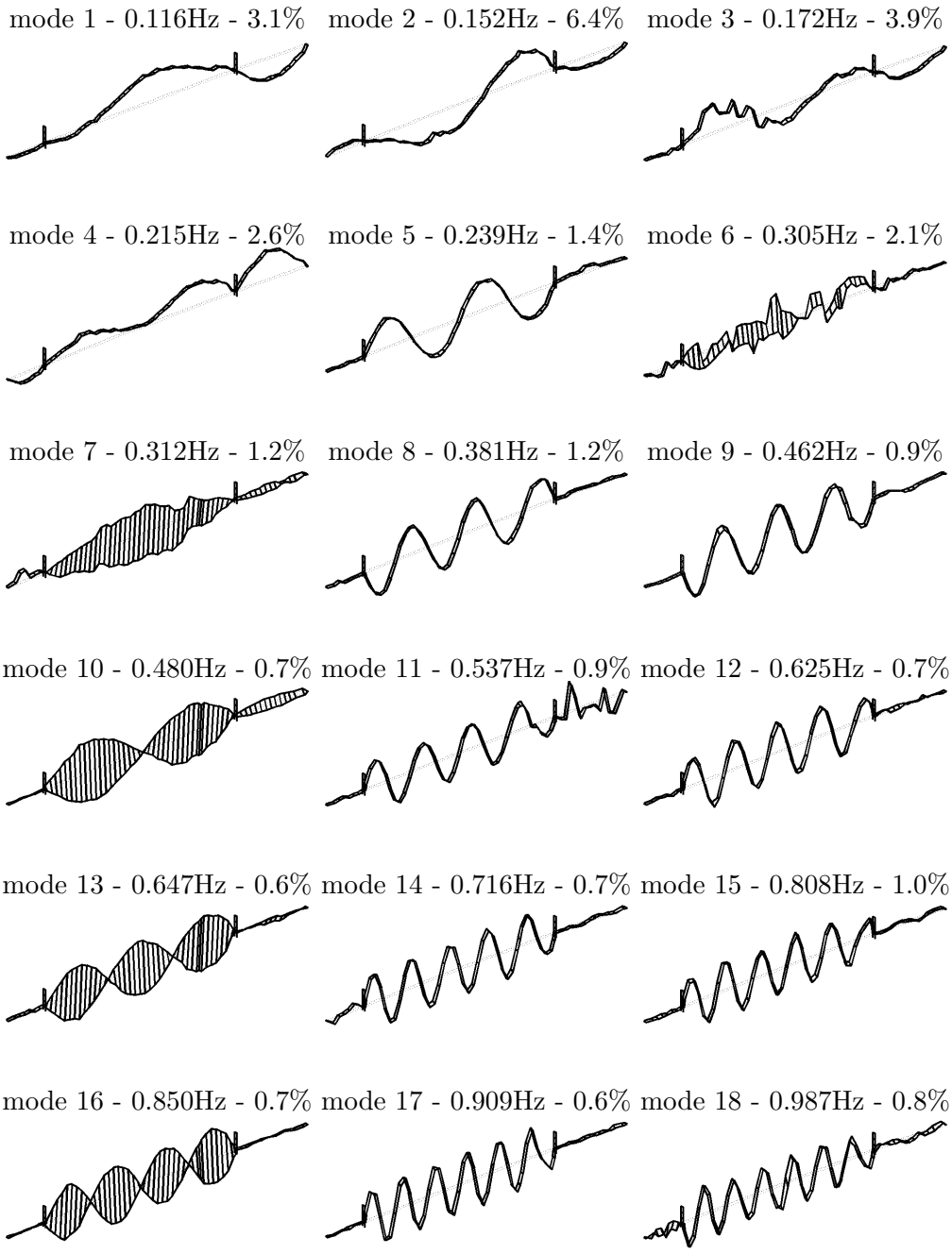

Figure 8.15 – Modes identified with data-driven SSI from the PoSER approach.

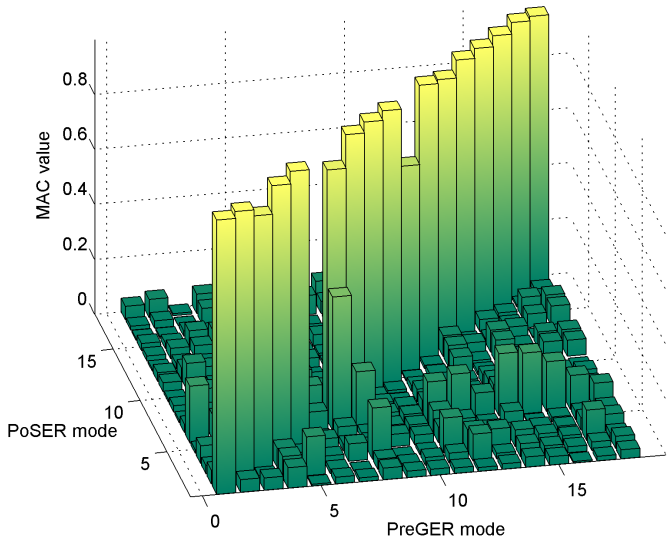

Figure 8.16 – MAC values between the real parts of the mode shapes obtained by PoSER and PreGER approach.

8.3.4 Heritage Court Tower

Within the collaboration with Structural Vibration Solutions A/S (Denmark) the merging methods from Chapter 4 were implemented in the commercial software ARTeMIS Extractor Pro [Str11]. A comparative study on a benchmark example in ARTeMIS, the Heritage Court Tower, was made between the classical PoSER and the new PreGER merging approach.

8.3.4.1 Description of the Heritage Court Tower and vibration measurements

The building considered in this study is the Heritage Court Tower (HCT) in downtown Vancouver, British Columbia in Canada. It is a relatively regular 15-story reinforced concrete shear core building. In plan, the building is essentially rectangular in shape with only small projections and setbacks. Typical floor dimensions of the upper floors are about 25 m by 31 m, while the dimensions of the lower three levels are about 36 m by 30 m. The footprint of the building below ground level is about 42 m by 36 m. Typical story heights are 2.70 m, while the first story height is 4.70 m. The elevator and stairs are concentrated at the center core of the building and form the main lateral resisting elements against potential wind and seismic lateral and torsional forces. The tower structure sits on top of four levels of reinforced concrete underground parking. The parking structure extends approximately 14 m beyond the tower in the south direction forming an L-shaped podium.

As reported in [VBDA01], a series of ambient vibration tests was conducted on April 28, 1998 by researchers from the University of British Columbia [DV98]. The vibration measurements were conducted using an eight-channel system (with force-balanced accelerometers) and were recorded in four different measurement setups. The accelerometers were typically located in the northwest and northeast corners of the building on every other floor starting from the roof down to the ground floor. Details of the field testing of this structure are given

in [DV98].

The tower model was simplified to a rectangle with nodes aligned vertically. The motions of the corners of this rectangle were computed from the measured motions by assuming rigid body motion of the floor slabs. The number of samples was 6560 and hence relatively low, amounting to 328 s at a sampling rate of 20 Hz.

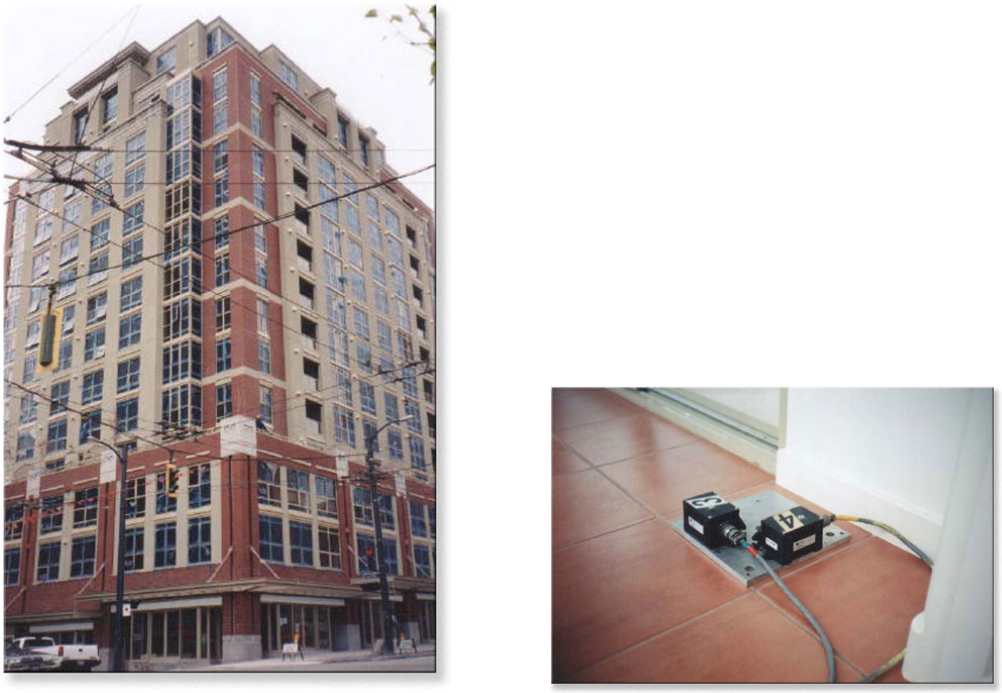

Figure 8.17 – HCT Building and setup close up.

8.3.4.2 Modal analysis with the PoSER and PreGER approaches

The modal analysis for both the PoSER and PreGER approach was tuned with the same parameters. The maximal considered model order was 80. The parameters for the modal extraction from the stabilization diagrams in ARTeMIS are shown in Figure 8.18.

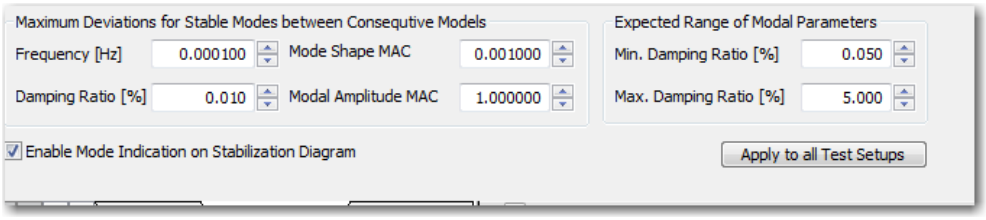

Figure 8.18 – Parameters of mode extraction from the stabilization diagram.

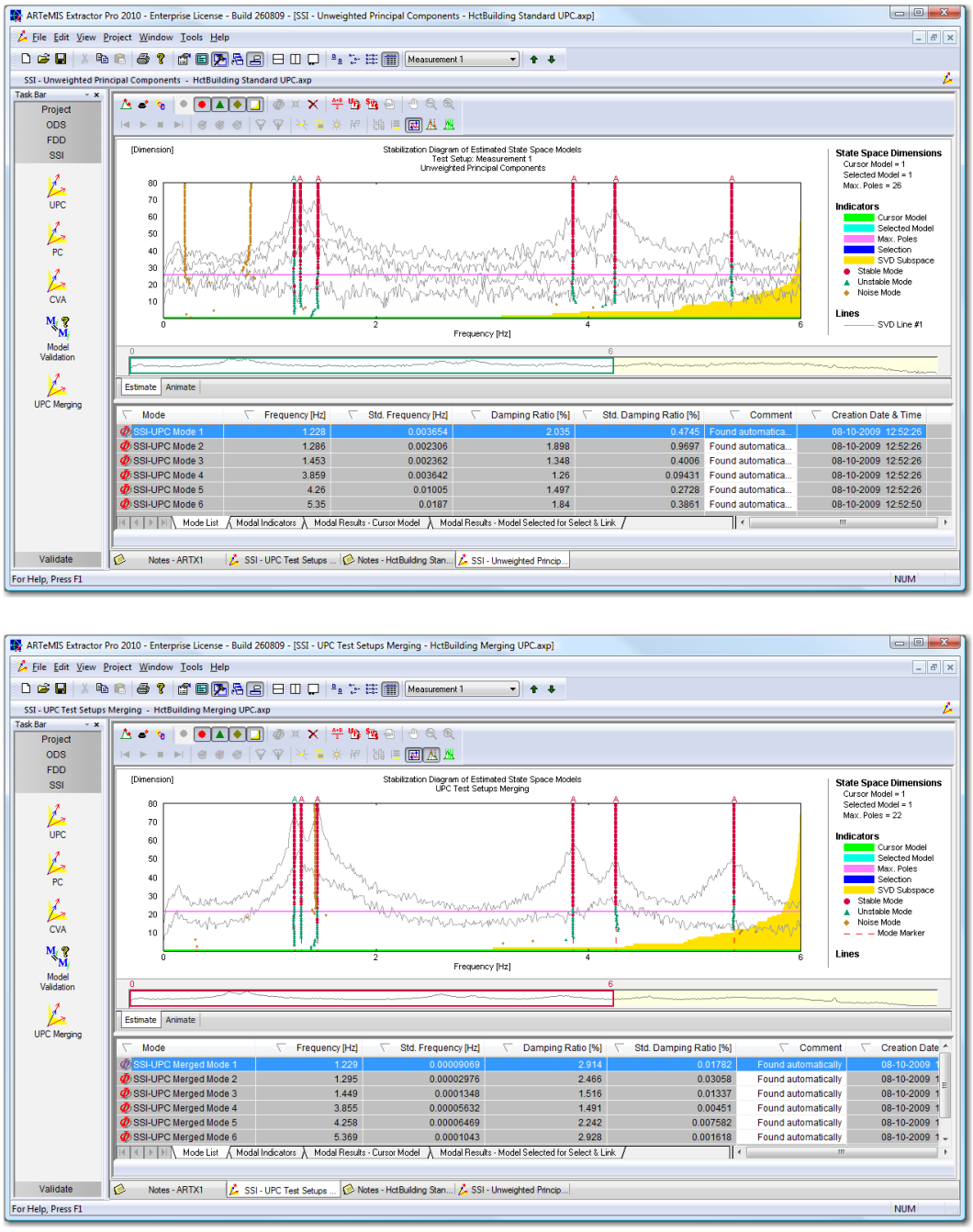

Figure 8.19 – PoSER stabilization diagram of first setup (top) and PreGER stabilization diagram (bottom).

The resulting stabilization diagrams are shown in Figure 8.19. As in previous studies [VBDA01], 6 modes were identified in the frequency range of interest [0–6 Hz]. Their natural frequencies and damping ratios are displayed in Table 8.2.

The mode shapes obtained by the PoSER and PreGER approaches are shown in Figure 8.20 and a MAC comparison between them is shown in Figure 8.21. The MAC values are very close to 1, indicating very similar mode shapes.

Table 8.2 – Frequencies ($\widehat{f}$) and damping coefficients ($\widehat{\rho}$) of obtained modes with both merging approaches.

	PoSER		PreGER	
Mode	$\widehat{f}$ (Hz)	$\widehat{\rho}$ (%)	$\widehat{f}$ (Hz)	$\widehat{\rho}$ (%)
1	1.228	2.04	1.229	2.91
2	1.286	1.90	1.295	2.47
3	1.453	1.35	1.449	1.52
4	3.859	1.26	3.855	1.49
5	4.260	1.50	4.258	2.24
6	5.350	1.84	5.369	2.93

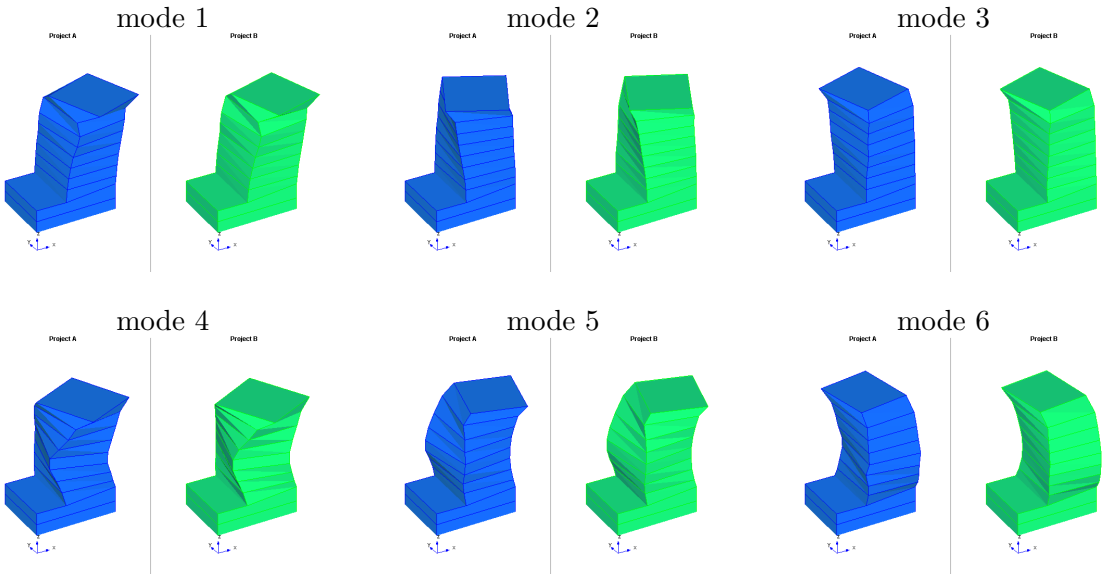

Figure 8.20 – First 6 mode shapes obtained with the PoSER (left in each figure) and the PreGER approach (right) of HCT.

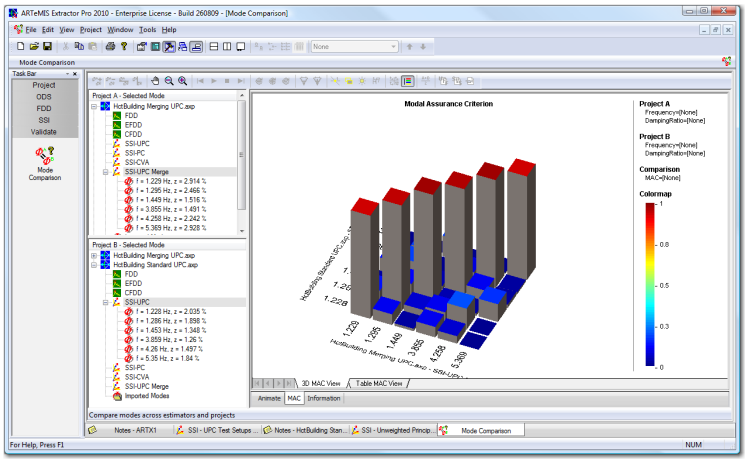

Figure 8.21 – MAC between mode shapes of HCT estimated by PoSER and PreGER approaches.

8.3.5 S101 Bridge

In a collaboration with the University of Tokyo, the system identification of the S101 Bridge was investigated within the IRIS project. Data-driven SSI with PoSER and PreGER merging approaches as well as system identification based on NExT-ERA with a frequency merging approach from [SF09] was compared.

8.3.5.1 Description of S101 Bridge and ambient vibration test

The tested bridge is the S101 Overpass Bridge located in Reibersdorf, Upper Austria west side of Vienna, Austria [SNF+10]. The bridge crossed over the national highway A1 Westautobahn Austria. It is a post-tensioned concrete bridge with the main span of 32 m, side spans of 12 m, and the width of 6.6 m (Figure 8.22). The deck is continuous over the piers and is built into

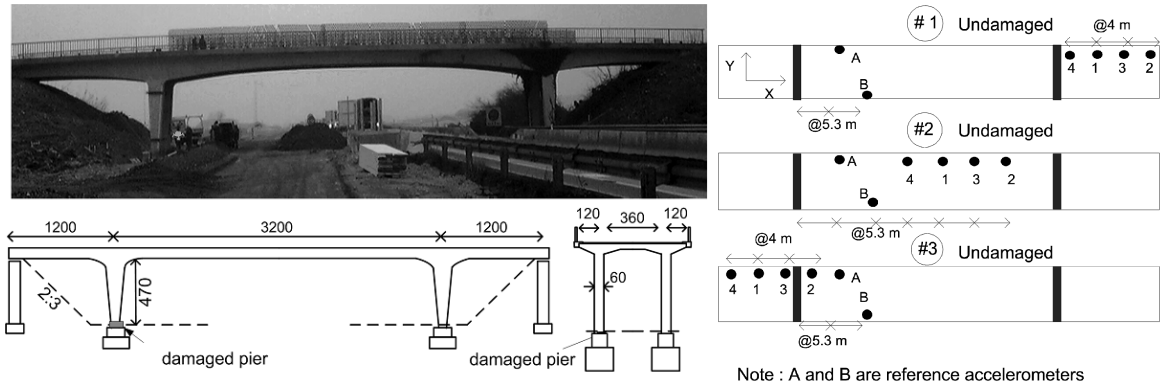

Figure 8.22 – S101 Bridge and sensor configuration.

abutment. The bridge built in 1960 had to be demolished due to some structural problems and to allow some space for additional lanes of the highway underneath.

The ambient vibration test was conducted to obtain estimates of the bridge modal parameters. The main source of vibration was from the highway traffic underneath the bridge. The sensing system consists of six triaxial accelerometers CV-373 produced by Tokyo Sokhushin. The sensors measured accelerations at six measurement nodes. Due to a limited number of sensors, three sensor arrangements were utilized (Figure 8.22). Two sensors (nodes A and B) were kept at the same places throughout measurement to provide reference for the normalization of the different ambient excitation level. Four other sensors were the roving sensors that moved from one end to the other end of the bridge. The data used in this study is sampled at a frequency of 100 Hz.

8.3.5.2 Modal analysis results

The PoSER and the PreGER merging approach were used with data-driven SSI and the re-scaling in frequency domain from [SF09] was used with NExT-ERA. Note that for a fast computation of the used stabilization diagrams, the algorithms from Section 5.3 can be applied for SSI and the algorithms from Section 5.4 can be applied for NExT-ERA. The system identification results of the first 5 modes in the frequency range [0–20 Hz] are presented in Table 8.3. Modes 1, 3 and 5 are vertical bending modes, while modes 2 and 4 are torsion modes.

Table 8.3 – Frequencies ($\widehat{f}$) and damping coefficients ($\widehat{\rho}$) of S101 Bridge with different SSI and merging approaches.

	PoSER (dat-SSI)		PreGER (dat-SSI)		NExT-ERA	
Mode	$\widehat{f}$ (Hz)	$\widehat{\rho}$ (%)	$\widehat{f}$ (Hz)	$\widehat{\rho}$ (%)	$\widehat{f}$ (Hz)	$\widehat{\rho}$ (%)
1	4.023	0.65	4.029	1.02	4.01	0.56
2	6.262	0.71	6.254	2.15	6.25	0.12
3	9.669	1.13	9.683	1.59	9.65	0.28
4	13.23	1.76	13.31	1.70	13.14	0.35
5	15.68	2.27	15.83	3.56	15.51	0.38

From Table 8.3 it can be noted that the obtained natural frequencies, especially for the first three modes, are very close. The values of the 4th and 5th frequency show slightly bigger differences, probably due to a lower excitation and bigger uncertainties of these modes. The damping value estimates show bigger deviations, with the PreGER SSI approach showing larger estimates than the PoSER SSI approach, while damping estimates from NExT-ERA show the lowest values.

The mode shapes obtained by NExT-ERA are displayed in Figure 8.23. Results from PoSER SSI and PreGER SSI show very similar results. Note that the sensor marked “B” is the reference sensor from the other side of the bridge deck (as shown in Figure 8.22) and hence indicating whether the mode is a vertical bending or a torsion mode.

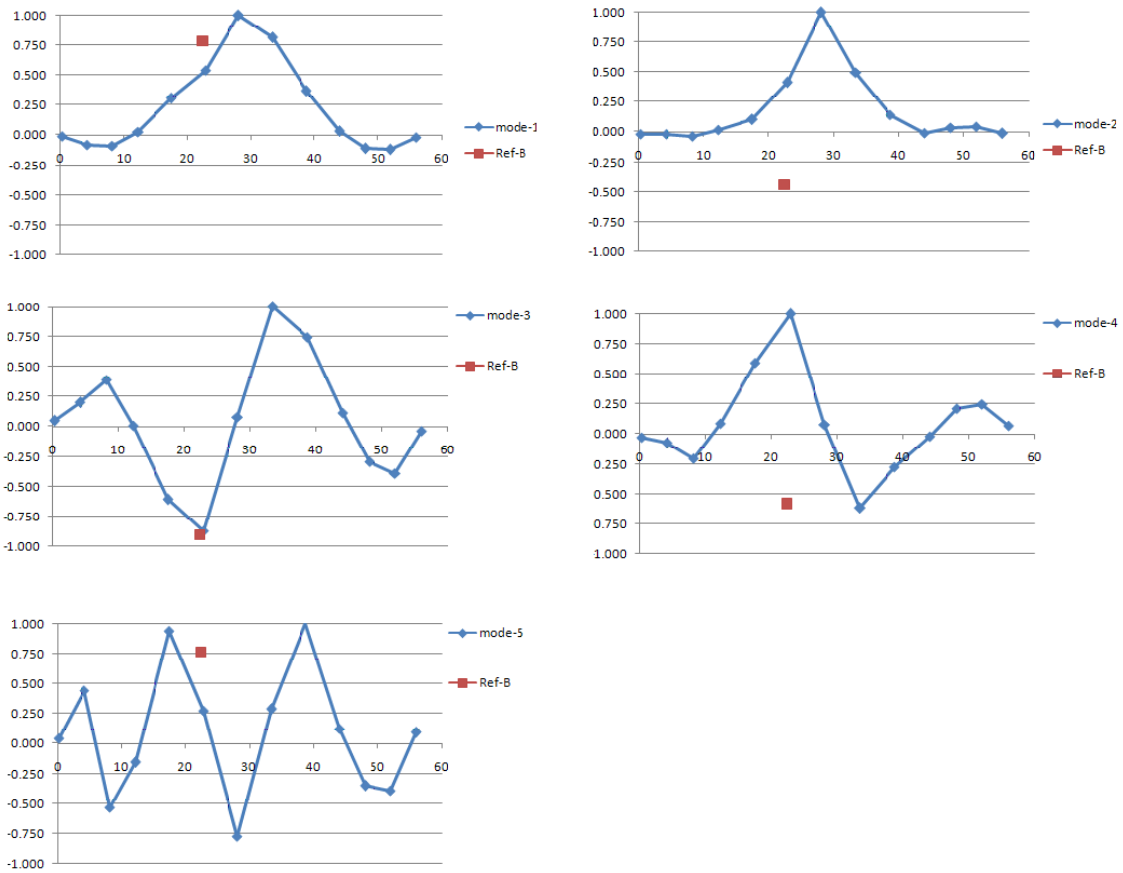

Figure 8.23 – Identified mode shapes of S101 Bridge from NExT-ERA.

8.4 Discussion

The eigenstructure identification results on structural vibration data with the new merging methods from Chapter 4 ("PreGER") have shown good accordance with established empirical merging methods ("PoSER", "PoGER").

One difference concerns the estimated damping ratios. In some of the estimates, the damping ratios of the PreGER approach are higher than in the other approaches. The PreGER methods were derived under the premise of the same state transition matrix A and observation matrix of the reference sensors $C^{(\mathrm{ref})}$ throughout all measurements. In practice however, this condition might not be entirely satisfied due to environmental changes between the measurements that affect the structure, e.g. temperature variations. Then, the natural frequencies in each setup are slightly different and the resulting frequency for each mode obtained by the PreGER approach is associated to a higher damping ratio, consequence from the merging of overlapping frequencies. However, the resulting mode shape estimates still show very good quality. Note that in the case of merging setups of a changing structure, only the identification of a mode shape estimate can be of interest, as frequency and damping

values change [PMDR01, BBMN09].

The quality of the obtained mode shapes from the PreGER approach is for all case studies comparable to other merging approaches. However, for closely spaced modes, identification results were improved: mode shape estimates identified with PreGER were clearly separated.

The PreGER approach is automated and yields one set of global modal parameters. Thus, no problems arise in analyzing many setups separately and matching identification results as in the PoSER approach, which usually also needs user interaction. As only one stabilization diagram needs to computed and analyzed, it is faster. Moreover, it is modular, processing setup after setup, and with its iterative computation, possible memory problems can be avoided. The PreGER approach is theoretically sound and avoids post-processing of the results.

8.5 Conclusions

In this chapter, the new merging algorithms of Chapter 4 were successfully applied to the modal analysis of several large-scale vibrating structures, thus validating their theoretical derivation. Compared to other established merging methods, they have proven very efficient and gave good results, both with covariance- and data-driven SSI.

Furthermore, first studies on the uncertainty quantification of the obtained eigenstructure identification results have been made [DLM11, DLAM11].

8.6 Dissemination

Parts of this chapter have been published in:

[DAM10] M. Döhler, P. Andersen, and L. Mevel. Data merging for multi-setup operational modal analysis with data-driven SSI. In *Proc. 28th International Modal Analysis Conference*, Jacksonville, FL, USA, 2010.

[DJMB11] M. Döhler, B. Jaishi, L. Mevel, and J.M.W. Brownjohn. Data fusion for system identification of the Humber Bridge. In *Proc. 29th International Modal Analysis Conference*, Jacksonville, FL, USA, 2011.

[DRM+10] M. Döhler, E. Reynders, F. Magalhães, L. Mevel, G. De Roeck, and Á. Cunha. Pre- and post-identification merging for multi-setup OMA with covariance-driven SSI. In *Proc. 28th International Modal Analysis Conference*, Jacksonville, FL, USA, 2010.

[DSM10] M. Döhler, D. Siringoringo, and L. Mevel. System identification under different ambient excitations. In *Proc. 3rd Asia-Pacific Workshop on Structural Health Monitoring*, Tokyo, Japan, 2010.

[LPD+10] M. Luczak, B. Peeters, M. Döhler, L. Mevel, W. Ostachowicz, P. Malinowski, T. Wandowski, and K. Branner. Damage detection in wind turbine blade panels using three different SHM techniques. In *Proc. 28th International Modal Analysis Conference*, Jacksonville, FL, USA, 2010.

Chapter 9

Damage detection and localization

9.1 Introduction

The statistical subspace-based fault detection test was introduced in Section 2.3. It has been proven to be useful for *Structural Health Monitoring (SHM)* of civil structures, whose underlying mechanical model was introduced in Section 2.4. For SHM, the parameters of the test (left null space S, covariance $\widehat{\Sigma}$, Jacobian $\widehat{\mathcal{J}}$) are set up in a reference period, where the structure is known to be safe. In the monitoring period, values of a χ^2-test statistics are computed and compared with a threshold to trigger an alarm.

The developments in this thesis are as follows for damage detection and localization. In Section 3.5, numerical improvements of the damage detection test were made regarding its applicability to real data. In Chapter 6, this damage detection test is extended to be robust to a changing ambient excitation. In Chapter 7, extensions to damage localization, i.e. to the change detection in the structural parameters were made, which take into account the mutual influence of structural parameters in the test and do not require a finite element model.

In the current chapter, the damage detection test is applied to a real large-scale structure during progressive artificial damage in order to validate its performance using the improvements of Section 3.5. This work was done in collaboration with the German Federal Institute for Materials Research and Testing (BAM). Also, the rejection of the mutual influence of structural parameters for damage localization (Chapter 7) is shown on a large-scale simulated bridge deck. Due to the lack of data for the damage detection test under a changing ambient excitation (Chapter 6), we refer to Section 6.6 for its application to a mass-spring model.

This chapter is organized as follows. In Section 9.2, the damage detection test is applied to vibration data from the progressive damage test of S101 Bridge and compared with system identification results of the monitoring data. The damage localization test is applied to a simulated bridge deck in Section 9.3.

9.2 Progressive damage test of S101 Bridge

Within the European research project "Integrated European Industrial Risk Reduction System (IRIS)" the prestressed concrete bridge S01 was artificially damaged [VCE09]. The damaging processes were accompanied by a permanent measurement of the static and dynamic behavior of the structure. Like this, a complete record of monitoring data during a defined loss of structural integrity on a typical bridge structure could be provided to test and evaluate SHM methods and applications. Note that the measurements used in this section are different from the setting in Section 8.3.5.

In order to validate its performance on a real structure, the damage detection test defined in Section 2.3 is applied to vibration data from the progressive damage test of S101 Bridge. As the implementation of the test in practice raises some numerical problems, the improved computation of the χ^2-test statistics for practical problems in Section 3.5 was taken into account.

9.2.1 The S101 Bridge

The S101 was a prestressed concrete bridge from the early 1960th spanning over the 4-lane highway A1 in Austria (Figure 9.1). The structural system was a three-field frame with a 32 m wide mean field and two 12 m wide side fields. The superstructures cross section was designed as a 7.2 m wide post-tensioned double T-beam with varying heights (Figure 9.2).

During recurring technical inspections of the bridge several deficiencies as cracks and spellings have been found. Since the crack pattern correlated with the geometric properties of the prestressing a significant deficit of structural reliability was assumed. Because of the subsequent determined limited load bearing capacity it was decided to replace the structure.

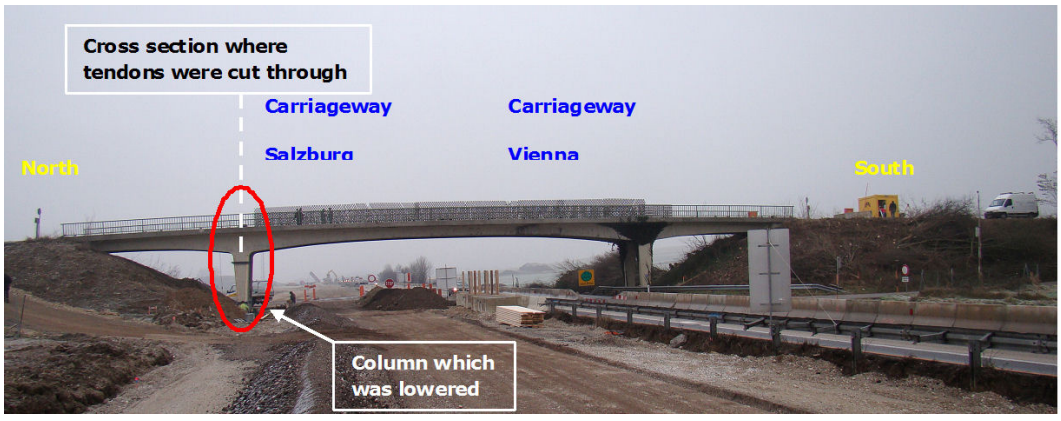

Figure 9.1 – S101 Bridge during damage test [VCE09].

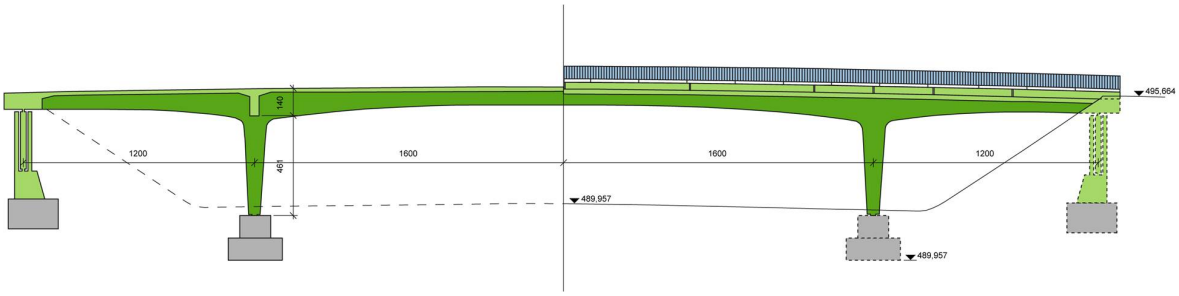

Figure 9.2 – System drawing of S101 Bridge [VCE09].

9.2.2 Damage description

The damage test took place from 10-13 December 2008. During the test the highway beneath the bridge was open in one direction. The second direction was closed for traffic because of construction work which in addition took place near the bridge.

Two major damage scenarios were artificially induced. First, a significant damage of one of the four columns was inserted by cutting through the column on its lower end. With this action a change in the global structural system was implemented. After a second cut a 5 cm thick slice of the column was removed and the column was lowered for altogether

Figure 9.3 – Destructive damaging; a) cutting through one of the columns, b) and c) successive intersecting of prestressing tendons [VCE09].

Table 9.1 – Damage scenarios during progressive damage test of S101 Bridge.

A	First cut through column	G	Uplifting column
B	Second cut through column	H	Exposing cables and cut through first cable
C	Lowering column (first step)	I	Cut through second cable
D	Lowering column (second step)	J	Cut through third cable
E	Lowering column (third step)	K	Cut through fourth cable
F	Inserting steel plates		

3 cm. Afterwards the column was uplifted again to its original position and secured there by steel plates. In a second damage scenario prestressing tendons of one of the beams were cut successively. All in all three and a quarter of a wire bundle were cut through. Between each intersection pauses of several hours were kept to let the structural system change into a new state of equilibrium. In Table 9.1 all damage actions are sorted in chronological order.

9.2.3 Measurement description

The measurement campaign was carried out by the Austrian company VCE and the University of Tokyo [VCE09]. For vibration measurement a BRIMOS measurement system containing a permanent sensor grid was used. The grid consisted out of 15 sensor locations on the bridge deck, see Figure 9.4, in each location three sensors for measurement in the bridge decks vertical, longitudinal and transversal direction. All in all, for vibration measurement 45 acceleration sensors were applied. Additionally, for verification of the static response of the structure to the damaging, the vertical displacement of the bridge deck was measured in three characteristic locations.

The measurement took place with a sampling frequency of 500 Hz. All values were recorded permanently and stored in files with 165 000 data points each. During the three days measurement campaign 714 data files each containing 45 channels were produced.

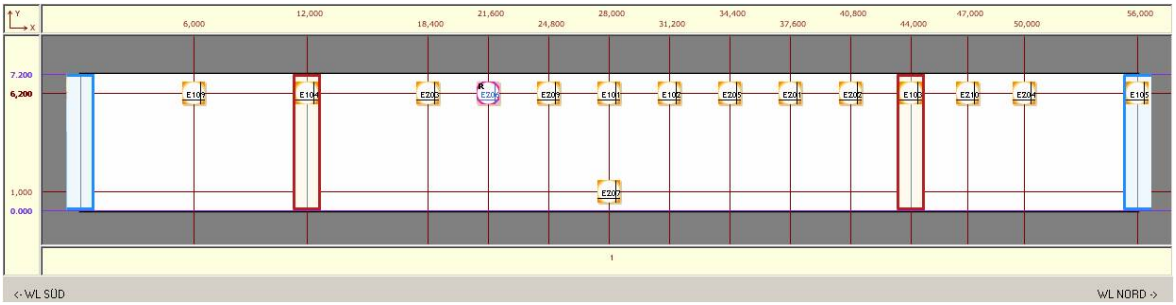

Figure 9.4 – Bridge deck with sensor grid for vibration measurement, on each location acceleration was measured in three directions [VCE09].

9.2.4 Damage detection on S101 Bridge

9.2.4.1 Data analysis

The output-only vibration data of the bridge were recorded throughout the whole three day long damage test, including the nights. To avoid disturbance of the detection, the files recorded during damaging activities were excluded. So, all in all 660 files, each of 45 acceleration channels were used in the analysis.

For damage detection, the non-parametric approach (cf. Section 2.3.4) was chosen in order to take into account the entire system response for the computation of the left null space. The reference state of the undamaged structure was then set by computing and averaging

the covariance-driven subspace matrices from several datasets in the reference state, from where the left null space $\widehat{S}$ and the residual covariance $\widehat{\Sigma}$ were obtained. With this approach, a possible disturbance by single excitation events or different environmental conditions is minimized. For computing the residual covariance matrix 100 datasets of the undamaged state were used.

In the test stage, the χ^2-test statistics is computed for every data set, which in real time means an indicator of damage for every 5.5 min.

9.2.4.2 Results

Figure 9.5 shows a bar plot of values as damage indicators of all consecutive tests within the three days campaign. The associated analysis used the covariance-driven SSI with all $r = r_0 = 45$ sensors. The abscissa of the plot describes the chronological sequence of the damage activities as noted in Table 9.1 as well as the 6am and 6pm points of time for orientation. Figure 9.6 shows the damage indicator during the several steps of the first damage scenario, the cutting and settling of one of the four bridge columns. With exception of the time periods of the direct mechanical destruction processes, which were excluded for containing strong noise, the displayed sequence of damage indicators has a consecutive course.

As can be seen in Figure 9.6, the three steps of the column settlement action are very distinctive in influencing the computed damage indicator. Obviously, the dynamic system has changed to quite some extend and the altogether 27 mm of elastic settlement can be detected clearly. Although not that distinctively visible, the cutting of the column (A+B) also caused an increase of the indicator of approximately 75%. However it has to be mentioned that the absolute effect is superimposed by noise effects. The inlet in Figure 9.6 shows a detail of that time period.

The column remained in the settled condition for approximately one day and was then uplifted again in its former position. The effect of the uplifting is again clearly visible in Figure 9.5 by a drop of the damage indicator. However, the χ^2-test did not drop completely to its original value, which is certainly due to the fact that the lowering of one column has led to cracking within the concrete structure to some extend and therefore also to a change of the dynamic signature of the system.

The use of so-called reference sensors or projection channels when computing the subspace matrices for the residual reduced the necessary memory and computational cost massively. The analysis using all 45 channels required an extent of memory space which is usually not provided on desktop computers.

Several numbers and constellations of projection channels were analyzed. Figure 9.7 shows a χ^2-value plot for only $r_0 = 4$ (instead of 45) projection channels, one vertical and one sensor with all three directions. Note that in the computation of the subspace matrix still all $r = 45$ sensors are used, cf. (2.2.3). As one can see, almost equal information about the damage indication could be achieved compared to Figure 9.5, and at the same calculation the computing time was cut to a fifth compared to a complete sensor analysis.

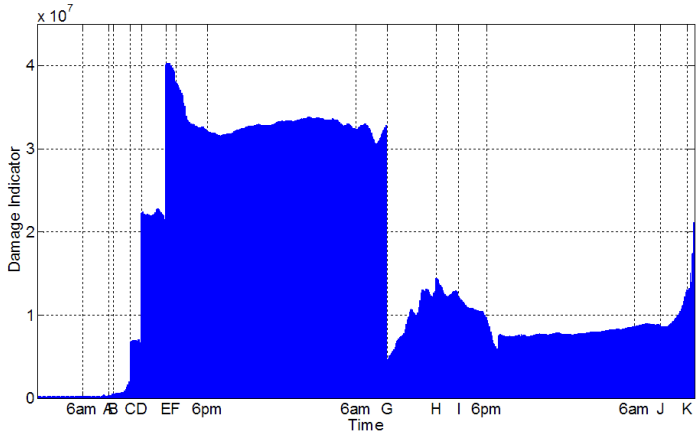

Figure 9.5 – χ^2-test results over the 3-day damage test.

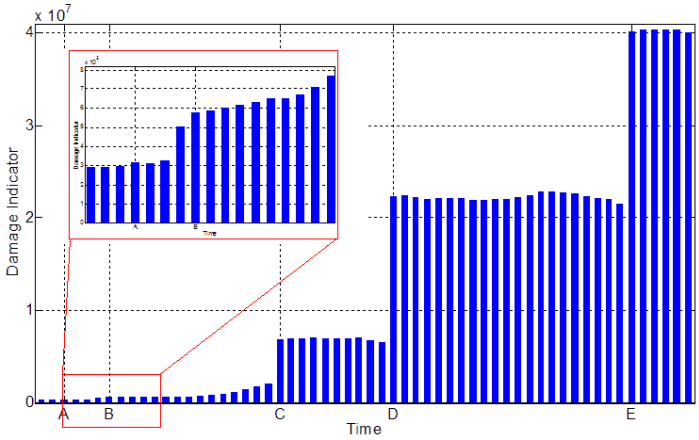

Figure 9.6 – χ^2-test for cutting and settling of one bridge column, detail of damage indicator for cutting through one bridge column.

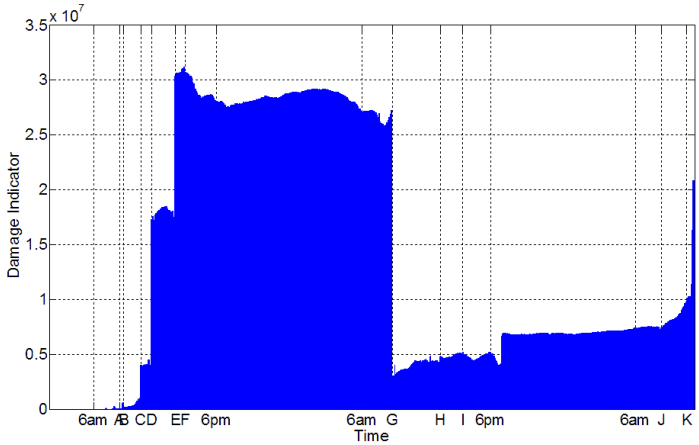

Figure 9.7 – χ^2-test results using $r_0 = 4$ projection channels.

9.2.5 Comparison to system identification results

9.2.5.1 Data analysis

System identification results of the S101 Bridge were obtained with covariance- and data-driven SSI. In order to compare results at the different damage states, confidence intervals on the obtained results were computed on the results based on [RPDR08]. The algorithm in [RPDR08] was derived for covariance-driven SSI and is extended to data-driven SSI using the covariance derivations in Section 3.5.2.

The system identification is done for the first five modes in the frequency range [0–18 Hz]. The data was downsampled from the original sampling rate 500 Hz by factor 8 and after a first examination only the sensors in vertical direction were chosen, as in this frequency range only vertical bending and torsional modes were present. For system identification and confidence interval computation the parameters $p + 1 = q = 11$ were chosen for the subspace matrices and the system orders $n = 1, \ldots, 70$ were considered for stabilization diagrams. Confidence bounds were obtained by cutting the data into 100 blocks.

9.2.5.2 System identification in reference state

In Figure 9.8, the stabilization diagrams of the natural frequencies from both SSI methods are presented, where the confidence interval of each frequency is plotted as a horizontal bar. The obtained confidence bounds on the frequencies were used to clean the diagrams: Modes with frequencies having big confidence bounds are likely to be spurious and are erased. In this case, all modes with confidence bounds bigger than 2% of the frequency value were deleted.

From the stabilization diagrams, the modes of the system are chosen. In Table 9.2, an overview of the obtained modal parameters and their confidence bounds at model order 40 is given. Note that all confidence bounds are relative values in percent, i.e. the standard deviation of a value divided by the value and multiplied by 100.

Table 9.2 – Overview of the estimated first 5 modes of S101 Bridge with natural frequencies $\widehat{f}$, their relative confidence bounds $\tilde{\sigma}_f = \widehat{\sigma}_f / \widehat{f} \cdot 100$, the damping ratios $\widehat{\rho}$ and their relative confidence bounds $\tilde{\sigma}_d = \widehat{\sigma}_\rho / \widehat{\rho} \cdot 100$.

	Covariance-driven SSI				Data-driven SSI (UPC)			
mode	$\widehat{f}$ (in Hz)	$\tilde{\sigma}_f$	$\widehat{\rho}$ (in %)	$\tilde{\sigma}_\rho$	$\widehat{f}$ (in Hz)	$\tilde{\sigma}_f$	$\widehat{\rho}$ (in %)	$\tilde{\sigma}_\rho$
1	4.039	0.34	1.1	23	4.031	0.21	1.3	22
2	6.292	0.19	0.6	52	6.282	0.11	0.7	19
3	9.730	3.42	3.0	92	9.872	1.17	2.1	32
4	13.19	0.67	1.3	73	13.31	0.38	1.4	22
5	15.72	0.70	1.8	20	15.73	0.39	1.8	19

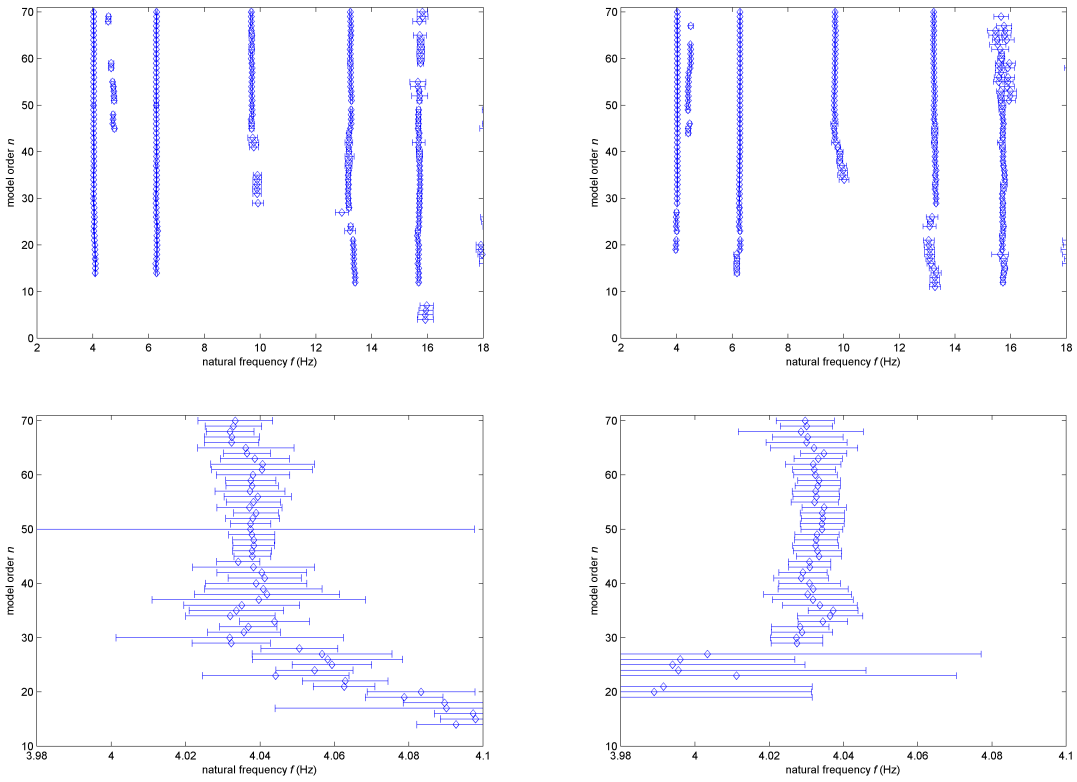

Figure 9.8 – Stabilization diagrams with covariance-driven SSI (left) and data-driven SSI (right) containing confidence intervals on the frequencies (top: full diagrams, bottom: zoom on first mode).

9.2.5.3 Frequency monitoring during damage test

An automated monitoring procedure was applied to each available dataset, which did the system identification and a confidence interval computation based on [RPDR08] automatically for each dataset. For each dataset a stabilization diagram was built with the SSI algorithms, containing model orders from 10 to 70. Then, the modes were chosen automatically using stabilization criteria such as thresholds for the damping estimates and confidence interval bounds, small frequency deviation between successive model orders, a minimum number of appearances of a frequency in the diagram and the MAC value between successive model orders.

The results of the frequency monitoring of all datasets are displayed in Figure 9.9 and the respective damage scenarios were explained in Table 9.1. Especially the frequency drop can be clearly seen when one column of the bridge was lowered before it was lifted up again (between A and G). This affected mainly the second, third and fourth mode, while the frequency changes in the first mode were less important. Especially the change in the fourth mode is remarkable, as it split in two modes during the lowering of the column, with one lower and one higher frequency than before. The frequency changes in the fifth mode cannot be evaluated, as its uncertainty is very high compared to the other modes.

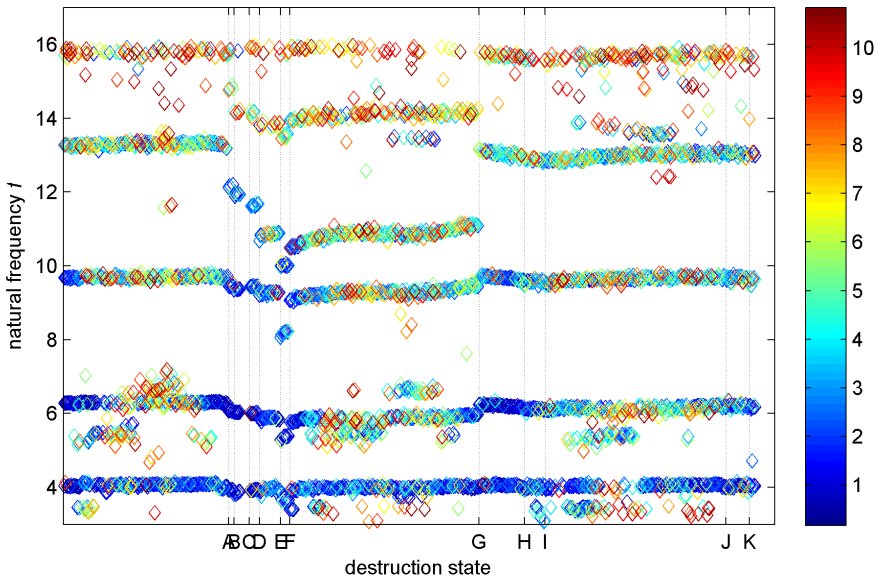

(a) covariance-driven SSI

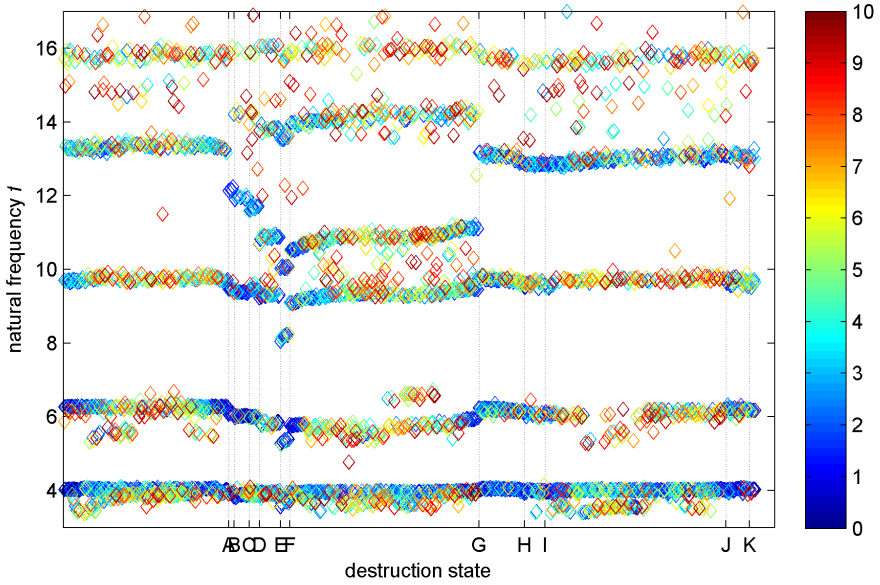

(b) data-driven SSI (UPC)

Figure 9.9 – Natural frequencies with confidence bounds during progressive damage test of S101 Bridge (damage incidents from Table 9.1). The color bar indicates the confidence bound in percent of the obtained frequency.

9.2.6 Discussion

With the statistical damage detection test, the change in the system response of the entire structure is evaluated. The link between the structural changes due to the artificially introduced damage cutting/lowering of one column and the behavior of the respective χ^2-test values at each test stage was clearly shown. Besides, a significant increase of the efficiency of the damage detection test was achieved by the use of projection channels.

Both the covariance- and data-driven SSI give practically identical estimates for system identification in this test case, when taking the obtained confidence bounds into account. However, the data-driven approach seems to yield frequency and damping estimates that have lower confidence bounds than the covariance-driven approach. Also, the damage scenarios "cutting/lowering of one column" could be clearly linked to changes in the natural frequencies.

9.3 Damage localization on a simulated bridge deck

The damage localization approach from Chapter 7 is demonstrated on a simulated bridge deck used in [BBM+08]. The emphasis here lies on the rejection approach (Section 7.3) in order to avoid the mutual influence of the clustered structural parameters in the associated χ^2-tests. The FE model-free localization approach is not considered in this section.

The FE model and the data of the bridge deck were provided by É. Balmès, SD Tools [BL06], which is gratefully acknowledged.

9.3.1 Finite element model of bridge deck

The data of the bridge deck and the sensitivities with respect to the stiffness parameters of the structural elements are obtained from a finite element model. The FE model of the bridge deck consists of 28 supports and a deck with height 3 m, width 6.6–10 m and length 100 m. The whole bridge span is modeled using 9600 standard 8-node isoparametric volume elements and 13 668 nodes [BBM+08]. A simplified model of the deck with 21 sensor position is illustrated in Figure 9.10.

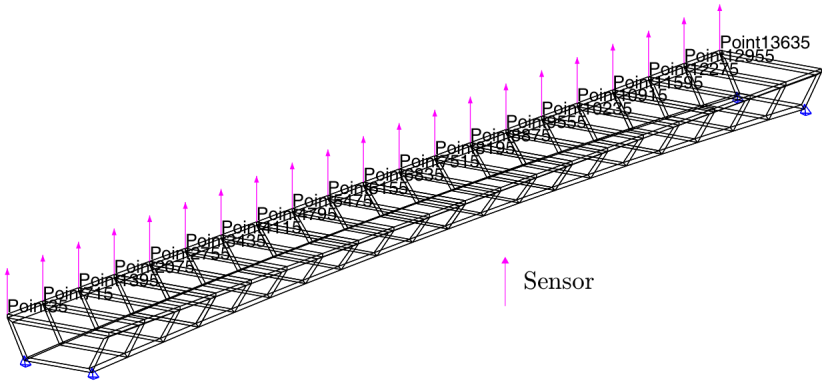

Figure 9.10 – Simplified model of the simulated bridge deck.

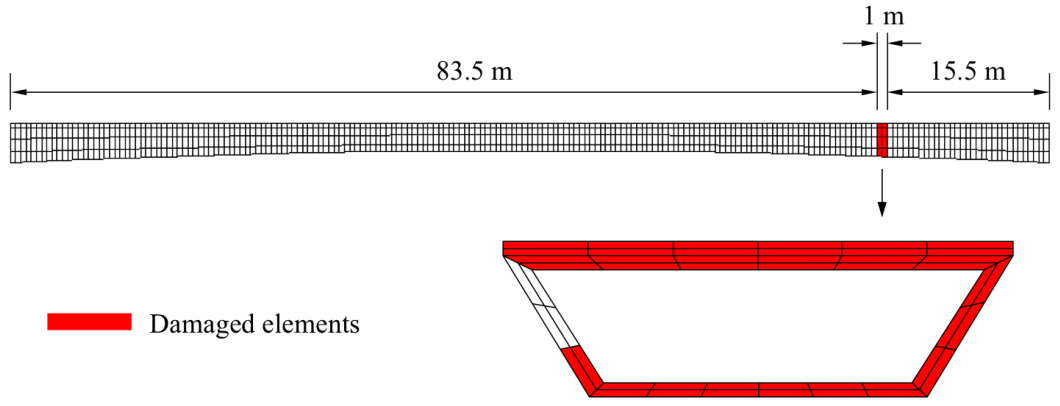

Figure 9.11 – The damaged area in the bridge.

In both the undamaged and damaged case, data at the 21 sensor positions was generated with a sampling frequency of 256 Hz, where each signal contains 100 000 data samples. Damage is introduced by the reduction of the material modulus of up to 30% in 44 elements as illustrated in Figure 9.11.

9.3.2 Damage localization

In the reference state, all the parameters of the χ^2-tests for damage localization (see Sections 7.2.3–7.2.4) need to be set up. From the FEM, the modal signature θ_{FE} is available, containing the first four modes (frequencies and mode shapes at the 21 measured coordinates). Furthermore, the sensitivities $\partial\theta_{\text{FE}}/\partial p_k$, $k = 1, \ldots, P$, with respect to the $P = 9600$ structural elements are available. Then, the following steps are done:

1. System identification from data of reference state with covariance-driven SSI – computation of modal signature θ_0 containing the same modes as θ_{FE} (but with possibly slightly different values as θ_0 is computed from data);

2. Computation of left null space $S(\theta_0)$ from parametric observability matrix $\mathcal{O}(\theta_0)$ and computation of the residual covariance $\widehat{\Sigma}$;

3. Computation of the residual sensitivity $\widehat{\mathcal{J}}(\theta_{\text{FE}})$ with respect to the modal parameters, using the scaled mode shapes from the FEM; and computation of the sensitivities $\widehat{\mathcal{J}}_k = \widehat{\mathcal{J}}(\theta_{\text{FE}})\partial\theta_{\text{FE}}/\partial p_k$, $k = 1, \ldots, P$, with respect to the structural parameters;

4. Computation of the change directions d_k, $k = 1, \ldots, P$, and clustering them with some cluster algorithm (Sections 7.3.2–7.3.3).

Note that the scaling of the mode shapes for the computation of the residual sensitivity with respect to the modal parameters $\mathcal{J}(\theta_0)$ (here $\mathcal{J}(\theta_{\text{FE}})$) must be the same as in the computation of the sensitivities $\partial\theta_0/\partial p_k$ (here $\partial\theta_{\text{FE}}/\partial p_k$) with respect to the structural parameters. With

Section 7.4.2, the latter can be computed from mass-normalized mode shapes, but in this case they were provided from the Structural Dynamics Toolbox [BL06].

For the sensitivity test (Section 7.2.4), where all the structural parameters are tested separately for a change, only the steps 1–3 from above are necessary. Its results are presented in Figure 9.12(a), where for each structural element its χ^2-value is plotted. The damaged area is correctly recognized by the highest χ^2-values.

For the clustering of the over 9000 structural parameters, step 4 from above is necessary. The results of the sensitivity test on the clusters are presented in Figure 9.12(b). It can be seen that in both Figures 9.12(a) and 9.12(b) also the undamaged elements react. In order to reject the influence of the damaged elements on the undamaged elements, the min-max test using the barycenters of the clusters (Section 7.3.3) was computed in Figure 9.12(c). It

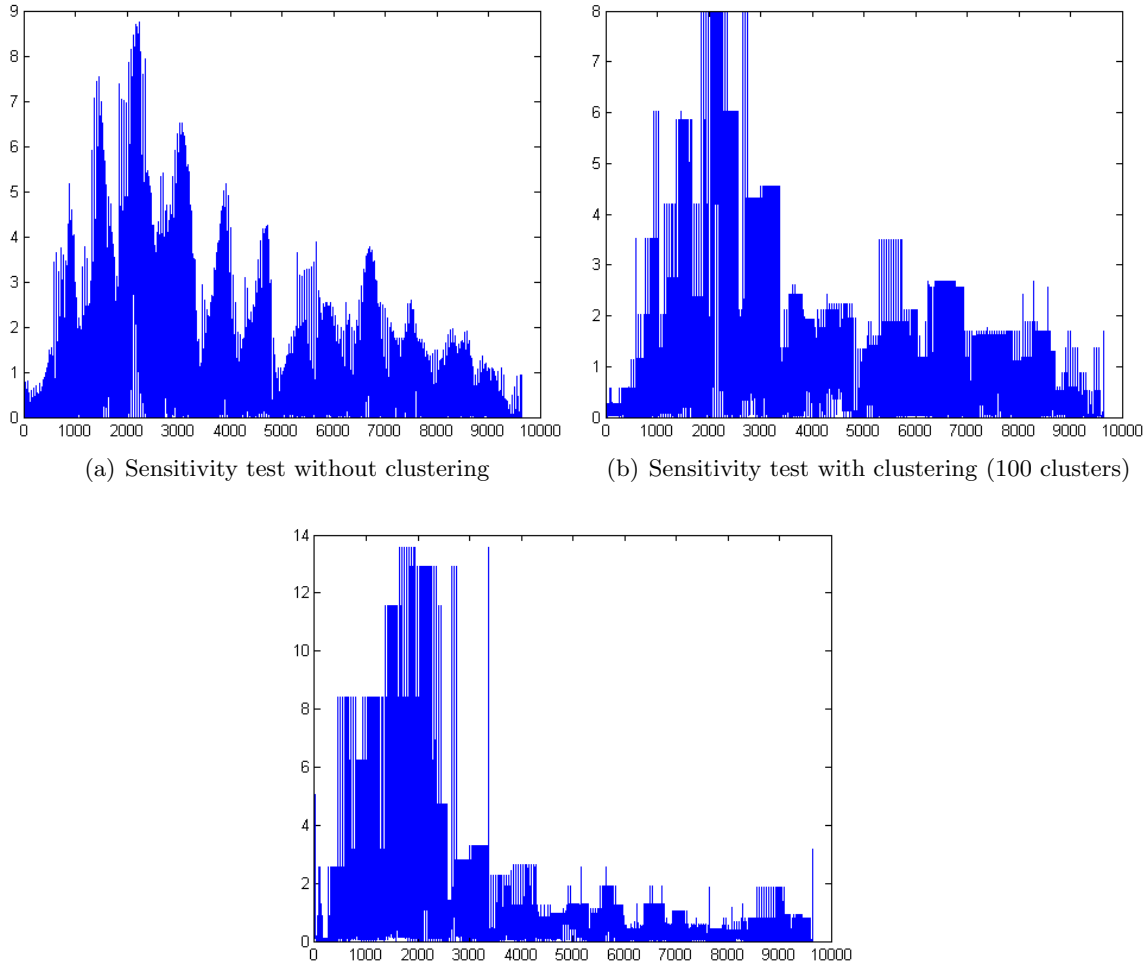

(a) Sensitivity test without clustering

(b) Sensitivity test with clustering (100 clusters)

(c) Min-max test with clustering (100 clusters)

Figure 9.12 – Damage localization in simulated bridge deck.

correctly localizes the damage, but the χ^2-values on the undamaged elements are much lower.

9.4 Conclusions

In this chapter, the statistical subspace-based damage detection test was successfully applied to output-only vibration data from a progressive damage test of the S101 Bridge. Its reactivity to artificially introduced damage on a civil structure was shown. An efficient and fast implementation of the damage detection test was made, which seems to be promising for online structural health monitoring.

Furthermore, the statistical damage localization was tested on a large-scale simulated bridge deck, where the rejection of the mutual influence of structural parameters in the χ^2-tests showed more contrasted damage localization results. Future work contains the application of the statistical damage localization on a real structure. Furthermore, the influence of the clustering on the rejection needs to be explored in detail.

9.5 Dissemination

Parts of this chapter have been published in:

[DHL+11] M. Döhler, F. Hille, X.-B. Lam, L. Mevel, and W. Rücker. Confidence intervals of modal parameters during progressive damage test. In *Proc. 29th International Modal Analysis Conference*, Jacksonville, FL, USA, 2011.

[DHMR11] M. Döhler, F. Hille, L. Mevel, and W. Rücker. Structural health monitoring during progressive damage test of S101 Bridge. In *Proc. 8th International Workshop on Structural Health Monitoring*, Stanford, CA, USA, 2011.

[HDMR11] F. Hille, M. Döhler, L. Mevel, and W. Rücker. Subspace based damage detection methods on a prestressed concrete bridge. In *Proc. 8th International Conference on Structural Dynamics (EURODYN)*, Leuven, Belgium, 2011.

Further applications of the damage detection test are published in [LPS+09, LPD+10, SDBM+10, ZLM+10].

Conclusions

In this thesis, methods for subspace-based system identification as well as fault detection and isolation have been developed, which find an important application in Operational Modal Analysis of vibrating structures. The developed techniques improve the practical usability of established subspace-based methods on real data. The resulting algorithms are faster, numerically more robust and can deal with large systems. They take the nature of in-operation data into account by being robust to changing excitation, noisy data and misspecified model order. Their practical relevance was shown on system identification and damage detection of several large-scale civil structures.

The developed methods in this work have a different degree of maturity. The methods on system identification from Part II have been tested extensively on real data from different large-scale structures. Both the *multi-setup* and the *fast multi-order subspace-based system identification* have been transferred to a commercial software product. The methods for damage detection and localization from Part III have been successfully tested on simulated data and still need to be validated on large-scale structures. The validation on structures in the lab is in progress in collaboration with IFSTTAR and BAM. These methods are also part of the European projects IRIS and ISMS.

A critical discussion of each developed method was made in the respective chapters. Advantages and shortcomings of the new methods can be summarized as follows:

(1) **Modular subspace-based system identification from multi-setup measurements:** A simple, theoretically sound method for global system identification of systems that are measured in multiple setups under possibly varying excitation has been proposed and successfully applied to the identification of large civil structures. It can be used with all subspace methods and shows convenient numerical properties. Because of a modular and iterative approach, a large number of sensors and setups can be handled. The merging is done under the assumption that the same system is observed in all the measurement setups. This can be a shortcoming, if the measurements of a structure are taken under different environmental conditions that affect the underlying system itself, such as temperature variations. This might lead to higher estimates of the damping ratios, but an effect on the mode shapes was not noticed.

The multi-setup methods were presented with subspace methods using time domain data, but can directly be adapted to data from the frequency domain with Remark 2.1. Besides, it seems easier to take into account different excitation levels in frequency domain in order to merge data from multiple setups, which can be done by normalizing

cross power spectra [PGC03]. Shifting the approach described in this thesis to the frequency domain and comparing it to other frequency domain methods (e.g. [RMDRC09]) is a natural extension of this work.

(2) **Fast multi-order subspace-based system identification:** A fast computation scheme for multi-order subspace-based system identification was proposed, that accelerates the computation of stabilization diagrams for structural vibration analysis significantly. A weak conceptual point might be the necessity of a preprocessing step at the maximal desired model order, but it was shown that the new method is already faster when doing the identification at quite low model orders. Note also that the stabilization diagram is a standard tool for modal analysis of structures. Thus, the new computation scheme finds a wide application. In particular, it can speed up the modal analysis of online monitoring data significantly.

(3) **Robust subspace-based fault detection under changing excitation:** Based on a residual function that is robust to changes in the excitation, a modified statistical subspace-based fault detection test was proposed. It was shown that the new test does not react on a change in the (unmeasured) excitation, but on damage to a simulated structure. In the reference state, sufficiently long data sets need to be available, each recorded under the same unmeasured excitation, in order to establish the parameters for a χ^2-test. Then, in the possibly damaged state, it can be decided with a very simple procedure if the eigenstructure related to the tested data deviates significantly from the reference state or not. In the new method, an additional step is added, which requires a SVD and its truncation at a chosen model order.

(4) **Robust subspace-based damage localization using mass-normalized mode shapes:** A statistical damage localization approach was modified to work without a finite element model, but with mass-normalized mode shapes obtained from measurements where a known mass perturbation is introduced on the investigated structure. Numerical simulations showed promising properties of this approach, which is probably the most "experimental" of the presented methods. Note that for damage localization, some extra information needs to be available compared to damage detection – either a FE model, measured excitation of a structure to obtain mass-normalized mode shapes, or in this case a known mass perturbation on the structure. With the rejection scheme of close structural parameters, more contrasted damage localization results were obtained. With this approach, a clustering step is necessary for large systems with many close structural parameters, which is not necessary without the rejection scheme. The mutual influence of structural parameters needs to be further studied and tested on real large scale examples.

The rejection approach can in general be used for any kind of parameter that can be mathematically modeled. For example, in [BBMN09] it was used to reject the influence of the temperature on the stiffness matrix for damage detection robust to temperature change. It can be extended in many ways to reject *nuisance parameters* in damage detection or localization tests, if an appropriate model exists.

With these points, possible areas of further developments of the proposed methods in this thesis are given.

The subspace-based system identification and fault detection and isolation algorithms are closely linked: The system matrices and the system's eigenstructure are identified from the *subspace matrix*. With the detection algorithms, changes in the system's eigenstructure are detected using the *subspace matrix* filled with new data. The covariance of the subspace matrix is used for the computation of the residual's covariance in the fault detection tests, and the same covariance matrix also leads to the uncertainty quantification of system identification results [RPDR08, DLM10a, DHL$^+$11, DLAM11, DLM11]. However, the problem of size reduction for detection is much more difficult as for identification, as *each dimension* of the involved covariance matrices are of the order of the *product of both dimensions* of the subspace matrix. The use of projection channels with $r_0 \ll r$ and strategies of Section 3.5.1 already increase the feasible problem sizes, and further development should contribute to this evolution.

The extensive use of numerical tools as QR and SVD decompositions and other matrix computations in all parts of this thesis led to improvements of the subspace-based identification and detection algorithms. For example, improvements are robustness to changing excitation, faster algorithms and, in general, the feasibility of higher problem sizes. This is especially important for applications in the future, where larger structures are instrumented with more and more sensors and problem sizes are continuously increasing. Further employment of numerical techniques and model reduction techniques will probably be needed to deal with even bigger problem sizes. New technologies as fiber optic sensors, distributed systems or wireless sensor networks push for this development.

Indeed, the motivation for this thesis was the treatment of large structures under realistic excitation assumptions for system identification and fault detection. Before this thesis, it has been shown that subspace methods effectively exhibit great potential to be used for both identification and fault detection of structures [MHVdA99, MGB03, MBB05, BBGM07]. They have interesting properties, such as non-stationary consistency [BM07], the possibility to reject the temperature effect for damage detection [BBB$^+$08, BBMN09] or the feasibility of uncertainty quantification of the identification results [RPDR08], but suffered in the context of large sized case studies. As such, subspace methods had some difficulties with large problem sizes, and several other approaches were once investigated before successfully going back to the subspace framework.

After over 20 years of the existence of subspace methods, contributions in both theoretical improvements and practical usability could still be achieved in this thesis. There is further room for developments especially for the size explosion regarding subspace-based fault detection or uncertainty quantification.

Resume in French

Introduction

Contexte de la thèse

L'identification des systèmes linéaires et la détection des changements dans les systèmes à partir de signaux mesurés est une branche de recherche multidisciplinaire dans les champs de la modélisation mathématique, de l'automatique, des statistiques et du traitement du signal. Au cours des dix à vingt dernières années, les méthodes d'identification des systèmes ont trouvé un intérêt particulier dans l'ingénierie des structures pour l'identification des *modes vibratoires* et de leurs *déformées modales*, mais également pour la détection des changements dans les caractéristiques de leurs vibrations, dans les deux cas sous conditions opérationnelles. Cette *analyse modale opérationnelle* (Operational Modal Analysis, OMA) est composée de trois éléments : acquisition de données, analyse des données collectées et évaluation des résultats. Les avancées dans les systèmes d'acquisition des données (capteurs moins chers, capteurs à fibre optique, réseaux de capteurs sans fils etc.) conduisent à de plus larges systèmes qui peuvent être surveillés au cours du temps et qui rendent ainsi nécessaire un développement plus poussé des techniques statistiques d'analyses de données. L'évaluation des résultats est effectuée par l'ingénieur mécanicien et a par exemple un impact sur la conception des structures, sur le recalage des modèles aux éléments finis ou au niveau de la détection du flottement aéroélastique.

Cette thèse se situe dans le cadre de l'analyse des données, où l'identification des systèmes linéaire ainsi que les méthodes de détection des pannes sont utilisés. En particulier, dans le contexte de l'OMA, il est nécessaire de prendre en compte les caractéristiques inhabituelles suivantes :

(a) Le nombre de capteurs peut être élevé (des centaines voire des milliers dans le futur au moyen de nouvelles technologies). Les capteurs peuvent également être déplacés d'un point de mesure à un autre ;

(b) Le nombre de modes peut également être élevé (jusqu'à cent et même au-delà) et ainsi nécessiter des méthodes qui peuvent prendre en compte des ordres de modèle très grands en un temps de calcul raisonnable;

(c) L'excitation appliquée à la structure n'est généralement pas mesurée, pas contrôlée et aussi turbulente et non stationnaire.

Dans cette thèse, sont développées des méthodes d'identification des systèmes et de détection des pannes qui prennent en compte les points (a–c) ci-dessus évoqués. Les techniques développées concernent la théorie de ces méthodes, mais tirent leur importance dans le cadre de l'OMA, où l'analyse de larges structures équipées de nombreux capteurs opérant sous conditions bruitées est courante.

Identification des systèmes

La conception et la maintenance des structures mécaniques, civiles et aéronautiques soumises au bruit et aux vibrations sont des sujets particulièrement intéressants en ingénierie des structures. Ces éléments contribuent au confort, par exemple pour les véhicules et les immeubles, et contribuent significativement aux aspects sécuritaires, entre autre pour les avions, les navettes spatiales, les structures civiles, les éoliennes, etc. Il est nécessaire de s'assurer que la force dynamique comme le flux de personnes, le trafic, le vent, les vagues ou les séismes, ne compromettent pas le bon fonctionnement de ces structures. Par exemple, la résonance ou le flottement aéroélastique doivent être évités. Afin d'étudier les propriétés dynamiques d'une structure, ses modes de vibration (fréquences naturelles et taux d'amortissement) et ses déformées modales sont analysés.

En conséquence, l'identification des modes de vibration et des déformées modales à partir des données mesurées est une étape de base pour l'ingénierie des structures, afin d'étudier et de surveiller les propriétés dynamiques d'une structure. Les caractéristiques des vibrations sont trouvées dans la structure propre d'un système linéaire, qui nécessite elle d'être identifiée à partir des données.

Les méthodes pour l'identification des systèmes sont souvent issues du domaine de l'automatique et se sont avérées fonctionner pour des petits ordres des systèmes et sous une excitation contrôlée. Elles ont été vérifiées en théorie, testées sur des données simulées et validées sur des structures artificiellement excitées en laboratoire. L'utilisation de ces méthodes sur des structures de terrain pour l'OMA, où les caractéristiques (a–c) doivent être prises en compte, représente la dernière étape dans ce développement et la principale motivation de cette thèse. Dans ce contexte, des techniques sont développées afin de palier à certains inconvénients de l'identification des systèmes dans le contexte de l'OMA.

Détection et diagnostic des pannes

La détection et le diagnostic des pannes sont établis dans le domaine de l'automatique pour détecter des conditions anormales de systèmes et pour identifier le sous-système où les pannes interviennent. Appliqué sur les données vibratoires pour des structures réelles, ce principe correspond à *la détection et la localisation des endommagements structurels* et est établi par détection des changements dans les caractéristiques vibratoires ou dans les paramètres structuraux d'une structure. La *surveillance des structures* (Structural Health Monitoring, SHM) avec de telles méthodes permet de surveiller par exemple les infrastructures civiles et aide à identifier les endommagements à un stade précoce.

Le SHM est devenu un champ de recherche important, dans lequel des techniques de détection non-destructive des endommagements sont utilisées pour surveiller ces structures.

De ce fait, les technologies SHM possèdent un large potentiel commercial et économique. Elles peuvent aider à identifier les endommagements à un stade précoce, où des actions correctives relativement mineures peuvent être entreprises au niveau de la structure avant que des détériorations plus importantes ne surviennent et ne nécessitent donc des actions plus lourdes. La surveillance des endommagements liés aux tremblements de terre représente également un exemple d'application SHM. Dans cette situation, le SHM permettrait d'assurer une remise en fonctionnement rapide des infrastructures civiles et des réseaux de transport, ce qui atténuerait l'importance de la perte économique associée à ces événements sismiques. L'utilisation de SHM dans un contexte de surveillance des infrastructures approchant ou ayant dépassé leur durée de vie initialement prévue, représente également un atout certain pour assurer leur fiabilité et maintenir économiquement des conditions de maintenance raisonnable. D'une manière générale, il est souhaitable de détecter les endommagements de façon automatisée afin de s'affranchir de la nécessité des inspections visuelles qui requièrent une forte main d'œuvre et qui sont difficiles à réaliser dans des environnements à risque ou inaccessibles. Les systèmes SHM permettraient aussi d'intégrer les informations apprises lors des constructions précédentes afin d'améliorer la performance des futures structures.

Des méthodes pour la détection et le diagnostic des pannes sont issues de la théorie de l'automatique. Elles offrent de prometteuses propriétés et peuvent déjà détecter de légers changements dans la structure propre des systèmes linéaires. Néanmoins, pour la détection et la localisation des endommagements pour SHM, les données vibratoires sont enregistrées sous des conditions opérationnelles où les caractéristiques (a–c) ci-dessus évoquées s'appliquent. Ils conduisent à adapter dans le cadre de cette thèse les méthodes actuelles de détection des endommagements à de plus réalistes hypothèses d'excitation. De plus, la robustesse numérique ainsi que le calcul rapide des indicateurs des endommagements doivent être assurés pour de larges structures sous conditions opérationnelles.

Méthodes proposées

Il a été démontré que les méthodes d'identification en sous-espace sont efficaces pour l'identification des systèmes linéaires invariants comprenant des entrées multiples et sorties multiples en utilisant des données mesurées sous des conditions d'excitations réalistes. Pour l'analyse opérationnelle modale des structures vibratoires, il est nécessaire d'identifier la structure propre (valeurs propres et vecteurs propres) du système linéaire de base à partir de laquelle *les fréquences naturelles*, *les taux d'amortissement* et *les déformées modales* sont obtenus. La convergence non-stationnaire de nombreuses méthodes en sous-espace a été prouvée pour l'identification de la structure propre, et en fait ainsi des méthodes phares pour OMA.

Les méthodes suivantes sont développées dans cette thèse, où chacune est motivée par un problème pratique de l'OMA :

1. Identification modulaire en sous-espace à partir de mesures multi-sessions,

2. Identification rapide en sous-espace aux ordres de système multiples et croissants,

3. Détection des pannes robuste aux changements de l'excitation par méthodes de sous-espace,

4. Localisation robuste des endommagements par méthodes de sous-espace en utilisant des déformées modales normalisées par rapport à la masse.

D'importantes propriétés théoriques sont établies pour ces méthodes. Elles sont validées sur des données vibratoires issues de structures réelles, quand ces données sont disponibles. Dans le cas contraire, des données simulées sont utilisées afin de valider les méthodes.

Chapitre 1 – L'état de l'art

Dans le domaine de l'identification des systèmes, dès les années 1960, des modèles mathématiques des systèmes dynamiques sont formulés pour des données mesurées entrée/sortie. Parmi les contributions importantes se trouvent les travaux de Ho et Kalman sur le problème de réalisation d'espace d'état [HK66], ceux d'Åström et Bohlin sur des méthodes de maximum de vraisemblance [AB65], ceux d'Akaike sur la théorie de la réalisation stochastique [Aka74c, Aka75], ceux de Ljung sur les méthodes d'erreur de prédiction [Lju78, LC79] et beaucoup d'autres. Un ouvrage de référence sur l'identification des systèmes est celui de [Lju99]. Dans [Gev06] se trouve une vue d'ensemble de l'histoire du développement de la recherche en identification des systèmes.

Pour l'identification des *systèmes linéaires invariants*, le modèle principal utilisé est *le modèle d'espace d'état*

$$\begin{cases} X_{k+1} = AX_k + BU_k + V_{k+1} \\ Y_k = CX_k + W_k \end{cases}$$

avec les états $X_k \in \mathbb{R}^n$, les entrées observées $U_k \in \mathbb{R}^m$, les sorties $Y_k \in \mathbb{R}^r$ et les distorsions non-observées de l'entrée et de la sortie V_k et W_k. L'identification des matrices de système A et C à partir des sorties Y_k et des entrées U_k (en cas d'entrées observées) est un des problèmes majeurs en identification des systèmes.

La problématique de détection et de diagnostic des pannes (fault detection and isolation, FDI) est de détecter les changements dans les paramètres d'un système dynamique (détection) et de distinguer les paramètres modifiés des paramètres non-modifiés (diagnostic). Il y a de nombreuses techniques FDI provenant du domaine de l'automatique [Wil76, PFC89, Fra90, BN93]. En général, ces problèmes FDI sont décomposés en deux étapes : 1/ l'obtention d'un résidu qui est dans l'idéal proche de zéro en absence de pannes, sensible le moins possible aux bruits et nuisances, et le plus sensible possible aux pannes ; et 2/ l'évaluation du résidu, c'est-à-dire le mise au point des règles de décision basées sur ce résidu [Bas98].

Dans ce chapitre, plusieurs contributions de la littérature par rapport à l'identification des systèmes et la détection des pannes sont présentées.

Chapitre 2 – Contexte des méthodes sous-espace pour l'identification des systèmes et détection des pannes

Les méthodes sous-espace pour l'identification des systèmes et détection des pannes ainsi que leur application à l'analyse des vibrations structurelles constituent le fondement de cette thèse. Elles sont expliquées en détail à partir de la littérature dans ce chapitre.

Pour l'identification en sous-espace, une *matrice sous-espace* $\mathcal{H}$ est construite à partir des données mesurées selon un algorithme sous-espace choisi. Avec une décomposition en valeurs singulières, la matrice d'observabilité $\mathcal{O}$ est obtenue, à partir de laquelle les matrices A et C du système de l'espace d'état sont calculées. La structure propre du système contient des paramètres canoniques et est obtenues à partir des valeurs et vecteurs propres de la matrice A et de la matrice C. Le travail est basé sur [BF85, VODM96, PDR99, BM07].

Pour la détection des pannes, des changements dans la structure propre d'un système linéaire sont détectés en confrontant de nouvelles données à un modèle de référence dans l'état sain. Avec l'approche asymptotique locale pour la détection de changements, un résidu asymptotique Gaussien est construit en utilisant un noyau gauche obtenu à partir du modèle de référence et une matrice sous-espace calculée à partir des données dans un état inconnu et éventuellement en panne. En utilisant un test χ^2 sur le résidu, une décision peut être prise si le résidu est significativement différent de zéro indiquant ainsi que le système est en panne. Ce travail est basé sur [BBM87, BAB00].

L'identification des systèmes et la détection des pannes sont souvent appliquées à l'analyse de vibrations structurelles. Le modèle mécanique de base des structures vibratoires est

$$\begin{cases} M\ddot{\mathcal{X}}(t) + C_1\dot{\mathcal{X}}(t) + K\mathcal{X}(t) = \upsilon(t) \\ Y(t) = L\mathcal{X}(t), \end{cases}$$

où t est le temps continu, M, C_1 et K sont les matrices de la masse, de l'amortissement et de la raideur, $\mathcal{X}(t)$ est le vecteur d'état qui indique les déplacements aux degrés de liberté de la structure, υ est la force externe non-mesurée, les mesures sont collectées dans le vecteur Y et la matrice L indique lesquels des degrés de liberté sont observés (où se trouvent des capteurs). Le modèle mécanique peut être transformé dans un modèle discret d'espace d'état, qui est utilisé pour l'identification et la détection. A partir de sa structure propre, les paramètres d'intérêt du modèle mécanique sont obtenus, soient *les fréquences naturelles*, *les taux d'amortissement* et *les déformées modales*.

Chapitre 3 – Quelques considérations numériques pour des algorithmes sous-espace

Quelques outils numériques nécessaires pour ce travail sont présentés et dérivés dans ce chapitre. Des propriétés supplémentaires de l'algorithme de détection des pannes sont prouvées et éclaircies afin d'augmenter la compréhension théorique de cet algorithme. De plus, quelques problèmes très pratiques pour le calcul d'un test χ^2 associé, concernant le traitement des matrices estimées et à rang déficients, sont résolus. Cette situation apparait

quand des ensembles de données mesurés sur des périodes de temps courtes sont utilisés. Une implémentation numériquement robuste est alors proposée. Ces points augmentent en pratique l'applicabilité de l'algorithme de détection

Chapitre 4 – Identification modulaire en sous-espace à partir de mesures multi-sessions

Un des problèmes dans le contexte de l'OMA est l'identification de la structure propre des larges structures comme des ponts ou des immeubles. Fréquemment, seul un nombre limité de capteurs est disponible. En conséquence, afin d'obtenir des déformées modales détaillées malgré une présence limitée de capteurs, des données vibratoires d'une structure sont mesurées en plusieurs groupes, où quelques capteurs restent fixes et d'autres sont déplacés entre les sessions de mesures. En fusionnant ces données de différents groupes d'une certaine manière, l'identification des systèmes est possible comme s'il y avait un très grand nombre de capteurs, allant même jusqu'à quelques centaines voir milliers. L'excitation entre les sessions peut varier et l'excitation différente non-mesurée doit être prise en compte pour fusionner les données. Basé sur [MBBG02a, MBBG02b], une approche globale de fusion est proposée, où dans une première étape les données de différents groupes sont normalisées et fusionnées, afin d'identifier dans une seconde étape le système global. Cette approche est entièrement automatisée et compatible avec toutes les méthodes d'identification en sous-espace. Elle est modulaire car les données de toutes les sessions sont traitées séquentiellement, et un très grand nombre de sessions et capteurs peut être traité sans se trouver confronté aux problèmes de mémoire. Pour ses propriétés théoriques, la consistance non-stationnaire et la robustesse par rapport à l'ordre de modèle mal spécifié sont prouvées, ce qui valide l'utilisation de cette approche de fusion sur structure réelle. Elle est appliquée avec succès à plusieurs structures civiles.

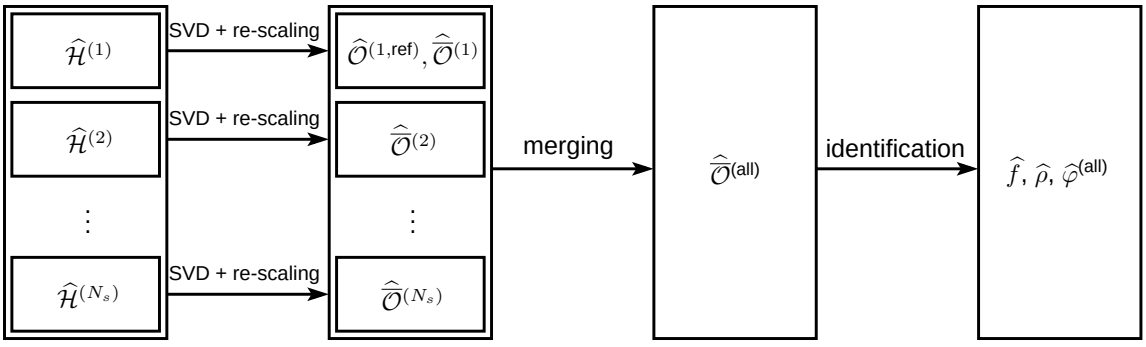

Figure 1 : Schéma de l'approche de fusion développée (Algorithme 4.4). Dans la première étape, les matrices d'observabilité sont obtenues à partir des données et ensuite normalisées. Après, elles sont fusionnées pour l'identification globale des systèmes.

Chapitre 5 – Identification rapide en sous-espace aux ordres de système multiples et croissants

Un problème général pour l'identification de la structure propre d'un système dans le contexte de l'OMA est la distinction entre les vrais modes physiques et les modes parasites qui apparaissent dans les modèles identifiés à cause, entre autre, du bruit coloré, des effets non-linéaires, de l'excitation non-stationnaire ou d'une spécification trop élevée de l'ordre de système. D'un autre côté, l'ordre de système doit être présumé plus élevé que le nombre de modes présents dans les données à cause des effets de bruit. Les modes physiques varient peu en comparant plusieurs estimations à différents ordres de modèle tandis que les modes parasites varient très fortement, il est donc possible de les distinguer grâce à *des diagrammes de stabilisation*, où les fréquences obtenues sont tracées contre les ordres de modèle. Pourtant, cette identification aux ordres multiples est couteuse, surtout pour les larges structures où les capteurs sont nombreux et les ordres de système élevés. Une procédure de calcul rapide est proposée dans cette thèse, qui peut être utilisée avec toutes les méthodes d'identification en sous-espace. Elle réduit le temps de calcul pour l'identification des matrices de système de $O(n_{\max}^4)$ à $O(n_{\max}^3)$, où $n_{\max}$ est l'ordre de modèle maximal. Par exemple, des réductions du temps de calcul par facteur 200 ont été obtenues.

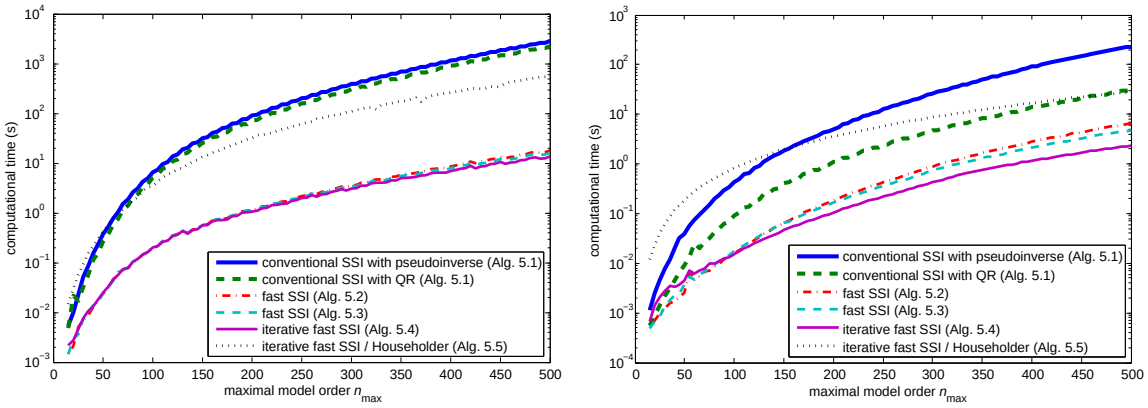

Figure 2 : Temps de calcul pour l'identification des matrices de système aux ordres multiples $1, 2, \ldots, n_{\max}$ *pour des différents ordres de modèle maximal* $n_{\max}$*. Les algorithmes 5.2–5.5 sont développés dans cette thèse.*

Chapitre 6 – Détection des pannes robuste aux changements de l'excitation par méthodes de sous-espace

Avec un test statistique en sous-espace pour la détection des pannes [BAB00], des données d'un état possiblement endommagé sont confrontées à un modèle de référence en utilisant un test χ^2 sur le résidu et en comparant le résultat du test à un seuil. En conséquence, une décision peut être prise si la structure propre d'un système correspondant aux nouvelles

données est toujours conforme ou non à la référence, sans identifier la structure propre dans le nouvel état. En utilisant des données de vibrations structurelles, des endommagements structurels peuvent être détectés avec cet algorithme. Dans le contexte de l'OMA, l'excitation ambiante n'est pas mesurée et peut varier, par exemple à cause des différences de trafic, de vent, etc. Toutefois, un changement de l'excitation a une influence sur la valeur χ^2 du test et peut produire des fausses alarmes. Un nouveau test de détection basé sur un résidu robuste aux changements dans l'excitation est proposé.

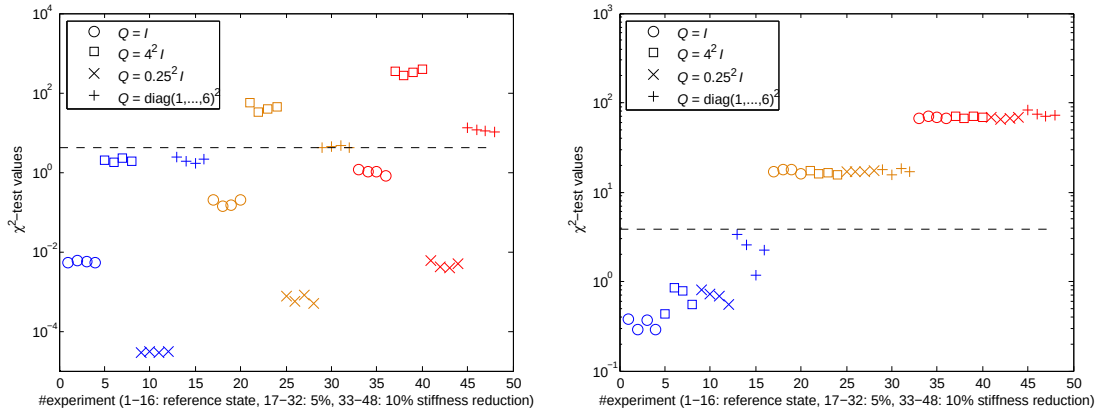

Figure 3 : Test de détection des pannes sous des excitations ambiantes différentes avec des données simulées. A gauche : test conventionnel, à droite : nouveau test proposé dans cette thèse. Les 16 premières valeurs χ^2 sont calculées dans le système de référence, les 16 valeurs χ^2 suivantes sont calculées dans le système en panne où la raideur d'un élément a été baissée de 5%, et les 16 dernières valeurs χ^2 sont calculées avec une baisse de raideur de 10%. Le nouveau test arrive à distinguer clairement les états de référence des états en panne.

Chapitre 7 – Localisation robuste des endommagements par méthodes de sous-espace en utilisant des déformées modales normalisées par rapport à la masse

Une approche de localisation des endommagements est basée sur la détection des changements dans les paramètres structuraux [BMG04, BBM$^+$08] en utilisant un test χ^2. Pour cette approche, des sensibilités par rapport aux paramètres structuraux, normalement obtenues d'un modèle aux éléments finis (finite element model, FEM), sont nécessaires. Dans cette thèse, une approche sans FEM est proposée, où les sensibilités nécessaires sont obtenues des déformées modales normalisées par rapport à la masse. Celles-ci peuvent être obtenues par exemple des données OMA en utilisant des mesures où une perturbation connue de la masse est introduite dans le système étudié. De plus, l'influence réciproque des paramètres structuraux dans les tests χ^2 est étudiée et un algorithme qui rejette cette influence est proposé. Cela conduit à des résultats plus contrastés dans les tests de localisation entre les éléments sains et endommagés et contribue à réduire les fausses alarmes.

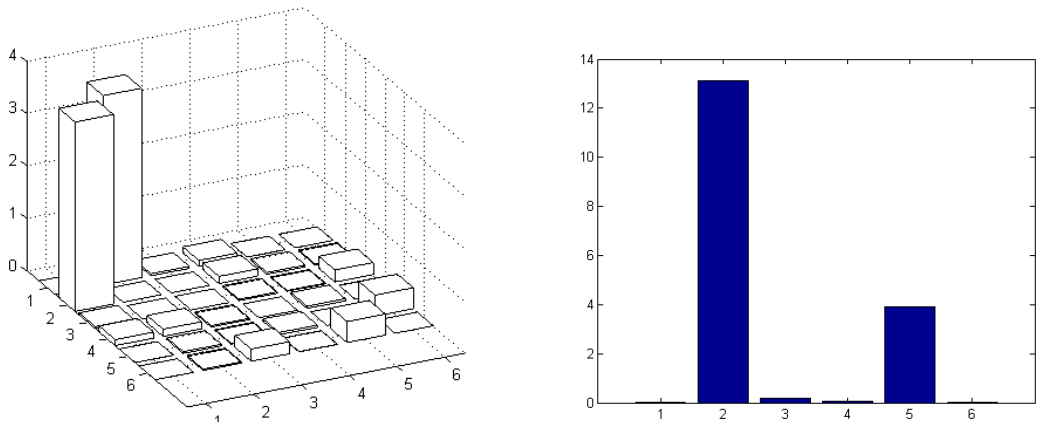

Figure 4 : Localisation des endommagements en détectant des changements dans les paramètres structuraux d'un système simulé à 6 degrés de liberté (DDL). A gauche : réduction de raideur de 5% de l'élément (1,2), à droite : augmentation de 5% de la masse à DDL 2.

Chapitres 8 and 9 – Applications

Dans ce chapitre, les nouveaux algorithmes de fusion pour l'identification des systèmes en multiples sessions sont appliqués à l'identification de la structure propre d'une plaque composite et de quatre structures civiles en utilisant des données sortie-seules. Les données de toutes les structures ont été enregistrées sous conditions opérationnelles, sauf la plaque composite qui a été enregistrée dans le laboratoire. Les analyses de ces structures ont été réalisées dans le cadre de nombreuses collaborations. Les structures étudiées sont :

- Une plaque composite utilisée dans les hélices d'éolienne, en collaboration avec LMS (Belgique), le laboratoire Risø (Danemark) et l'Académie Polonaise des Sciences ;
- Le pont Luiz I (Portugal), en collaboration avec KU Leuven (Belgique) et l'Université de Porto (Portugal) ;
- Le pont Humber (Royaume-Uni), en collaboration avec l'Université de Sheffield ;
- L'immeuble Heritage Court Tower (Canada), en collaboration avec Structural Vibration Solutions A/S (Danemark) ;
- Le pont S101 (Autriche), en collaboration avec l'Université de Tokyo.

De plus, le test de détection d'endommagement est appliqué à une structure réelle de grande taille au cours de dommages artificiels progressifs afin de valider sa performance en utilisant des améliorations de la Section 3.5. Ce travail a été réalisé en collaboration avec l'institut fédéral allemand de recherche sur les matériaux (BAM). De plus, le rejet de l'influence réciproque des paramètres structuraux pour la localisation des endommagements (Chapitre 7) est démontré sur des données fournies par l'Ecole Centrale de Paris, simulée à partir d'un modèle d'un pont de grande taille.

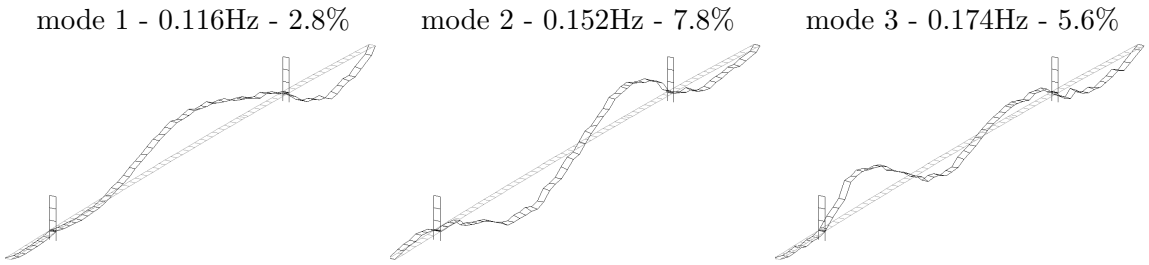

Figure 5 : Les premiers trois modes du pont Humber. Les données vibratoires du pont Humber ont été enregistrées en 26 sessions sous des conditions opérationnelles.

Conclusions

Dans cette thèse, des méthodes théoriques ont été développées pour l'identification des systèmes ainsi que pour la détection et le diagnostic des pannes, qui s'appliquent à l'analyse modale opérationnelle des données vibratoires structurelles. Les techniques développées améliorent l'applicabilité des méthodes sous-espace établies sur des données réelles. Les algorithmes résultants sont plus rapides, numériquement plus robustes et peuvent traiter des systèmes de plus grande dimension. Ils prennent en compte les propriétés intrinsèques des données opérationnelles en étant robustes aux changements dans l'excitation, aux éventuelles nuisances et à une spécification trop élevée de l'ordre de système. L'utilisation des outils numériques partout dans cette thèse, comme les décompositions QR ou SVD et d'autres calculs matriciels, a rendu possible ces améliorations. L'importance pratique des algorithmes développés a été démontrée pour l'identification des systèmes et la détection des endommagements de plusieurs structures civiles de grande taille.

Les méthodes développées dans cette thèse sont de différents degrés de maturité. Les méthodes d'identification des systèmes des Chapitres 4 et 5 ont été testées sur des données opérationnelles de différentes structures de grande taille. Les algorithmes pour l'identification modulaire en sous-espace à partir de mesures multi-sessions et pour l'identification rapide en sous-espace aux ordres de système multiples et croissants ont été transférés à un logiciel commercial. Les méthodes de détection et de localisation des Chapitres 6 et 7 ont été testées avec succès sur des données simulées et doivent encore être validées sur des structures de grande taille. Leur validation sur des structures en laboratoire et en cours en collaborations avec l'IFSSTAR et BAM. Ces méthodes font aussi partie des projets européens IRIS et ISMS.

Bibliography

[AB65] K.J. Aström and T. Bohlin. Numerical identification of linear dynamic systems from normal operating records. In *Proc. IFAC Symposium on Self Adaptive Systems*, Teddington, UK, 1965.

[Akç10] H. Akçay. An insight into instrumental variable frequency-domain subspace identification. *Automatica*, 46(2):375–382, 2010.

[Aka74a] H. Akaike. A new look at the statistical model identification. *IEEE Transactions on Automatic Control*, 19(6):716–723, 1974.

[Aka74b] H. Akaike. Markovian representation of stochastic processes and its application to the analysis of autoregressive moving average processes. *Annals of the Institute of Statistical Mathematics*, 26(1):363–387, 1974.

[Aka74c] H. Akaike. Stochastic theory of minimal realization. *IEEE Transactions on Automatic Control*, 19(6):667–674, 1974.

[Aka75] H. Akaike. Markovian representation of stochastic processes by canonical variables. *SIAM Journal on Control*, 13:162–173, 1975.

[AMR09] M. Abdolvahab, L. Mevel, and L. Ramos. Rejection of temperature effect in subspace-based damage monitoring systems: Application to two historical monuments. In *Proc. 3rd International Operational Modal Analysis Conference*, Ancona, Italy, 2009.

[Au11] S.-K. Au. Assembling mode shapes by least squares. *Mechanical Systems and Signal Processing*, 25(1):163–179, 2011.

[AWDR99] M.M. Abdel Wahab and G. De Roeck. Damage detection in bridges using modal curvatures: application to a real damage scenario. *Journal of Sound and Vibration*, 226(2):217–235, 1999.

[BA03] R. Brincker and P. Andersen. A way of getting scaled mode shapes in output only modal testing. In *Proc. 21st International Modal Analysis Conference*, Kissimmee, Florida, USA, 2003.

[BAB97] M. Basseville, M. Abdelghani, and A. Benveniste. Subspace-based fault detection and isolation methods - application to vibration monitoring. Technical Report 3299, INRIA, 1997.

[BAB00] M. Basseville, M. Abdelghani, and A. Benveniste. Subspace-based fault detection algorithms for vibration monitoring. *Automatica*, 36(1):101–109, 2000.

[Bak11] P.G. Bakir. Automation of the stabilization diagrams for subspace based system identification. *Expert Systems with Applications*, 38(12):14390–14397, 2011.

[Bas97] M. Basseville. Information criteria for residual generation and fault detection and isolation. *Automatica*, 33(5):783–803, 1997.

[Bas98] M. Basseville. On-board component fault detection and isolation using the statistical local approach. *Automatica*, 34(11):1391–1415, 1998.

[Bas99] M. Basseville. An invariance property of some subspace-based detection algorithms. *IEEE Transactions on Signal Processing*, 47(12):3398–3400, 1999.

[Bau01] D. Bauer. Order estimation for subspace methods. *Automatica*, 37(10):1561–1573, 2001.

[Bau05] D. Bauer. Asymptotic properties of subspace estimators. *Automatica*, 41(3):359–376, 2005.

[BAZM79] D.L. Brown, R.J. Allemang, R.D. Zimmerman, and M. Mergeay. Parameter estimation techniques for modal analysis. *SAE Transactions*, 88:828–846, 1979. SAE Paper Number 689110.

[BB11] D. Bernal and Y. Bulut. A modified whiteness test for damage detection using Kalman filter innovations. In *Proc. 27th International Modal Analysis Conference*, Jacksonville, Fl, USA, 2011.

[BBB+08] É. Balmès, M. Basseville, F. Bourquin, L. Mevel, H. Nasser, and F. Treyssède. Merging sensor data from multiple temperature scenarios for vibration-based monitoring of civil structures. *Structural Health Monitoring*, 7(2):129–142, 2008.

[BBG+01] M. Basseville, A. Benveniste, M. Goursat, L. Hermans, L. Mevel, and H. Van der Auweraer. Output-only subspace-based structural identification: from theory to industrial testing practice. *Journal of Dynamic Systems, Measurement, and Control*, 123(4):668–676, 2001.

[BBGM06] A. Benveniste, M. Basseville, M. Goursat, and L. Mevel. The local approach to change detection, diagnosis, and model validation: application to vibration mechanics. In Torkel Glad, editor, *Forever Ljung in system identification - Workshop on the occasion of Lennart Ljung's 60th birthday*, pages 3–35. Studentlitteratur, Lund, SE, 2006.

[BBGM07] M. Basseville, A. Benveniste, M. Goursat, and L. Mevel. In-flight monitoring of aeronautic structures: vibration-based on-line automated identification versus detection. *IEEE Control Systems Magazine*, 27(5):27–42, 2007.

[BBM87] A. Benveniste, M. Basseville, and G. Moustakides. The asymptotic local approach to change detection and model validation. *IEEE Transactions on Automatic Control*, 32(7):583–592, 1987.

[BBM+06] M. Basseville, F. Bourquin, L. Mevel, H. Nasser, and F. Treyssède. Merging sensor data from multiple temperature scenarios for vibration-based monitoring of civil structures. In *Proc. 3rd European Workshop on Structural Health Monitoring*, pages 499–506, Granada, Spain, 2006.

[BBM+08] É. Balmès, M. Basseville, L. Mevel, H. Nasser, and W. Zhou. Statistical model-based damage localization: a combined subspace-based and substructuring approach. *Structural Control and Health Monitoring*, 15(6):857–875, 2008.

[BBM+10] M. Basseville, F. Bourquin, L. Mevel, H. Nasser, and F. Treyssède. Handling the temperature effect in vibration monitoring: two subspace-based analytical approaches. *Journal of Engineering Mechanics*, 136(3):367–378, 2010.

[BBMN09] É. Balmès, M. Basseville, L. Mevel, and H. Nasser. Handling the temperature effect in vibration-based monitoring of civil structures: a combined subspace-based and nuisance rejection approach. *Control Engineering Practice*, 17(1):80–87, 2009.

[BDS99] D. Bauer, M. Deistler, and W. Scherrer. Consistency and asymptotic normality of some subspace algorithms for systems without observed inputs. *Automatica*, 35(7):1243–1254, 1999.

[BDST87] J.M.W. Brownjohn, A.A. Dumanoglu, R.T. Severn, and C.A. Taylor. Ambient vibration measurements of the Humber suspension bridge and comparison with calculated characteristics. In *Proc. of the Institution of Civil Engineers (London)*, volume 83, pages 561–600, 1987.

[Ber02] D. Bernal. Load vectors for damage localization. *Journal of Engineering Mechanics*, 128(1):7–14, 2002.

[Ber04] D. Bernal. Modal scaling from known mass perturbations. *Journal of Engineering Mechanics*, 130(9):1083–1088, 2004.

[Ber06] D. Bernal. Flexibility-based damage localization from stochastic realization results. *Journal of Engineering Mechanics*, 132(6):651–658, 2006.

[Ber10] D. Bernal. Load vectors for damage location in systems identified from operational loads. *Journal of Engineering Mechanics*, 136(1):31–39, 2010.

[Ber11a] D. Bernal. Eigenvector normalization from mass perturbations: a review. In *Proc. International Symposium on Nondestructive Testing of Materials and Structures*, Istanbul, Turkey, 2011.

[Ber11b] D. Bernal. Kalman filter detection under variable noise statistics. In *Proc. 4th International Operational Modal Analysis Conference*, Istanbul, Turkey, 2011.

[Ber11c] D. Bernal. The receptance approach to complex operational mode normalization. In *Proc. 4th International Operational Modal Analysis Conference*, Istanbul, Turkey, 2011.

[Ber11d] D. Bernal. A receptance based formulation for modal scaling using mass perturbations. *Mechanical Systems and Signal Processing*, 25(2):621–629, 2011.

[BF85] A. Benveniste and J.-J. Fuchs. Single sample modal identification of a nonstationary stochastic process. *IEEE Transactions on Automatic Control*, AC-30(1):66–74, 1985.

[BG63] R.E.D. Bishop and G.M.L. Gladwell. An investigation into the theory of resonance testing. *Philosophical Transactions of the Royal Society A: Mathematical and Physical Sciences*, 255(1055):241–280, 1963.

[BL02] D. Bauer and L. Ljung. Some facts about the choice of the weighting matrices in Larimore type of subspace algorithms. *Automatica*, 38(5):763–773, 2002.

[BL06] É. Balmès and J.-M. Leclère. Structural Dynamics Toolbox, User's Guide Version 5.3, SD Tools, 2006.

[BM07] A. Benveniste and L. Mevel. Non-stationary consistency of subspace methods. *IEEE Transactions on Automatic Control*, AC-52(6):974–984, 2007.

[BMCC10] J.M.W. Brownjohn, F. Magalhães, E. Caetano, and Á. Cunha. Ambient vibration re-testing and operational modal analysis of the Humber Bridge. *Engineering Structures*, 32(8):2003–2018, 2010.

[BMG04] M. Basseville, L. Mevel, and M. Goursat. Statistical model-based damage detection and localization: subspace-based residuals and damage-to-noise sensitivity ratios. *Journal of Sound and Vibration*, 275(3):769–794, 2004.

[BMP90] A. Benveniste, M. Metivier, and P. Priouret. *Adaptive Algorithms and Stochastic Approximations*, volume 22 of *Applications of Mathematics*. Springer-Verlag, New York, 1990.

[BN93] M. Basseville and I. Nikiforov. *Detection of Abrupt Changes - Theory and Applications*. Information and System Sciences Series. Prentice Hall, Englewood Cliffs, NJ, 1993.

[BNSR98] T. Bastogne, H. Noura, P. Sibille, and A. Richard. Multivariable identification of a winding process by subspace methods for tension control. *Control Engineering Practice*, 6(9):1077–1088, 1998.

[BP93] J.S. Bendat and A.G. Piersol. *Engineering Applications of Correlation and Spectral Analysis*. John Wiley & Sons, New York, USA, 2nd edition, 1993.

[BP08] E. Bura and R. Pfeiffer. On the distribution of the left singular vectors of a random matrix and its applications. *Statistics & Probability Letters*, 78(15):2275–2280, 2008.

[Bro03] J.M.W. Brownjohn. Ambient vibration studies for system identification of tall buildings. *Earthquake Engineering & Structural Dynamics*, 32(1):71–95, 2003.

[Bro11] M. Brookes. The matrix reference manual, 2011. `http://www.ee.imperial.ac.uk/hp/staff/dmb/matrix/intro.html`.

[BVA01] R. Brincker, C.E. Ventura, and P. Andersen. Damping estimation by frequency domain decomposition. In *Proc. 19th International Modal Analysis Conference*, Kissimmee, FL, USA, 2001.

[BZA01] R. Brincker, L. Zhang, and P. Andersen. Modal identification of output-only systems using frequency domain decomposition. *Smart Materials and Structures*, 10(3):441–445, 2001.

[CBP06] J. Ching, J.L. Beck, and K.A. Porter. Bayesian state and parameter estimation of uncertain dynamical systems. *Probabilistic Engineering Mechanics*, 21(1):81–96, 2006.

[CF04] E.P. Carden and P. Fanning. Vibration based condition monitoring: a review. *Structural Health Monitoring*, 3(4):355–377, 2004.

[CGDV02] B. Cauberghe, P. Guillaume, B. Dierckx, and P. Verboven. Identification of modal parameters from inconsistent data. In *Proc. 20th International Modal Analysis Conference*, pages 809–815, Los Angeles, CA, USA, 2002.

[CGPV06] B. Cauberghe, P. Guillaume, R. Pintelon, and P. Verboven. Frequency-domain subspace identification using FRF data from arbitrary signals. *Journal of Sound and Vibration*, 290(3-5):555–571, 2006.

[CGV+05] B. Cauberghe, P. Guillaume, P. Verboven, S. Vanlanduit, and E. Parloo. On the influence of the parameter constraint on the stability of the poles and the discrimination capabilities of the stabilisation diagrams. *Mechanical Systems and Signal Processing*, 19(5):989–1014, 2005.

[CGVP03] B. Cauberghe, P. Guillaume, P. Verboven, and E. Parloo. Identification of modal parameters including unmeasured forces and transient effects. *Journal of Sound and Vibration*, 265(3):609–625, 2003.

[CK95] Y.M. Cho and T. Kailath. Fast subspace-based system identification: An instrumental variable approach. *Automatica*, 31(6):903–905, 1995.

[CMC06] Á. Cunha, F. Magalhães, and E. Caetano. Output-only modal identification of Luiz I bridge before and after rehabilitation. In *Proc. 22th International Conference on Noise and Vibration Engineering (ISMA2006)*, Leuven, Belgium, 2006.

[CMK01] G. Camba-Mendez and G. Kapetanios. Testing the rank of the Hankel covariance matrix: A statistical approach. *IEEE Transactions on Automatic Control*, 46(2):331–336, 2001.

[Col68] H.A. Cole. On-the-line analysis of random vibrations. *AIAA Paper No. 68-288*, 1968.

[CP04a] A. Chiuso and G. Picci. Asymptotic variance of subspace methods by data orthogonalization and model decoupling: a comparative analysis. *Automatica*, 40(10):1705–1717, 2004.

[CP04b] A. Chiuso and G. Picci. Subspace identification by data orthogonalization and model decoupling. *Automatica*, 40(10):1689–1703, 2004.

[DAM10] M. Döhler, P. Andersen, and L. Mevel. Data merging for multi-setup operational modal analysis with data-driven SSI. In *Proc. 28th International Modal Analysis Conference*, Jacksonville, FL, USA, 2010.

[DB97] B. Delyon and A. Benveniste. On the relationship between identification and local tests. In *Proc. 36th IEEE Conference on Decision and Control*, pages 139–144, 1997.

[DBMS11] M. Döhler, D. Bernal, L. Mevel, and D. Siegert. Statistical-based model-free damage localization. In *Proc. 4th International Operational Modal Analysis Conference*, Istanbul, Turkey, 2011.

[DDSG10] C. Devriendt, G. De Sitter, and P. Guillaume. An operational modal analysis approach based on parametrically identified multivariable transmissibilities. *Mechanical Systems and Signal Processing*, 24(5):1250–1259, 2010. Special Issue: Operational Modal Analysis.

[DFP98] S.W. Doebling, C.R. Farrar, and M.B. Prime. A summary review of vibration-based damage identification methods. *Shock and Vibration Digest*, 30(2):91–105, 1998.

[DHL+11] M. Döhler, F. Hille, X.-B. Lam, L. Mevel, and W. Rücker. Confidence intervals of modal parameters during progressive damage test. In *Proc. 29th International Modal Analysis Conference*, Jacksonville, FL, USA, 2011.

[DHMR11] M. Döhler, F. Hille, L. Mevel, and W. Rücker. Structural health monitoring during progressive damage test of S101 Bridge. In *Proc. 8th International Workshop on Structural Health Monitoring*, Stanford, CA, USA, 2011.

[DJMB11] M. Döhler, B. Jaishi, L. Mevel, and J.M.W. Brownjohn. Data fusion for system identification of the Humber Bridge. In *Proc. 29th International Modal Analysis Conference*, Jacksonville, FL, USA, 2011.

[DLAM11] M. Döhler, X.-B. Lam, P. Andersen, and L. Mevel. Uncertainty quantification for stochastic subspace identification of multi-setup measurements. In *Proc. 4th International Operational Modal Analysis Conference*, Istanbul, Turkey, 2011.

[DLM10a] M. Döhler, X.-B. Lam, and L. Mevel. Confidence intervals on modal parameters in stochastic subspace identification. In *Proc. 34th International Symposium on Bridge and Structural Engineering*, Venice, Italy, 2010.

[DLM10b] M. Döhler, X.-B. Lam, and L. Mevel. Crystal clear data fusion in subspace system identification and damage detection. In *Proc. 5th International Conference on Bridge Maintenance, Safety and Management*, Philadelphia, PA, USA, 2010.

[DLM11] M. Döhler, X.-B. Lam, and L. Mevel. Uncertainty quantification for stochastic subspace identification on multi-setup measurements. In *Proc. 50th IEEE Conference on Decision and Control*, Orlando, FL, USA, 2011.

[DM10] M. Döhler and L. Mevel. Modular subspace-based system identification and damage detection on large structures. In *Proc. 34th International Symposium on Bridge and Structural Engineering*, Venice, Italy, 2010.

[DM11a] M. Döhler and L. Mevel. Fast multi-order stochastic subspace-based system identification. 2011. *Control Engineering Practice*, under revision.

[DM11b] M. Döhler and L. Mevel. Fast multi-order stochastic subspace identification. In *Proc. 18th IFAC World Congress*, Milan, Italy, 2011.

[DM11c] M. Döhler and L. Mevel. Modular subspace-based system identification from multi-setup measurements. 2011. *IEEE Transactions on Automatic Control*, under revision.

[DM11d] M. Döhler and L. Mevel. Robust subspace based fault detection. In *Proc. 18th IFAC World Congress*, Milan, Italy, 2011.

[DMB11] M. Döhler, L. Mevel, and D. Bernal. Statistical subspace-based model-free damage localization. In *Proc. Engineering Mechanics Institute Conference*, Boston, USA, 2011.

[DPS95] M. Deistler, K. Peternell, and W. Scherrer. Consistency and relative efficiency of subspace methods. *Automatica*, 31(12):1865–1875, 1995.

[DRM+10] M. Döhler, E. Reynders, F. Magalhães, L. Mevel, G. De Roeck, and Á. Cunha. Pre- and post-identification merging for multi-setup OMA with covariance-driven SSI. In *Proc. 28th International Modal Analysis Conference*, Jacksonville, FL, USA, 2010.

[DSM10] M. Döhler, D. Siringoringo, and L. Mevel. System identification under different ambient excitations. In *Proc. 3rd Asia-Pacific Workshop on Structural Health Monitoring*, Tokyo, Japan, 2010.

[DV98] C. Dyck and C.E. Ventura. Ambient Vibration Measurements of Heritage Court Tower. *EQ LAB, University of British Columbia, Earthquake Engineering Research*, 1998.

[Ewi84] D.J. Ewins. *Modal testing: theory and practice*. Research Studies Press Ltd., Letchworth, Hertfordshire, UK, 1984.

[Fac05] P.L. Fackler. Notes on matrix calculus. Technical report, North Carolina State University, 2005.

[FDN01] C.R. Farrar, S.W. Doebling, and D.A. Nix. Vibration-based structural damage identification. *Philosophical Transactions of the Royal Society A: Mathematical, Physical and Engineering Science*, 359(1778):131–149, 2001.

[Fis05] R.F.H. Fischer. *Precoding and Signal Shaping for Digital Transmission*, chapter Appendix A: Wirtinger Calculus, pages 405–413. John Wiley & Sons, Inc., 2005.

[FJI97] C.R. Farrar and G.H. James III. System identification from ambient vibration measurements on a bridge. *Journal of Sound and Vibration*, 205(1):1–18, 1997.

[FJK98] C.-P. Fritzen, D. Jennewein, and T. Kiefer. Damage detection based on model updating methods. *Mechanical Systems and Signal Processing*, 12(1):163–186, 1998.

[FK09] C.-P. Fritzen and P. Kraemer. Self-diagnosis of smart structures based on dynamical properties. *Mechanical Systems and Signal Processing*, 23(6):1830–1845, 2009. Special Issue: Inverse Problems.

[FM02] C.-P. Fritzen and G. Mengelkamp. Detection of delaminations in composite materials using a smart structures concept. In *Proc. First European Workshop on Structural Health Monitoring*, Paris, France, 2002.

[FMG03] C.-P. Fritzen, G. Mengelkamp, and A. Guemes. Elimination of temperature effects on damage detection within a smart structure concept. In *Proc. 4th International Workshop on Structural Health Monitoring*, Stanford, CA, USA, 2003.

[Fra90] P.M. Frank. Fault diagnosis in dynamic systems using analytical and knowledge-based redundancy: A survey and some new results. *Automatica*, 26(3):459–474, 1990.

[GD91] B. Gach-Devauchelle. *Diagnostic Mécanique des Fatigues sur les Structures Soumises à des Vibrations en Ambiance de Travail (In French).* PhD thesis, Université de Paris IX Dauphine, Paris, FR, 1991.

[Ger74] W. Gersch. On the achievable accuracy of structural system parameter estimates. *Journal of Sound and Vibration*, 34(1):63–79, 1974.

[Gev06] M. Gevers. A personal view of the development of system identification. *IEEE Control Systems Magazine*, 26(6):93–105, 2006.

[GM03] A. Guyader and L. Mevel. Covariance-driven subspace methods: input/output vs. output-only. In *Proc. 21th International Modal Analysis Conference*, Kissimmee, FL, USA, 2003.

[GP96] P. Guillaume and R. Pintelon. A gauss-newton-like optimization algorithm for "weighted" nonlinear least-squares problems. *IEEE Transactions on Signal Processing*, 44(9):2222–2228, 1996.

[Gra84] R.M. Gray. Vector quantization. *IEEE ASSP Magazine*, 1(2):4–29, 1984.

[GS08] H.M. Gomes and N.R.S. Silva. Some comparisons for damage detection on structures using genetic algorithms and modal sensitivity method. *Applied Mathematical Modelling*, 32(11):2216–2232, 2008.

[Gus98] T. Gustafsson. Instrumental variable subspace tracking using projection approximation. *IEEE Transactions on Signal Processing*, 46(3):669–681, 1998.

[GVC+03] P. Guillaume, P. Verboven, B. Cauberghe, S. Vanlanduit, E. Parloo, and G. De Sitter. Frequency-domain system identification techniques for experimental and operational modal analysis. In *Proc. 13th IFAC Symposium on System Identification*, Rotterdam, The Netherlands, 2003.

[GVL96] G.H. Golub and C.F. Van Loan. *Matrix computations.* Johns Hopkins University Press, 3rd edition, 1996.

[GVV98] P. Guillaume, P. Verboven, and S. Vanlanduit. Frequency-domain maximum likelihood identification of modal parameters with confidence intervals. In *Proc. 24th International Seminar on Modal Analysis (ISMA)*, 1998.

[GVV+03] P. Guillaume, P. Verboven, S. Vanlanduit, H. Van der Auweraer, and B. Peeters. A poly-reference implementation of the least-squares complex frequency-domain estimator. In *Proc. 21th International Modal Analysis Conference*, Kissimmee, FL, USA, 2003.

[GZ08] M.P. González and J.L. Zapico. Seismic damage identification in buildings using neural networks and modal data. *Computers & Structures*, 86(3-5):416–426, 2008.

[HDMR11] F. Hille, M. Döhler, L. Mevel, and W. Rücker. Subspace based damage detection methods on a prestressed concrete bridge. In *Proc. 8th International Conference on Structural Dynamics (EURODYN)*, Leuven, Belgium, 2011.

[HK66] B.L. Ho and R.E. Kalman. Effective construction of linear state-variable models from input/output functions. *Regelungstechnik*, 14(12):545–548, 1966.

[HLS98] W. Heylen, S. Lammens, and P. Sas. *Modal Analysis Theory and Testing*. Katholieke Universiteit Leuven, Belgium, 1998.

[HVdA99] L. Hermans and H. Van der Auweraer. Modal testing and analysis of structures under operational conditions: industrial application. *Mechanical Systems and Signal Processing*, 13(2):193–216, 1999.

[Ibr77] S.R. Ibrahim. Random decrement technique for modal identification of structures. *Journal of Spacecraft and Rockets*, 14(11):696–700, 1977.

[IM76] S.R. Ibrahim and E.C. Mikulcik. The experimental determination of vibration parameters from time responses. *Shock and Vibration Bulletin*, 46(5):187–196, 1976.

[JICL95] G.H. James III, T.G. Carne, and J.P. Lauffer. The natural excitation technique (NExT) for modal parameter extraction from operating structures. *Modal Analysis - The International Journal of Analytical and Experimental Modal Analysis*, 10:260–277, 1995.

[JP85] J.-N. Juang and R.S. Pappa. Eigensystem realization algorithm for modal parameter identification and model reduction. *Journal of Guidance, Control and Dynamics*, 8(5):620–627, 1985.

[JR06] B. Jaishi and W.X. Ren. Damage detection by finite element model updating using modal flexibility residual. *Journal of Sound and Vibration*, 290(1-2):369–387, 2006.

[JSL01] B.C. Juricek, D.E. Seborg, and W.E. Larimore. Identification of the Tennessee Eastman challenge process with subspace methods. *Control Engineering Practice*, 9(12):1337–1351, 2001.

[Jua94] J.-N. Juang. *Applied system identification*. Prentice Hall, Englewood Cliffs, NJ, USA, 1994.

[KM04] H. Kim and H. Melhem. Damage detection of structures by wavelet analysis. *Engineering Structures*, 26(3):347–362, 2004.

[KS95] J.T. Kim and N. Stubbs. Model-uncertainty impact and damage-detection accuracy in plate girder. *Journal of Structural Engineering*, 121(10):1409–1417, 1995.

[KS02] J.T. Kim and N. Stubbs. Improved damage identification method based on modal information. *Journal of Sound and Vibration*, 252(2):223–238, 2002.

[Kul03] J. Kullaa. Damage detection of the Z24 Bridge using control charts. *Mechanical Systems and Signal Processing*, 17(1):163–170, 2003.

[Kun78] S.Y. Kung. A new identification and model reduction algorithm via singular value decomposition. In *Proc. 12th Asilomar Conference on Circuits, Systems, and Computers*, pages 705–714, Pacific Grove, CA, USA, 1978.

[Lar83] W.E. Larimore. System identification, reduced order filters and modelling via canonical variate analysis. In *Proc. American Control Conference*, pages 445–451, San Francisco, 1983.

[LBG80] Y. Linde, A. Buzo, and R.M. Gray. An algorithm for vector quantizer design. *IEEE Transactions on Communications*, 28(1):84–95, 1980.

[LC56] L. Le Cam. On the asymptotic theory of estimation and testing hypotheses. In *Proc. 3rd Berkeley Symposium on Mathematical Statistics and Probability*, pages 129–156, University of California, 1956.

[LC79] L. Ljung and P.E. Caines. Asymptotic normality of prediction error estimators for approximate system models. *Stochastics – An International Journal of Probability and Stochastic Processes*, 3(1):29–46, 1979.

[LC86] L. Le Cam. *Asymptotic Methods in Statistical Decision Theory*. Series in Statistics. Springer, NY, 1986.

[Lju78] L. Ljung. Convergence analysis of parametric identification methods. *IEEE Transactions on Automatic Control*, 23(5):770–783, 1978.

[Lju99] L. Ljung. *System identification: theory for the user*. Prentice Hall, Englewood Cliffs, NJ, USA, 1999.

[LPD+10] M. Luczak, B. Peeters, M. Döhler, L. Mevel, W. Ostachowicz, P. Malinowski, T. Wandowski, and K. Branner. Damage detection in wind turbine blade panels using three different SHM techniques. In *Proc. 28th International Modal Analysis Conference*, Jacksonville, FL, USA, 2010.

[LPS+09] M. Luczak, B. Peeters, W. Szkudlarek, L. Mevel, M. Döhler, W. Ostachowicz, K. Martyniuk, and K. Branner. Comparison of the three different approaches for damage detection in the part of the composite wind turbine blade. In *Proc. 7th International Workshop on Structural Health Monitoring*, Stanford, CA, USA, 2009.

[LS10] M. Luczak and W. Szkudlarek. Damage detecting in E-glass composite material. Technical report, LMS, 2010.

[LW98] K.M. Liew and Q. Wang. Application of wavelet theory for crack identification in structures. *Journal of Engineering Mechanics*, 124(2):152–157, 1998.

[MaCC08] F. Magalhães, Á. Cunha, and E. Caetano. Dynamic monitoring of a long span arch bridge. *Engineering Structures*, 30(11):3034–3044, 2008.

[MaCC10] F. Magalhães, Á. Cunha, and E. Caetano. Continuous dynamic monitoring of an arch bridge: strategy to eliminate the environmental and operational effects and detect damages. In *Proc. 24th International Conference on Noise and Vibration Engineering (ISMA2010)*, Leuven, Belgium, 2010.

[MAL96] T. McKelvey, H. Akçay, and L. Ljung. Subspace-based multivariable system identification from frequency response data. *IEEE Transactions on Automatic Control*, 41(7):960–979, 1996.

[MB86] G.V. Moustakides and A. Benveniste. Detecting changes in the AR parameters of a nonstationary ARMA process. *Stochastics – An International Journal of Probability and Stochastic Processes*, 16(1):137–155, 1986.

[MBB05] L. Mevel, M. Basseville, and A. Benveniste. Fast in-flight detection of flutter onset: a statistical approach. *AIAA Journal of Guidance, Control, and Dynamics*, 28(3):431–438, 2005.

[MBB+06] L. Mevel, A. Benveniste, M. Basseville, M. Goursat, B. Peeters, H. Van der Auweraer, and A. Vecchio. Input/output versus output-only data processing for structural identification - application to in-flight data analysis. *Journal of Sound and Vibration*, 295(3):531–552, 2006.

[MBBG02a] L. Mevel, M. Basseville, A. Benveniste, and M. Goursat. Merging sensor data from multiple measurement setups for nonstationary subspace-based modal analysis. *Journal of Sound and Vibration*, 249(4):719–741, 2002.

[MBBG02b] L. Mevel, A. Benveniste, M. Basseville, and M. Goursat. Blind subspace-based eigenstructure identification under nonstationary excitation using moving sensors. *IEEE Transactions on Signal Processing*, SP-50(1):41–48, 2002.

[MBG03] L. Mevel, M. Basseville, and M. Goursat. Stochastic subspace-based structural identification and damage detection - Application to the steel-quake benchmark. *Mechanical Systems and Signal Processing*, 17(1):91–101, 2003. Special issue on COST F3 Benchmarks.

[MDR03] J. Maeck and G. De Roeck. Description of Z24 benchmark. *Mechanical Systems and Signal Processing*, 17(1):127–131, 2003.

[MGB03] L. Mevel, M. Goursat, and M. Basseville. Stochastic subspace-based structural identification and damage detection and localization - Application to the Z24 Bridge benchmark. *Mechanical Systems and Signal Processing*, 17(1):143–151, 2003. Special issue on COST F3 Benchmarks.

[MH99] T. Marwala and H.E.M. Hunt. Fault identification using finite element models and neural networks. *Mechanical Systems and Signal Processing*, 13(3):475–490, 1999.

[MHVdA99] L. Mevel, L. Hermans, and H. Van der Auweraer. Application of subspace-based fault detection methods to industrial structures. *Mechanical Systems and Signal Processing*, 13(6):823–838, 1999.

[MK00] R.L. Mayes and S.E. Klenke. Consolidation of modal parameters from several extraction sets. Technical report, Sandia National Labs., Albuquerque, NM, and Livermore, CA (US), 2000.

[MKS+01] N. Mastronardi, D. Kressner, V. Sima, P. Van Dooren, and S. Van Huffel. A fast algorithm for subspace state-space system identification via exploitation of the displacement structure. *Journal of Computational and Applied Mathematics*, 132(1):71–81, 2001.

[MLVH01] N. Mastronardi, P. Lemmerling, and S. Van Huffel. The structured total least squares problem. *Contemporary Mathematics*, 280-1(12):157–176, 2001.

[MMBF07] I.D. Mendoume Minko, P. Bernard, and M. Fogli. Asymptotic analysis of the random decrement. *Probabilistic Engineering Mechanics*, 22(3):250–256, 2007.

[MS97] N.M. Maia and J.M. Silva. *Theoretical and Experimental Modal Analysis*. John Wiley & Sons, 1997.

[MWVH+05] I. Markovsky, J.C. Willems, S. Van Huffel, B. De Moor, and R. Pintelon. Application of structured total least squares for system identification and model reduction. *IEEE Transactions on Automatic Control*, 50(10):1490–1500, 2005.

[OKC02] W. Ostachowicz, M. Krawczuk, and M. Cartmell. The location of a concentrated mass on rectangular plates from measurements of natural vibrations. *Computers & Structures*, 80(16-17):1419–1428, 2002.

[Par03] E. Parloo. *Application of frequency-domain system identification techniques in the field of operational modal analysis*. PhD thesis, Vrije Universiteit Brussel, 2003.

[PB94] A.K. Pandey and M. Biswas. Damage detection in structures using changes in flexibility. *Journal of Sound and Vibration*, 169(1):3–17, 1994.

[PBS91] A.K. Pandey, M. Biswas, and M.M. Samman. Damage detection from changes in curvature mode shapes. *Journal of Sound and Vibration*, 145(2):321–332, 1991.

[PDR99] B. Peeters and G. De Roeck. Reference-based stochastic subspace identification for output-only modal analysis. *Mechanical Systems and Signal Processing*, 13(6):855–878, 1999.

[PDR01] B. Peeters and G. De Roeck. Stochastic system identification for operational modal analysis: a review. *Journal of Dynamic Systems, Measurement, and Control*, 123(4):659–667, 2001.

[Pee00] B. Peeters. *System identification and damage detection in civil engineering*. PhD thesis, Katholieke Universiteit Leuven, 2000.

[PFC89] R.J. Patton, P.M. Frank, and R.N. Clarke. *Fault diagnosis in dynamic systems: theory and application*. Prentice Hall, Englewood Cliffs, NJ, 1989.

[PGC03] E. Parloo, P. Guillaume, and B. Cauberghe. Maximum likelihood identification of non-stationary operational data. *Journal of Sound and Vibration*, 268(5):971–991, 2003.

[PGS07] R. Pintelon, P. Guillaume, and J. Schoukens. Uncertainty calculation in (operational) modal analysis. *Mechanical Systems and Signal Processing*, 21(6):2359–2373, 2007.

[Pin02] R. Pintelon. Frequency-domain subspace system identification using non-parametric noise models. *Automatica*, 38(8):1295–1311, 2002.

[PL08] Y. Pan and J.H. Lee. Modified subspace identification for long-range prediction model for inferential control. *Control Engineering Practice*, 16(12):1487–1500, 2008.

[PMDR01] B. Peeters, J. Maeck, and G. De Roeck. Vibration-based damage detection in civil engineering: excitation sources and temperature effects. *Smart Materials and Structures*, 10(3):518–527, 2001.

[POB+91] M. Prevosto, M. Olagnon, A. Benveniste, M. Basseville, and G. Le Vey. State-space formulation, a solution to modal parameter estimation. *Journal of Sound and Vibration*, 148(2):329–342, 1991.

[PS01] R. Pintelon and J. Schoukens. *System Identification, A Frequency Domain Approach*. IEEE Press, New York, 2001.

[PSV97] R. Pintelon, J. Schoukens, and G. Vandersteen. Frequency domain system identification using arbitrary signals. *IEEE Transactions on Automatic Control*, 42(12):1717–1720, 1997.

[PVdAGL04] B. Peeters, H. Van der Auweraer, P. Guillaume, and J. Leuridan. The PolyMAX frequency-domain method: a new standard for modal parameter estimation? *Shock and Vibration*, 11(3-4):395–409, 2004.

[PVGVO02] E. Parloo, P. Verboven, P. Guillaume, and M. Van Overmeire. Sensitivity-based operational mode shape normalisation. *Mechanical Systems and Signal Processing*, 16(5):757–767, 2002.

[RBS+00] R.G. Rohrmann, M. Baessler, S. Said, W. Schmid, and W.F. Rücker. Structural causes of temperature affected modal data of civil structures obtained by long time monitoring. In *Proc. 18th International Modal Analysis Conference*, San Antonio, TX, USA, 2000.

[RDR02a] W.X. Ren and G. De Roeck. Structural damage identification using modal data. I: Simulation verification. *Journal of Structural Engineering*, 128(1):87–95, 2002.

[RDR02b] W.X. Ren and G. De Roeck. Structural damage identification using modal data. II: Test verification. *Journal of Structural Engineering*, 128(1):96–104, 2002.

[RDR08] E. Reynders and G. De Roeck. Reference-based combined deterministic-stochastic subspace identification for experimental and operational modal analysis. *Mechanical Systems and Signal Processing*, 22(3):617–637, 2008.

[RDR10] E. Reynders and G. De Roeck. A local flexibility method for vibration-based damage localization and quantification. *Journal of Sound and Vibration*, 329(12):2367–2383, 2010.

[RHDR11] E. Reynders, J. Houbrechts, and G. De Roeck. Automated interpretation of stability diagrams. In *Proc. 29th International Modal Analysis Conference*, Jacksonville, FL, USA, 2011.

[Ris78] J. Rissanen. Modeling by shortest data description. *Automatica*, 14(5):465–471, 1978.

[RMDRC09] E. Reynders, F. Magalhães, G. De Roeck, and Á. Cunha. Merging strategies for multi-setup operational modal analysis: application to the Luiz I steel arch bridge. In *Proc. 27th International Modal Analysis Conference*, Orlando, FL, USA, 2009.

[RML+10] L.F. Ramos, L. Marques, P.B. Lourenço, G. De Roeck, A. Campos-Costa, and J. Roque. Monitoring historical masonry structures with operational modal analysis: Two case studies. *Mechanical Systems and Signal Processing*, 24(5):1291–1305, 2010. Special Issue: Operational Modal Analysis.

[RMLDR08] L. Ramos, L. Mevel, P.B. Lourenço, and G. De Roeck. Dynamic monitoring of historical masonry structures for damage identification. In *Proc. 26th International Modal Analysis Conference*, Orlando, Fl, USA, 2008.

[RPDR08] E. Reynders, R. Pintelon, and G. De Roeck. Uncertainty bounds on modal parameters obtained from stochastic subspace identification. *Mechanical Systems and Signal Processing*, 22(4):948–969, 2008.

[RTDR10] E. Reynders, A. Teughels, and G. De Roeck. Finite element model updating and structural damage identification using OMAX data. *Mechanical Systems and Signal Processing*, 24(5):1306–1323, 2010.

[Ryt93] A. Rytter. *Vibrational based inspection of civil engineering structures*. PhD thesis, Aalborg University, Denmark, 1993.

[SBMT08] D. Siegert, O. Ben Mekki, and F. Toutlemonde. Vibration-based monitoring of a 10-meter span composite uhpfrc-carbon fibre-timber bridge mockup. In *Proc. Advances in Geomaterials and Structures*, Hammamet, Tunisia, 2008.

[Söd07] T. Söderström. Errors-in-variables methods in system identification. *Automatica*, 43(6):939–958, 2007.

[SDBM+10] D. Siegert, M. Döhler, O. Ben Mekki, L. Mevel, M. Goursat, and F. Toutlemonde. Vibration monitoring of a small span composite bridge. In *Proc. 28th International Modal Analysis Conference*, Jacksonville, FL, USA, 2010.

[SF08] D.M. Siringoringo and Y. Fujino. System identification of suspension bridge from ambient vibration response. *Engineering Structures*, 30(2):462–477, 2008.

[SF09] D.M. Siringoringo and Y. Fujino. Noncontact operational modal analysis of structural members by laser doppler vibrometer. *Computer-Aided Civil and Infrastructure Engineering*, 24(4):249–265, 2009.

[SL05] M. Scionti and J.P. Lanslots. Stabilisation diagrams: Pole identification using fuzzy clustering techniques. *Advances in Engineering Software*, 36(11-12):768–779, 2005.

[SMR+09] D. Siegert, L. Mevel, E. Reynders, G. De Roeck, and M. Goursat. Variation of modal parameter estimates of a prestressed concrete bridge. In *Proc. 27th International Modal Analysis Conference*, Orlando, Fl, USA, 2009.

[SNF+10] D. M. Siringoringo, T. Nagayama, Y. Fujino, D. Su, and C. Tandian. Observed dynamic characteristics of an overpass bridge during destructive testing. In *Proc. 5th International Conference on Bridge Maintenance, Safety and Management*, Philadelphia, PA, USA, 2010.

[SPG03] O.A.Z. Sotomayor, S.W. Park, and C. Garcia. Multivariable identification of an activated sludge process with subspace-based algorithms. *Control Engineering Practice*, 11(8):961–969, 2003.

[SPVG97] J. Schoukens, R. Pintelon, G. Vandersteen, and P. Guillaume. Frequency-domain system identification using non-parametric noise models estimated from a small number of data sets. *Automatica*, 33(6):1073–1086, 1997.

[SS81] T. Söderström and P. Stoica. Comparison of some instrumental variable methods–consistency and accuracy aspects. *Automatica*, 17(1):101–115, 1981.

[STAB88] C.Y. Shih, Y.G. Tsuei, R.J. Allemang, and D.L. Brown. Complex mode indication function and its applications to spatial domain parameter estimation. *Mechanical Systems and Signal Processing*, 2(4):367–377, 1988.

[Str11] Structural Vibration Solutions A/S. ARTeMIS Extractor Pro, 2011. Release 5.3. `http://www.svibs.com`.

[Uhl05] T. Uhl. Identification of modal parameters for nonstationary mechanical systems. *Archive of Applied Mechanics*, 74(11):878–889, 2005.

[VBDA01] C.E. Ventura, R. Brincker, E. Dascotte, and P. Andersen. FEM updating of the Heritage Court Building structure. In *Proc. 19th International Modal Analysis Conference*, Kissimmee, FL, USA, 2001.

[VCE09] VCE. Progressive damage test S101 Flyover Reibersdorf / draft. Technical Report 08/2308, VCE, 2009.

[VdAGVV01] H. Van der Auweraer, P. Guillaume, P. Verboven, and S. Vanlanduit. Application of a fast-stabilizing frequency domain parameter estimation method. *ASME Journal of Dynamic Systems, Measurement, and Control*, 123(4):651–658, 2001.

[VdALMH00] H. Van der Auweraer, W. Leurs, P. Mas, and L. Hermans. Modal parameter estimation from inconsistent data sets. In *Proc. 18th International Modal Analysis Conference*, pages 763–771, San Antonio, TX, USA, 2000.

[VdAP04] H. Van der Auweraer and B. Peeters. Discriminating physical poles from mathematical poles in high order systems: use and automation of the stabilization diagram. In *Proc. 21st IEEE Instrumentation and Measurement Technology Conference*, pages 2193–2198, 2004.

[Ver93] M. Verhaegen. Subspace model identification part 3. Analysis of the ordinary output-error state-space model identification algorithm. *International Journal of Control*, 58(3):555–586, 1993.

[Ver94] M. Verhaegen. Identification of the deterministic part of MIMO state space models given in innovations form from input-output data. *Automatica*, 30(1):61–74, 1994. Special issue on statistical signal processing and control.

[VHG10] N. Viet Hà and J.C. Golinval. Localization and quantification of damage in beam-like structures using sensitivities of principal component analysis results. *Mechanical Systems and Signal Processing*, 24(6):1831–1843, 2010.

[Vib95] M. Viberg. Subspace-based methods for the identification of linear time-invariant systems. *Automatica*, 31(12):1835–1851, 1995.

[VODM94] P. Van Overschee and B. De Moor. N4SID: Subspace algorithms for the identification of combined deterministic-stochastic systems. *Automatica*, 30(1):75–93, 1994.

[VODM96] P. Van Overschee and B. De Moor. *Subspace Identification for Linear Systems: Theory, Implementation, Applications*. Kluwer, 1996.

[VODMDS97] P. Van Overschee, B. De Moor, W. Dehandschutter, and J. Swevers. A subspace algorithm for the identification of discrete time frequency domain power spectra. *Automatica*, 33(12):2147–2157, 1997.

[VWO97] M. Viberg, B. Wahlberg, and B. Ottersten. Analysis of state space system identification methods based on instrumental variables and subspace fitting. *Automatica*, 33(9):1603–1616, 1997.

[Wes86] W.M. West. Illustration of the use of modal assurance criterion to detect structural changes in an orbiter test specimen. In *Proc. 4th International Modal Analysis Conference*, Los Angeles, CA, USA, 1986.

[WFMP07] K. Worden, C.R. Farrar, G. Manson, and G. Park. The fundamental axioms of structural health monitoring. *Proceedings of the Royal Society A: Mathematical, Physical and Engineering Science*, 463(2082):1639–1664, 2007.

[Wil76] A.S. Willsky. A survey of design methods for failure detection in dynamic systems. *Automatica*, 12(6):601–611, 1976.

[WMF00] K. Worden, G. Manson, and N.R.J. Fieller. Damage detection using outlier analysis. *Journal of Sound and Vibration*, 229(3):647–667, 2000.

[WSF02] K. Worden, H. Sohn, and CR Farrar. Novelty detection in a changing environment: regression and interpolation approaches. *Journal of Sound and Vibration*, 258(4):741–761, 2002.

[WVE10] H. Wenzel and R. Veit-Egerer. Determination of a performance baseline for lifecycle consideration of bridges. In *Proc. 5th International Conference on Bridge Maintenance, Safety and Management*, Philadelphia, PA, USA, 2010.

[WZ01] Z. Waszczyszyn and L. Ziemiański. Neural networks in mechanics of structures and materials-new results and prospects of applications. *Computers & Structures*, 79(22-25):2261–2276, 2001.

[YG05] A.-M. Yan and J.-C. Golinval. Structural damage localization by combining flexibility and stiffness methods. *Engineering Structures*, 27(12):1752–1761, 2005.

[YG06] A.-M. Yan and J.-C. Golinval. Null subspace-based damage detection of structures using vibration measurements. *Mechanical Systems and Signal Processing*, 20(3):611–626, 2006.

[YKDBG05a] A.-M. Yan, G. Kerschen, P. De Boe, and J.-C. Golinval. Structural damage diagnosis under varying environmental conditions–Part I: A linear analysis. *Mechanical Systems and Signal Processing*, 19(4):847–864, 2005.

[YKDBG05b] A.-M. Yan, G. Kerschen, P. De Boe, and J.-C. Golinval. Structural damage diagnosis under varying environmental conditions–part II: local PCA for non-linear cases. *Mechanical Systems and Signal Processing*, 19(4):865–880, 2005.

[Zab05] V. Zabel. A wavelet-based approach for damage detection on civil engineering structures. In *Proc. 23rd International Modal Analysis Conference*, Orlando, FL, USA, 2005.

[ZB03] Q. Zhang and M. Basseville. Advanced numerical computation of χ^2–tests for fault detection and isolation. In *5th Symp. Fault Detection, Supervision and Safety for Technical Processes (SAFEPROCESS)*, pages 211–216, Washington, USA, 2003.

[ZBB94] Q. Zhang, M. Basseville, and A. Benveniste. Early warning of slight changes in systems. *Automatica*, 30(1):95–113, 1994.

[ZLM+10] W. Zhou, H. Li, L. Mevel, M. Döhler, X.-B. Lam, C. Mao, and J. Ou. Seismic damage assessment for a residential masonry building using aftershock monitoring ofwenchuan earthquake. In *Proc. 24th International Conference on Noise and Vibration Engineering (ISMA2010)*, Leuven, Belgium, 2010.

[ZWM10] W. Zhou, Z. Wu, and L. Mevel. Vibration-based damage detection to the composite tank filled with fluid. *Structural Health Monitoring*, 9(5):433–445, 2010.

Résumé

L'identification des modes vibratoires est un sujet prioritaire dans le cadre de la surveillance des structures civiles. Certaines techniques d'identification, les méthodes sous espace, ont prouvé leur adéquation pour l'identification et la détection de changements dans les caractéristiques vibratoires, ceci sous des conditions opérationnelles. Le but de cette thèse est l'amélioration de l'efficacité et de la robustesse de ces approches pour l'identification vibratoire et pour la détection des pannes dans les structures de grande taille, équipées d'un grand nombre de capteurs et fonctionnant en conditions environnementales diverses et bruitées. Dans cette thèse, quatre verrous majeurs ont été levés. D'abord, à partir de mesures collectées à différents points de mesure et sous différentes conditions environnementales, un algorithme d'extraction des déformées est proposé, alliant simplicité, modularité et compacité. Ensuite, une reformulation d'un problème moindre carrés amène à une amélioration conséquente du temps de calcul, lors du calcul multi ordre utilisé pour séparer les vrais modes de structures des modes parasites. D'autre part, une approche statistique pour la détection de pannes est améliorée et modifiée par l'usage d'un résidu robuste aux variations dans l'excitation ambiante inconnue. Finalement est considéré le problème de localisation de fautes quand l'absence de modèle aux éléments finis doit être compensée par un calcul direct de sensibilités à partir des données mesurées. Les différentes méthodes sont validées sur simulations et sont appliquées avec succès pour l'identification et la détection de fautes sur plusieurs structures civiles de grande taille.

Abstract

System identification methods are especially attractive to structural engineering for the identification of vibration modes and mode shapes of structures, as well as for detecting changes in their vibration characteristics, both under real operation conditions. Focusing on the class of subspace-based methods, the goal of this thesis is to improve the efficiency and robustness of system identification and fault detection of large in-operational structures, which are heavily instrumented and work under noisy and varying environmental conditions. In this thesis, four different hurdles are cleared. Firstly, an algorithm is derived for directly merging sensor data from multiple measurement sessions at different sensor positions and under different excitation conditions. With a modular and memory efficient approach, global subspace-based system identification of large structures is possible. Secondly, a reformulation of a least squares problem leads to a significantly faster computation of system identification results at multiple model orders, which is used to distinguish true physical modes of a structure from spurious modes under in-operation conditions. Thirdly, a statistical subspace-based fault detection method is improved using a residual that is robust to changes in the unmeasured ambient excitation. Finally, a statistical damage localization test is derived, where required sensitivities are computed from measured data without the need of finite element model. The proposed methods are validated on simulations and are successfully applied to system identification and damage detection of several large-scale civil structures.